Multilevel Coding and Unequal Error Protection for Multiple-Access Communications and Ultra-Wideband Communications in the Presence of Interference

by

Chih-Wei Wang

A dissertation submitted in partial fulfillment
of the requirements for the degree of
Doctor of Philosophy
(Electrical Engineering: Systems)
in The University of Michigan
2010

Doctoral Committee:

Professor Wayne E. Stark, Chair
Professor Hendrikus Derksen
Associate Professor Achilleas Anastasopoulos
Assistant Professor David D. Wentzloff

To my family.

ACKNOWLEDGEMENTS

I would like to express my sincere gratitude to my advisor Professor Wayne E. Stark for his guidance and support throughout my doctoral study. I appreciate the ways in which he has helped me develop my ideas and research, and I gained invaluable experiences from working with him. This thesis would not have been possible without his advice. I would also like to thank other committee members, Professor Hendrikus Derksen, Professor Achilleas Anastasopoulos, and Professor David D. Wentzloff for their constructive feedback and comments on my thesis.

A special thank you goes to Dr. Kurt Metzger. His passion for DSP and dedication to teaching set up a good example for me. His life experiences are great resources for me to overcome challenges I encountered. I deeply appreciate his mentoring and encouragement.

I would like to thank my colleagues in the Wireless Communication Laboratory, Do-Sik Yoo, Hua Wang, Ping-Cheng Yeh, Kar-Peo Yar, Shih-Yu Chang, Jinho Kim, and Changhun Bae. Their friendship and support made my graduate study here a wonderful experience. Some good research ideas were stimulated from conversations with them. I would also like to thank many good friends here in Ann Arbor. I am grateful for their care for me and making my life filled with joy and happiness.

I want to thank my parents for their tremendous love and support for me. I also thank my brother for taking care of things back at home so I can concentrate on my study.

The work presented in this thesis was supported in part by Jet Propulsion Labora-

tory Autonomous Radio for Proximity Link Project and Air Force Office of Scientific Research (FA9550-07-1-0456). I appreciate their support for my graduate study at the University of Michigan.

TABLE OF CONTENTS

LIST OF TABLES

Table

LIST OF FIGURES

Figure

LIST OF APPENDICES

APPENDIX

CHAPTER 1

Introduction

The advances in technology and emerging applications and services define the era of a wireless world. There is a huge and increasing demand for data transmission but a fixed and scarce radio resource (the electromagnetic spectrum). In addition, energy/power is a system resource that is limited. Low energy/power consumption is desirable in many applications. These constraints make the design of wireless systems a challenge.

The concept of radio resource sharing is a key to the efficient use of the wireless spectrum. Multiple-access schemes are designed to achieve the goal of sharing radio resource. In multiple-access schemes, multiple transmissions often take place simultaneously over a common communication medium (channel), which causes interference to one another, and degrades the reliability of the communication links. Interference is one of the major factors that degrade the performance of a communication system. Various types of interference in different scenarios result in different effect on the system performance. It is important to design systems to combat interference in order to assure the desired performance. Most existing systems deal with the interference problem by coordinating users so that the transmissions are orthogonal in time or frequency, or through coding. By adjusting transmission power, it may be possible to control the received interference power at individual receivers to achieve the link quality goals. Another issue in modern wireless (mobile/cellular) communication systems is

the ability to provide versatile broadband services (voice/data/media streaming) simultaneously through the limited radio resource with *quality of service* (QoS) and possibly energy/power constraints. In this scenario, a simple coding and modulation scheme deployed at the transmitter and a smart receiver to recover data of different levels of QoS requirements is necessary. These two problems motivate our research presented in this thesis.

There exists a rich body of previous research to solve these problems. In general, they are treated from two aspects:

- From the *physical layer* point of view, interference can be managed and suppressed through signal processing. Multiple users can access the limited radio resource through coding and modulation techniques.

- From the *network layer* point of view, protocols for power control, routing, and scheduling can be used to optimize the system in different ways.

Traditionally, physical and network layer solutions are considered separately. However, this is not the most efficient way to design wireless systems. A more general concept to deal with the issue is to consider both physical and network layers when designing systems. *Cross-layer* design is a promising way for future wireless systems.

In this thesis, we consider the interference management at the physical layer. In order to enhance the performance (bit error rate, throughput, link quality, complexity, etc.), the receiver needs to have knowledge about the interference, such as the probability distribution, the signal-to-interference ratio, etc. By exploiting the knowledge about interference (such as the statistical properties), it can be suppressed to enhance the link quality.

This thesis contains two main topics: multilevel coding (MLC) for unequal error protection (UEP) and receiver design for ultra-wideband (UWB) communications to suppress interference. Both topics deal with interference in different ways, and face

different design challenges. In the next two sections, we describe the two topics and address the issues we are facing and problem we try to solve. In the final section of this chapter, we outline the organization of this thesis.

1.1 Multilevel Coding and Unequal Error Protection

As mentioned earlier, an issue in modern wireless (mobile/cellular) communication systems is the ability to provide different services simultaneously through a limited radio resource with different QoS and energy/power constraints. In order to overcome the time-varying effect of the wireless channel, channel estimation at the receiver and the feedback between the transmitter and the receiver regarding the channel information is useful. With the channel information, the transmitter can adaptively adjust the coding and modulation scheme to match the channel condition to make the communication efficient. However, the feedback link from the receiver to the transmitter costs extra energy. In order to process the channel information and update coding and modulation schemes, a complex transmitter structure is expected. For some applications, it is desired to have a simple transmitter structure to satisfy an energy/power constraint, and have a powerful receiver to handle most of the processing. This motivates us to find a different solution to this problem.

The idea is to design a fixed coding and modulation scheme at the transmitter with fixed transmitting power. In this case, the receiver has to be smart enough to get the most information out of the received data depending on the channel situation and the SNR. The design of the coding and modulation scheme has to be able to handle different data streams with different QoS requirements for transmission. With careful design on the coding and modulation scheme, the receiver is able to extract information from the received signal at different rates and data quality by adaptively using different decoding

and demodulation strategies according the current channel condition.

A similar problem to ours is the multilevel multicast transmission in wireless networks [1][2][3][4][5][6][7] and the unequal error protection (UEP) problem [8][9][10]. The key idea in these proposed methods is to provide different levels of protection to different classes of data. This is essential when different portions of the source data do not contribute evenly to the overall quality of the decoded information. In a broadcast wireless network, the system is designed to provide reliable transmission to different users which may use various types of equipment and be located at distinct sites. Due to the different reception capabilities of the intended receivers suffering from varying severity of fading channels, it is necessary to design a transmission scheme that guarantees the reliable reception at a minimum transmission rate to the "disadvantaged" users and higher transmission rate for other users. The UEP technique is a simple and efficient method to achieve such requirement. The basic idea is to use constellations with non-uniformly spaced signal points in the modulation scheme. The non-uniform nature of such constellation results in different distances between sets of signals and provide different levels of capability against noise and hence unequal error protection for different bits of the symbol.

Multilevel coding (MLC) [11] is another way to provide unequal error protection for different streams of information with different levels of importance in a communication system. In multilevel coding, the system performance is optimized by choosing the specific coding and modulation scheme. The idea of MLC is to protect each bit of a signal point in the modulation constellation by an individual binary code. The various choices of the component codes enable different strategies for creating a UEP capable system.

The major goal of our work is to design and analyze the system performance of a DS-CDMA system with asymmetric phase-shift-keying (PSK) modulation and MLC in the AWGN channel. The analysis includes probability of bit error of different levels

of the UEP and MLC schemes, and the capacity and throughput of the MLC scheme combined with 8-PSK modulation.

1.2 Interference Mitigation in UWB Communications

Considerable amount of research has focused on analyzing and mitigating interference caused from UWB to other existing systems (such as 802.11 Wireless LANs, GPS, etc.). However, the existing systems can also cause strong interference to UWB. It is important to investigate the impact of the interference to UWB, and design algorithms to mitigate interference for UWB. In designing algorithms to suppress interference, there are two major concerns:

1. *Understanding the interference*

   In order to successfully combat interference, it is necessary to understand the structure of the interference. Random interference can be described by its probability density function (PDF). For theoretical analysis, interference can be modeled according to the application and the exact PDF can be obtained. In practice, interference is unknown and varies with time (non-stationary). Thus, its PDF has to be estimated and adaptively updated.

2. *Implementing the algorithm – the complexity issue*

   When designing and analyzing the optimum receiver based on the maximum a posteriori probability (MAP) criterion, the knowledge of the PDF of the interference is required. With this knowledge, if the PDF is complicated, it is difficult to utilize it for the receiver design in the practical sense. In this case, suboptimum receivers with low complexity that can perform nearly as well as the optimum receiver are desirable.

There are several types of interference we should consider in the design of UWB communication systems – intersymbol interference (ISI) due to the multipath channels, multiple-access interference (MAI) in multiuser scenario, narrowband interference (NBI) from existing systems, possible jamming signal, and lastly, additive white Gaussian noise (AWGN) in the system. All these types of interference mentioned above degrade the UWB system performance in different ways and to different levels. This points out the importance of interference mitigation in UWB communications.

In this work we analyze the performance of UWB communications in the presence of MAI and jamming interference. We consider a nonlinear interference suppression technique for time-hopping (TH) pulse-position modulation (PPM) UWB systems. We consider the synchronous single path AWGN channel, and the transmitted signal is corrupted by interference. In practice, the interference is not Gaussian distributed, and hence the total interference plus noise is not Gaussian, and the optimum receiver can be very complex and quite difficult to realize physically. Previously the Gaussian approximation to the interference is used when evaluating the system performance. Since Gaussian interference is actually the worst case, substantial improvement can be made when the actual non-Gaussian interference is properly taken into account. In our work, we find the probability distribution of the total interference by computing the exact probability density function (PDF). Therefore the exact bit error rate (BER) can be evaluated. Furthermore, this PDF can be used in a locally optimum Bayes detector (LOBD) to derive the suboptimum receiver with less complexity. In the first part of this work, we derive the PDF of the total interference in a multiple access TH-PPM UWB system. By applying the conventional pulse correlation receiver, a closed-form PDF of the total interference of the correlator output is found for the special case when the impulse signal is rectangular. Next, we apply the LOBD algorithm using the interference PDF to derive the nonlinearity for interference suppression. Lastly, we apply this locally optimum detector at the receiver to evaluate the system performance,

and compare the results with the performance of the traditional linear receiver. In the second part of the work, we apply the same procedures to deal with the Gaussian on-off jamming interference. The last part of this work is to adaptively estimate and update the interference PDF for the LOBD receiver for the real-time processing of the receiver.

1.3 Thesis Outline

This thesis contains two major parts. The first part is composed of Chapter 2 through Chapter 4 with a focus on multilevel coding for unequal error protection. Asymmetric modulation and multilevel coding are considered to achieve the goal of unequal error protection. The second part of the thesis is composed of Chapter 5 through Chapter 7 with an emphasis on the receiver design for ultra-wideband communications in the presence of interference. The goal is to design receivers with low complexity for practical implementation while performance asymptotically approaches the optimum receiver performance. Each chapter in this thesis is briefly described in the following.

In Chapter 2, we analyze a quaternary DS-CDMA system with asymmetric QPSK modulation. We derive the exact BER performance of the system by analyzing the probability density function of the multiple-access interference utilizing the characteristic function method. We also approximate the BER using Gaussian approximation to the interference. Lastly, we investigate the near-far problem by generalizing the system model to the case where users have different transmitting power. The results show that the less protected data bits are more sensitive to the near-far effect in a multiple-access environment.

In Chapter 3, we extende the analysis of a DS-CDMA system QPSK modulation studied in Chapter 2 to the 8-PSK modulation case in combination with multilevel coding to further achieve the goal of an unequal error protection system. In the proposed system, we analyze the performance of multilevel coding and multistage decoding with

BCH codes as component codes, and derive the approximate BER by approximating the multiple-access interference as a Gaussian random variable and assuming the use of random signature sequences for spreading.

In Chapter 4, we analyze the capacity and throughput of the 8-PSK multilevel coding scheme using BCH codes of various block length and error correcting capability. The results show that the MLC scheme outperforms the regular scheme in the low SNR region. However, in the high SNR region, MLC scheme has a lower throughput than the regular scheme due to the low reliability on the low level.

In Chapter 5, receiver design for multiple-access ultra-wideband communications is investigated. We examine the performance of the suboptimum linear receiver, and design the suboptimum nonlinear receiver to suppress interference based on the LOBD algorithm. The results show the effectiveness of the proposed nonlinear receiver to mitigate strong interference.

In Chapter 6, we apply the technique described in Chapter 5 to receiver design for ultra-wideband communications to suppress Gaussian on-off jammer. We examined the optimum receiver and compare it to the proposed suboptimum receiver. Various jamming scenarios are examined to show the interference suppression capability of the proposed receiver structure.

In Chapter 7, implementation of the LOBD receiver proposed in Chapters 5 and 6 is discussed. A LOBD receiver with real-time processing is implemented by continuously monitoring the interference and adaptively estimate and update the interference density function and the signal processing function of the LOBD receiver. The adaptive LOBD algorithm makes the proposed receiver implementation practical to deal with different types of interference.

This thesis is concluded in Chapter 8.

CHAPTER 2

Analysis of a DS-CDMA System with Asymmetric QPSK Modulation

2.1 Introduction

In the design of a wireless communication system, feedback between the transmitter and receiver regarding the channel condition is useful for adapting the radio transmission rate to match the channel conditions [12][13][14][15][16]. When the channel condition is good, the data rate is increased, while when the channel condition is bad, the data rate is decreased. However, in some cases the transmitter does not know the condition of the channel and still desires to match the data rate to the channel. In this case, modulation and demodulation techniques are needed that allow more data to be transmitted when the channel is good and less when the channel is bad, without the transmitter knowing in advance the condition of the channel.

Consider for example the transmission of an image. Suppose that there are two modes of operation at the receiver with respect to high and low signal-to-noise ratios (SNRs). The two modes have different demodulation and decoding strategies according to two different rates and image qualities. In the high SNR mode, the receiver can demodulate and decode the data at high rate (or full rate) and recover the image with its high quality. In the low SNR mode, the protection available with coding and

modulation is not adequate to protect all the data. However, it may be possible to decode only a subset of the bits that have higher error protection. In this case, the receiver demodulates and decodes the data at a lower rate, and recovers the image with lower quality as compared to the high-quality image.

In a wireless network, the channel condition can vary for several reasons. One reason is just the change in the distance between the transmitter and the receiver. Another reason is that the multiple-access interference produces time-varying channel conditions.

The key idea in designing such a system is to introduce modulation and coding schemes that provide different error protection to different classes of data. The earlier work on multicasting [1][2][3][4][6][5][7] and unequal error protection (UEP) [8][9][10] examined such a system in the case of a mobile network downlink. This idea is essential when different portions of the source do not contribute evenly to the overall quality of the decoded information. The UEP technique is a simple and efficient method to satisfy such a requirement. The basic idea is to use a constellation with non-uniformly spaced signal points in the modulation scheme. The non-uniform nature of such a constellation results in different distances between sets of signals and provides different levels of reliability against noise and interference and, hence, unequal error protection on different bits of a symbol. An asymmetric quadrature phase-shift-keying (AQPSK) constellation can be regarded as the simplest modulation scheme to provide the system with UEP capability. A comparison of QPSK and AQPSK is shown in Figure 2.1. As can be seen, in the example shown in Figure 2.1b, the I-channel data (bit) is better protected than the Q-channel data.

In [17], a quaternary direct-sequence code-division multiple-access (DS-CDMA) system is analyzed and an expression for the SNR is determined. However, the exact bit-error rate (BER) performance is not derived. In [18] and [19], the case of binary DS-CDMA with random signature sequences is investigated for binary phase-shift-keying (BPSK). Also, the Gaussian approximation to the interference is used to approximate

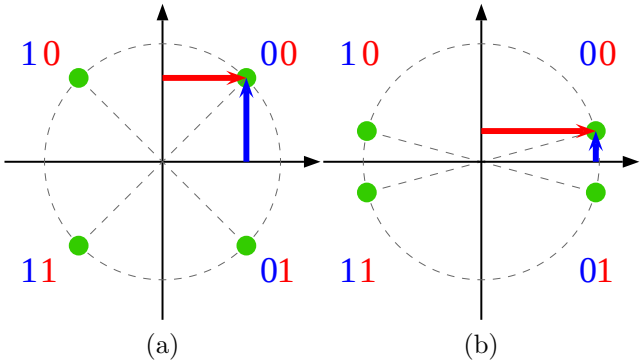

Figure 2.1: Comparison of QPSK and AQPSK.

the performance. In this chapter, we derive the exact BER for a quaternary DS-CDMA system and also derive the approximate BER using a Gaussian approximation to the interference for AQPSK. We consider a direct-sequence spread-spectrum modulation technique with asymmetric QPSK modulation that allows higher data rate transmission if the channel is good and a lower transmission rate when the channel condition is poor. We analyze the performance of a quaternary DS-CDMA communication using AQPSK modulation over an additive white Gaussian noise (AWGN) channel, with a correlation receiver that is coherent to the desired user. We look at both the cases of specific and random signature sequences being used in the system.

This chapter is organized as follows. In Section 2.2, the system model is introduced. In Section 2.3, we derive the exact BER performance of the system. This also includes the derivation of the probability density function (pdf) of the multiple-access interference (MAI). A numerical example is given to illustrate the performance using a specific set of signature sequences. In Section 2.4, the random signature-sequence case is considered. The Gaussian approximation is used to model the MAI, and the approximate BER performance is obtained. In Section 2.5, we generalize the signal model and examine the nearfar effect on the system performance.

2.2 System Model

In this section, we describe the mathematical model of an asymmetric QPSK modulation system and characterize the receiver output. We consider an extension of the model described in [17] for asynchronous quaternary DS-CDMA. The model is shown in Figure 2.2. The difference from [17] is that we consider asymmetric QPSK so that the in-phase (I)-channel and quadrature-phase (Q)-channel bits have unequal energy. Suppose there are K users in the system. The quaternary signal of the kth user is given by

$$s_k(t) = s_k^I(t) + s_k^Q(t) \tag{2.1}$$

where

$$s_k^I(t) = \sqrt{2P} \cdot \cos(\beta) \cdot a_k^I(t) b_k^I(t) \cos(2\pi f_c t + \theta_k), \tag{2.2}$$

$$s_k^Q(t) = \sqrt{2P} \cdot \sin(\beta) \cdot a_k^Q(t) b_k^Q(t) \sin(2\pi f_c t + \theta_k). \tag{2.3}$$

In the above expressions, P is the transmitted power, β is the angle of the signal points in the asymmetrical constellation, $a_k^I(t)$ and $a_k^Q(t)$ are the spreading signals for the I and Q channels, $b_k^I(t)$ and $b_k^Q(t)$ are the user information being transmitted in the I and Q channels, θ_k is the initial phase of the kth user and is assumed to be uniformly distributed over the interval $[0, 2\pi]$. The modulation constellation is shown in Figure 2.3. In this scheme, we choose $0 < \beta < \frac{\pi}{4}$.

The information being transmitted by user k is represented by

$$b_k^I(t) = \sum_{j=-\infty}^{\infty} b_{k,j}^I \cdot p_T(t - jT) \tag{2.4}$$

$$b_k^Q(t) = \sum_{j=-\infty}^{\infty} b_{k,j}^Q \cdot p_T(t - jT) \tag{2.5}$$

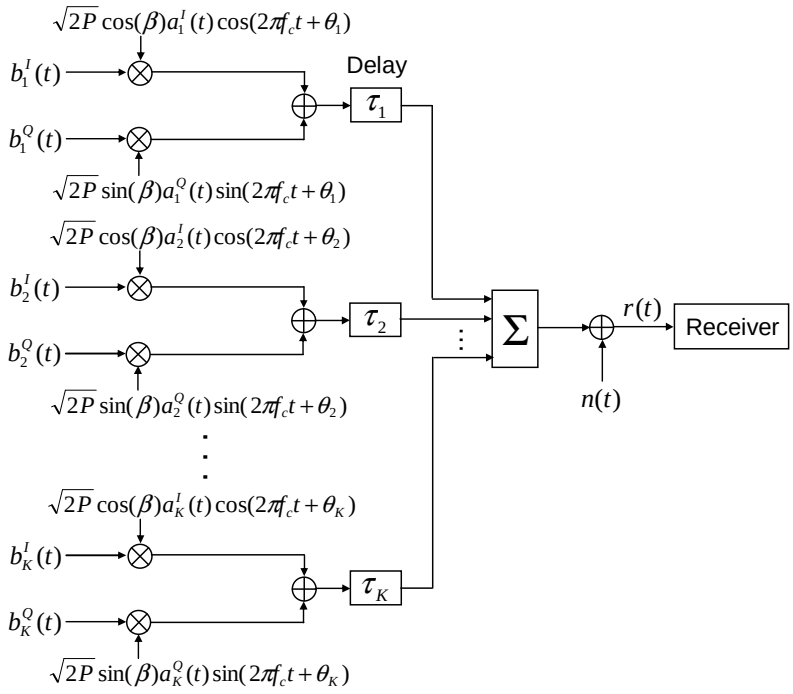

Figure 2.2: A quaternary DS-CDMA communication system model.

where $b_{k,j}^I$, $b_{k,j}^Q \in \{\pm 1\}$, T is the symbol duration, and

$$p_T(t) = \begin{cases} 1, & 0 \le t \le T \\ 0, & \text{otherwise.} \end{cases} \tag{2.6}$$

The spreading signals are expressed as

$$a_k^I(t) = \sum_{j=-\infty}^{\infty} a_{k,j}^I \cdot \psi(t - jT_c) \tag{2.7}$$

$$a_k^Q(t) = \sum_{j=-\infty}^{\infty} a_{k,j}^Q \cdot \psi(t - jT_c) \tag{2.8}$$

where $a_{k,j}^I$, $a_{k,j}^Q \in \{\pm 1\}$ are the signature sequences for the I and Q channels, T_c is the chip duration such that $T = NT_c$, and $\psi(t)$ is the chip waveform which is nonzero for $0 \le t \le T_c$. In general we can choose any pulse shape as the chip waveform. However, to simplify the analysis, in the following we will assume the rectangular pulse is used

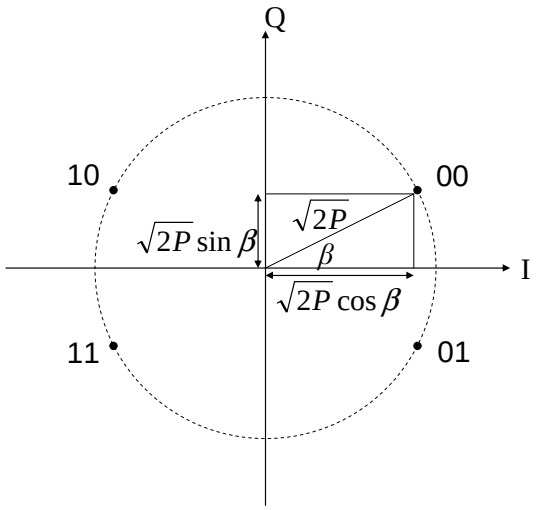

Figure 2.3: Asymmetric QPSK constellation.

as the chip waveform, i.e. $\psi(t) = p_{T_c}(t)$.

The receiver is assumed to consist of a simple correlator matched to the desired signal. We examine both the time synchronous and asynchronous cases. Even though the asynchronous case is the more realistic case of the two, the synchronous case is more easily analyzed than the asynchronous case. When considering channel coding using linear block codes, it is very difficult to analyze the asynchronous case due to the dependency of bit errors within one block.

2.2.1 Asynchronous System

We first consider the asynchronous case. The received signal is given by

$$\begin{aligned} r(t) &= \sum_{k=1}^{K} s_k(t-\tau_k) + n(t) \\ &= \sum_{k=1}^{K} \sqrt{2P}\cos(\beta) a_k^I(t-\tau_k) b_k^I(t-\tau_k)\cos(2\pi f_c(t-\tau_k)+\theta_k) \\ &\quad + \sum_{k=1}^{K} \sqrt{2P}\sin(\beta) a_k^Q(t-\tau_k) b_k^Q(t-\tau_k)\sin(2\pi f_c(t-\tau_k)+\theta_k) + n(t) \\ &= \sum_{k=1}^{K} \sqrt{2P}\cos(\beta) a_k^I(t-\tau_k) b_k^I(t-\tau_k)\cos(2\pi f_c t+\phi_k) \\ &\quad + \sum_{k=1}^{K} \sqrt{2P}\sin(\beta) a_k^Q(t-\tau_k) b_k^Q(t-\tau_k)\sin(2\pi f_c t+\phi_k) + n(t) \end{aligned} \tag{2.9}$$

where $n(t)$ is an additive white Gaussian noise with zero mean and two-sided power spectral density $N_0/2$. The time delay of the kth signal is represented by τ_k and $\phi_k = \theta_k - 2\pi f_c \tau_k \pmod{2\pi}$.

The analysis here basically follows the methods in [17] and [20]. Consider the output of the correlation receiver for the first user. The output of the I-channel correlator for the data bit $b_{1,0}^I$ can be decomposed into terms corresponding to the desired signal, the

interference, and noise as follows:

$$\begin{aligned}
Z_1^I &= \int_0^T r(t)a_1^I(t)\cos(2\pi f_c t)dt \\
&= \int_0^T \sqrt{2P}\cos(\beta)a_1^I(t)b_1^I(t)\cos(2\pi f_c t)a_1^I(t)\cos(2\pi f_c t)dt \\
&\quad + \int_0^T \sqrt{2P}\sin(\beta)a_1^Q(t)b_1^Q(t)\sin(2\pi f_c t)a_1^I(t)\cos(2\pi f_c t)dt \\
&\quad + \sum_{k=2}^{K}\int_0^T \sqrt{2P}\cos(\beta)a_k^I(t-\tau_k)b_k^I(t-\tau_k)\cos(2\pi f_c t+\phi_k)a_1^I(t)\cos(2\pi f_c t)dt \\
&\quad + \sum_{k=2}^{K}\int_0^T \sqrt{2P}\sin(\beta)a_k^Q(t-\tau_k)b_k^Q(t-\tau_k)\sin(2\pi f_c t+\phi_k)a_1^I(t)\cos(2\pi f_c t)dt \\
&\quad + \int_0^T n(t)a_1^I(t)\cos(2\pi f_c t)dt. \qquad (2.10)
\end{aligned}$$

In the above expression, the output due to the desired signal is

$$\begin{aligned}
A &= \int_0^T \sqrt{2P}\cos(\beta)b_1^I(t)\left(a_1^I(t)\right)^2\cos^2(2\pi f_c t)dt \\
&= \sqrt{2P}\cos(\beta)b_{1,0}^I\int_0^T \frac{1}{2}[1+\cos(4\pi f_c t)]dt \\
&= T\sqrt{P/2}\cos(\beta)b_{1,0}^I \qquad (2.11)
\end{aligned}$$

where the double frequency term is negligible since we assume $f_c >> (T_c)^{-1}$. Because of the assumption of coherent reception, the component of the I-channel correlator output due to the Q-channel signal is

$$\begin{aligned}
B &= \int_0^T \sqrt{2P}\sin(\beta)a_1^Q(t)b_1^Q(t)\sin(2\pi f_c t)a_1^I(t)\cos(2\pi f_c t)dt \\
&= \sqrt{2P}\sin(\beta)b_{1,0}^Q\int_0^T a_1^Q(t)a_1^I(t)\sin(2\pi f_c t)\cos(2\pi f_c t)dt \\
&= 0. \qquad (2.12)
\end{aligned}$$

The interference component of the I-channel correlator output due to a I-channel inter-

ferer is given by

$$\begin{aligned}
C_k &= \int_0^T \sqrt{2P}\cos(\beta)a_k^I(t-\tau_k)b_k^I(t-\tau_k)\cos(2\pi f_c t+\phi_k)a_1^I(t)\cos(2\pi f_c t)dt \\
&= \sqrt{2P}\cos(\beta)\int_0^T b_k^I(t-\tau_k)a_k^I(t-\tau_k)a_1^I(t)\cos(2\pi f_c t+\phi_k)\cos(2\pi f_c t)dt \\
&= \sqrt{2P}\cos(\beta)\int_0^T b_k^I(t-\tau_k)a_k^I(t-\tau_k)a_1^I(t)\frac{1}{2}\Big[\cos(\phi_k)+\cos(4\pi f_c t+\phi_k)\Big]dt \\
&= \sqrt{P/2}\cos(\beta)\cos(\phi_k)\int_0^T b_k^I(t-\tau_k)a_k^I(t-\tau_k)a_1^I(t)dt \\
&= \sqrt{P/2}\cos(\beta)\cos(\phi_k)\Big[b_{k,-1}^I R_{k,1}^{II}(\tau_k)+b_{k,0}^I\hat{R}_{k,1}^{II}(\tau_k)\Big] \qquad (2.13)
\end{aligned}$$

where the time cross-correlations $R_{k,i}^{II}(\tau)$ and $\widehat{R}_{k,i}^{II}(\tau)$ are defined as [17][1]

$$R_{k,i}^{II}(\tau) = \int_0^\tau a_k^I(t-\tau)a_i^I(t)dt \qquad (2.14)$$

$$\widehat{R}_{k,i}^{II}(\tau) = \int_\tau^T a_k^I(t-\tau)a_i^I(t)dt. \qquad (2.15)$$

Letting

$$I_{k,i}^{II}(\underline{b}_k^{II},\tau,\phi) = T^{-1}\Big[b_{k,-1}^I R_{k,1}^{II}(\tau_k)+b_{k,0}^I\widehat{R}_{k,1}^I(\tau_k)\Big]\cos(\phi), \qquad (2.16)$$

then Equation (2.13) can be written as

$$C_k = T\sqrt{P/2}\cos(\beta)I_{k,1}^{II}(\underline{b}_k^I,\tau_k,\phi_k). \qquad (2.17)$$

The total I-channel interference is then

$$\sum_{k=2}^K C_k = T\sqrt{P/2}\cos(\beta)\sum_{k=2}^K I_{k,1}^{II}(\underline{b}_k^I,\tau_k,\phi_k) \qquad (2.18)$$

where $\underline{b}^I = (b_{2,-1}^I, b_{2,0}^I, \cdots, b_{K,-1}^I, b_{K,0}^I)$. Similarly, the component of the I-channel cor-

[1]Note that the "hat" notation on the cross-correlation functions is used to denote the correlation over the complementary (with respect to the symbol duration) portion of the integration interval.

relator output due to a Q-channel interferer is

$$\begin{aligned}
D_k &= \int_0^T \sqrt{2P}\sin(\beta)a_k^Q(t-\tau_k)b_k^Q(t-\tau_k)\sin(2\pi f_c t+\phi_k)a_1^I(t)\cos(2\pi f_c t)dt \\
&= \sqrt{2P}\sin(\beta)\int_0^T b_k^Q(t-\tau_k)a_k^Q(t-\tau_k)a_1^I(t)\sin(2\pi f_c t+\phi_k)\cos(2\pi f_c t)dt \\
&= \sqrt{2P}\sin(\beta)\int_0^T b_k^Q(t-\tau_k)a_k^Q(t-\tau_k)a_1^I(t)\frac{1}{2}\Big[\sin(\phi_k)+\sin(4\pi f_c t+\phi_k)\Big]dt \\
&= \sqrt{P/2}\sin(\beta)\sin(\phi_k)\int_0^T b_k^Q(t-\tau_k)a_k^Q(t-\tau_k)a_1^I(t)dt \\
&= \sqrt{P/2}\sin(\beta)\sin(\phi_k)\Big[b_{k,-1}^Q R_{k,1}^{QI}(\tau_k)+b_{k,0}^Q\widehat{R}_{k,1}^{QI}(\tau_k)\Big] \qquad (2.19)
\end{aligned}$$

where, analogously to Equations (2.14) through (2.16), we define

$$R_{k,i}^{QI}(\tau) = \int_0^\tau a_k^Q(t-\tau)a_i^I(t)dt \qquad (2.20)$$

$$\widehat{R}_{k,i}^{QI}(\tau) = \int_\tau^T a_k^Q(t-\tau)a_i^I(t)dt \qquad (2.21)$$

and

$$I_{k,i}^{QI}(\underline{b}_k^Q,\tau,\phi) = T^{-1}\Big[b_{k,-1}^Q R_{k,1}^{QI}(\tau_k)+b_{k,0}^Q\widehat{R}_{k,1}^{QI}(\tau_k)\Big]\sin(\phi). \qquad (2.22)$$

Then Equation (2.19) can be written as

$$D_k = T\sqrt{P/2}\sin(\beta)I_{k,1}^{QI}(\underline{b}_k^Q,\tau_k,\phi_k) \qquad (2.23)$$

and hence the total Q-channel interference is

$$\sum_{k=2}^K D_k = T\sqrt{P/2}\sin(\beta)\sum_{k=2}^K I_{k,1}^{QI}(\underline{b}_k^Q,\tau_k,\phi_k) \qquad (2.24)$$

where $\underline{b}^Q = (b_{2,-1}^Q, b_{2,0}^Q, \cdots, b_{K,-1}^Q, b_{K,0}^Q)$. The noise component of the I-channel correlator output is

$$n_1^I = \int_0^T n(t)a_1^I(t)\cos(2\pi f_c t)dt. \qquad (2.25)$$

Note that n_1^I is Gaussian with zero mean and variance $N_0T/4$. In summary, we have

$$\begin{aligned} Z_1^I &= T\sqrt{\frac{P}{2}}\cos(\beta)b_{1,0}^I + \sum_{k=2}^{K} T\sqrt{\frac{P}{2}}\cos(\beta)I_{k,1}^{II}(\underline{b}_k^I,\tau_k,\phi_k) \\ &\quad + \sum_{k=2}^{K} T\sqrt{\frac{P}{2}}\sin(\beta)I_{k,1}^{QI}(\underline{b}_k^Q,\tau_k,\phi_k) + n_1^I \\ &= T\sqrt{\frac{P}{2}}\left\{ b_{1,0}^I\cos(\beta) + \cos(\beta)\sum_{k=2}^{K} I_{k,1}^{II}(\underline{b}_k^I,\tau_k,\phi_k) \right. \\ &\quad \left. + \sin(\beta)\sum_{k=2}^{K} I_{k,1}^{QI}(\underline{b}_k^Q,\tau_k,\phi_k) \right\} + n_1^I \\ &= T\sqrt{\frac{P}{2}}\cos(\beta)(b_{1,0}^I + I_I) \end{aligned} \tag{2.26}$$

where

$$I_I = \sum_{k=2}^{K} I_{k,1}^{II}(\underline{b}_k^I,\tau_k,\phi_k) + \tan(\beta)\cdot I_{k,1}^{QI}(\underline{b}_k^Q,\tau_k,\phi_k) \tag{2.27}$$

Similarly, for the Q-channel correlator output we have

$$\begin{aligned} Z_1^Q &= T\sqrt{\frac{P}{2}}\left\{ b_{1,0}^Q\sin(\beta) + \cos(\beta)\sum_{k=2}^{K} I_{k,1}^{IQ}(\underline{b}_k^I,\tau_k,\phi_k) \right. \\ &\quad \left. + \sin(\beta)\sum_{k=2}^{K} I_{k,1}^{QQ}(\underline{b}_k^Q,\tau_k,\phi_k) \right\} + n_1^Q \\ &= T\sqrt{\frac{P}{2}}\sin(\beta)(b_{1,0}^Q + I_Q) \end{aligned} \tag{2.28}$$

where

$$I_Q = \sum_{k=2}^{K} I_{k,1}^{QQ}(\underline{b}_k^I,\tau_k,\phi_k) + \cot(\beta)\cdot I_{k,1}^{IQ}(\underline{b}_k^Q,\tau_k,\phi_k) \tag{2.29}$$

$$I_{k,i}^{IQ}(\underline{b}_k^I,\tau,\phi) = T^{-1}\left[b_{k,-1}^I R_{k,1}^{IQ}(\tau_k) + b_{k,0}^I \widehat{R}_{k,1}^{IQ}(\tau_k) \right]\sin(-\phi) \tag{2.30}$$

$$I_{k,i}^{QQ}(\underline{b}_k^Q,\tau,\phi) = T^{-1}\left[b_{k,-1}^Q R_{k,1}^{QQ}(\tau_k) + b_{k,0}^Q \widehat{R}_{k,1}^{QQ}(\tau_k) \right]\cos(\phi) \tag{2.31}$$

and

$$R_{k,i}^{IQ}(\tau) = \int_0^{\tau} a_k^I(t-\tau)a_i^Q(t)dt, \tag{2.32}$$

$$\widehat{R}_{k,i}^{IQ}(\tau) = \int_{\tau}^{T} a_k^I(t-\tau)a_i^Q(t)dt, \tag{2.33}$$

$$R_{k,i}^{QQ}(\tau) = \int_0^{\tau} a_k^Q(t-\tau)a_i^Q(t)dt, \tag{2.34}$$

$$\widehat{R}_{k,i}^{QQ}(\tau) = \int_{\tau}^{T} a_k^Q(t-\tau)a_i^Q(t)dt. \tag{2.35}$$

Also, n_1^Q is Gaussian with zero mean and variance $N_0T/4$.

2.2.2 Synchronous System

For the synchronous case wherein $\tau_k = 0$ for all $k = 1, 2, \cdots, K$, the received signal is given by

$$r(t) = \sum_{k=1}^{K} s_k(t) + n(t). \tag{2.36}$$

With arguments similar to those in the asynchronous case, we have the correlation receiver outputs

$$Z_1^I = n_1^I + T\sqrt{P/2}\cdot\cos(\beta)\left[b_{1,0}^I + \sum_{k=2}^{K} I_{k,1}^I(\mathbf{b}_k, \theta_k)\right] \tag{2.37}$$

$$Z_1^Q = n_1^Q + T\sqrt{P/2}\cdot\sin(\beta)\left[b_{1,0}^Q + \sum_{k=2}^{K} I_{k,1}^Q(\mathbf{b}_k, \theta_k)\right] \tag{2.38}$$

where n_1^I and n_1^Q are Gaussian with zero mean and variance $N_0T/4$, $\mathbf{b}_k = (b_{k,0}^I, b_{k,0}^Q)$, and

$$I_{k,1}^I(\mathbf{b}_k, \theta_k) = I_{k,1}^{II}(b_{k,0}^I, \theta_k) + \tan(\beta)\cdot I_{k,1}^{QI}(b_{k,0}^Q, \theta_k) \tag{2.39}$$

$$I_{k,1}^Q(\mathbf{b}_k, \theta_k) = I_{k,1}^{IQ}(b_{k,0}^I, \theta_k) + \cot(\beta)\cdot I_{k,1}^{QQ}(b_{k,0}^Q, \theta_k) \tag{2.40}$$

with

$$I_{k,1}^{II}(b_{k,0}^{I},\theta_k) = T^{-1}\cdot b_{k,0}^{I}\cdot R_{k,1}^{II}(0)\cdot\cos(\theta_k), \tag{2.41}$$

$$I_{k,1}^{QI}(b_{k,0}^{Q},\theta_k) = T^{-1}\cdot b_{k,0}^{Q}\cdot R_{k,1}^{QI}(0)\cdot\sin(\theta_k), \tag{2.42}$$

$$I_{k,1}^{IQ}(b_{k,0}^{I},\theta_k) = T^{-1}\cdot b_{k,0}^{I}\cdot R_{k,1}^{IQ}(0)\cdot\sin(-\theta_k), \tag{2.43}$$

$$I_{k,1}^{QQ}(b_{k,0}^{Q},\theta_k) = T^{-1}\cdot b_{k,0}^{Q}\cdot R_{k,1}^{QQ}(0)\cdot\cos(\theta_k). \tag{2.44}$$

Since there is no delay between users, we have

$$R_{k,1}^{II}(0) = \int_0^T a_k^I(t)a_1^I(t)dt = \sum_{j=0}^{N-1} a_{k,j}^I a_{1,j}^I \int_0^{T_c}\psi^2(t)dt, \tag{2.45}$$

$$R_{k,1}^{QI}(0) = \int_0^T a_k^Q(t)a_1^I(t)dt = \sum_{j=0}^{N-1} a_{k,j}^Q a_{1,j}^I \int_0^{T_c}\psi^2(t)dt, \tag{2.46}$$

$$R_{k,1}^{IQ}(0) = \int_0^T a_k^I(t)a_1^Q(t)dt = \sum_{j=0}^{N-1} a_{k,j}^I a_{1,j}^Q \int_0^{T_c}\psi^2(t)dt, \tag{2.47}$$

$$R_{k,1}^{QQ}(0) = \int_0^T a_k^Q(t)a_1^Q(t)dt = \sum_{j=0}^{N-1} a_{k,j}^Q a_{1,j}^Q \int_0^{T_c}\psi^2(t)dt. \tag{2.48}$$

Furthermore, since we use a rectangular chip waveform, that is, $\psi(t) = p_{T_c}(t)$, then $\int_0^{T_c}\psi^2(t)dt = T_c$, and we can further simplify the above expressions as

$$R_{k,1}^{II}(0) = T_c\sum_{j=0}^{N-1} a_{k,j}^I a_{1,j}^I, \tag{2.49}$$

$$R_{k,1}^{QI}(0) = T_c\sum_{j=0}^{N-1} a_{k,j}^Q a_{1,j}^I, \tag{2.50}$$

$$R_{k,1}^{IQ}(0) = T_c\sum_{j=0}^{N-1} a_{k,j}^I a_{1,j}^Q, \tag{2.51}$$

$$R_{k,1}^{QQ}(0) = T_c\sum_{j=0}^{N-1} a_{k,j}^Q a_{1,j}^Q. \tag{2.52}$$

2.3 Exact Performance Analysis

Our goal is to analyze the bit-error rate (BER) of such a system. In order to find the exact BER, we need to find the probability distribution of the interference. In this section, we derive the pdf of the interference for both synchronous and asynchronous cases.

2.3.1 Average Probability of Error

The average probability of bit error is given by

$$P_e = \frac{1}{2}\left(P_e^I + P_e^Q\right) \tag{2.53}$$

where P_e^I and P_e^Q are the average probabilities of bit error of the I and Q channels, respectively, and are evaluated as follows:

$$\begin{aligned}
P_e^I &= \frac{1}{2}\left\{Pr\left(Z_1^I \le 0 | b_{1,0}^I = +1\right) + Pr\left(Z_1^I > 0 | b_{1,0}^I = -1\right)\right\} \\
&= \frac{1}{2}\left\{Pr\left(T\sqrt{P/2}\cos(\beta)(1+I_I) + n_1^I \le 0\right)\right. \\
&\quad \left. + Pr\left(T\sqrt{P/2}\cos(\beta)(-1+I_I) + n_1^I > 0\right)\right\} \\
&= \frac{1}{2}\left\{Pr\left(\frac{n_1^I}{T\sqrt{P/2}\cos(\beta)} \le -1 - I_I\right) + Pr\left(\frac{n_1^I}{T\sqrt{P/2}\cos(\beta)} > 1 - I_I\right)\right\} \\
&= \frac{1}{2}\left\{Pr\left(n_I + I_I \le -1\right) + Pr\left(n_I + I_I > 1\right)\right\} \\
&= \frac{1}{2}\left\{1 - Pr\left(-1 < n_I + I_I \le 1\right)\right\}
\end{aligned} \tag{2.54}$$

where $n_I = n_1^I/(T\sqrt{P/2}\cos\beta)$ is Gaussian with zero mean and variance $(2E_b^I/N_0)^{-1}$, $E_b^I = PT\cos^2\beta = E_s\cos^2\beta$, and $E_s = PT$. Similarly, we have

$$P_e^Q = \frac{1}{2}\Big\{1 - Pr\left(-1 < n_Q + I_Q \le 1\right)\Big\} \tag{2.55}$$

where $n_Q = n_1^Q/(T\sqrt{P/2}\sin\beta)$ is Gaussian with zero mean and variance $(2E_b^Q/N_0)^{-1}$, $E_b^Q = PT\sin^2\beta = E_s\sin^2\beta$.

In order to evaluate P_e^I and P_e^Q, we use the characteristic function method in [20] to compute these probabilities. In order to compute P_e, we need to know the probability distribution of the sum of the noise and interference. We first obtain the characteristic functions of the random variables, and then derive P_e^I and P_e^Q from the characteristic functions.

Let $\Phi_{n_I}(v)$, $\Phi_{I_I}(v)$, and $\Phi_I(v)$ be the characteristic functions of n_I, I_I, and $I = n_I + I_I$. Note that they are even functions ($\Phi(v) = \Phi(-v)$), and $\Phi_I(v) = \Phi_{n_I}(v)\Phi_{I_I}(v)$ by the independence of n_I and I_I. The probability needed to compute P_e^I is obtained as

$$\begin{aligned}
\Pr\left(-1 < n_I + I_I \le 1\right) &= \int_{-1}^{1} f_I(x)dx \\
&= 2\int_{0}^{1} f_I(x)dx \\
&= 2\int_{0}^{1}\left(\frac{1}{2\pi}\int_{-\infty}^{\infty}\Phi_I(v)e^{-jvx}dv\right)dx \\
&= \frac{2}{\pi}\int_{0}^{1}\left(\int_{0}^{\infty}\Phi_I(v)\cos(vx)dv\right)dx \\
&= \frac{2}{\pi}\int_{0}^{\infty}\Phi_I(v)\left(\int_{0}^{1}\cos(vx)dx\right)dv \\
&= \frac{2}{\pi}\int_{0}^{\infty}\Phi_I(v)v^{-1}\sin(v)dv. \qquad (2.56)
\end{aligned}$$

The characteristic function of the interference in the I-channel, $\Phi_I(v)$, can be written as

$$\Phi_I(v) = \Phi_{n_I}(v)\Phi_{I_I}(v) = \Phi_{n_I}(v) - \Phi_{n_I}(v) + \Phi_{n_I}(v)\Phi_{I_I}(v) = \Phi_{n_I}(v) - \Phi_{n_I}(v)\left[1 - \Phi_{I_I}(v)\right] \qquad (2.57)$$

thus

$$\begin{aligned}\Pr\left(-1 < n_I + I_I \leq 1\right) &= \frac{2}{\pi}\int_0^\infty \Phi_{n_I}(v)v^{-1}\sin(v)dv \\ &\quad -\frac{2}{\pi}\int_0^\infty v^{-1}\sin(v)\Phi_{n_I}(v)\big[1-\Phi_{I_I}(v)\big]dv \end{aligned} \tag{2.58}$$

where

$$\Phi_{n_I}(v) = \exp\left(-\frac{N_0}{4E_b^I}v^2\right). \tag{2.59}$$

The average probability of error of the I-channel is then given by

$$\begin{aligned} P_e^I &= \frac{1}{2} - \frac{1}{2}P\left(-1 < n_I + I_I \leq 1\right) \\ &= \frac{1}{2} - \frac{1}{\pi}\int_0^\infty v^{-1}\sin(v)\Phi_{n_I}(v)dv + \frac{1}{\pi}\int_0^\infty v^{-1}\sin(v)\Phi_{n_I}(v)\big[1-\Phi_{I_I}(v)\big]dv \\ &= Q\left(\sqrt{\frac{2E_b^I}{N_0}}\right) + \frac{1}{\pi}\int_0^\infty v^{-1}\sin(v)\Phi_{n_I}(v)[1-\Phi_{I_I}(v)]dv \end{aligned} \tag{2.60}$$

where

$$Q(x) = \frac{1}{\sqrt{2\pi}}\int_x^\infty e^{-t^2/2}dt,\ x \geq 0. \tag{2.61}$$

Similarly, let $\Phi_{n_Q}(v)$, $\Phi_{I_Q}(v)$, and $\Phi_Q(v)$ be the characteristic functions of n_Q, I_Q, and $Q = n_Q + I_Q$. $\Phi_Q(v) = \Phi_{n_Q}(v)\Phi_{I_Q}(v)$. Then we have

$$\begin{aligned}\Pr\left(-1 < n_Q + I_Q \leq 1\right) &= \frac{2}{\pi}\int_0^\infty v^{-1}\sin(v)\Phi_{n_Q}(v)dv \\ &\quad -\frac{2}{\pi}\int_0^\infty v^{-1}\sin(v)\Phi_{n_Q}(v)[1-\Phi_{I_Q}(v)]dv \end{aligned} \tag{2.62}$$

and

$$\begin{aligned} P_e^Q &= \frac{1}{2} - \frac{1}{\pi}\int_0^\infty v^{-1}\sin(v)\Phi_{n_Q}(v)dv + \frac{1}{\pi}\int_0^\infty v^{-1}\sin(v)\Phi_{n_Q}(v)[1-\Phi_{I_Q}(v)]dv \\ &= Q\left(\sqrt{\frac{2E_b^Q}{N_0}}\right) + \frac{1}{\pi}\int_0^\infty v^{-1}\sin(v)\Phi_{n_Q}(v)[1-\Phi_{I_Q}(v)]dv. \end{aligned} \tag{2.63}$$

Therefore, the average probability of error is given by

$$\begin{aligned} P_e &= \frac{1}{2}\Big\{Q\left(\sqrt{\frac{2E_b^I}{N_0}}\right) + Q\left(\sqrt{\frac{2E_b^Q}{N_0}}\right)\Big\} \\ &\quad + \frac{1}{2\pi}\int_0^\infty v^{-1}\sin(v)\Big\{\Phi_{n_I}(v)[1-\Phi_{I_I}(v)] + \Phi_{n_Q}(v)[1-\Phi_{I_Q}(v)]\Big\}dv. \quad (2.64) \end{aligned}$$

Note that by representing the error probability in this way it is clear what the contribution to error probability is from noise and interference. When there is no MAI, i.e., the single user case, the MAI term in the above expression is zero, and the probability of error is the same as in the case of an AWGN channel. In general, the MAI term in the above expression does not have a closed-form solution and needs to be evaluated numerically. However, in order to evaluate it numerically, we need to find expressions for $\Phi_{I_I}(v)$ and $\Phi_{I_Q}(v)$.

2.3.2 Asynchronous Case

Here we begin to derive the characteristic function of the interference in the asynchronous case. The I-channel interference is given by

$$I_I = \sum_{k=2}^{K} I_{k,1}^{II}(\underline{b}_k^I, \tau_k, \phi_k) + \tan(\beta) I_{k,1}^{QI}(\underline{b}_k^Q, \tau_k, \phi_k). \quad (2.65)$$

where

$$I_{k,1}^{II}(\underline{b}_k^I, \tau_k, \phi_k) = \frac{\cos(\phi_k)}{T}\Big[b_{k,-1}^I R_{k,1}^{II}(\tau_k) + b_{k,0}^I \widehat{R}_{k,1}^{II}(\tau_k)\Big], \quad (2.66)$$

$$I_{k,1}^{QI}(\underline{b}_k^Q, \tau_k, \phi_k) = \frac{\sin(\phi_k)}{T}\Big[b_{k,-1}^Q R_{k,1}^{QI}(\tau_k) + b_{k,0}^Q \widehat{R}_{k,1}^{QI}(\tau_k)\Big]. \quad (2.67)$$

Now consider $lT_c \le \tau_k \le (l+1)T_c$. In this case, we have

$$\begin{aligned} R_{k,1}^{II}(\tau_k) &= C_{k,1}^{II}(l-N)\widehat{R}_\psi(\tau_k - lT_c) + C_{k,1}^{II}(l+1-N)R_\psi(\tau_k - lT_c), \quad (2.68) \\ \widehat{R}_{k,1}^{II}(\tau_k) &= C_{k,1}^{II}(l)\widehat{R}_\psi(\tau_k - lT_c) + C_{k,1}^{II}(l+1)R_\psi(\tau_k - lT_c) \quad (2.69) \end{aligned}$$

where $\widehat{R}_\psi(\tau)$ and $R_\psi(\tau)$ are the autocorrelation functions of the chip waveform defined as

$$\widehat{R}_\psi(\tau) = \int_\tau^{T_c} \psi(t)\psi(t-\tau)dt, \tag{2.70}$$

$$R_\psi(\tau) = \int_0^{\tau} \psi(t)\psi(t+T_c-\tau)dt. \tag{2.71}$$

Similarly,

$$R_{k,1}^{QI}(\tau_k) = C_{k,1}^{QI}(l-N)\widehat{R}_\psi(\tau_k - lT_c) + C_{k,1}^{QI}(l+1-N)R_\psi(\tau_k - lT_c), \tag{2.72}$$

$$\widehat{R}_{k,1}^{QI}(\tau_k) = C_{k,1}^{QI}(l)\widehat{R}_\psi(\tau_k - lT_c) + C_{k,1}^{QI}(l+1)R_\psi(\tau_k - lT_c). \tag{2.73}$$

In the above expressions, $C_{k,i}^{II}(l)$ and $C_{k,i}^{QI}(l)$ are the aperiodic cross-correlation functions defined as

$$C_{k,i}^{II}(l) = \begin{cases} \sum_{j=0}^{N-1-l} a_{k,j}^I a_{i,j+l}^I, & 0 \le l \le N-1 \\ \sum_{j=0}^{N-1+l} a_{k,j-l}^I a_{i,j}^I, & 1-N \le l < 0 \\ 0, & |l| \ge N \end{cases} \tag{2.74}$$

$$C_{k,i}^{IQ}(l) = \begin{cases} \sum_{j=0}^{N-1-l} a_{k,j}^I a_{i,j+l}^Q, & 0 \le l \le N-1 \\ \sum_{j=0}^{N-1+l} a_{k,j-l}^I a_{i,j}^Q, & 1-N \le l < 0 \\ 0, & |l| \ge N \end{cases} \tag{2.75}$$

Here $\{a^I_{k,j}\}$ and $\{a^Q_{k,j}\}$ are the spreading sequences of the I and Q channels of the kth user. The characteristic function of I_I is given by

$$
\begin{aligned}
\Phi_{I_I}(v) &= E\left\{\exp(jvI_I)\right\} \\
&= E\left\{\exp\left[jv\left(\sum_{k=2}^{K} I^{II}_{k,1}(\underline{b}^I_k,\tau_k,\phi_k)+\tan(\beta)I^{QI}_{k,1}(\underline{b}^Q_k,\tau_k,\phi_k)\right)\right]\right\} \\
&= \prod_{k=2}^{K} E\left\{\exp\left[jv\left(I^{II}_{k,1}(\underline{b}^I_k,\tau_k,\phi_k)+\tan(\beta)I^{QI}_{k,1}(\underline{b}^Q_k,\tau_k,\phi_k)\right)\right]\right\} \\
&= \prod_{k=2}^{K}\left\{\frac{1}{2\pi}\frac{1}{T}\frac{1}{4}\frac{1}{4}\sum_{\underline{b}^I_k}\sum_{\underline{b}^Q_k}\right. \\
&\qquad \left.\int_0^{2\pi}\int_0^{T}\exp\left[jv\left(I^{II}_{k,1}(\underline{b}^I_k,\tau,\phi)+\tan(\beta)I^{QI}_{k,1}(\underline{b}^Q_k,\tau,\phi)\right)\right]d\tau d\phi\right\} \\
&= \prod_{k=2}^{K}\left\{\frac{1}{32\pi T}\sum_{\underline{b}^I_k}\sum_{\underline{b}^Q_k}\int_0^{2\pi}\sum_{l=0}^{N-1}\int_{lT_c}^{(l+1)T_c}\right. \\
&\qquad \exp\left[jv\frac{\cos(\phi)}{T}\left[b^I_{k,-1}\left(C^{II}_{k,1}(l-N)\widehat{R}_\psi(\tau-lT_c)\right.\right.\right. \\
&\qquad + C^{II}_{k,-1}(l+1-N)R_\psi(\tau-lT_c)\big) \\
&\qquad + b^I_{k,0}\left(C^{II}_{k,1}(l)\widehat{R}_\psi(\tau-lT_c)+C^{II}_{k,1}(l+1)R_\psi(\tau-lT_c)\right)\Big] \\
&\qquad + jv\tan(\beta)\frac{\sin(\phi)}{T}\left[b^Q_{k,-1}\left(C^{QI}_{k,1}(l-N)\widehat{R}_\psi(\tau-lT_c)\right.\right. \\
&\qquad \left.+C^{QI}_{k,-1}(l+1-N)R_\psi(\tau-lT_c)\right) \\
&\qquad \left.\left.\left.+\ b^Q_{k,0}\left(C^{QI}_{k,1}(l)\widehat{R}_\psi(\tau-lT_c)+C^{QI}_{k,1}(l+1)R_\psi(\tau-lT_c)\right)\right]\right]d\tau d\phi\right\} \qquad (2.76)
\end{aligned}
$$

With further simplification (see Appendix A), we obtain

$$\Phi_{I_I}(v)=\prod_{k=2}^{K}\left\{\frac{1}{8N}\sum_{l=0}^{N-1}\left(\sum_{i=1}^{8} f(v;l,g_i(l),h_i(l),\alpha_i)\right)\right\} \qquad (2.77)$$

where

$$f(v;l,g(l),h(l),\alpha) \triangleq \frac{1}{2\pi T_c}\int_0^{2\pi}\int_0^{T_c}\cos\Big\{\frac{v}{T}\Big[(\cos\phi\cdot g(l)+\alpha\sin\phi\cdot h(l))\,\widehat{R}_\psi(\tau) + (\cos\phi\cdot g(l+1)+\alpha\sin\phi\cdot h(l+1))\,R_\psi(\tau)\Big]\Big\}d\tau d\phi \quad (2.78)$$

and

$$g_1(l)=\theta_{k,1}^{II},\ h_1(l)=\theta_{k,1}^{QI},\ \alpha_1=+\tan\beta, \quad (2.79)$$

$$g_2(l)=\theta_{k,1}^{II},\ h_2(l)=\widehat{\theta}_{k,1}^{QI},\ \alpha_2=-\tan\beta, \quad (2.80)$$

$$g_3(l)=\theta_{k,1}^{II},\ h_3(l)=\widehat{\theta}_{k,1}^{QI},\ \alpha_3=+\tan\beta, \quad (2.81)$$

$$g_4(l)=\theta_{k,1}^{II},\ h_4(l)=\theta_{k,1}^{QI},\ \alpha_4=-\tan\beta, \quad (2.82)$$

$$g_5(l)=\widehat{\theta}_{k,1}^{II},\ h_5(l)=\theta_{k,1}^{QI},\ \alpha_5=-\tan\beta, \quad (2.83)$$

$$g_6(l)=\widehat{\theta}_{k,1}^{II},\ h_6(l)=\widehat{\theta}_{k,1}^{QI},\ \alpha_6=+\tan\beta, \quad (2.84)$$

$$g_7(l)=\widehat{\theta}_{k,1}^{II},\ h_7(l)=\widehat{\theta}_{k,1}^{QI},\ \alpha_7=-\tan\beta, \quad (2.85)$$

$$g_8(l)=\widehat{\theta}_{k,1}^{II},\ h_8(l)=\theta_{k,1}^{QI},\ \alpha_8=+\tan\beta. \quad (2.86)$$

If we consider a rectangular chip waveform, we can further simplify equation (2.78) as (see Appendix A)

$$\begin{aligned} f(v;l,g(l),h(l),\alpha) &= \frac{1}{2\pi}\int_0^{2\pi}\operatorname{sinc}\Big\{\frac{v}{2\pi N}\Big(\cos\phi((g(l+1)-g(l)) \\ &\quad +\alpha\sin\phi((h(l+1)-h(l))\Big)\Big\} \\ &\quad \cdot\cos\Big\{\frac{v}{2N}\Big(\cos\phi((g(l+1)+g(l)) \\ &\quad +\alpha\sin\phi((h(l+1)+h(l))\Big)\Big\}d\phi. \end{aligned} \quad (2.87)$$

This expression is simple to evaluate numerically, which allows us to compute the characteristic function and the average error probability. From the above expression, we see that the characteristic function of the interference does not depend on the signal

energy or SNR. The advantage is that we need to compute the characteristic function of the interference only once, and it can be applied to different SNR values to compute the probability of error.

2.3.3 Synchronous Case

For the synchronous case, the derivation is similar to the asynchronous case. The expressions for the bit-error probability for the I and Q channels are the same as for the asynchronous case. The only difference is in the expressions for the characteristic functions of the interference. These are given by

$$\begin{aligned}\Phi_{I_I}(v) &= \prod_{k=2}^{K}\left\{\frac{1}{4\pi}\int_0^{2\pi}\cos\left(\frac{v}{T}[\cos\phi\cdot R_{k,1}^{II}(0)+\tan\beta\cdot\sin\phi\cdot R_{k,1}^{QI}(0)]\right)\right. \\ &\quad \left.+\cos\left(\frac{v}{T}[\cos\phi\cdot R_{k,1}^{II}(0)-\tan\beta\cdot\sin\phi\cdot R_{k,1}^{QI}(0)]\right)d\phi\right\}, \qquad (2.88)\\ \Phi_{I_Q}(v) &= \prod_{k=2}^{K}\left\{\frac{1}{4\pi}\int_0^{2\pi}\cos\left(\frac{v}{T}[\cos\phi\cdot R_{k,1}^{QQ}(0)+\cot\beta\cdot\sin\phi\cdot R_{k,1}^{IQ}(0)]\right)\right. \\ &\quad \left.+\cos\left(\frac{v}{T}[\cos\phi\cdot R_{k,1}^{QQ}(0)-\cot\beta\cdot\sin\phi\cdot R_{k,1}^{IQ}(0)]\right)d\phi\right\}. \qquad (2.89)\end{aligned}$$

2.3.4 Numerical Examples

Here we present a numerical example for the asynchronous case. In [20], the average error probability for a direct-sequence spread-spectrum multiple-access (DS-SSMA) system with symmetric QPSK modulation is investigated. The performance is evaluated using auto-optimal, least side-lobe energy (AO/LSE) sequences [21] as the spreading codes for the users in the system. For the quaternary system, the spreading factor is chosen to be $N = 127$, and there are 9 pairs of codes listed. In each pair of codes, the I- and Q-channel sequences are the reverse of each other. The AO/LSE codes for $N = 127$ are listed in Table 2.1.

Each row represents a pair of codes. The generator polynomial coefficients are

Table 2.1: AO/LSE codes ($N = 127$).

H	$\underline{\alpha}_0$	H^{-1}	$\underline{\alpha}_0^{-1}$	$\widehat{M}$	$\widehat{L}$	S
211	0010000	221	1001101	17	6	2183
217	0000101	361	1111111	15	12	2015
235	0001100	271	1000101	17	10	2283
247	0010111	345	0110001	17	8	2255
277	1110001	375	0101010	19	4	2295
357	1110010	367	0110101	17	4	2563
323	1110111	313	1000111	17	4	2203
203	1101101	301	0010010	17	4	2087
325	0000101	253	1101100	19	6	2483

denoted by H and H^{-1} in octal. The initial values in the shift registers are denoted by $\underline{\alpha}_0$ and $\underline{\alpha}_0^{-1}$. The in-phase interference characteristic function from the second user to the first user using the above spreading codes with $\beta = \pi/4$ is shown in Figure 2.4. Since in the symmetric constellation the I- and Q-channel signals have the same power, the resulting characteristic functions of the I- and Q-channel interference are the same. Therefore, we show only the characteristic function of the I channel. For $\beta = \pi/8$, even though we use mutually reversed spreading codes for in-phase and quadrature-phase components, the characteristic functions are different. This is due to the unequal power of the I- and Q-channel signals in the asymmetric constellation and the cross-correlation nature of the spreading codes. The characteristic functions of the interference from the second user to the first user when $\beta = \pi/8$ are shown in Figure 2.5. The average probability of error when the number of users varies from 1 to 9 is shown in Figure 2.6. The performance is worse than the symmetric case as shown in [20]. This is because the performance is dominated by the Q-channel performance, which is bad due to the low transmitted power.

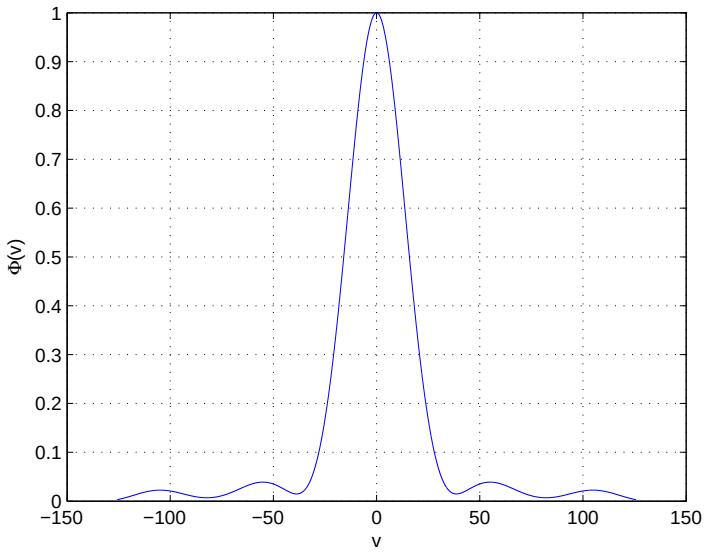

Figure 2.4: In-phase interference characteristic function ($N = 127$, $\beta = \pi/4$).

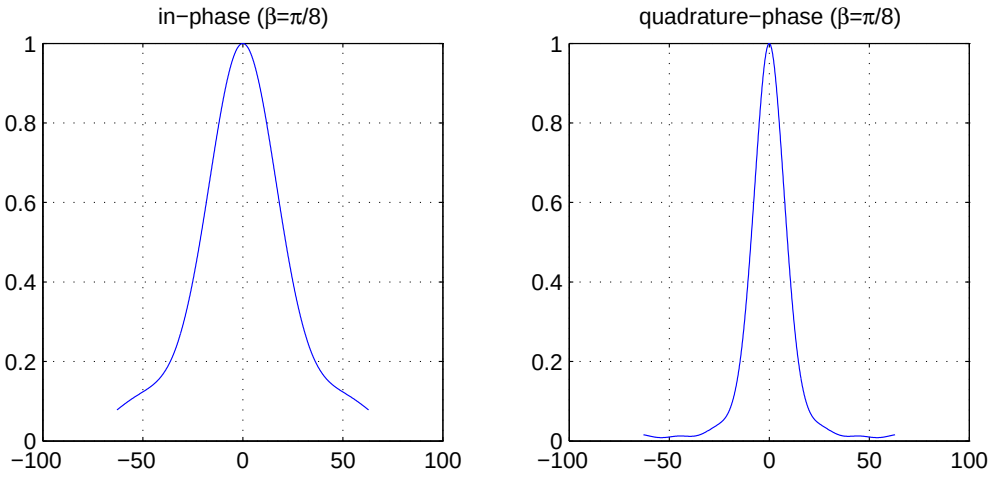

Figure 2.5: Interference characteristic functions ($N = 127$, $\beta = \pi/8$).

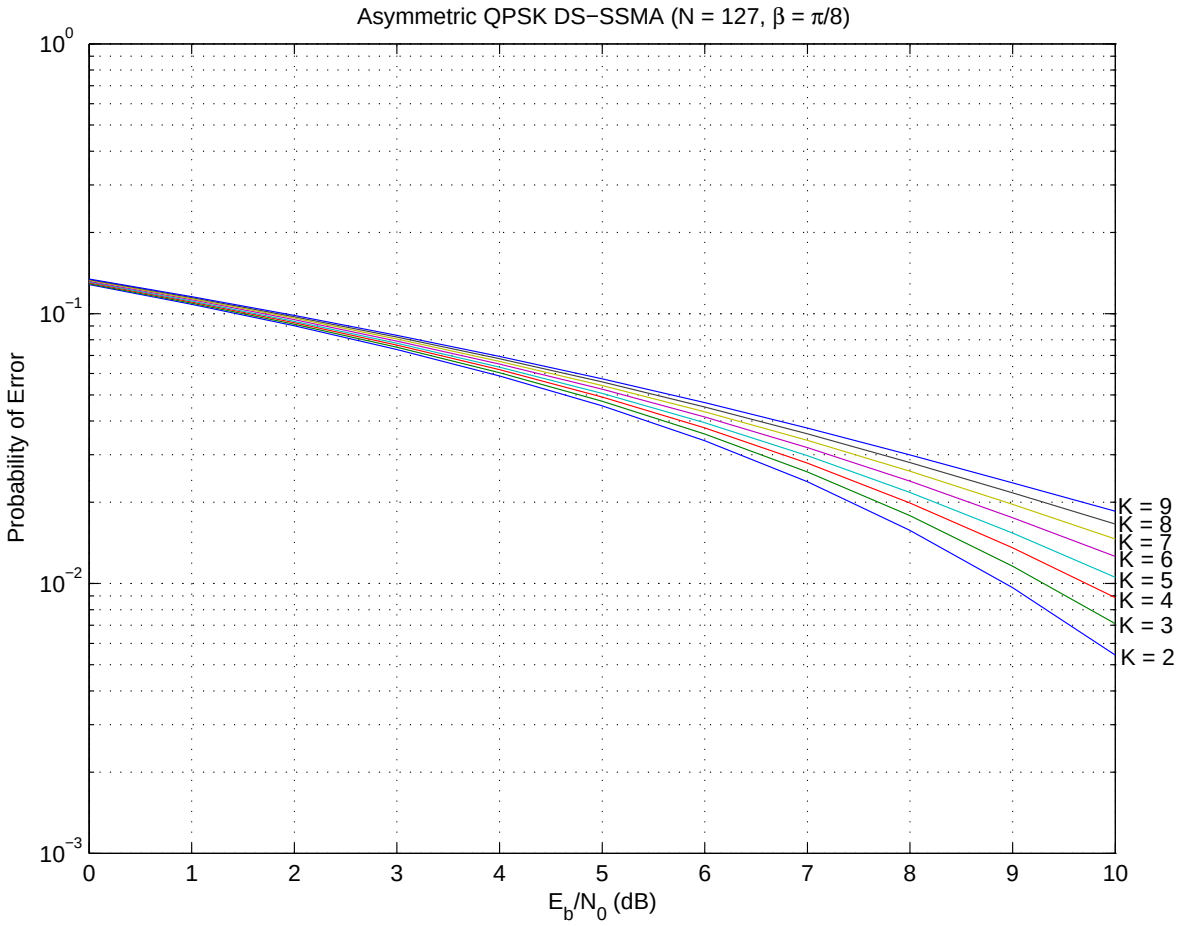

Figure 2.6: Probability of error for asymmetric QPSK DS-SSMA ($N = 127$, $\beta = \pi/8$) for $K = 2$ to 9 users.

2.4 Approximate Performance Analysis

As seen in the previous section, the expressions for the interference are very complicated, and the evaluation for the exact performance is computationally tedious. Also, as in the numerical example, the results are for a specific set of signature sequences. One way to solve this problem is to use a Gaussian approximation to model the interference and to use random signature sequences in the analysis. Then a simple approximate expression for the BER can be obtained involving only the signal-to-interference-plus-noise ratio (SINR) and the Q function. In this section, we approximate the interference as a Gaussian random variable and assume random signature sequences. We find the variance of the interference and examine the approximate system performance.

2.4.1 Asynchronous Case

In order to find the approximate BER performance, we approximate the interference as a Gaussian random variable and find its variance. We first find the conditional variance of the interference, and then average over the random variables to find the variance. Therefore, we can obtain an expression for the SINR, and thus the approximate BER.

The decision statistics at the output of the correlation receiver for user 1 are

$$Z_1^I = n_1^I + T\sqrt{\frac{P}{2}} \cdot \cos\beta \cdot b_{1,0}^I + \sqrt{\frac{P}{2}} \sum_{k=2}^{K} \cos\beta \cdot W_k^{II} \cdot \cos(\phi_k) + \sin\beta \cdot W_k^{QI} \cdot \sin(\phi_k) \tag{2.90}$$

$$Z_1^Q = n_1^Q + T\sqrt{\frac{P}{2}} \cdot \cos\beta \cdot b_{1,0}^Q + \sqrt{\frac{P}{2}} \sum_{k=2}^{K} \sin\beta \cdot W_k^{QQ} \cdot \cos(\phi_k) - \cos\beta \cdot W_k^{IQ} \cdot \sin(\phi_k) \tag{2.91}$$

where

$$W_k^{II} = b_{k,-1}^I \cdot R_{k,1}^{II}(\tau_k) + b_{k,0}^I \cdot \widehat{R}_{k,1}^{II}(\tau_k), \tag{2.92}$$

$$W_k^{QI} = b_{k,-1}^Q \cdot R_{k,1}^{QI}(\tau_k) + b_{k,0}^Q \cdot \widehat{R}_{k,1}^{QI}(\tau_k), \tag{2.93}$$

$$W_k^{QQ} = b_{k,-1}^Q \cdot R_{k,1}^{QQ}(\tau_k) + b_{k,0}^Q \cdot \widehat{R}_{k,1}^{QQ}(\tau_k), \tag{2.94}$$

$$W_k^{IQ} = b_{k,-1}^I \cdot R_{k,1}^{IQ}(\tau_k) + b_{k,0}^I \cdot \widehat{R}_{k,1}^{IQ}(\tau_k). \tag{2.95}$$

To find the variance of the multiple access interference (MAI) of Z_1^I and Z_1^Q, we start by writing Z_1^I in the form

$$Z_1^I = n_1^I + T\sqrt{P/2} \cdot b_{1,0}^I \cdot \cos\beta + W \tag{2.96}$$

where

$$W = \sqrt{P/2} \cdot \cos\beta \sum_{k=2}^{K} W_k^{II} \cdot \cos(\phi_k) + \sqrt{P/2} \cdot \sin\beta \sum_{k=2}^{K} W_k^{QI} \cdot \sin(\phi_k) = W^I + W^Q \tag{2.97}$$

with

$$W^I = \sqrt{P/2} \cdot \cos\beta \sum_{k=2}^{K} W_k^{II} \cdot \cos(\phi_k), \tag{2.98}$$

$$W^Q = \sqrt{P/2} \cdot \sin\beta \sum_{k=2}^{K} W_k^{QI} \cdot \sin(\phi_k). \tag{2.99}$$

The variances of W^I and W^Q are given by (see Appendix B)

$$\mathrm{Var}[W^I] = \frac{(K-1)NPT_c^2\cos^2(\beta)}{6} \tag{2.100}$$

$$\mathrm{Var}[W^Q] = \frac{(K-1)NPT_c^2\sin^2(\beta)}{6}. \tag{2.101}$$

Hence the variance of the MAI in Z_1^I is given by

$$\mathrm{Var}[W] = \mathrm{Var}[W^I] + \mathrm{Var}[W^Q] = \frac{(K-1)NPT_c^2}{6}. \tag{2.102}$$

The SINR of Z_1^I is then

$$\begin{aligned} \mathrm{SINR}_I &= \frac{T^2P/2 \cdot \cos^2\beta}{\frac{N_0T}{4} + \frac{(K-1)NPT_c^2}{6}} \\ &= \frac{6E_s \cdot \cos^2\beta}{3N_0 + 2E_s\frac{(K-1)}{N}} \\ &= \frac{12E_b \cdot \cos^2\beta}{3N_0 + 4E_b\frac{(K-1)}{N}} \end{aligned} \tag{2.103}$$

where $E_s = NPT_c$ is the symbol energy, and $E_b = (1/2)E_s$ is the average bit energy. Similarly, for the Q-channel, the SINR of Z_1^Q is given by

$$\mathrm{SINR}_Q = \frac{6E_s \cdot \sin^2\beta}{3N_0 + 2E_s\frac{(K-1)}{N}} = \frac{12E_b \cdot \sin^2\beta}{3N_0 + 4E_b\frac{(K-1)}{N}}. \tag{2.104}$$

Then the approximate BER can be expressed as

$$P_{e,GA}^I = Q\left(\sqrt{\frac{12E_b \cdot \cos^2\beta}{3N_0 + 4\overline{E}_b\frac{(K-1)}{N}}}\right), \tag{2.105}$$

$$P_{e,GA}^Q = Q\left(\sqrt{\frac{12E_b \cdot \sin^2\beta}{3N_0 + 4\overline{E}_b\frac{(K-1)}{N}}}\right). \tag{2.106}$$

2.4.2 Synchronous Case

The analysis for the synchronous case is similar to that for the asynchronous case presented in the previous subsection. We can rewrite the decision statistic as

$$Z_1^I = n_1^I + T\sqrt{P/2} \cdot \cos(\beta) \cdot b_{1,0}^I + W \tag{2.107}$$

where

$$W = \sum_{k=2}^{K} W_k^I \tag{2.108}$$

and

$$W_k^I = \sqrt{P/2}\left(\cos\beta \cdot b_{k,0}^I \cdot R_{k,1}^{II}(0) \cdot \cos(\theta_k) + \sin\beta \cdot b_{k,0}^Q \cdot R_{k,1}^{QI}(0) \cdot \sin(\theta_k)\right) \tag{2.109}$$

We want to find the variance of the MAI W_k^I. Note that $R_{k,1}^{II}(0)$ and $R_{k,1}^{QI}(0)$ are both functions of $\{a_{1,j}^I\}$. Thus the variance of W_k^I conditioned on $\{a_{1,j}^I\}$ and θ_k is

$$\begin{aligned}
\mathrm{Var}\left[W_k^I \mid \{a_{1,j}^I\}, \theta_k\right] &= \mathrm{Var}\left[\sqrt{P/2} \cdot \cos\beta \cdot b_{k,0}^I \cdot R_{k,1}^{II}(0) \cdot \cos\theta_k \mid \{a_{1,j}^I\}, \theta_k\right] \\
&\quad + \mathrm{Var}\left[\sqrt{P/2} \cdot \sin\beta \cdot b_{k,0}^Q \cdot R_{k,1}^{QI}(0) \cdot \sin\theta_k \mid \{a_{1,j}^I\}, \theta_k\right] \\
&= \frac{P}{2}\left(\cos^2\beta \cdot \cos^2\theta_k \cdot \mathrm{Var}[b_{k,0}^I \cdot R_{k,1}^{II}(0) \mid \{a_{1,j}^I\}]\right. \\
&\quad \left. + \sin^2\beta \cdot \sin^2\theta_k \cdot \mathrm{Var}[b_{k,0}^Q \cdot R_{k,1}^{QI}(0) \mid \{a_{1,j}^I\}]\right).
\end{aligned} \tag{2.110}$$

Because we assume random signature sequences, given $\{a_{1,j}^I\}$, $R_{k,1}^{II}(0)$ and $R_{k,1}^{QI}(0)$ are independent identically distributed (i.i.d.) with PDF

$$p_R(rT_c) = \binom{N}{\frac{r+N}{2}} 2^{-N} \tag{2.111}$$

for $r = -N, -N+2, \cdots, N-2, N$. Since both $b_{k,0}^I$ and $R_{k,1}^{II}$ have zero mean and they are independent, we have

$$\begin{aligned}
\mathrm{Var}\left[b_{k,0}^I \cdot R_{k,1}^{II}(0) \mid \{a_{1,j}^I\}\right] &= E\left[\left(b_{k,0}^I \cdot R_{k,1}^{II}(0)\right)^2 \mid \{a_{1,j}^I\}\right] \\
&= E\left[\left(b_{k,0}^I\right)^2\right] E\left[\left(R_{k,1}^{II}(0)\right)^2 \mid \{a_{1,j}^I\}\right] \\
&= 1 \cdot NT_c^2 \\
&= NT_c^2
\end{aligned} \tag{2.112}$$

Note that even though $R_{k,1}^{II}(0)$ depends on $\{a_{1,j}^I\}$, the mean and variance do not depend on the particular realization of $\{a_{1,j}^I\}$. This is different from the asynchronous case. However, this property helps reduce the complexity of analysis. Similarly, we have $\text{Var}\left[b_{k,0}^Q \cdot R_{k,1}^{QI}(0)|\{a_{1,j}^I\}\right] = NT_c^2$. Therefore the conditional variance of W_k^I is

$$\text{Var}\left[W_k^I \mid \theta_k, \{a_{1,j}^I\}\right] = \frac{NPT_c^2}{2}\left(\cos^2\beta \cdot \cos^2\theta_k + \sin^2\beta \cdot \sin^2\theta_k\right) \tag{2.113}$$

Let $\mathbf{\Theta} = (\theta_1, \cdots, \theta_K)$. Then the conditional variance of W is given by

$$\begin{aligned}\text{Var}\left[W \mid \mathbf{\Theta}, \{a_{1,j}^I\}\right] &= \sum_{k=2}^{K} \text{Var}\left[W_k^I \mid \theta_k, \{a_{1,j}^I\}\right] \\ &= (K-1)\frac{NPT_c^2}{2}\left(\cos^2\beta \cdot \cos^2\theta_k + \sin^2\beta \cdot \sin^2\theta_k\right) \end{aligned} \tag{2.114}$$

Note that the above expression now depends only on θ_k. By averaging over θ_k, the variance of W is

$$\begin{aligned}\text{Var}\left[W\right] &= \sum_{k=2}^{K} E_{\theta_k}\left[\text{Var}\left[W_k^I \mid \theta_k\right]\right] \\ &= (K-1)E_{\theta_k}\left[\frac{NPT_c^2}{2}\left(\cos^2\beta \cdot \cos^2\theta_k + \sin^2\beta \cdot \sin^2\theta_k\right)\right] \\ &= \frac{(K-1)NPT_c^2}{2}\left(\cos^2\beta \cdot E_{\theta_k}[\cos^2\theta_k] + \sin^2\beta \cdot E_{\theta_k}[\sin^2\theta_k]\right) \\ &= \frac{(K-1)NPT_c^2}{2}\left(\cos^2\beta \cdot \frac{1}{2} + \sin^2\beta \cdot \frac{1}{2}\right) \\ &= \frac{(K-1)NPT_c^2}{4}. \end{aligned} \tag{2.115}$$

Therefore, the SINR is

$$\begin{aligned}
\mathrm{SINR}_I &= \frac{T^2 P/2 \cdot \cos^2\beta}{N_0 T/4 + (K-1)NPT_c^2/4} \\
&= \frac{2NT_c E_s \cos^2\beta}{N_0 N T_c + (K-1)T_c E_s} \\
&= \frac{2E_s \cos^2\beta}{N_0 + \frac{(K-1)}{N} E_s} \qquad (2.116) \\
&= \frac{4E_b \cos^2\beta}{N_0 + \frac{2(K-1)}{N} E_b} \qquad (2.117)
\end{aligned}$$

By approximating the MAI as Gaussian with variance $(K-1)NP/4$, the approximate I-channel average probability of bit error is

$$P_{e,GA}^I = Q\left(\sqrt{\mathrm{SINR}_I}\right) = Q\left(\sqrt{\frac{4E_b \cos^2\beta}{N_0 + \frac{2(K-1)}{N} E_b}}\right). \qquad (2.118)$$

Similarly, it can be shown that, for the Q channel, the approximate average probability of bit error is

$$P_{e,GA}^Q = Q\left(\sqrt{\frac{4E_b \sin^2\beta}{N_0 + \frac{2(K-1)}{N} E_b}}\right). \qquad (2.119)$$

2.5 A Generalized Model and the Near-Far Problem

In this section, we consider a general model for the AQPSK DS-CDMA system. The main difference from the model in the previous sections is that the users can have different transmission power. This causes what is referred to as "the near-far problem". We are interested in the near-far effect on system performance.

2.5.1 Analysis

In the general model, the in-phase and quadrature components are given by

$$s_k^I(t) = A_k \cos(\beta) a_k^I(t) b_k^I(t) \cos(2\pi f_c t + \theta_k) \tag{2.120}$$

$$s_k^Q(t) = A_k \sin(\beta) a_k^Q(t) b_k^Q(t) \sin(2\pi f_c t + \theta_k) \tag{2.121}$$

where A_1, A_2, $\cdots$, A_K can be different. Without loss of generality, let user 1 be the desired user. The correlation receiver output of the in-phase and quadrature phase channels are

$$\begin{aligned} Z_1^I = \frac{1}{2} A_1 T \Bigg\{ & b_{1,0}^I \cos(\beta) + \cos(\beta) \sum_{k=2}^{K} \frac{A_k}{A_1} I_{k,1}^I(\underline{b}_k^I, \tau_k, \phi_k) \\ & + \sin(\beta) \sum_{k=2}^{K} \frac{A_k}{A_1} I_{k,1}^{QI}(\underline{b}_k^Q, \tau_k, \phi_k) \Bigg\} + n_1^I, \end{aligned} \tag{2.122}$$

$$\begin{aligned} Z_1^Q = \frac{1}{2} A_1 T \Bigg\{ & b_{1,0}^Q \sin(\beta) + \cos(\beta) \sum_{k=2}^{K} \frac{A_k}{A_1} I_{k,1}^{IQ}(\underline{b}_k^I, \tau_k, \phi_k) \\ & + \sin(\beta) \sum_{k=2}^{K} \frac{A_k}{A_1} I_{k,1}^{Q}(\underline{b}_k^Q, \tau_k, \phi_k) \Bigg\} + n_1^Q. \end{aligned} \tag{2.123}$$

The average probability of error is given by

$$P_e = \frac{1}{2} \left(P_e^I + P_e^Q \right) \tag{2.124}$$

with

$$P_e^I = \frac{1}{2} \left\{ 1 - P \left(-1 < \frac{2n_1^I}{A_1 T \cos\beta} + I_1^I \leq 1 \right) \right\} \tag{2.125}$$

$$P_e^Q = \frac{1}{2} \left\{ 1 - P \left(-1 < \frac{2n_1^Q}{A_1 T \sin\beta} + I_1^Q \leq 1 \right) \right\} \tag{2.126}$$

where

$$I_1^I = \sum_{k=2}^{K} \frac{A_k}{A_1} \left[I_{k,1}^{II}(\underline{b}_k^I, \tau_k, \phi_k) + \tan\beta I_{k,1}^{QI}(\underline{b}_k^Q, \tau_k, \phi_k) \right] \tag{2.127}$$

$$I_1^Q = \sum_{k=2}^{K} \frac{A_k}{A_1} \left[I_{k,1}^{QQ}(\underline{b}_k^Q, \tau_k, \phi_k) + \cot\beta I_{k,1}^{IQ}(\underline{b}_k^I, \tau_k, \phi_k) \right]. \tag{2.128}$$

The characteristic function of I_1^I is

$$\Phi_{I_1^I}(v) = \prod_{k=2}^{K} \Phi_{I_{k,1}^I}(v) \tag{2.129}$$

where

$$\Phi_{I_{k,1}^I}(v) = \frac{1}{8N} \sum_{l=0}^{N-1} \sum_{i=1}^{8} f\left(v; l, g_{k,i}^I(l), h_{k,i}^I(l), \alpha_i^I, \frac{A_k}{A_1} \right) \tag{2.130}$$

and

$$\begin{aligned} f(v; l, g(l), h(l), \alpha, \gamma) = \frac{1}{2\pi} \int_0^{2\pi} & \operatorname{sinc}\left\{ \gamma \frac{v}{2\pi N} \left(\cos\phi(g(l+1) - g(l)) \right.\right. \\ & \left.\left. + \alpha \sin\phi(h(l+1) - h(l)) \right)\right\} \\ & \cdot \cos\left\{ \gamma \frac{v}{2N} \left(\cos\phi(g(l+1) + g(l)) \right.\right. \\ & \left.\left. + \alpha \sin\phi(h(l+1) + h(l)) \right)\right\} d\phi \end{aligned} \tag{2.131}$$

with

$$g^I_{k,1}(l) = \theta^{II}_{k,1},\ h^I_{k,1}(l) = \theta^{QI}_{k,1},\ \alpha^I_1 = +\tan\beta, \tag{2.132}$$

$$g^I_{k,2}(l) = \theta^{II}_{k,1},\ h^I_{k,2}(l) = \widehat{\theta}^{QI}_{k,1},\ \alpha^I_2 = -\tan\beta, \tag{2.133}$$

$$g^I_{k,3}(l) = \theta^{II}_{k,1},\ h^I_{k,3}(l) = \widehat{\theta}^{QI}_{k,1},\ \alpha^I_3 = +\tan\beta, \tag{2.134}$$

$$g^I_{k,4}(l) = \theta^{II}_{k,1},\ h^I_{k,4}(l) = \theta^{QI}_{k,1},\ \alpha^I_4 = -\tan\beta, \tag{2.135}$$

$$g^I_{k,5}(l) = \widehat{\theta}^{II}_{k,1},\ h^I_{k,5}(l) = \theta^{QI}_{k,1},\ \alpha^I_5 = -\tan\beta, \tag{2.136}$$

$$g^I_{k,6}(l) = \widehat{\theta}^{II}_{k,1},\ h^I_{k,6}(l) = \widehat{\theta}^{QI}_{k,1},\ \alpha^I_6 = +\tan\beta, \tag{2.137}$$

$$g^I_{k,7}(l) = \widehat{\theta}^{II}_{k,1},\ h^I_{k,7}(l) = \widehat{\theta}^{QI}_{k,1},\ \alpha^I_7 = -\tan\beta, \tag{2.138}$$

$$g^I_{k,8}(l) = \widehat{\theta}^{II}_{k,1},\ h^I_{k,8}(l) = \theta^{QI}_{k,1},\ \alpha^I_8 = +\tan\beta. \tag{2.139}$$

Similarly, we have

$$\Phi_{I^Q_1}(v) = \prod_{k=2}^{K} \Phi_{I^Q_{k,1}}(v) \tag{2.140}$$

where

$$\Phi_{I^Q_{k,1}}(v) = \frac{1}{8N} \sum_{l=0}^{N-1} \sum_{i=1}^{8} f\left(v; l, g^Q_{k,i}(l), h^Q_{k,i}(l), \alpha^Q_i, \frac{A_k}{A_1}\right) \tag{2.141}$$

and

$$g^Q_{k,1}(l) = \theta^{QQ}_{k,1},\ h^Q_{k,1}(l) = \theta^{IQ}_{k,1},\ \alpha^Q_1 = -\cot\beta, \tag{2.142}$$

$$g^Q_{k,2}(l) = \theta^{QQ}_{k,1},\ h^Q_{k,2}(l) = \widehat{\theta}^{IQ}_{k,1},\ \alpha^Q_2 = +\cot\beta, \tag{2.143}$$

$$g^Q_{k,3}(l) = \theta^{QQ}_{k,1},\ h^Q_{k,3}(l) = \widehat{\theta}^{IQ}_{k,1},\ \alpha^Q_3 = -\cot\beta, \tag{2.144}$$

$$g^Q_{k,4}(l) = \theta^{QQ}_{k,1},\ h^Q_{k,4}(l) = \theta^{IQ}_{k,1},\ \alpha^Q_4 = +\cot\beta, \tag{2.145}$$

$$g^Q_{k,5}(l) = \widehat{\theta}^{QQ}_{k,1},\ h^Q_{k,5}(l) = \theta^{IQ}_{k,1},\ \alpha^Q_5 = +\cot\beta, \tag{2.146}$$

$$g^Q_{k,6}(l) = \widehat{\theta}^{QQ}_{k,1},\ h^Q_{k,6}(l) = \widehat{\theta}^{IQ}_{k,1},\ \alpha^Q_6 = -\cot\beta, \tag{2.147}$$

$$g^Q_{k,7}(l) = \widehat{\theta}^{QQ}_{k,1},\ h^Q_{k,7}(l) = \widehat{\theta}^{IQ}_{k,1},\ \alpha^Q_7 = +\cot\beta, \tag{2.148}$$

$$g^Q_{k,8}(l) = \widehat{\theta}^{QQ}_{k,1},\ h^Q_{k,8}(l) = \theta^{IQ}_{k,1},\ \alpha^Q_8 = -\cot\beta. \tag{2.149}$$

2.5.2 Numerical Examples

Here we show some numerical examples. To see the near-far effect on the error probability, we consider the cases where there are five users in the system and the desired users power is four times the power of the interferers, while the interferers have the same power, that is, $P_1 = 4P_2 = 4P_3 = 4P_4 = 4P_5$. Here the total interference power is the same as P_1. We compare it with the case when there are two users having the same power, i.e., $P_1 = P_2$. In this case also, the total interference power is P_1. AQPSK modulation is used by all the users. The spreading codes are the AO/LSE codes listed in Table 2.1.

Figure 2.7 shows the average probability of error for both I and Q channels with $\beta = \pi/8$ and $N = 127$. Due to the unequal error protection for the I and Q channels by the modulation scheme, we can see that the I channel has much lower error probability than that of the Q channel. Figures 2.8 and 2.9 show the average error probability for the I and Q channels for the two cases when $\beta = \pi/8$ and $N = 127$. As can be seen, in the case with the near-far effect, the performance is better as SNR increases. This is because even though the total interference power is the same, the effect of each interferer on the desired user is not the same due to the different correlation relations of the spreading codes. In this case, the interference effect is not four times that of any one interferer since it is unlikely that all interferers spreading codes have simultaneously large correlation with the desired user.

2.6 Conclusions

In this chapter, the exact and an approximate BER performance were derived for a quaternary asymmetric QPSK DS-CDMA system. The variance and pdf of the MAI were analyzed. The results showed that the AQPSK scheme can provide a significant difference in the amount of error protection for different bits of a symbol. Therefore,

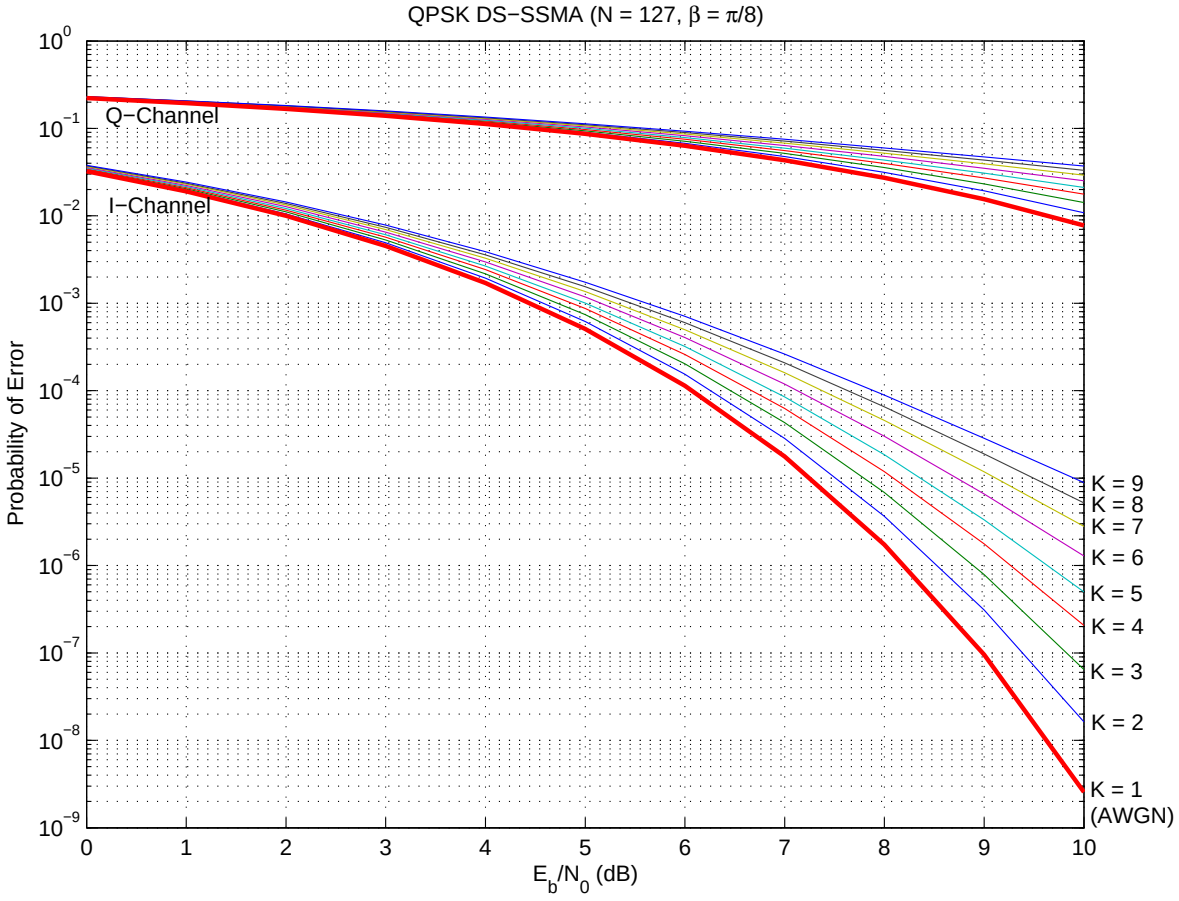

Figure 2.7: Probability of error for asymmetric QPSK DS-SSMA ($N = 127$, $\beta = \pi/8$).

it is advantageous to use AQPSK when designing a UEP system for its simplicity and efficiency. We also examined the nearfar problem by generalizing the system model to the case where users have different transmit power. The results showed that the Q-channel (less power) is more sensitive to the nearfar effect than the I-channel is in a multiple-access environment.

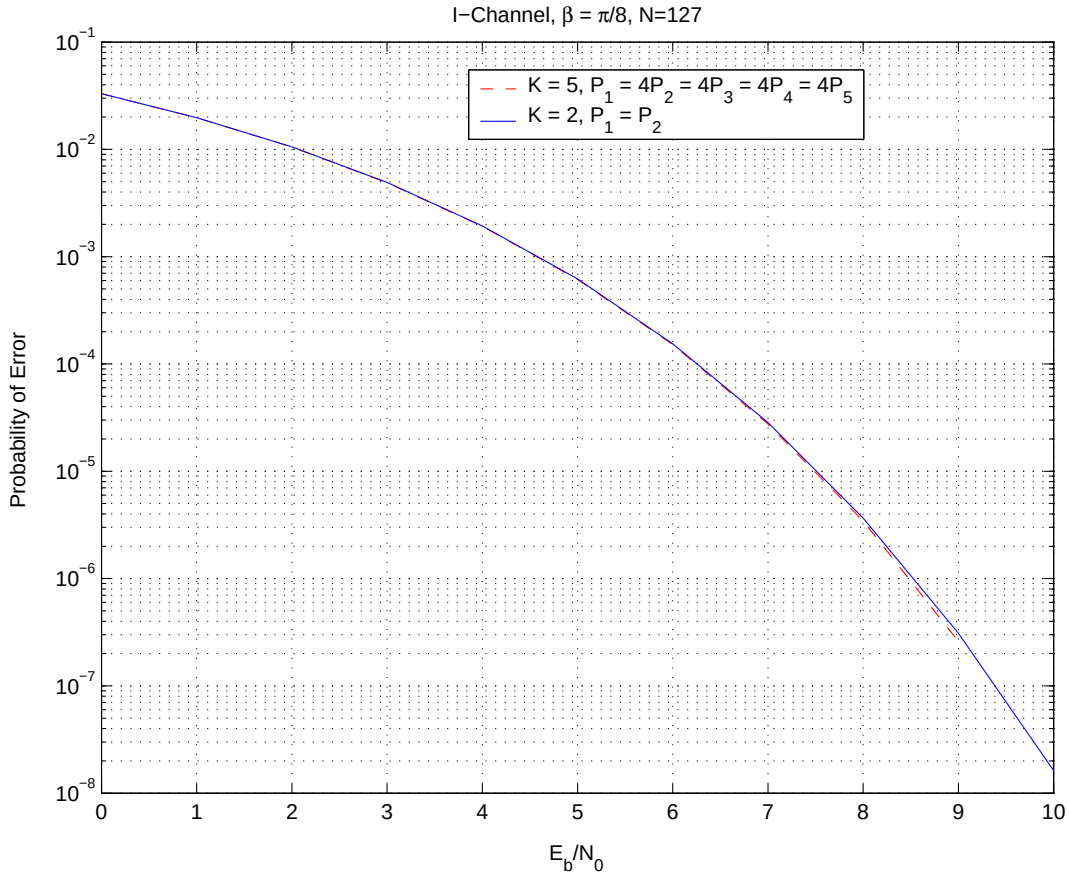

Figure 2.8: Probability of error for asymmetric QPSK DS-SSMA I-Channel($\beta = \pi/8$, $N = 127$).

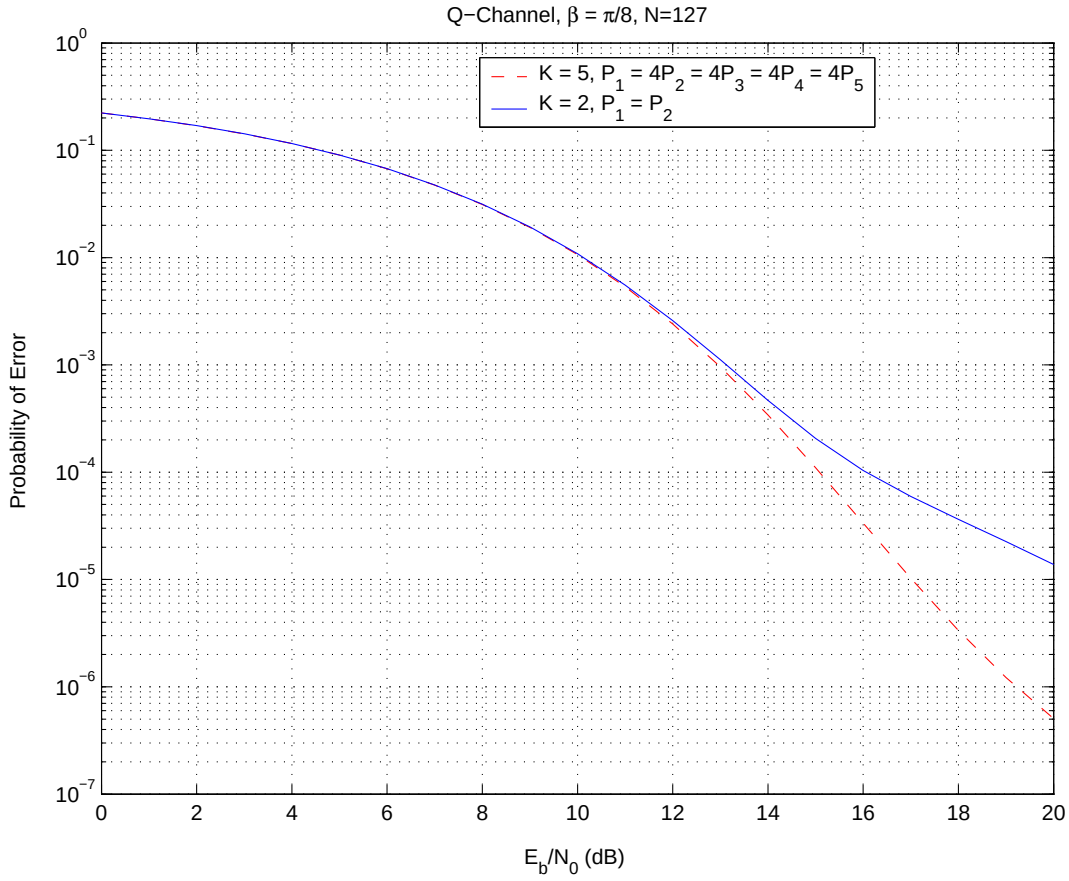

Figure 2.9: Probability of error for asymmetric QPSK DS-SSMA Q-Channel($\beta = \pi/8$, $N = 127$).

CHAPTER 3

Analysis of A Multilevel Coded 8-PSK CDMA System with UEP Capability

3.1 Introduction

Multilevel coding (MLC) is a way to provide unequal error protection for different streams of information with different levels of importance in a communication system. MLC is based on the concept of coded modulation, which combines coding scheme and modulation scheme in the system design to optimize the performance. Based on the code structure, there are two basic types of coded modulation: trellis coded modulation (TCM) and block coded modulation (BCM). TCM was first introduced by Ungerboeck in 1982 [22], and BCM was first introduced by Imai and Hirakawa in 1977 [11]. In this chapter, we focus on the use of BCM. However, the design and analysis demonstrated in this work can easily be extended to the TCM case.

Imai and Hirakawa's work was referred to as multilevel coding (MLC). The idea is to protect each bit in the signal point in the modulation constellation by an individual binary code. Originally it was proposed for one-dimensional signaling combined with labeling by binary counting of the signal levels. In general, it can be applied to any two-dimensional modulation scheme.

3.1.1 MLC Encoding Scheme

Consider M information streams at the output of the source encoder. Each of them has different levels of importance. The goal is to design the channel encoder using MLC to provide different levels of error protection to these streams of data. Two main parts in the system design for the transmitter employing MLC are the code construction (MLC channel encoder) and how the codewords are mapped to the signal space (symbol mapper).

MLC Channel Encoder

The MLC encoding scheme at the transmitter is shown in Figure 3.1. Let $b_1, b_2, \ldots, b_M$ denote the information streams. They are sent into the multilevel/UEP channel encoder. The encoder output is mapped to the signal point in the modulation constellation by the mapping rule $\mathcal{M}$, and then sent through the channel.

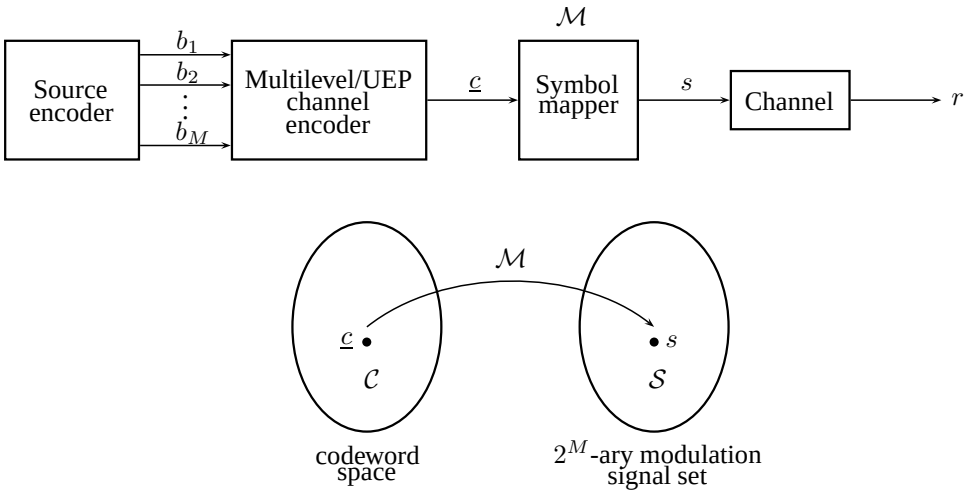

Figure 3.1: Multilevel encoding system.

We consider block coded modulation, and in this case $b_1, b_2, \ldots, b_M$ are encoded with binary block codes $C_1, C_2, \ldots, C_M$, respectively. In the MLC setup, we refer the level corresponding to b_i as the ith level. Let C_i be a (n_i, k_i, d_i) code as the component code of the ith level for $i = 1, 2, \ldots, M$. For the purpose of analysis, we assume all

the codes have the same block length n. Thus the ith code has rate $R_i = k_i/n$, and the overall code rate is $R = \sum_{i=1}^{M} R_i$. The overall MLC encoding process and the *code array* for $M = 3$ is shown in Figure 3.2.

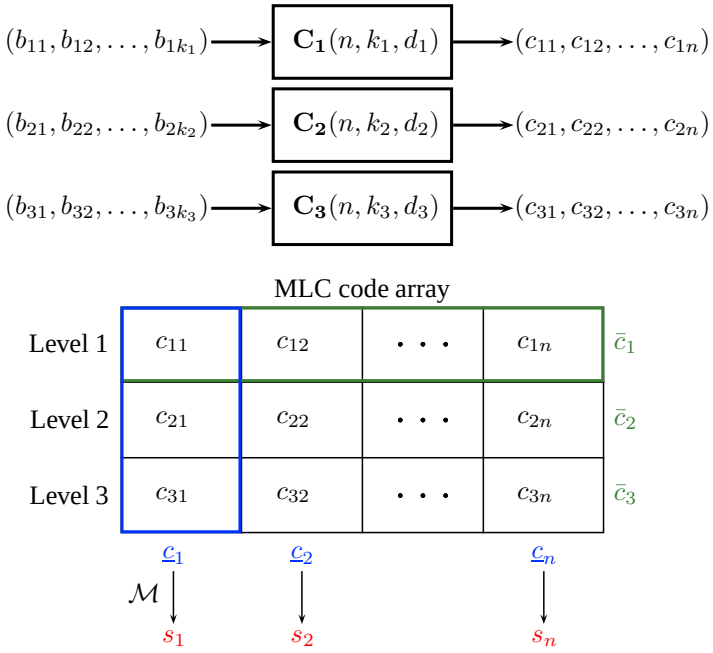

Figure 3.2: MLC encoder and code array ($M = 3$).

Each information stream is first encoded by sending k_i bits $(b_{i1}, b_{i2}, \ldots, b_{ik_i})$ into its corresponding encoder, and the encoder output is a codeword $\bar{c}_i = (c_{i1}, c_{i2}, \ldots, c_{in})$ of block length n. These M codewords are arranged row by row to form a M-by-n code matrix. Then each column of the matrix $\underline{c}_j = (c_{1j}, c_{2j}, \ldots, c_{Mj})^T$ is sent to the symbol mapper $\mathcal{M}$ to generate the corresponding signal point s_j in the constellation of the modulation scheme. For example, in Figure 3.2, the three bits (c_{11}, c_{21}, c_{31}) of $\underline{c}_1$ are mapped to s_1 according to the mapping rule $\mathcal{M}$. The code construction is done by appropriately choosing $C_1, C_2, \ldots, C_M$ to make the system suitable for various channels while achieving the desired error protection levels. In the code array generation described above, each row of the code array is a codeword generated from one of the component codes, and all the codewords are generated in parallel. Thus, the codewords $\bar{c}_1, \bar{c}_2, \ldots, \bar{c}_M$ are generated independently. It might be possible to add interdependency

among codewords by encoding them in a different way. However, in this chapter we only consider the case that there is no interdependency among component codewords in the code array.

Symbol Mapping by Partitioning

There are many different strategies for the design of the symbol mapper $\mathcal{M}$ proposed in the literature [22][11][23][24]. The basic idea is to map the codeword to the signal space such that the minimum Euclidean distance of the coded sequences is maximized. In Imai and Hirakawa's paper [11], the mapping is very simple by binary counting off the signal levels. This is shown in Figure 3.3 for the case of 8-PSK modulation.

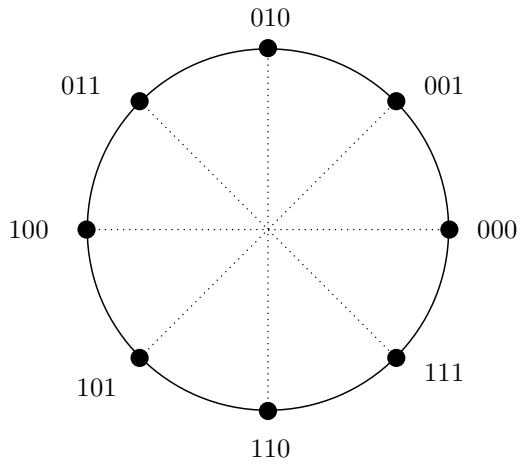

Figure 3.3: Imai and Hirakawa's partitioning for 8-PSK constellation.

Ungerboeck's approach is the mapping rule called "mapping by set partitioning" [22]. This mapping follows from successive partitioning of a signal set into subsets with increasing minimum distances between the signals of these subsets. Thus the minimum intra-subset Euclidean distance is maximized. This partitioning strategy is widely used in coded modulation. An example for 8-PSK modulation is shown in Figure 3.4.

Another mapping strategy is called "block partitioning" [23][24]. By using this rule, at each partition level, all the signal points within a subset are contained in disjoint half planes. This results in a small number of nearest neighbors. However, unlike

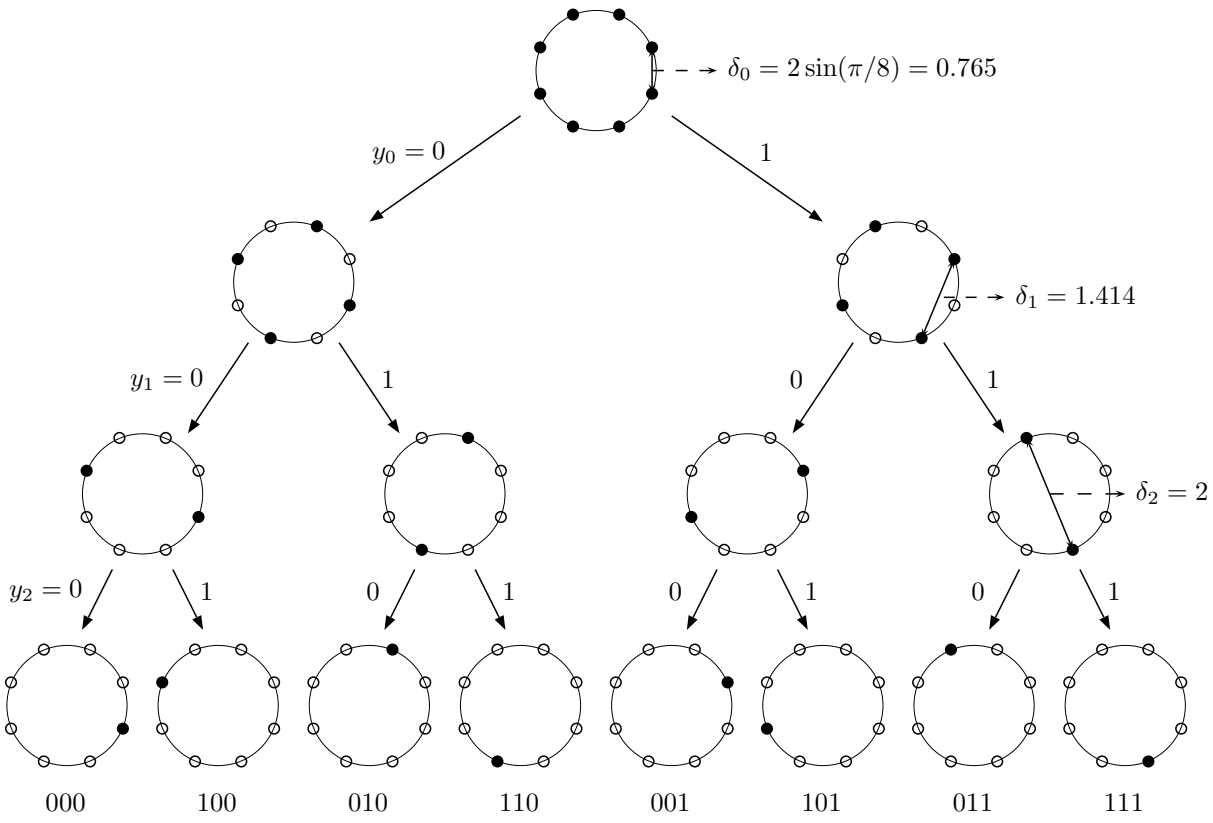

Figure 3.4: Ungerboeck's mapping by set partitioning for 8-PSK constellation.

Ungerboeck's partitioning, the minimum intraset distance at each level of the partition is a constant. An example of 8-PSK modulation using blocking partitioning is shown in Figure 3.5. Note that in the 8-PSK case, the first level (most significant bit) determines which of the horizontal half-plane the symbol lies in, and the second levels (the second most significant bit) determines which of the vertical half-plane the symbol lies in. This implies that the first and second level decoders can be implemented in parallel.

By combining Ungerboeck's partitioning and block partitioning, a strategy called "hybrid partitioning" [23][24] was proposed. It takes advantage of both the reduction of error coefficients, achieved by block partitioning, and the increasing minimum intraset distance associated with Ungerboeck's partitioning. An example for 8-PSK modulation is shown in Figure 3.6. The first partition level is identical to block partitioning, and the remaining levels are partitioned using Ungerboeck's rule.

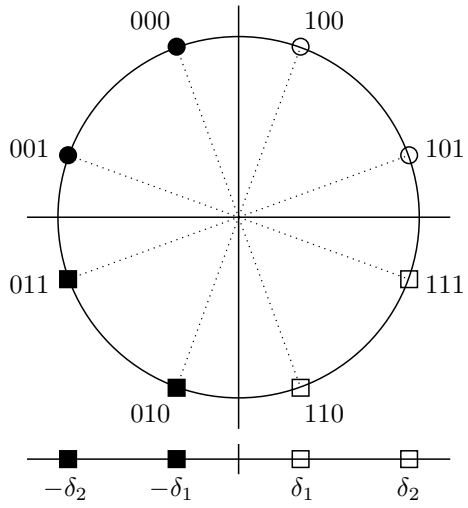

Figure 3.5: Block partitioning for 8-PSK constellation.

3.1.2 MSD Decoding Scheme

The decoding procedure for MLC is called "multistage decoding" (MSD). In general, for basic MLC with independent component codes, each code C_i can be decoded individually. However, due to the coded modulation structure, codeword bits of all levels are related in the signal space. Thus, in the MSD scheme, the decoding process starts at the first level codewords, and the decoding at a later level has to take into account the decoder outputs of prior decoding stages. To be specific, consider the transmission of one code array as shown in Figure 3.2. As mentioned earlier, each column of the code array is mapped to a symbol, then sent through the channel. Let $\underline{c}_j = (c_{1j}, c_{2j}, \ldots, c_{Mj})^T$ be mapped to s_j and transmitted, and r_j is the received symbol for $j = 1, 2, \ldots, n$. Let $f(r_j|s_j)$ be the conditional probability density function (PDF) of the channel output r_j given the channel input s_j. Also define $f(r_j|c_{1j}, c_{2j}, \ldots, c_{ij})$ to be the conditional PDF of r_j given that the encoder outputs from the first to the ith level are $c_{1j}, c_{2j}, \ldots, c_{ij}$, respectively, for $i = 1, 2, \ldots, M$. Therefore, we have

$$f(r_j|c_{1j}, c_{2j}, \ldots, c_{Mj}) = f(r_j|s_j) \tag{3.1}$$

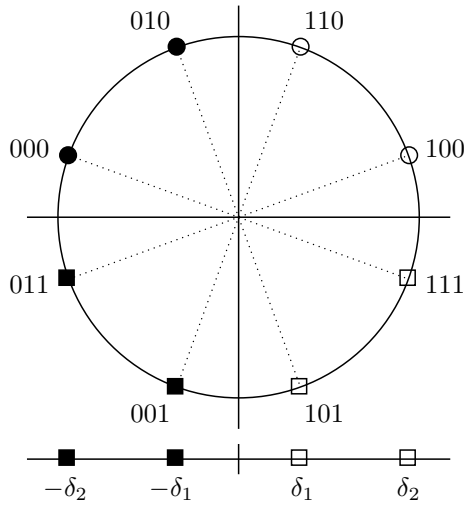

Figure 3.6: Hybrid partitioning for 8-PSK constellation.

where $f(r_j|c_{1j}, c_{2j}, \ldots, c_{ij})$ can be computed as

$$f(r_j|c_{1j}, c_{2j}, \ldots, c_{ij}) = \sum_{c_{(i+1)j}=0}^{1} \cdots \sum_{c_{Mj}=0}^{1} f(r_j|c_{1j}, c_{2j}, \ldots, c_{Mj}) P(c_{(i+1)j}, \ldots, c_{Mj}) \quad (3.2)$$

where $P(c_{(i+1)j}, \ldots, c_{Mj})$ is the joint probability of $c_{(i+1)j}, \ldots, c_{Mj}$. Define $P(c_{1j}|r_j)$ to be the conditional probability of c_{1j} given the channel output r_j. Also define $P(c_{ij}|r_j, c_{1j}, \ldots, c_{(i-1)j})$ to be the conditional probability of c_{ij} given r_j and $c_{1j}, \ldots, c_{(i-1)j}$. Let $f(r_j)$ be the PDF of r_j and $P(c_{1j}, \ldots, c_{(i-1)j})$ be the joint probability of $c_{1j}, \ldots, c_{(i-1)j}$, then we have

$$P(c_{1j}|r_j) = \frac{f(r_j|c_{1j})P(c_{1j})}{f(r_j)} \quad (3.3)$$

$$P(c_{ij}|r_j, c_{1j}, \ldots, c_{(i-1)j}) = \frac{f(r_j|c_{1j}, \ldots, c_{ij})P(c_{1j}, \ldots, c_{ij})}{f(r_j|c_{1j}, \ldots, c_{(i-1)j})P(c_{1j}, \ldots, c_{(i-1)j})} \quad (3.4)$$

for $i = 2, \ldots, M$ and $j = 1, 2, \ldots, n$.

To estimate c_{ij} when given r_j and $c_{1j}, \ldots, c_{(i-1)j}$, using MAP rule, we have

$$P(0|r_j, c_{1j}, \ldots, c_{(i-1)j}) \geq P(1|r_j, c_{1j}, \ldots, c_{(i-1)j}) \implies \widetilde{c}_{ij} = 0 \quad (3.5)$$

$$P(0|r_j, c_{1j}, \ldots, c_{(i-1)j}) < P(1|r_j, c_{1j}, \ldots, c_{(i-1)j}) \implies \widetilde{c}_{ij} = 1 \quad (3.6)$$

where $\widetilde{c}_{ij}$ is from the detection of the received symbol r_j before the decoding process, and is called the *intermediate estimate* for c_{ij}, which might be different from the final estimate $\widehat{c}_{ij}$ after decoding.

In practice, the receiver does not know $c_{1j}, \ldots, c_{(i-1)j}$. However, if $\widehat{c}_{1j}, \ldots, \widehat{c}_{(i-1)j}$ are equal to $c_{1j}, \ldots, c_{(i-1)j}$ with high probability, then $\widehat{c}_{1j}, \ldots, \widehat{c}_{(i-1)j}$ can be used in the above equations to replace $c_{1j}, \ldots, c_{(i-1)j}$ for the estimation of c_{ij}. The decoding process can be described as the following.

- The first step is to estimate c_{1j} by observing r_j using $P(0|r_j)$ and $P(1|r_j)$ for $j = 1, 2, \ldots, n$. At this point $\widetilde{c}_{1j}$ is obtained. Then after the intermediate estimates $(\widetilde{c}_{11}, \widetilde{c}_{12}, \ldots, \widetilde{c}_{1n})$ are obtained, they are sent into decoder D_1 for error correction and form the final estimates $(\widehat{c}_{11}, \widehat{c}_{12}, \ldots, \widehat{c}_{1n})$.

- The ith step is to estimate c_{ij} using the probabilities $P(0|r_j, \widehat{c}_{1j}, \ldots, \widehat{c}_{(i-1)j})$ and $P(1|r_j, \widehat{c}_{1j}, \ldots, \widehat{c}_{(i-1)j})$. Then the intermediate estimates $(\widetilde{c}_{i1}, \widetilde{c}_{i2}, \ldots, \widetilde{c}_{in})$ are sent into decoder D_i and form the final estimates $(\widehat{c}_{i1}, \widehat{c}_{i2}, \ldots, \widehat{c}_{in})$. This part is applied for $i = 2, \ldots, M$.

If we assume that basic MLC scheme is used, then $c_{1j}, c_{2j}, \ldots, c_{Mj}$ are independent, and $P(c_{ij}|r_j, \widehat{c}_{1j}, \ldots, \widehat{c}_{(i-1)j})$ can be replaced with $f(r_j|\widehat{c}_{1j}, \ldots, \widehat{c}_{(i-1)j}, c_{ij})$, which can be computed by

$$f(r_j|c_{1j}, \ldots, c_{ij}) = \frac{1}{2^{M-i}} \sum_{c_{(i+1)j}=0}^{1} \cdots \sum_{c_{Mj}=0}^{1} f(r_j|c_{1j}, \ldots, c_{Mj}) \tag{3.7}$$

3.1.3 Outline of the Chapter

In this chapter, we analyze the performance of a code-division multiple-access (CDMA) system with coded modulation. MLC is used at the transmitter with asymmetric 8-PSK modulation to achieve unequal error protection (UEP). BCH codes are used in the encoder and multistage decoding (MSD) is used at the receiver for data recovery. The

approximate bit error performance is obtained by approximating the multiple-access interference (MAI) as a Gaussian random variable. The rest of the chapter is organized as the following. In Section 3.2, we introduce the system model. In Section 3.3, we analyze the performance of MLC with 8-PSK modulation in the single-user case. In Section 3.4, we analyze the overall system performance by combining the analysis of 8-PSK MLC with the quaternary DS-CDMA scheme. Then this chapter is concluded in Section 3.5.

3.2 System Model

The overall system we consider is a direct-sequence code-division multiple-access (DS-CDMA) system where each user employs MLC coded modulation to achieve UEP for various data streams of different priorities/quality of service (QoS) requirements. Specifically, we consider 8-PSK modulation where three data streams are multilevel coded at the transmitter. The receiver employs multistage decoding (MSD). This is shown in Figure 3.7. The detail information about each component in the system is described in the following.

3.2.1 Multilevel/UEP Channel Encoder

In the proposed system, we consider three bit streams generated from the source encoder to the input of the multilevel/UEP channel encoder as shown in Figure 3.7. The multilevel encoder and the code array structure is shown in Figure 3.2 as an example. The component codes used in the system are BCH codes since given a block length, it is possible to find BCH codes with different error correcting capability, which suits our needs well in the design of the UEP system. The shortest BCH codes $[n, k, t]$ with 3 different error correcting capability are $[15, 11, 1]$, $[15, 7, 2]$ and $[15, 5, 3]$ BCH codes where n is the block length, k is the message length, and t is the error correcting

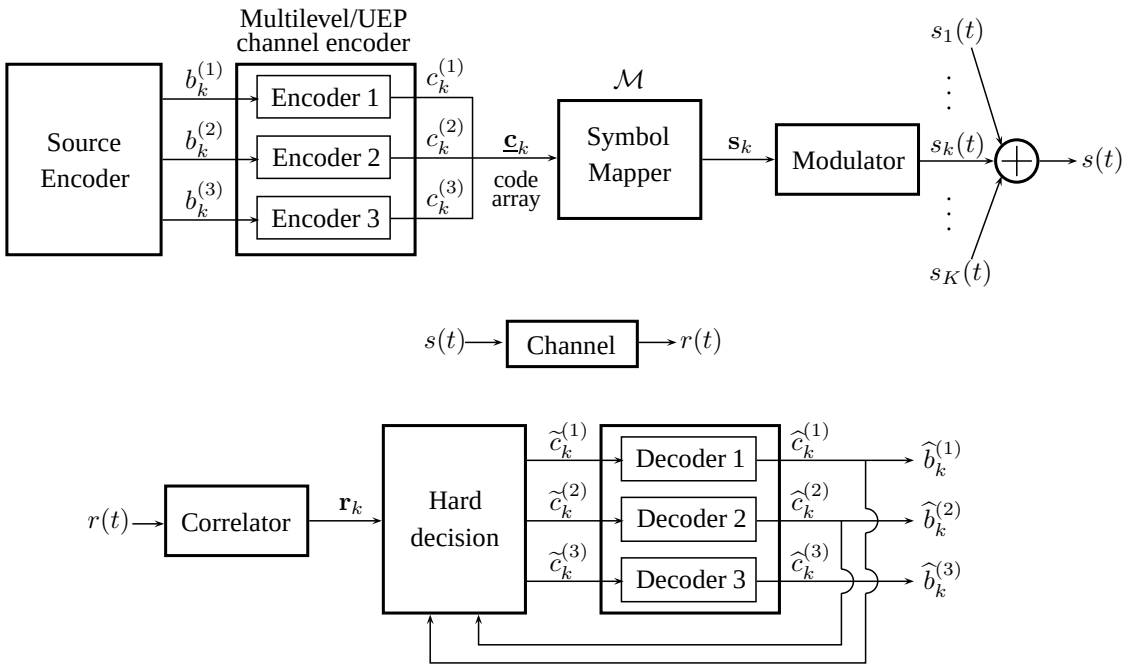

Figure 3.7: A MLC coded modulation quaternary DS-CDMA system with MSD.

capability of the code. These three codes have rates 0.73, 0.46, and 0.33 and can correct 1, 2, and 3 errors, respectively. We use these three codes as the component codes in the MLC scheme in the proposed system.

3.2.2 Asymmetric 8-PSK Modulation

The modulation scheme we consider in the system is asymmetric 8-PSK constellation as shown in Figure 3.8. The asymmetry of the constellation makes the system design flexible for the UEP purpose. The partitioning scheme (symbol mapping) considered in this system is block partitioning. The symbol mapper $\mathcal{M}$ maps every three coded bits $(c_k^{(1)}c_k^{(2)}c_k^{(3)}) \in \{0,1\}^3$ from $\underline{\mathbf{c}}_k$ column by column to one of the 8-PSK symbols. As can be seen in Figure 3.8, the eight symbols are distributed non-uniformly around the circle. The values α and β denote the angles corresponding to the symbols in the constellation. In each quadrant, there are two symbols located symmetrically about the angle β with an angle shift of either $+\alpha$ or $-\alpha$. For the eight symbols, there are two

possible values for the phase of the symbol ϕ_k, $\beta-\alpha$ and $\beta+\alpha$, which is determined by $c_k^{(3)}$. For example, in the first quadrant, when $c_k^{(3)}=0$, $\phi_k=\beta-\alpha$, and when $c_k^{(3)}=1$, $\phi_k=\beta+\alpha$.

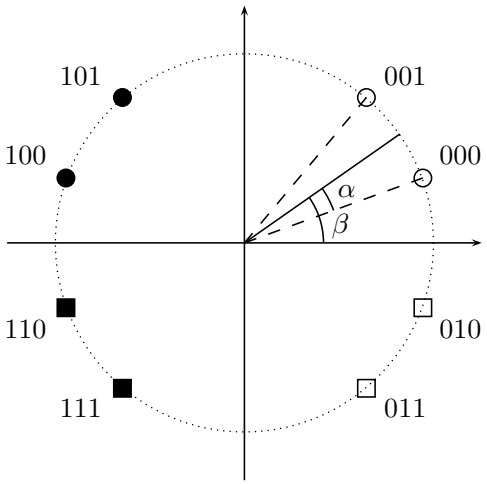

Figure 3.8: Asymmetric 8-PSK constellation.

Symbol Mapping at the Transmitter

In general, the symbol mapper output is not the angle of the constellation point but the in-phase and quadrature phase components of the baseband complex signal. By examining the modulation constellation, we have the following mapping as shown in Table 3.1.

$(c_k^{(1)}c_k^{(2)}c_k^{(3)})$	I	Q
(000)	$+\sqrt{2P}\cos(\beta-\alpha)$	$+\sqrt{2P}\sin(\beta-\alpha)$
(001)	$+\sqrt{2P}\cos(\beta+\alpha)$	$+\sqrt{2P}\sin(\beta+\alpha)$
(010)	$+\sqrt{2P}\cos(\beta-\alpha)$	$-\sqrt{2P}\sin(\beta-\alpha)$
(011)	$+\sqrt{2P}\cos(\beta+\alpha)$	$-\sqrt{2P}\sin(\beta+\alpha)$
(100)	$-\sqrt{2P}\cos(\beta-\alpha)$	$+\sqrt{2P}\sin(\beta-\alpha)$
(101)	$-\sqrt{2P}\cos(\beta+\alpha)$	$+\sqrt{2P}\sin(\beta+\alpha)$
(110)	$-\sqrt{2P}\cos(\beta-\alpha)$	$-\sqrt{2P}\sin(\beta-\alpha)$
(111)	$-\sqrt{2P}\cos(\beta+\alpha)$	$-\sqrt{2P}\sin(\beta+\alpha)$

Table 3.1: In-phase(I) and quadrature-phase(Q) components of 8-PSK modulation.

From Table 3.1, we can write the I and Q components in the general form

$$\text{I-component: } \sqrt{2P}\cos(\phi_k)d_k^{(1)} \tag{3.8}$$

$$\text{Q-component: } \sqrt{2P}\sin(\phi_k)d_k^{(2)} \tag{3.9}$$

where $d_k^{(i)} = 1 - 2c_k^{(i)}$ for $i = 0, 1$, and ϕ_k is determined by $c_k^{(3)}$.

Symbol Detection at the Receiver

We begin by considering optimum detection in an AWGN channel. The detection rule is equivalent to the minimum distance rule for symbol detection. However, we can divide the process into stages for detecting individual bits. The reason is because when combining this modulation scheme with MLC, this detection scheme can be combined nicely with MSD.

The detection of $c_k^{(1)}$ and $c_k^{(2)}$ is the same as QPSK modulation since for the transmitted symbol, the I-component is solely determined by $c_k^{(1)}$ and the Q-component is solely determined by $c_k^{(2)}$. This is a result of block partitioning when designing the symbol mapper. Let Z^I and Z^Q denote the I and Q components of the receiver correlator output for one symbol. Then the detection rule for $c_k^{(1)}$ and $c_k^{(2)}$ can be summarized as

$$\widetilde{c}_k^{(1)} = \begin{cases} 0, & Z^I \geq 0; \\ 1, & Z^I < 0, \end{cases} \tag{3.10}$$

and

$$\widetilde{c}_k^{(2)} = \begin{cases} 0, & Z^Q \geq 0; \\ 1, & Z^Q < 0. \end{cases} \tag{3.11}$$

The detection of $c_k^{(3)}$ requires a bit more work. From the modulation scheme, the quadrant where the symbol is located is determined by $c_k^{(1)}$ and $c_k^{(2)}$. Once the quadrant is determined, $c_k^{(3)}$ determines the symbol among the two. Thus, the detection of $c_k^{(3)}$

is based on $\widetilde{c}_k^{(1)}$ and $\widetilde{c}_k^{(2)}$. When considering coding combined with modulation, the detection of $c_k^{(3)}$ is based on the decoder output $\widehat{c}_k^{(1)}$ and $\widehat{c}_k^{(2)}$. Within a quadrant, $c_k^{(3)}$ can be regarded as the case of BPSK modulation with two symbols along the line determined by the angles $\beta+\alpha$ and $\beta-\alpha$. Since the two symbols are centered around the angle β, we can rotate the received symbol by the angle $\pm\beta$ to make it center around angle zero, and the decision is based on the Q-component as in the BPSK case. To be specifically, the detection of $c_k^{(3)}$ can be made by a decision statistic Z based on Z^I and Z^Q, which is given by

$$Z = Z^Q \cos\beta - (-1)^{|\widetilde{c}_k^{(1)} - \widetilde{c}_k^{(2)}|} \cdot Z^I \sin\beta. \tag{3.12}$$

Based on Z, the detection of $c_k^{(3)}$ is summarized in Table 3.2.

$(\widetilde{c}_k^{(1)}\widetilde{c}_k^{(2)})$	Angle of rotation	$Z \geq 0$	$Z < 0$
(00)	$-\beta$	$\widetilde{c}_k^{(3)} = 1$	$\widetilde{c}_k^{(3)} = 0$
(01)	$+\beta$	$\widetilde{c}_k^{(3)} = 0$	$\widetilde{c}_k^{(3)} = 1$
(10)	$+\beta$	$\widetilde{c}_k^{(3)} = 1$	$\widetilde{c}_k^{(3)} = 0$
(11)	$-\beta$	$\widetilde{c}_k^{(3)} = 0$	$\widetilde{c}_k^{(3)} = 1$

Table 3.2: Detection of $c_k^{(3)}$ in 8-PSK modulation.

3.2.3 Multiuser Scheme

We consider a multiple-user system with K users being active simultaneously. Multiple-access is achieved by employing quaternary DS-CDMA as shown in Figure 3.9. The transmitted signal of the kth user is given by

$$s_k(t) = s_k^I(t) + s_k^Q(t) \tag{3.13}$$

with

$$s_k^I(t) = \sqrt{2P}\cos(\phi_k(t))a_k^I(t)d_k^{(1)}(t)\cos(2\pi f_c t + \theta_k) \quad (3.14)$$

$$s_k^Q(t) = \sqrt{2P}\sin(\phi_k(t))a_k^Q(t)d_k^{(2)}(t)\sin(2\pi f_c t + \theta_k) \quad (3.15)$$

where $\phi_k(t)$ is the phase of the constellation point in the modulation scheme, and θ_k is the phase of the kth user's carrier.

We consider the synchronous case ($\tau_k = 0$ for all k), and the received signal can be written as

$$r(t) = \sum_{k=1}^{K} s_k(t) + n(t) \quad (3.16)$$

where $n(t)$ is an additive white Gaussian random process with zero mean and two-sided power spectral density $\frac{N_0}{2}$.

Consider the correlator receiver of the first user for $0 \leq t < T$. Then we can write $\phi_k(t)$ as ϕ_k. Assume θ_1 is known to the first user's receiver. Therefore the in-phase and quadrature phase components of the receiver correlator output can be written as

$$Z_1^I = \int_0^T r(t)a_1^I(t)\cos(2\pi f_c t)dt, \quad (3.17)$$

$$Z_1^Q = \int_0^T r(t)a_1^Q(t)\sin(2\pi f_c t)dt. \quad (3.18)$$

These two terms are used for symbol detection at the receiver as mentioned earlier. However, in a multiple-access scheme, both Z_1^I and Z_1^Q contain multiple-access interference (MAI) from other users in the system that can degrade the system performance. A detailed analysis on Z_1^I, Z_1^Q, and the MAI terms will be conducted in Section 3.4 in order to evaluate the overall system performance.

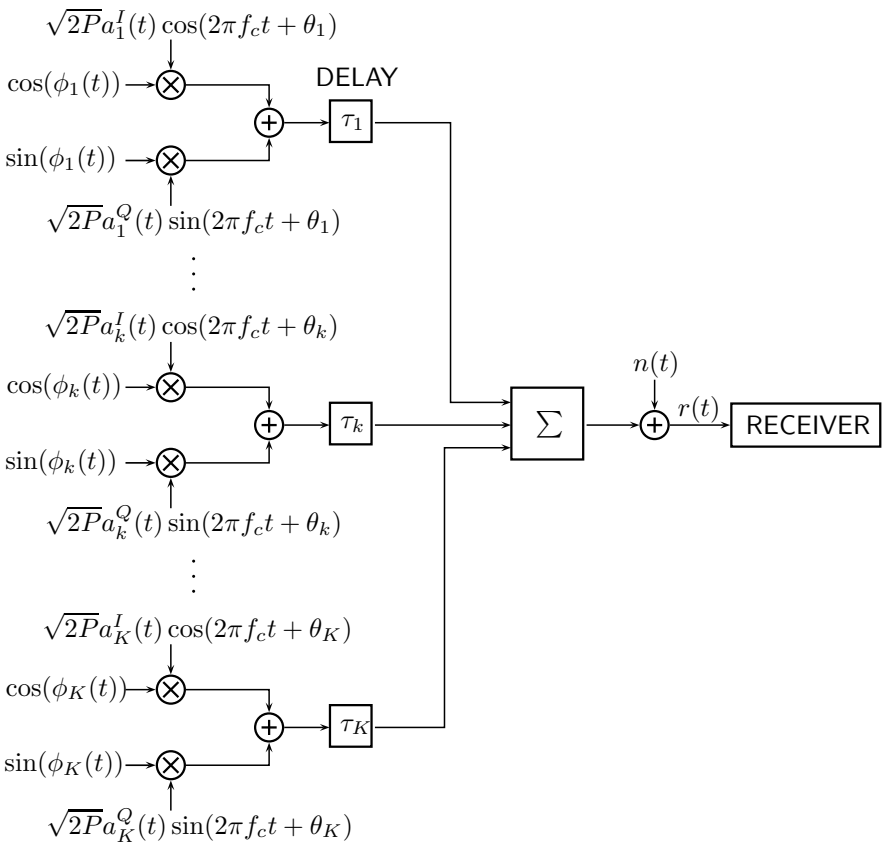

Figure 3.9: A quartenary DS-CDMA communication system.

3.3 Multilevel Coding with BCH Codes

In this section, we analyze a single-user communication system using MLC with 8-PSK modulation and MSD at the receiver. The multiple-user case will be discussed in the next section.

3.3.1 BCH Codes

In our proposed system, we apply MLC to the asymmetric 8-PSK constellation. The code array is shown in Figure 3.2. As mentioned earlier, with BCH codes, it is possible to find codes of the same block length with different error correcting capability, which suits our needs well in the design of the UEP system. We choose the shortest BCH codes of block length $n = 15$ as an example in the analysis. These codes are $[15, 11, 1]$,

[15, 7, 2] and [15, 5, 3] BCH codes. According to [25], the bit error probability for binary BCH codes when used in a binary symmetric channel (BSC) with crossover probability p is upper bounded by the probability that more than t errors occur, which is given by

$$P_b \leq \sum_{i=t+1}^{n} \frac{i+t}{n} \binom{n}{i} p^i (1-p)^{n-i}. \tag{3.19}$$

This quantity includes both the cases of undetected errors and failure to decode. In the case that the BSC is from an AWGN channel with BPSK modulation and hard decision demodulation, $p = Q\left(\sqrt{2E/N_0}\right)$ where $E = E_b/r$ is the normalized bit energy, E_b is the uncoded bit energy, and $r = k/n$ is the code rate. To verify the upper bound, we simulate the three codes with BPSK modulation in the AWGN channel. In the simulation, the decoder first detects the number of errors in the received codeword with hard decision detection. If the number of errors is within the error correcting capability of the code, the decoder corrects the error bits and output the corrected codeword. If the number of errors is beyond the error correcting capability of the code, the decoder does nothing and outputs the received codeword. The simulation results and the upper bounds for the three codes with BPSK modulation in the AWGN channel are shown in Figure 3.10, 3.11, and 3.12.

It can be seen that the upper bound is very close to the actual performance, and thus it is possible to use it as an approximation. Also for the [15,11,1] BCH code, the upper bound is equal to the actual performance. This is because the [15,11,1] BCH code is actually a Hamming code, which is a perfect code. In this case, the decoder corrects exactly t or fewer errors in a codeword and cannot for more than t errors in a codeword. Thus the upper bound mentioned above becomes exact. We are interested in the performance of the three codes since we want to achieve unequal error protection by using them. Figure 3.13 shows the performance of the three codes for comparison. We can see that for codes with higher error correcting capability, the performance is worse.

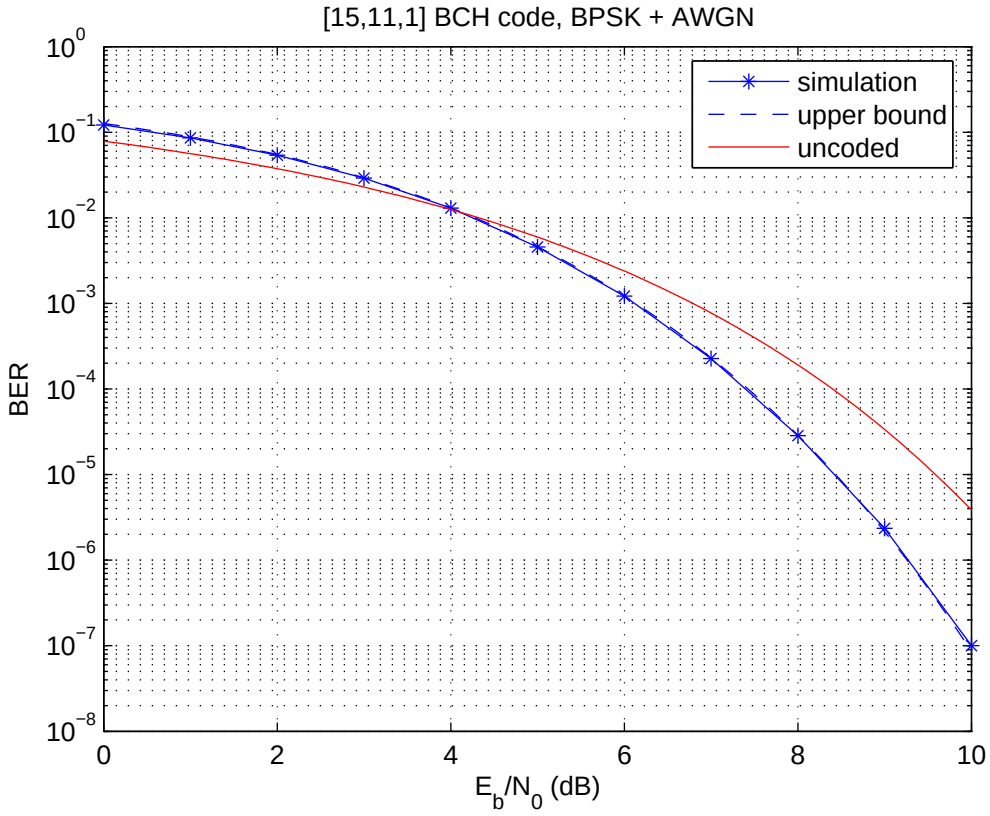

Figure 3.10: Performance of [15,11,1] BCH code.

This is because for codes with high error correcting capability, the message length k is small and the rate R is low. Thus the energy used to transmit the whole block of coded bits is low. However, when we apply the coding scheme with asymmetric 8-PSK constellation, the symbol energy is distributed unequally to $b_k^{(1)}$, $b_k^{(2)}$, and $b_k^{(3)}$, thus the performance of the codes combined with modulation can still be different. Our idea is to apply the codes with larger t to bits of more importance. Thus we will apply [15,5,3] code to $b_k^{(1)}$, [15,7,2] code to $b_k^{(2)}$, and [15,11,1] code to $b_k^{(3)}$ and see what is the overall coded modulation performance.

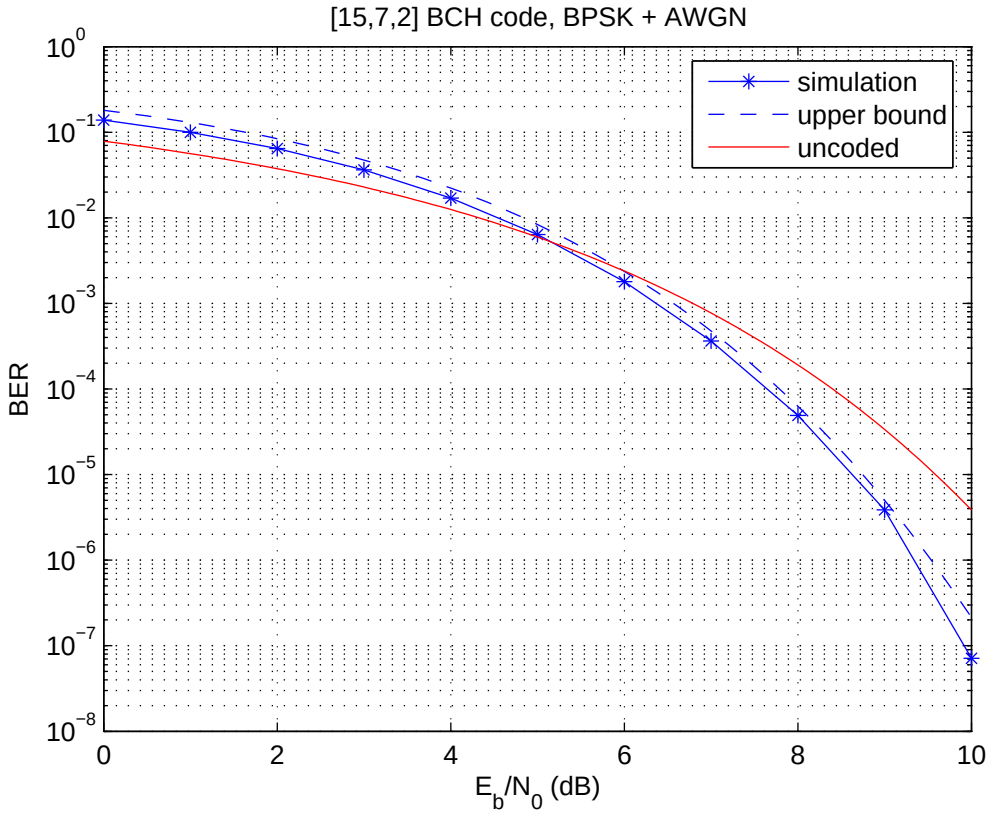

Figure 3.11: Performance of [15,7,2] BCH code.

3.3.2 Upper Bound to the BER using BCH Codes – Single-User Case

We first examine the BCH coded MLC scheme for the single-user case in AWGN channel. Later the multiple-user case can be extended from this case. The detection and decoding error probability of the ith level in the MLC scheme are defined as

$$P_{det_i} = P(c_k^{(i)} \neq \widehat{c}_k^{(i)}), \tag{3.20}$$

and

$$P_{dec_i} = P(b_k^{(i)} \neq \widehat{b}_k^{(i)}), \tag{3.21}$$

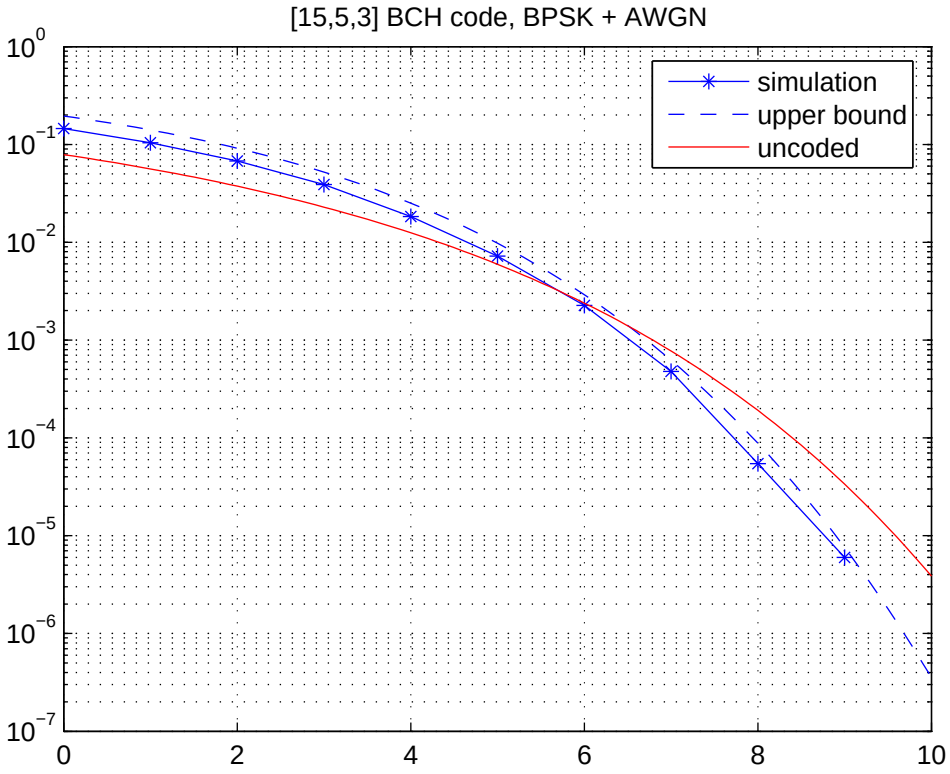

Figure 3.12: Performance of [15,5,3] BCH code.

respectively, for $i = 1, 2, 3$. The detection error probability is defined as the error probability between encoder output and decoder input, which occurs during transmission over the AWGN channel with hard decision detector at the receiver. The decoding error probability is defined as the error probability between the uncoded bits at the encoder input and the decoded bits at the decoder output. Depending on the number of errors occur in a codeword during transmission, the decoder may or may not be able to correct the errors, which causes decoding error. For a $[n, k, t]$ BCH code, the decoding error probability can be upper bounded by equation (3.19), and the simulation results show that for BCH codes, this upper bound is very close to the actual decoding error probability, and thus can be used as an approximation to P_{dec_i}. Therefore, for the proposed BCH coded 8-PSK UEP system, the upper bound of the overall bit error probability

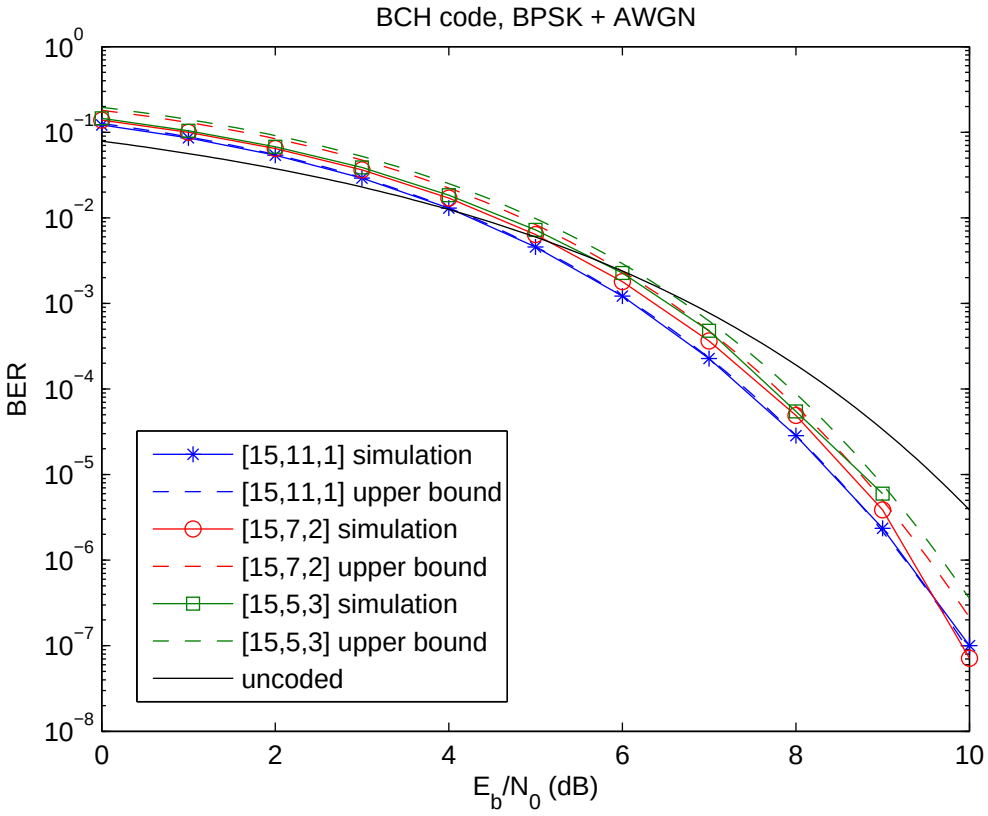

Figure 3.13: Comparison of BCH codes performance.

for the three levels can then be approximated by

$$P_{dec_i} \simeq \sum_{j=t_i+1}^{n} \frac{j+t_i}{n} \binom{n}{j} P_{det_i}^{j} (1 - P_{det_i})^{n-j}. \tag{3.22}$$

In order to find the upper bound (approximation), we need to obtain the detection error probability P_{det_i}. For level-1 ($b_k^{(1)}$) and level-2 ($b_k^{(2)}$), we have [26]

$$P_{det_1} = \frac{1}{2}\left[Q\left(\sqrt{\frac{4E_s\cos^2(\beta+\alpha)}{N_0}}\right) + Q\left(\sqrt{\frac{4E_s\cos^2(\beta-\alpha)}{N_0}}\right)\right], \tag{3.23}$$

$$P_{det_2} = \frac{1}{2}\left[Q\left(\sqrt{\frac{4E_s\sin^2(\beta+\alpha)}{N_0}}\right) + Q\left(\sqrt{\frac{4E_s\sin^2(\beta-\alpha)}{N_0}}\right)\right]. \tag{3.24}$$

where E_s is the symbol energy. For level-3, the derivation of P_{det_3} is more complicated than that of P_{det_1} and P_{det_2} because of the multistage decoding (MSD). It can be shown that (Appendix C)

$$\begin{aligned} P_{det_3} &= Q\left(\sqrt{\frac{4E_s \sin^2 \alpha}{N_0}}\right)(1 - P_{dec_1} - P_{dec_2}) \\ &\quad + \frac{1}{2}\left[1 - Q\left(\sqrt{\frac{4E_s \sin^2(2\beta - \alpha)}{N_0}}\right) + Q\left(\sqrt{\frac{4E_s \sin^2(2\beta + \alpha)}{N_0}}\right)\right] P_{dec_1} \\ &\quad + \frac{1}{2}\left[1 + Q\left(\sqrt{\frac{4E_s \sin^2(2\beta - \alpha)}{N_0}}\right) - Q\left(\sqrt{\frac{4E_s \sin^2(2\beta + \alpha)}{N_0}}\right)\right] P_{dec_2}. \end{aligned} \tag{3.25}$$

Therefore, from (3.22), (3.23), (3.24), and (3.25), we can obtain the approximate decoding error probability for P_{dec_1}, P_{dec_2}, and P_{dec_3}. It can be observed that P_{det_3} (and thus P_{dec_3}) depends on P_{dec_1} and P_{dec_2}, which is due to the structure of MSD. The independence of P_{dec_1} and P_{dec_2} is because of the block partitioning. Hence, when P_{dec_1} and P_{dec_2} are very small, P_{dec_3} is dominated by the value of α.

3.3.3 Numerical Examples

Now we demonstrate numerical examples of applying [15,11,1], [15,7,2], and [15,5,3] BCH codes to the asymmetric 8-PSK multilevel coding (MLC) system and observe the bit error performance of the three levels. In the simulation, the [15,5,3] code is applied to the first level, the [15,7,2] code is applied to the second level, and the [15,11,1] code is applied to the third level. We consider the single user case in the AWGN channel. Figure 3.14 shows the bit error probability of the three levels when $\beta = 45°$ with $\alpha = 10°$, 15°, 20°, and 25°. The solid lines are the simulation results and the dash lines are the upper bound (3.22) shown in the previous section. For $\beta = 45°$, the constellation is the same as the case proposed in [24]. As can be seen, when α increases, the third level

bit error probability decreases. This is consistent with (3.25) that the performance is dominated by α when P_{det_1} and P_{det_2} are small. It can also be observed that the change of α does not affect P_{dec_1} and P_{dec_2} very much. As to the upper bound, we can see that it is very close to the actual performance and can be used as an approximation when BCH codes are applied. Figure 3.15 shows the results when $\beta = 35°$ with $\alpha = 5°$, $10°$, $15°$, and $20°$. As can be seen, by changing β, P_{dec_1} and P_{dec_2} can be further adjusted to differentiate the level of unequal error protection. Note that when $\alpha = 20°$ and SNR is greater than about 13 dB, the level-2 performance is worse than the level-3 performance. Thus in the system design, in order to have distinguishable error protection levels, it is important to choose the right values of α and β. Figure 3.16 shows the SNR required to achieve a bit error probability of 10^{-5} for the three levels for different α and β. It can be observed that for the third level, there is an optimal value of α that requires the least SNR to achieve a bit error probability of 10^{-5}. However, at the optimal point, the level-2 performance is very close to the level-3 performance and is worse than the level-3 performance when α goes beyond the optimal point. This result is also shown in [24]. Thus, the optimal point of α for the third level might not be the optimal point for the overall system.

3.4 CDMA with 8-PSK Modulation

In this section, we analyze the performance of the proposed 8-PSK MLC system in the multiple-user scenario employing DS-CDMA as the multiple-access scheme. From the analysis in Section 3.4, the 8-PSK MLC performance for single-user case can be evaluated using detection and decoding error probability at each level. In the multiple-user case, there is MAI in the received signal, and the detection and decoding error probability is different. In order to evaluate the performance, we first need to analyze the MAI in the system.

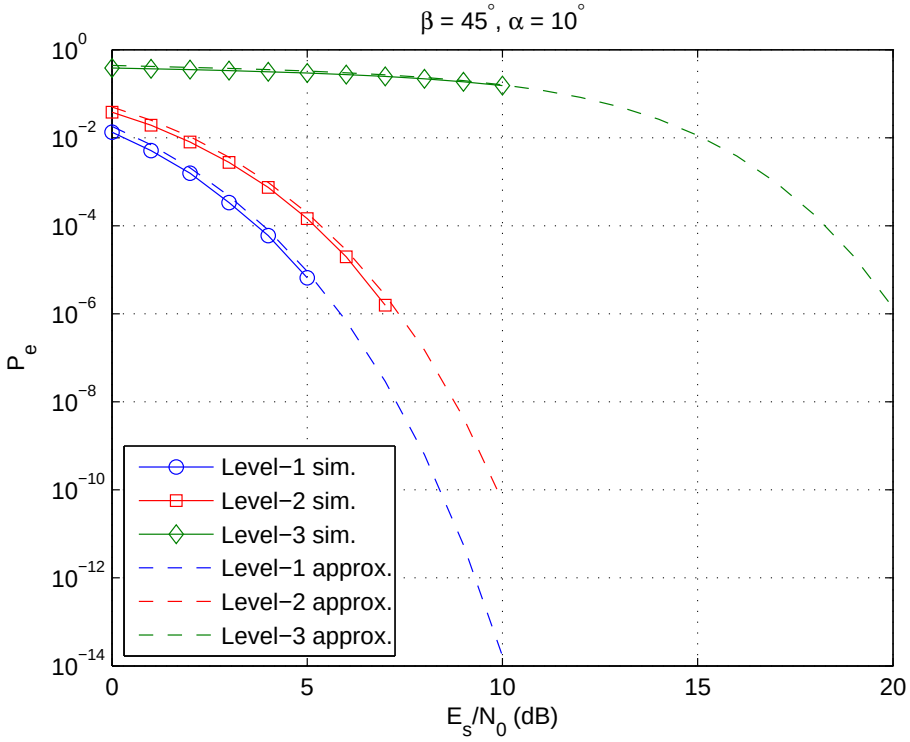

(a)

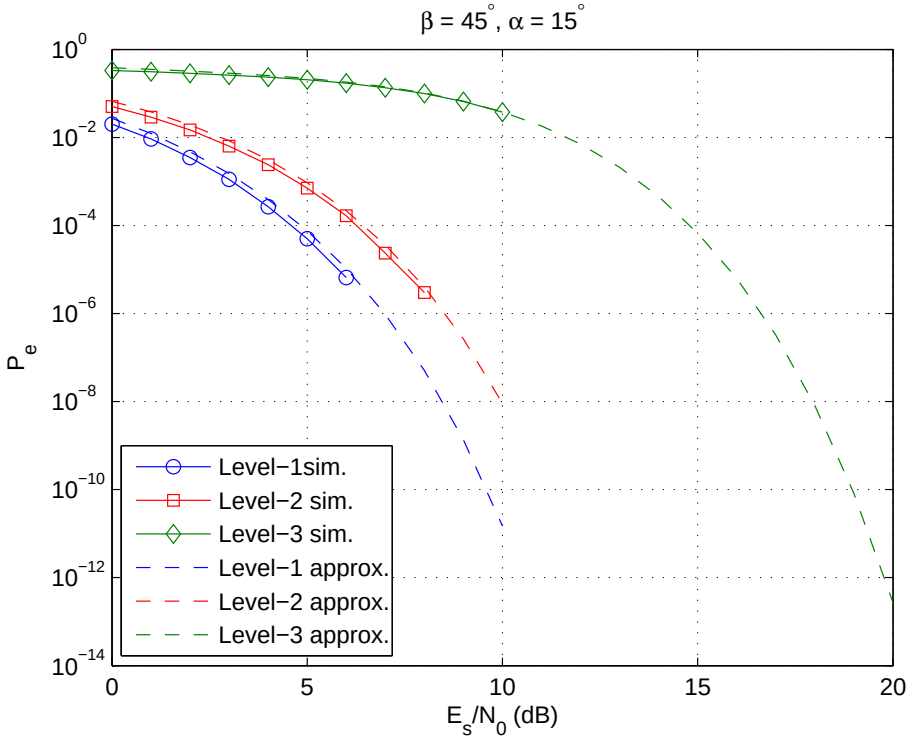

(b)

Figure 3.14: (a) $\beta = 45°$, $\alpha = 10°$ (b) $\beta = 45°$, $\alpha = 15°$

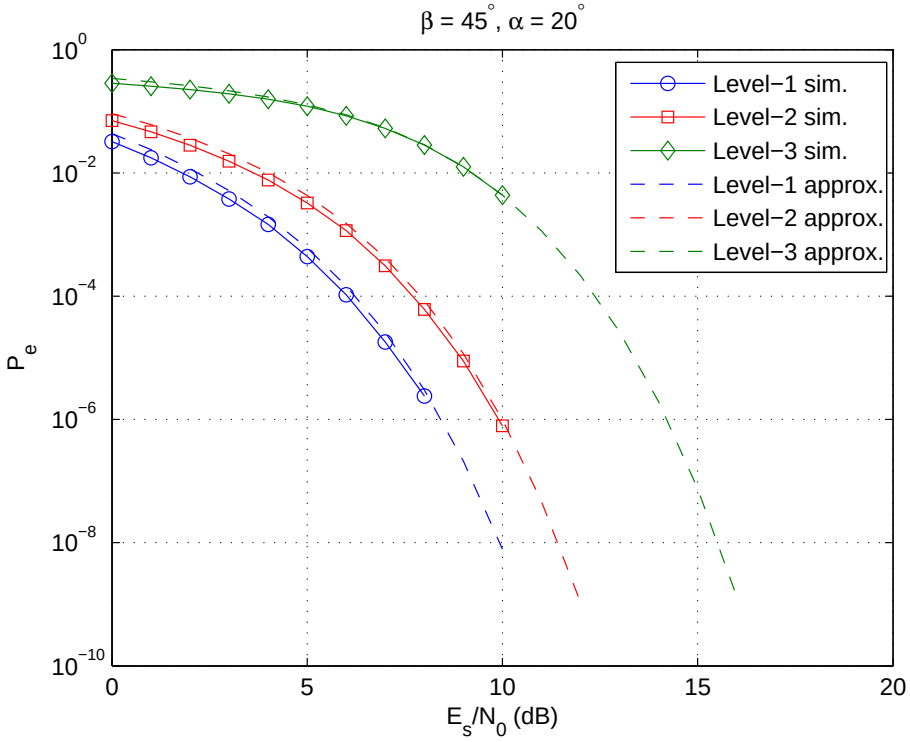

(c)

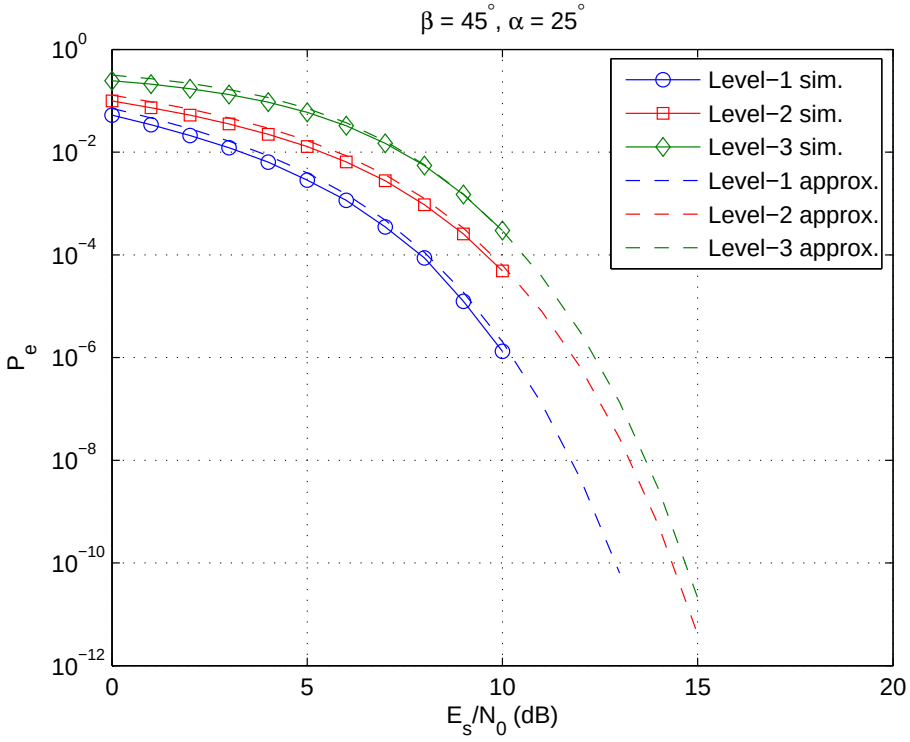

(d)

Figure 3.14: (c) $\beta = 45°$, $\alpha = 20°$ (d) $\beta = 45°$, $\alpha = 25°$

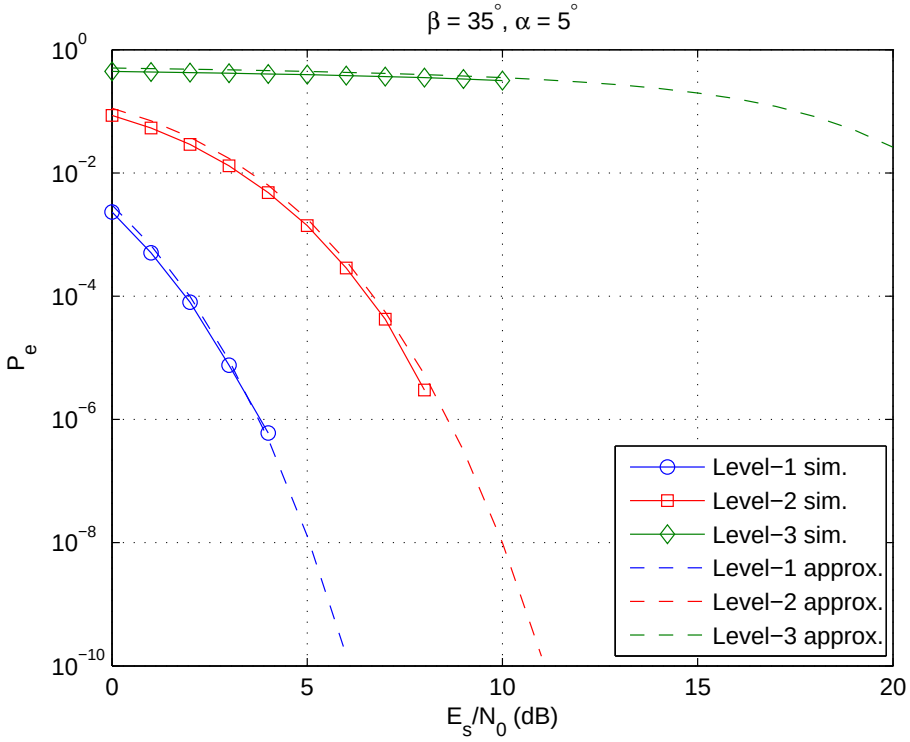

(a)

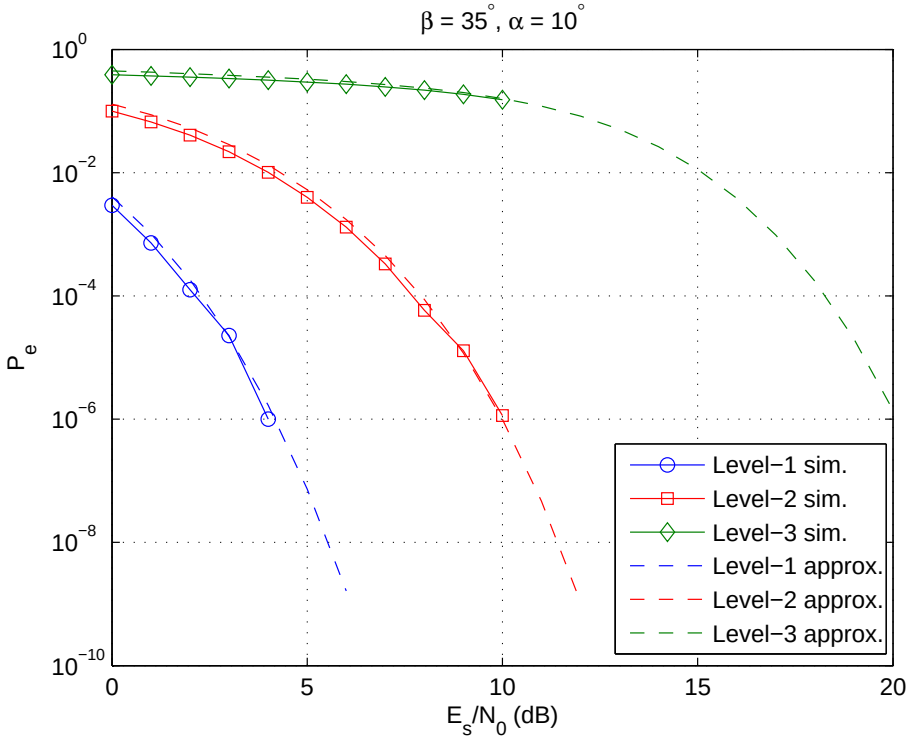

(b)

Figure 3.15: (a) $\beta = 35°$, $\alpha = 5°$ (b) $\beta = 35°$, $\alpha = 10°$

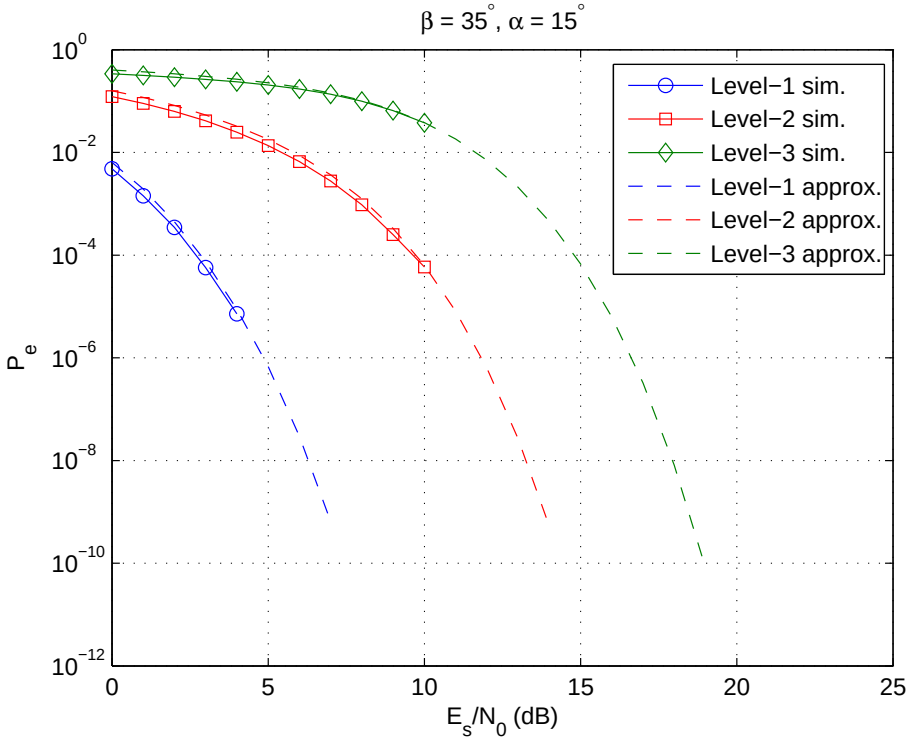

(c)

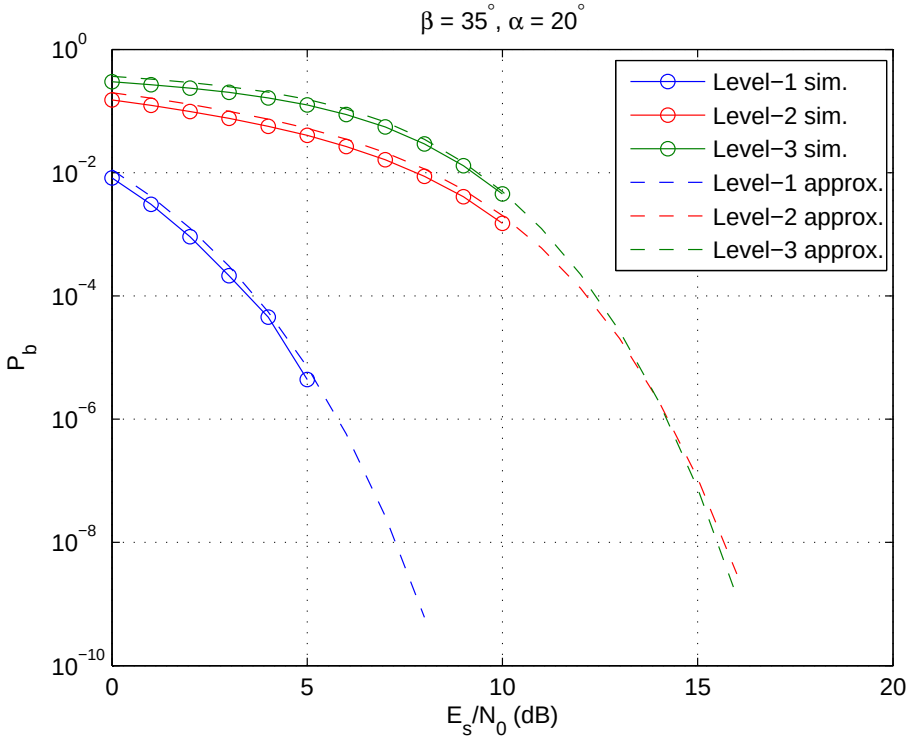

(d)

Figure 3.15: (c) $\beta = 35°$, $\alpha = 15°$ (d) $\beta = 35°$, $\alpha = 20°$

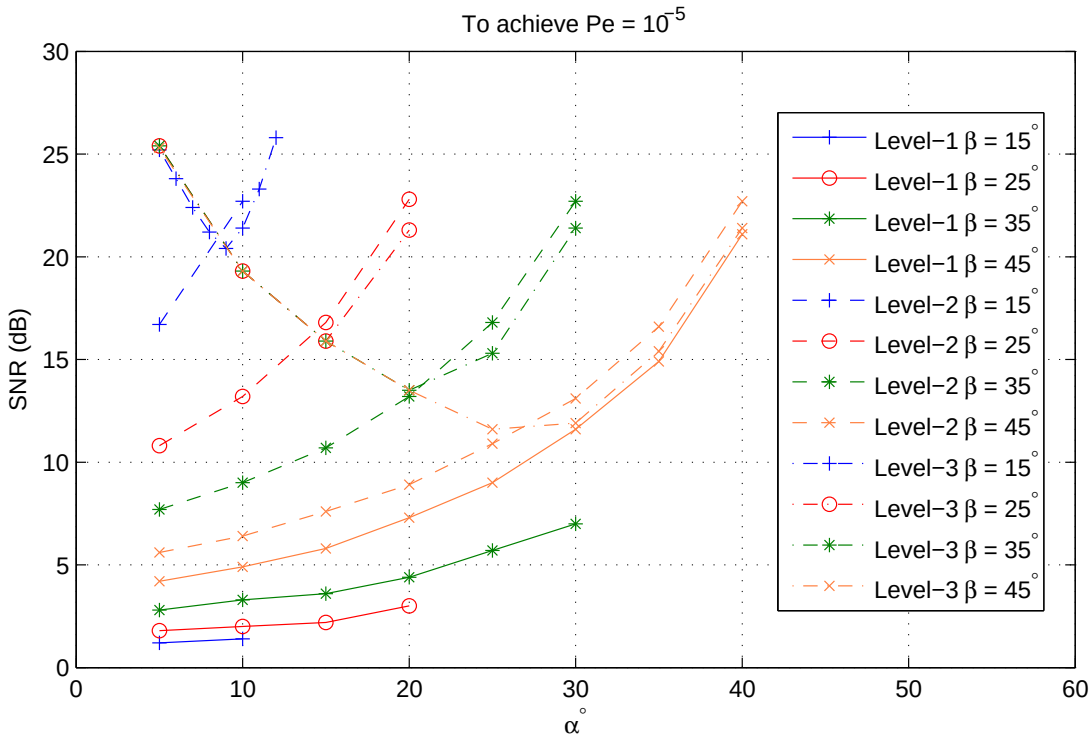

Figure 3.16: SNR required to achieve $P_e = 10^{-5}$.

3.4.1 Correlator Receiver

We begin with the analysis on the correlator receiver output. Let user 1 be the user of interest. Without loss of generality, we assume $\theta_1 = 0$. Recall in Section 3.2, the correlator receiver output of user 1 of the quaternary DS-CDMA system is given by

$$Z_1^I = \int_0^T r(t)a_1^I(t)\cos(2\pi f_c t)dt, \tag{3.26}$$

$$Z_1^Q = \int_0^T r(t)a_1^Q(t)\sin(2\pi f_c t)dt. \tag{3.27}$$

If we expand (3.26), we have

$$\begin{aligned} Z_1^I &= \int_0^T \sqrt{2P}\cos(\phi_1)a_1^I(t)d_1^{(1)}(t)\cos(2\pi f_c t)a_1^I(t)\cos(2\pi f_c t)dt \\ &\quad + \int_0^T \sqrt{2P}\sin(\phi_1)a_1^Q(t)d_1^{(2)}(t)\sin(2\pi f_c t)a_1^I(t)\cos(2\pi f_c t)dt \\ &\quad + \sum_{k=2}^{K}\int_0^T \sqrt{2P}\cos(\phi_k)a_k^I(t)d_k^{(1)}(t)\cos(2\pi f_c t+\theta_k)a_1^I(t)\cos(2\pi f_c t)dt \\ &\quad + \sum_{k=2}^{K}\int_0^T \sqrt{2P}\sin(\phi_k)a_k^Q(t)d_k^{(2)}(t)\sin(2\pi f_c t+\theta_k)a_1^I(t)\cos(2\pi f_c t)dt \\ &\quad + \int_0^T n(t)a_1^I(t)\cos(2\pi f_c t)dt \\ &= A+B+\sum_{k=2}^{K}C_k+\sum_{k=2}^{K}D_k+n_1^I. \end{aligned} \tag{3.28}$$

For $0 \le t < T$, we can write $d_k^{(i)}(t)$ as $d_k^{(i)}$ since they are constants throughout one symbol duration. In the above expression, the output due to the desired signal is

$$A = \sqrt{2P}\cos(\phi_1)d_1^{(1)}\int_0^T (a_1^I(t))^2\cos^2(2\pi f_c t)dt = \sqrt{P/2}T\cos(\phi_1)d_1^{(1)}. \tag{3.29}$$

The output of the I-channel receiver due to the Q-channel signal is (assuming $f_c T \gg 1$)

$$B = \sqrt{2P}\cos(\phi_1)d_1^{(2)}\int_0^T a_1^I(t)a_1^Q(t)\sin(2\pi f_c t)\cos(2\pi f_c t)dt = 0. \tag{3.30}$$

The output of the I-channel interference is given by

$$\begin{aligned} C_k &= \int_0^T \sqrt{2P}\cos(\phi_k)a_k^I(t)d_k^{(1)}(t)\cos(2\pi f_c t+\theta_k)a_1^I(t)\cos(2\pi f_c t)a_1^I(t)\cos(2\pi f_c t)dt \\ &= \sqrt{2P}\cos(\phi_k)d_k^{(1)}\int_0^T a_k^I(t)a_1^I(t)\cos(2\pi f_c t+\theta_k)\cos(2\pi f_c t)dt \\ &= \sqrt{P/2}\cos(\phi_k)d_k^{(1)}\cos(\theta_k)\int_0^T a_k^I(t)a_1^I(t)dt \\ &= \sqrt{P/2}\cos(\phi_k)d_k^{(1)}\cos(\theta_k)R_{k,1}^{II} \end{aligned} \tag{3.31}$$

where

$$R_{k,1}^{II} = \int_0^T a_k^I(t) a_1^I(t) dt = \sum_{j=0}^{N-1} a_{k,j}^I a_{1,j}^I \int_0^{T_c} \psi^2(t) dt \tag{3.32}$$

and $\psi(t)$ is the chip waveform. If we use a rectangular chip waveform, that is, $\psi(t) = p_{T_c}(t)$, then $\int_0^{T_c} \psi^2(t) dt = T_c$, and $R_{k,1}^{II} = T_c \sum_{j=0}^{N-1} a_{k,j}^I a_{1,j}^I$. Similarly, the output of the interference due to the Q-channel signal is

$$D_k = \sqrt{P/2} \sin(\phi_k) d_k^{(2)} \sin(\theta_k) R_{k,1}^{QI} \tag{3.33}$$

where

$$R_{k,1}^{QI} = \int_0^T a_k^Q(t) a_1^I(t) dt = T_c \sum_{j=0}^{N-1} a_{k,j}^Q a_{1,j}^I \tag{3.34}$$

assuming rectangular chip waveform. The noise at the receiver output is

$$n_1^I = \int_0^T n(t) a_1^I(t) \cos(2\pi f_c t) dt. \tag{3.35}$$

Note that n_1^I is Gaussian with zero mean and variance $\frac{N_0 T}{4}$. In summary, we have

$$\begin{aligned} Z_1^I &= T\sqrt{P/2} \cos(\phi_1) d_1^{(1)} + \sum_{k=2}^{K} \sqrt{P/2} \cos(\phi_k) d_k^{(1)} \cos(\theta_k) R_{k,1}^{II} \\ &\quad + \sum_{k=2}^{K} \sqrt{P/2} \sin(\phi_k) d_k^{(1)} \sin(\theta_k) R_{k,1}^{QI} + n_1^I \\ &= T\sqrt{P/2} \left\{ d_1^{(1)} \cos(\phi_1) + \sum_{k=2}^{K} \left[\cos(\phi_k) I_{k,1}^{II}(d_k^{(1)}, \theta_k) + \sin(\phi_k) I_{k,1}^{QI}(d_k^{(2)}, \theta_k) \right] \right\} + n_1^I \end{aligned} \tag{3.36}$$

where

$$I_{k,1}^{II}(d_k^{(1)}, \theta_k) = \frac{1}{T} d_k^{(1)} R_{k,1}^{II} \cos(\theta_k), \tag{3.37}$$

$$I_{k,1}^{QI}(d_k^{(2)}, \theta_k) = \frac{1}{T} d_k^{(2)} R_{k,1}^{QI} \sin(\theta_k). \tag{3.38}$$

Since we only consider a single symbol transmission in the time interval $[0, T]$, we can simplify the subscript for the data bits, and write Z_1^I as

$$Z_1^I = T\sqrt{P/2}\left\{d_1^{(1)}\cos(\phi_1) + \sum_{k=2}^{K}\left[\cos(\phi_k)I_{k,1}^{II}(d_k^{(1)},\theta_k) + \sin(\phi_k)I_{k,1}^{QI}(d_k^{(2)},\theta_k)\right]\right\} + n_1^I. \tag{3.39}$$

By similar arguments, we have

$$Z_1^Q = T\sqrt{P/2}\left\{d_1^{(2)}\sin(\phi_1) + \sum_{k=2}^{K}\left[\cos(\phi_k)I_{k,1}^{IQ}(d_k^{(1)},\theta_k) + \sin(\phi_k)I_{k,1}^{QQ}(d_k^{(2)},\theta_k)\right]\right\} + n_1^Q \tag{3.40}$$

where

$$I_{k,1}^{IQ}(d_k^{(1)},\theta_k) = \frac{1}{T}d_k^{(1)}R_{k,1}^{IQ}\sin(-\theta_k), \tag{3.41}$$

$$I_{k,1}^{QI}(d_k^{(2)},\theta_k) = \frac{1}{T}d_k^{(2)}R_{k,1}^{QQ}\cos(\theta_k), \tag{3.42}$$

and

$$R_{k,1}^{IQ} = \int_0^T a_k^I(t)a_1^Q(t)dt = T_c\sum_{j=0}^{N-1}a_{k,j}^I a_{1,j}^Q, \tag{3.43}$$

$$R_{k,1}^{QQ} = \int_0^T a_k^Q(t)a_1^Q(t)dt = T_c\sum_{j=0}^{N-1}a_{k,j}^Q a_{1,j}^Q. \tag{3.44}$$

As shown in the system model, we use hard decisions to obtain $\widetilde{c}_1^{(1)}$ and $\widetilde{c}_1^{(2)}$. Thus if $Z_1^I \geq 0$, the receiver decides $\widetilde{c}_1^{(1)} = 0$, otherwise $\widetilde{c}_1^{(1)} = 1$. Similarly, if $Z_1^Q \geq 0$, the receiver decides $\widetilde{c}_1^{(2)} = 0$, otherwise $\widetilde{c}_1^{(2)} = 1$.

3.4.2 Bit Error Probability

Let P_{det_1} and P_{det_2} be the detection error probability of $c_1^{(1)}$ and $c_1^{(2)}$, respectively. The bit error probability P_{det_1} can be written as

$$\begin{aligned}
P_{det_1} &= \frac{1}{2}\left\{P(Z_1^I < 0 \mid c_1^{(1)} = 0) + P(Z_1^I \geq 0 \mid c_1^{(1)} = 1)\right\} \\
&= \frac{1}{2}\left\{P\left[\sqrt{P/2}T(\cos(\phi_1) + I_1^I) + n_1^I < 0\right]\right. \\
&\quad \left. + P\left[\sqrt{P/2}T(-\cos(\phi_1) + I_1^I) + n_1^I \geq 0\right]\right\} \\
&= \frac{1}{2}\left\{P\left[\frac{n_1^I}{\sqrt{P/2}T} < -\cos(\phi_1) - I_1^I\right] + P\left[\frac{n_1^I}{\sqrt{P/2}T} \geq \cos(\phi_1) - I_1^I\right]\right\} \\
&= \frac{1}{2}\left\{P\left[\frac{n_1^I}{\sqrt{P/2}T} + I_1^I < -\cos(\phi_1)\right] + P\left[\frac{n_1^I}{\sqrt{P/2}T} + I_1^I \geq \cos(\phi_1)\right]\right\} \\
&= \frac{1}{2}\left\{1 - P\left[-\cos(\phi_1) \leq \frac{n_1^I}{\sqrt{P/2}T} + I_1^I < -\cos(\phi_1)\right]\right\} \\
&= P\left(-1 \leq n_I + I_I < 1\right) \qquad (3.45)
\end{aligned}$$

where

$$n_I = \frac{2n_1^I}{\sqrt{P/2}T\cos(\phi_1)}, \qquad (3.46)$$

and

$$I_I = \sum_{k=2}^{K} \frac{\cos(\phi_k)}{\cos(\phi_1)} I_{k,1}^{II}(d_k^{(1)}, \theta_k) + \frac{\sin(\phi_k)}{\cos(\phi_1)} I_{k,1}^{QI}(d_k^{(2)}, \theta_k). \qquad (3.47)$$

Let $I = n_I + I_I$ denote the total normalized interference plus noise, and $f_I(x)$ denote its probability density function, then P_{c_1} can be written as

$$\begin{aligned} P_{det_1} &= \int_{-1}^{1} f_I(x)dx \\ &= 2\int_{0}^{1} f_I(x)dx \\ &= 2\int_{0}^{1} \left(\frac{1}{2\pi}\int_{-\infty}^{\infty} \Phi_I(v)e^{-jvx}dv\right)dx \\ &= \frac{2}{\pi}\int_{0}^{1}\int_{0}^{\infty} \Phi_I(v)\cos(vx)dvdx \\ &= \frac{2}{\pi}\int_{0}^{\infty} \Phi_I(v)\int_{0}^{1} \cos(vx)dxdv \\ &= \frac{2}{\pi}\int_{0}^{\infty} \Phi_I(v)v^{-1}\sin(v)dv \end{aligned} \tag{3.48}$$

where $\Phi_I(v)$ is the characteristic function of I, which can be written as $\Phi_I(v) = \Phi_{n_I}(v)\Phi_{I_I}(v)$, the product of the characteristic functions of n_I and I_I. Since n_I is Gaussian with a known characteristic function, we need to derive Φ_{I_I} in order to evaluate P_{c_1}.

Characteristic Function of I_I

If we expand the I-channel and Q-channel interference terms in I_I, we have

$$I_I = \sum_{k=2}^{K} \frac{\cos(\phi_k)}{T\cos(\phi_1)} d_k^{(1)} R_{k,1}^{II} \cos(\theta_k) + \frac{\sin(\phi_k)}{T\cos(\phi_1)} d_k^{(2)} R_{k,1}^{QI} \sin(\theta_k). \tag{3.49}$$

The characteristic function conditioned on ϕ_1 can be written as

$$\begin{aligned}
\Phi_{I_I|\phi_1}(v) &= E\left[\exp\left(jvI_I\right)\right] \\
&= E\left[\exp\left(\frac{jv}{T\cos(\phi_1)}\sum_{k=2}^{K}\cos(\phi_k)\cos(\theta_k)d_k^{(1)}R_{k,1}^{II}\right.\right. \\
&\quad \left.\left.+\sin(\phi_k)\sin(\theta_k)d_k^{(2)}R_{k,1}^{QI}\right)\right] \\
&= \prod_{k=2}^{K}E\left\{\exp\left[\frac{jv}{T\cos(\phi_1)}\left(\cos(\phi_k)\cos(\theta_k)d_k^{(1)}R_{k,1}^{II}\right.\right.\right. \\
&\quad \left.\left.\left.+\sin(\phi_k)\sin(\theta_k)d_k^{(2)}R_{k,1}^{QI}\right)\right]\right\} \\
&= \prod_{k=2}^{K}\frac{1}{16\pi}\left(\triangle_1+\triangle_2\right). \qquad (3.50)
\end{aligned}$$

where

$$\triangle_1=\sum_{d_k^{(1)}}\sum_{d_k^{(2)}}\int_0^{2\pi}\exp\left[\frac{jv}{T\cos(\phi_1)}\left(\cos(\beta-\alpha)\cos(\theta_k)d_k^{(1)}R_{k,1}^{II}+\sin(\beta-\alpha)d_k^{(2)}R_{k,1}^{QI}\right)\right]d\theta_k, \qquad (3.51)$$

and

$$\triangle_2=\sum_{d_k^{(1)}}\sum_{d_k^{(2)}}\int_0^{2\pi}\exp\left[\frac{jv}{T\cos(\phi_1)}\left(\cos(\beta+\alpha)\cos(\theta_k)d_k^{(1)}R_{k,1}^{II}+\sin(\beta+\alpha)d_k^{(2)}R_{k,1}^{QI}\right)\right]d\theta_k. \qquad (3.52)$$

To further simplify $\triangle_1$, consider the four cases for the pair $(d_k^{(1)}, d_k^{(2)})$. Then $\triangle_1$ can be written as

$$\triangle_1=\sum_{i=1}^{4}\int_0^{2\pi}\exp\left(jv\frac{1}{T}\gamma_i\right)d\theta_k \qquad (3.53)$$

where

$$\gamma_1 = \frac{\cos(\beta-\alpha)}{\cos(\phi_1)}\cos(\theta_k)R_{k,1}^{II} + \frac{\sin(\beta-\alpha)}{\cos(\phi_1)}\sin(\theta_k)R_{k,1}^{QI}, \tag{3.54}$$

$$\gamma_2 = \frac{\cos(\beta-\alpha)}{\cos(\phi_1)}\cos(\theta_k)R_{k,1}^{II} - \frac{\sin(\beta-\alpha)}{\cos(\phi_1)}\sin(\theta_k)R_{k,1}^{QI}, \tag{3.55}$$

$$\gamma_3 = -\frac{\cos(\beta-\alpha)}{\cos(\phi_1)}\cos(\theta_k)R_{k,1}^{II} + \frac{\sin(\beta-\alpha)}{\cos(\phi_1)}\sin(\theta_k)R_{k,1}^{QI}, \tag{3.56}$$

$$\gamma_4 = -\frac{\cos(\beta-\alpha)}{\cos(\phi_1)}\cos(\theta_k)R_{k,1}^{II} - \frac{\sin(\beta-\alpha)}{\cos(\phi_1)}\sin(\theta_k)R_{k,1}^{QI}. \tag{3.57}$$

As can be seen, $\gamma_1 = -\gamma_4$, and $\gamma_2 = -\gamma_3$. Therefore,

$$\exp\left(jv\frac{1}{T}\gamma_1\right) + \exp\left(jv\frac{1}{T}\gamma_4\right) = 2\cos\left(\frac{v}{T}\gamma_1\right), \tag{3.58}$$

$$\exp\left(jv\frac{1}{T}\gamma_2\right) + \exp\left(jv\frac{1}{T}\gamma_3\right) = 2\cos\left(\frac{v}{T}\gamma_2\right), \tag{3.59}$$

and we have

$$\begin{aligned}\triangle_1 &= 2\int_0^{2\pi}\cos\left(\frac{v}{T}W_1\right) + \cos\left(\frac{v}{T}W_2\right)d\theta_k \\ &= 2\int_0^{2\pi}\cos\left[\frac{v}{T}\left(\frac{\cos(\beta-\alpha)}{\cos(\phi_1)}\cos(\theta_k)R_{k,1}^{II} + \frac{\sin(\beta-\alpha)}{\cos(\phi_1)}\sin(\theta_k)R_{k,1}^{QI}\right)\right] \\ &\quad + \cos\left[\frac{v}{T}\left(\frac{\cos(\beta-\alpha)}{\cos(\phi_1)}\cos(\theta_k)R_{k,1}^{II} - \frac{\sin(\beta-\alpha)}{\cos(\phi_1)}\sin(\theta_k)R_{k,1}^{QI}\right)\right]d\theta_k.\end{aligned} \tag{3.60}$$

Similarly,

$$\begin{aligned}\triangle_2 &= 2\int_0^{2\pi}\cos\left[\frac{v}{T}\left(\frac{\cos(\beta+\alpha)}{\cos(\phi_1)}\cos(\theta_k)R_{k,1}^{II} + \frac{\sin(\beta+\alpha)}{\cos(\phi_1)}\sin(\theta_k)R_{k,1}^{QI}\right)\right] \\ &\quad + \cos\left[\frac{v}{T}\left(\frac{\cos(\beta+\alpha)}{\cos(\phi_1)}\cos(\theta_k)R_{k,1}^{II} - \frac{\sin(\beta+\alpha)}{\cos(\phi_1)}\sin(\theta_k)R_{k,1}^{QI}\right)\right]d\theta_k.\end{aligned} \tag{3.61}$$

Therefore, the characteristic function of I_I condition on ϕ_1 is given by

$$\begin{aligned}\Phi_{I_I|\phi_1}(v) &= \prod_{k=2}^{K}\frac{1}{8\pi}\int_0^{2\pi}\left\{\cos\left[\frac{v}{T}\left(\frac{\cos(\beta-\alpha)}{\cos(\phi_1)}\cos(\theta_k)R_{k,1}^{II}+\frac{\sin(\beta-\alpha)}{\cos(\phi_1)}\sin(\theta_k)R_{k,1}^{QI}\right)\right]\right. \\ &+\cos\left[\frac{v}{T}\left(\frac{\cos(\beta-\alpha)}{\cos(\phi_1)}\cos(\theta_k)R_{k,1}^{II}-\frac{\sin(\beta-\alpha)}{\cos(\phi_1)}\sin(\theta_k)R_{k,1}^{QI}\right)\right] \\ &+\cos\left[\frac{v}{T}\left(\frac{\cos(\beta+\alpha)}{\cos(\phi_1)}\cos(\theta_k)R_{k,1}^{II}+\frac{\sin(\beta+\alpha)}{\cos(\phi_1)}\sin(\theta_k)R_{k,1}^{QI}\right)\right] \\ &\left.+\cos\left[\frac{v}{T}\left(\frac{\cos(\beta+\alpha)}{\cos(\phi_1)}\cos(\theta_k)R_{k,1}^{II}-\frac{\sin(\beta+\alpha)}{\cos(\phi_1)}\sin(\theta_k)R_{k,1}^{QI}\right)\right]\right\}d\theta_k.\end{aligned} \tag{3.62}$$

Then, by averaging over ϕ_1, we have

$$\Phi_{I_I}(v)=\frac{1}{2}\left(\Phi_{I_I|\phi_1=\beta-\alpha}(v)+\Phi_{I_I|\phi_1=\beta+\alpha}(v)\right). \tag{3.63}$$

As can be seen, the expression for $\Phi_{I_I}(v)$ is complicated, and it is difficult to find a closed form solution. However, it can be computed numerically.

The error probability P_{det_2} can also be computed in a similar way using the characteristic function method. For the error probability P_{det_3} of the third level, we can follow similar analysis as shown in Section 3.3 utilizing the decoding error probability P_{dec_1} and P_{dec_2}. However, we still have to analyze the effect of MAI using the characteristic function analysis. As can be seen, the characteristic function method results in complicated solutions that need to be evaluated numerically. This leads to the analysis of approximating the MAI with Gaussian distribution.

3.4.3 Gaussian Approximation to the MAI

Recall the correlator receiver output in equations (3.39) and (3.40). We can rewrite them as

$$Z_1^I = T\sqrt{P/2}\cdot\cos\phi_1 + W_1^I + n_1^I \tag{3.64}$$

$$Z_1^Q = T\sqrt{P/2}\cdot\sin\phi_1 + W_1^Q + n_1^Q \tag{3.65}$$

where the MAI terms are represented by

$$W_1^I = \sum_{k=2}^{K} W_{k,1}^I = \sum_{k=2}^{K} \sqrt{P/2}\left(\cos\phi_k\cdot\cos\theta_k\cdot R_{k,1}^{II} + \sin\phi_k\cdot\sin\theta_k\cdot R_{k,1}^{QI}\right) \tag{3.66}$$

$$W_1^Q = \sum_{k=2}^{K} W_{k,1}^Q = \sum_{k=2}^{K} \sqrt{P/2}\left(\sin\phi_k\cdot\cos\theta_k\cdot R_{k,1}^{QQ} - \cos\phi_k\cdot\sin\theta_k\cdot R_{k,1}^{IQ}\right) \tag{3.67}$$

with the crosscorrelations of the signature sequences defined as in equations (3.32), (3.34), (3.43), and (3.44). The noise terms n_1^I and n_1^Q are both Gaussian random variables with zero mean and variance $N_0T/4$. As can be seen, the MAI terms are complicated, and as shown in the characteristic function analysis, the probability density function of the MAI is also complicated. In order to simplify the analysis, we apply Gaussian approximation to the MAI assuming the use of random signature sequences [18].

In order to approximate the MAI as Gaussian, we need to find the variance of the MAI. By assuming the use of random signature sequences and following similar arguments for the QPSK case [26], it can be shown that (Appendix D) the variance of W_1^I and W_1^Q is $\frac{(K-1)NPT_c^2}{4}$.

Following the analysis of detection and decoding error probability of the MSD in the single-user case, the approximated detection error probability in the first and second

level can be written as

$$P_{det_1} = \frac{1}{2}\left[Q\left(\sqrt{\frac{2E_s\cos^2(\beta-\alpha)}{N_0+\frac{K-1}{N}E_s}}\right)+Q\left(\sqrt{\frac{2E_s\cos^2(\beta+\alpha)}{N_0+\frac{K-1}{N}E_s}}\right)\right] \quad (3.68)$$

$$P_{det_2} = \frac{1}{2}\left[Q\left(\sqrt{\frac{2E_s\sin^2(\beta-\alpha)}{N_0+\frac{K-1}{N}E_s}}\right)+Q\left(\sqrt{\frac{2E_s\sin^2(\beta+\alpha)}{N_0+\frac{K-1}{N}E_s}}\right)\right] \quad (3.69)$$

where $E_s = PT$ is the symbol energy. Then depending on what error correcting code is used as the component codes, the decoding error probability P_{dec_1} and P_{dec_2} can be obtained using P_{det_1} and P_{det_2}. For the third level, the approximate detection error probability is given by

$$\begin{aligned} P_{det_3} = {} & Q\left(\sqrt{\frac{2E_s\sin^2\alpha}{N_0+\frac{K-1}{N}E_s}}\right)(1-P_{dec_1}-P_{dec_2}) \\ & +\frac{1}{2}\left[1-Q\left(\sqrt{\frac{2E_s\sin^2(2\beta-\alpha)}{N_0+\frac{K-1}{N}E_s}}\right)+Q\left(\sqrt{\frac{2E_s\sin^2(2\beta+\alpha)}{N_0+\frac{K-1}{N}E_s}}\right)\right]P_{dec_1} \\ & +\frac{1}{2}\left[1+Q\left(\sqrt{\frac{2E_s\sin^2(2\beta-\alpha)}{N_0+\frac{K-1}{N}E_s}}\right)-Q\left(\sqrt{\frac{2E_s\sin^2(2\beta+\alpha)}{N_0+\frac{K-1}{N}E_s}}\right)\right]P_{dec_2} \end{aligned} \quad (3.70)$$

Again, the approximate decoding error probability P_{dec_3} can then be obtained using P_{det_3}.

3.4.4 Numerical Examples

The average bit error probability of the overall system, denoted by P_{av}, is defined as

$$P_{av} = \frac{P_{dec_1}\cdot R_1 + P_{dec_2}\cdot R_2 + P_{dec_3}\cdot R_3}{R} \quad (3.71)$$

where R_1, R_2, and R_3 are the code rates of the component codes of the first, second, and third level in the multilevel coding, respectively, and $R = R_1+R_2+R_3$ is the overall rate. Figure 3.17 shows the approximate average bit error probability for different number of

users K from 1 to 5 with $\beta = 45°$, $\alpha = 22.5°$ (symmetric 8-PSK), and $N = 127$ using Gaussian approximation to the MAI and random signature sequences. The component codes are [15,5,3], [15,7,2], and [15,11,1] BCH codes, and the decoding error probability is approximated by the upper bound in equation (3.22). If we change β from 45° to 35°, then as shown in Figure 3.18, the overall performance gets worse than the symmetric constellation case. This is because even though the first level bit has an improvement in the bit error performance, it takes the least part among the three levels (R_1/R) in P_{av} and cannot compensate for the performance loss caused by the increment in the second level bit error probability.

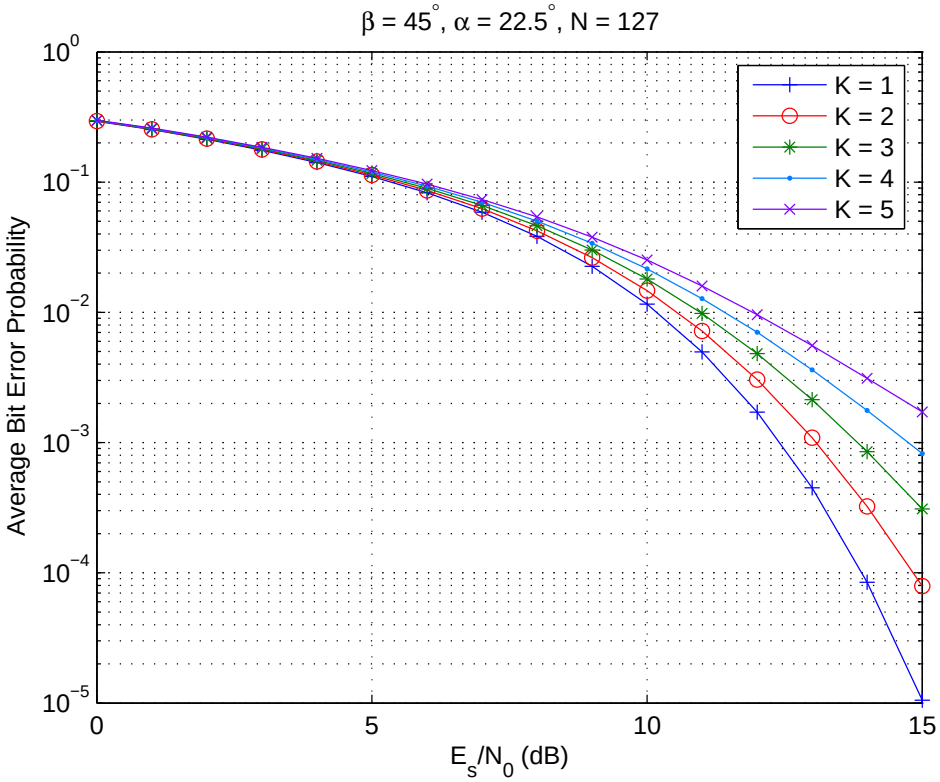

Figure 3.17: Average bit error probability for different number of users.

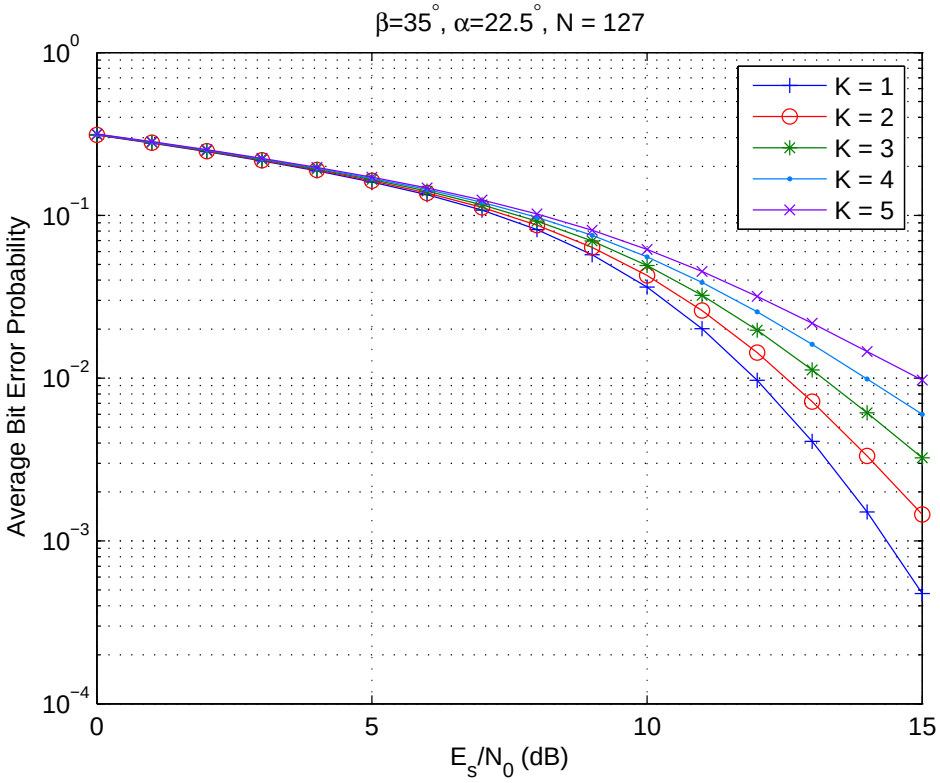

Figure 3.18: Average bit error probability for different number of users.

3.5 Conclusions

In this chapter, we consider the performance of a CDMA system with coded modulation. Multilevel coding (MLC) is used at the transmitter with asymmetric 8-PSK modulation to achieve unequal error protection (UEP). BCH codes are used for encoding, and multistage decoding (MSD) is used at the receiver for data recovery. The approximate bit error performance is obtained by approximating the multiple-access interference (MAI) as a Gaussian random variable and assuming the use of random signature sequences for spreading. The numerical results show that the BCH code upper bound is a good and simple approximation to the bit error performance. It also shows that the symmetric constellation results in a better average bit error probability than that of the asymmetric one. However, the tradeoff is the flexibility in the designing for the UEP capability of the system, which can not be quantified.

CHAPTER 4

Capacity of MLC with 8-PSK Modulation

4.1 Introduction

In this chapter, we analyze the capacity of the MLC scheme and compare it with the case without MLC. From the analysis, we can find situations when substantial performance gain can be obtained when applying MLC in the system.

4.2 Capacity Analysis

4.2.1 MPSK Capacity in AWGN Channel

Let $\mathbf{s} = \{s_0, s_1, \ldots, s_{M-1}\}$ be the set of symbols of a M-ary phase-shift-keying (MPSK) modulation scheme. Consider an AWGN channel with zero mean and variance σ^2 along each dimension. According to [22], the capacity of MPSK with equiprobable occurrence of channel input ($p(S_i) = 1/M \ \forall \ i$) is given by

$$C = \log_2(M) - \frac{1}{M} \sum_{k=0}^{M-1} \int_w \log_2 \left(\sum_{i=0}^{M-1} \exp \left(-\frac{(s_k + w - s_i)^2 - w^2}{2\sigma^2} \right) \right) dw \qquad (4.1)$$

and can be evaluated numerically. Figure 4.1 shows the capacity of MPSK for M=1 (BPSK), 2 (QPSK), and 3 (8-PSK).

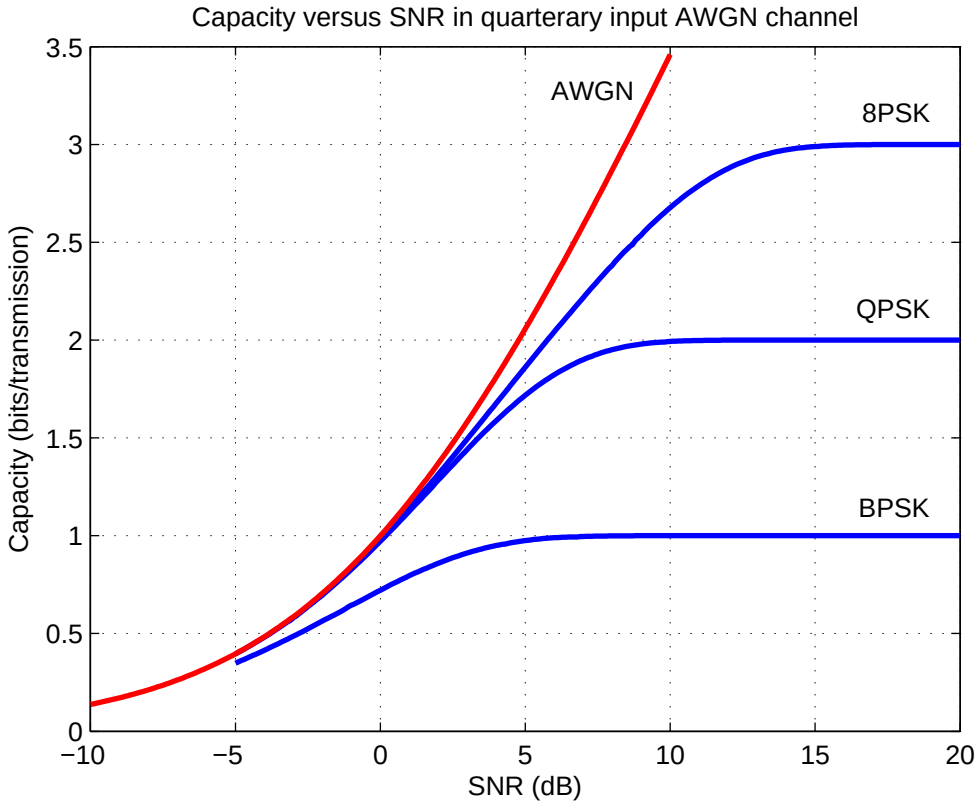

Figure 4.1: Channel capacity of MPSK modulation in AWGN channel.

4.2.2 Capacity of MLC

The MPSK capacity in (4.1) is a general formula for any set of MPSK signals $\mathbf{s}$ (uniform or nonuniform). We are interested in evaluating the capacity of the MLC scheme with nonuniform 8-PSK modulation. Consider the 8-PSK modulation with block partitioning as shown in Figure 4.2.

Let X be the AWGN channel input and Y the output. Let (X_1, X_2, X_3) be the three bits corresponding to the symbol X. Assume all 8-PSK symbols are equiprobable. The mutual information between X and Y is given by

$$\begin{aligned} I(Y;X) &= I(Y;X_1,X_2,X_3) \\ &= I(Y;X_1) + I(Y;X_2|X_1) + I(Y;X_3|X_1,X_2). \end{aligned} \tag{4.2}$$

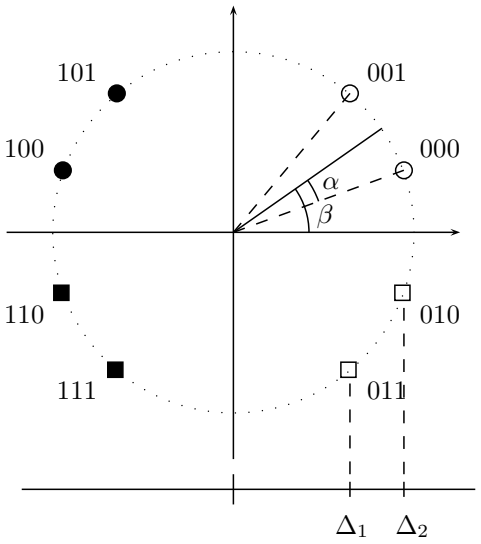

Figure 4.2: Nonuniform 8-PSK modulation with block partitioning.

It can be shown that (see Appendix E)

$$\begin{aligned} I(Y;X_1) &= \frac{1}{2}g_1\left(\frac{\sqrt{E_s}\cdot\cos(\beta+\alpha)}{\sigma},\frac{\sqrt{E_s}\cdot\cos(\beta-\alpha)}{\sigma}\right) \\ &\quad +\frac{1}{2}g_1\left(-\frac{\sqrt{E_s}\cdot\cos(\beta+\alpha)}{\sigma},-\frac{\sqrt{E_s}\cdot\cos(\beta-\alpha)}{\sigma}\right) \end{aligned} \tag{4.3}$$

$$\begin{aligned} I(Y;X_2|X_1) &= \frac{1}{2}g_1\left(\frac{\sqrt{E_s}\cdot\sin(\beta+\alpha)}{\sigma},\frac{\sqrt{E_s}\cdot\sin(\beta-\alpha)}{\sigma}\right) \\ &\quad +\frac{1}{2}g_1\left(-\frac{\sqrt{E_s}\cdot\sin(\beta+\alpha)}{\sigma},-\frac{\sqrt{E_s}\cdot\sin(\beta-\alpha)}{\sigma}\right) \end{aligned} \tag{4.4}$$

where

$$\begin{aligned} g_1(x,y) &= \frac{1}{2\sqrt{2\pi}}\int_{-\infty}^{\infty}\left(e^{-\frac{(u-x)^2}{2}}+e^{-\frac{(u-y)^2}{2}}\right)\cdot \\ &\quad \log_2\left(\frac{2\left(e^{-\frac{(u-x)^2}{2}}+e^{-\frac{(u-y)^2}{2}}\right)}{e^{-\frac{(u-x)^2}{2}}\left(1+e^{-2xu}\right)+e^{-\frac{(u-y)^2}{2}}\left(1+e^{-2yu}\right)}\right)du \end{aligned} \tag{4.5}$$

and

$$I(Y;X_3|X_1,X_2)=\frac{1}{2}g_2\left(\frac{\sqrt{E_s}\cdot\sin\alpha}{\sigma}\right)+\frac{1}{2}g_2\left(-\frac{\sqrt{E_s}\cdot\sin\alpha}{\sigma}\right) \tag{4.6}$$

where

$$g_2(x)=\frac{1}{\sqrt{2\pi}}\int_{-\infty}^{\infty}e^{-\frac{(u-x)^2}{2}}\cdot\log_2\left(\frac{2}{1+e^{-2xu}}\right)du \tag{4.7}$$

Figure 4.3 shows the capacity of the nonuniform 8-PSK MLC scheme when $\alpha = 22.5°$ and $\beta = 45°$, $35°$, $25°$, and $22.5°$. The case $\beta = 45°$ and $\alpha = 22.5°$ shown in Figure 4.3a is actually the uniform 8-PSK constellation and the result is the same as the one shown in Figure 4.1. As can be seen, the nonuniform scheme might result in a smaller capacity, but the capacity in individual levels might be improved compared to the uniform scheme. Figure 4.4 shows the capacity with fixed $\beta = 45°$ and various α values. This is to demonstrate how level 3 (b_3) capacity $I(Y;X_3|X_1,X_2)$ varies with α. It is observed that $I(Y;X_3|X_1,X_2)$ is an increasing function of α, which intuitively makes sense.

4.3 Throughput Analysis

The throughput analysis is complementary to the capacity analysis. The capacity tells us the theoretical limit of the MLC scheme, and the throughput tells us when various channel codes are applied to the MLC scheme, how the system performs in terms of bits per transmission or bandwidth efficiency (bits/sec/Hz).

The throughput of the 8-PSK MLC system at each level is computed as the following. For each level, the bit error probability of detection P_{det_i} is obtained in (3.23), (3.24), and (3.25). With P_{det_i}, the packet error probability can be computed as

$$P_{E_i}=\sum_{j=t_i+1}^{n}\binom{n}{j}P_{c_i}^{j}(1-P_{c_i})^{n-j} \tag{4.8}$$

where t_i is the error-correcting capability of the code, and n is the block length. This

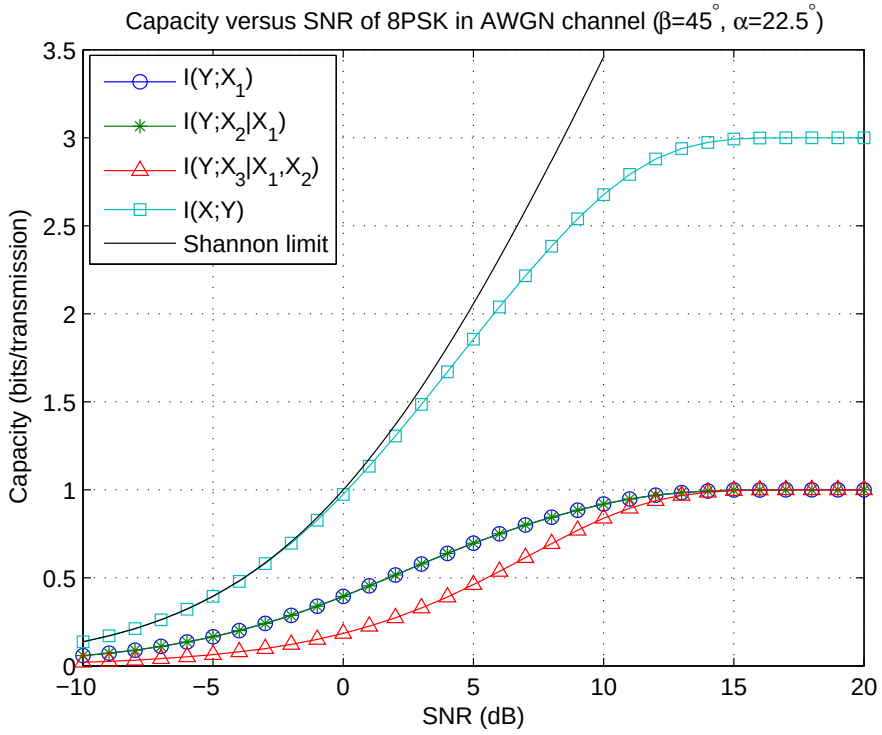

(a)

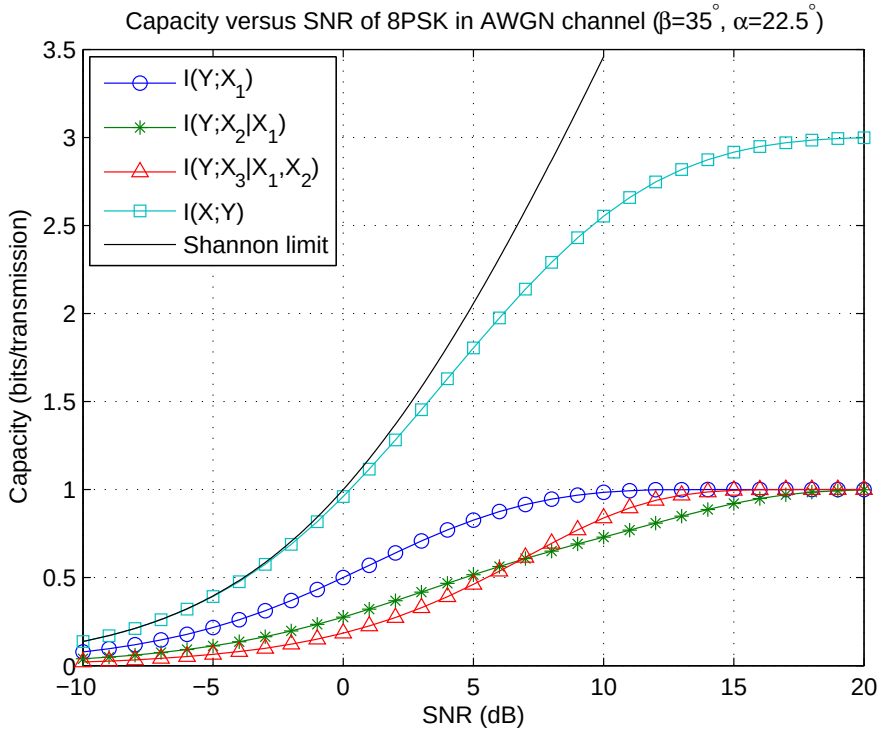

(b)

Figure 4.3: 8-PSK MLC capacity ($\alpha = 22.5°$) (a)$\beta = 45°$ (b)$\beta = 35°$.

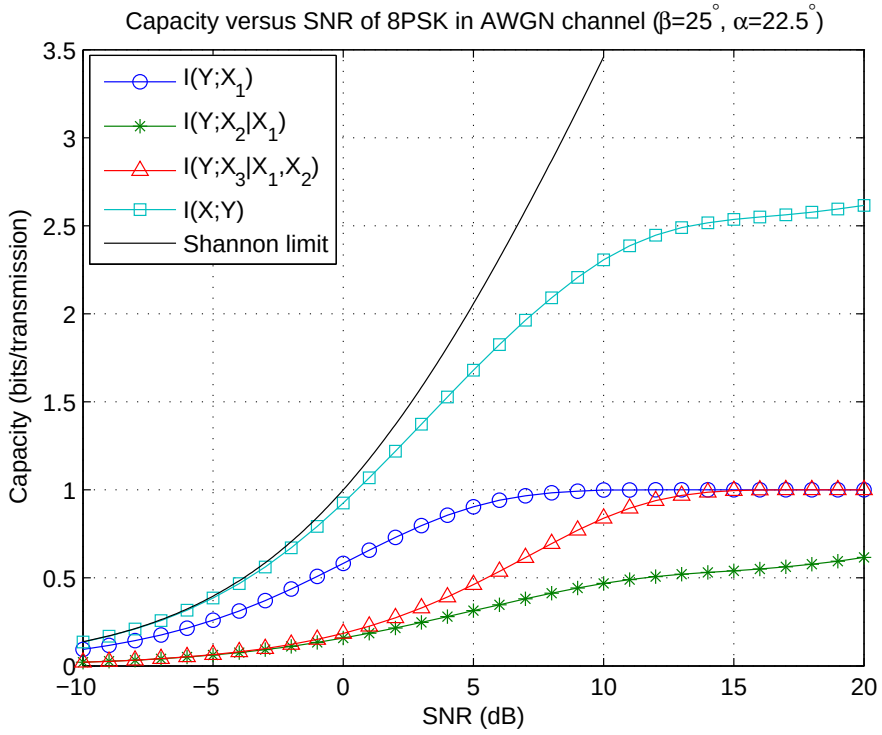

(c)

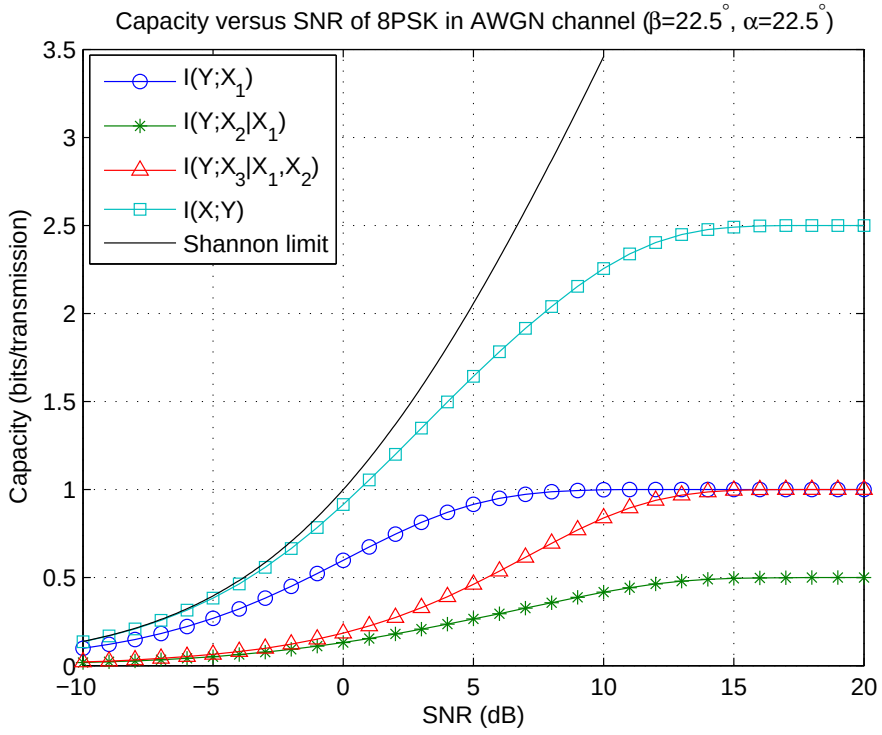

(d)

Figure 4.3: 8-PSK MLC capacity ($\alpha = 22.5°$) (c)$\beta = 25°$ (d)$\beta = 22.5°$.

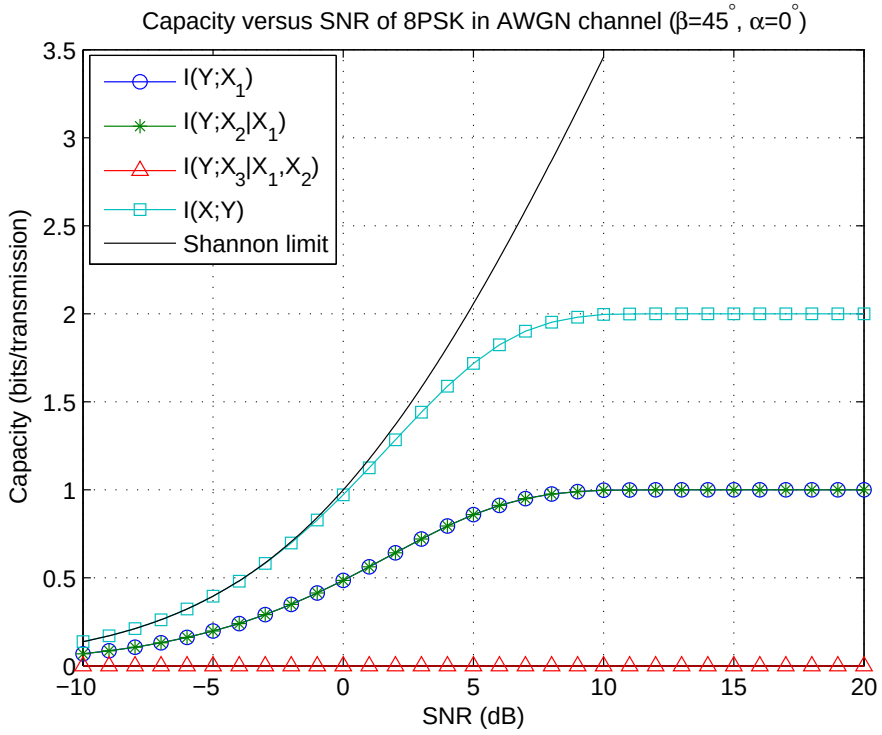

(a)

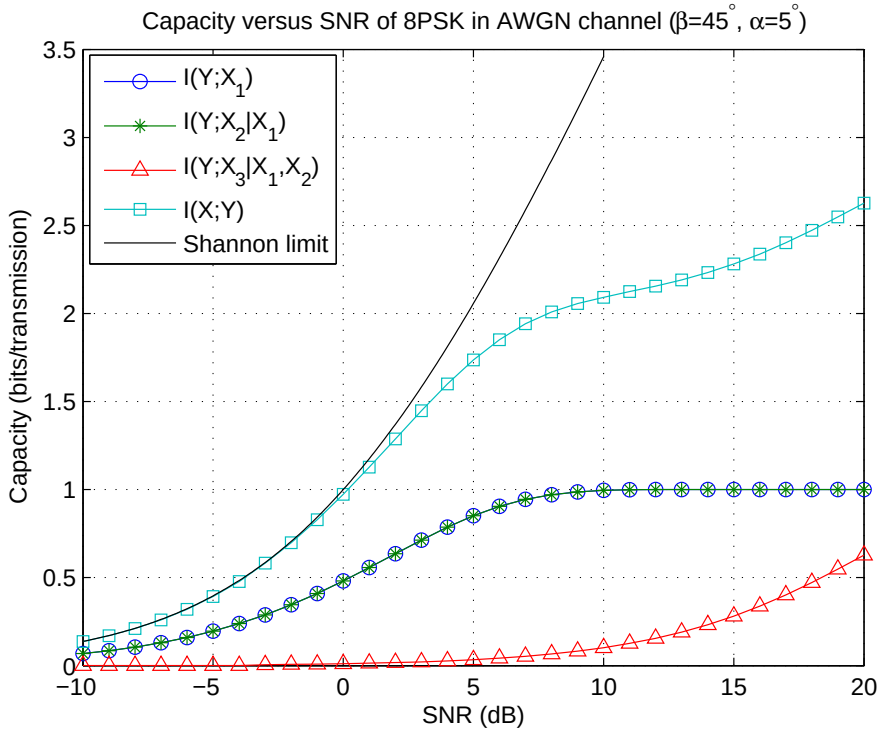

(b)

Figure 4.4: 8-PSK MLC capacity ($\beta = 45°$) (a)$\alpha = 0°$ (b)$\alpha = 5°$.

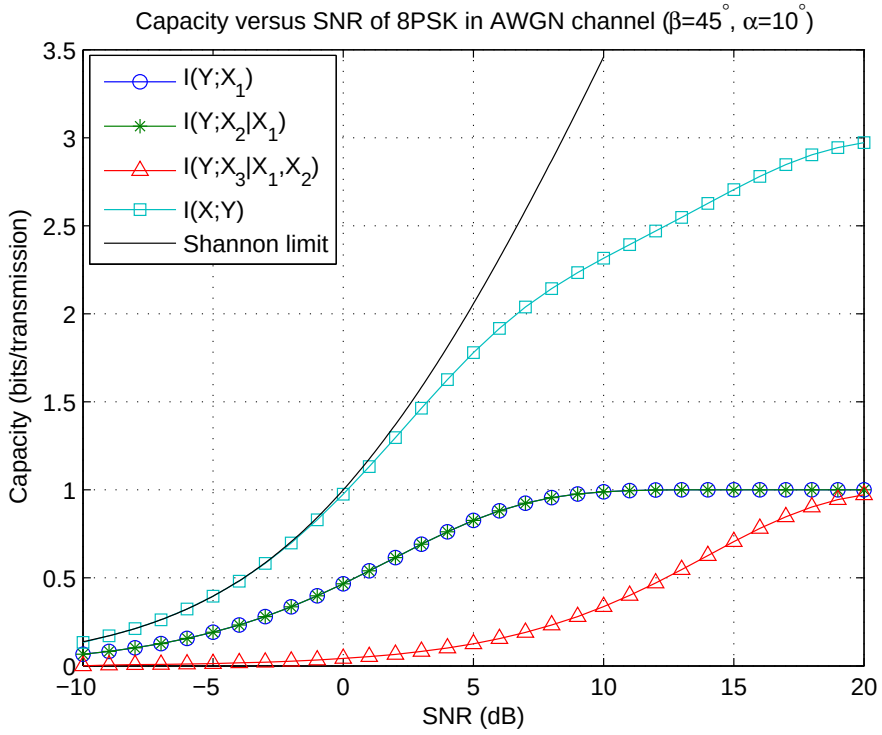

(c)

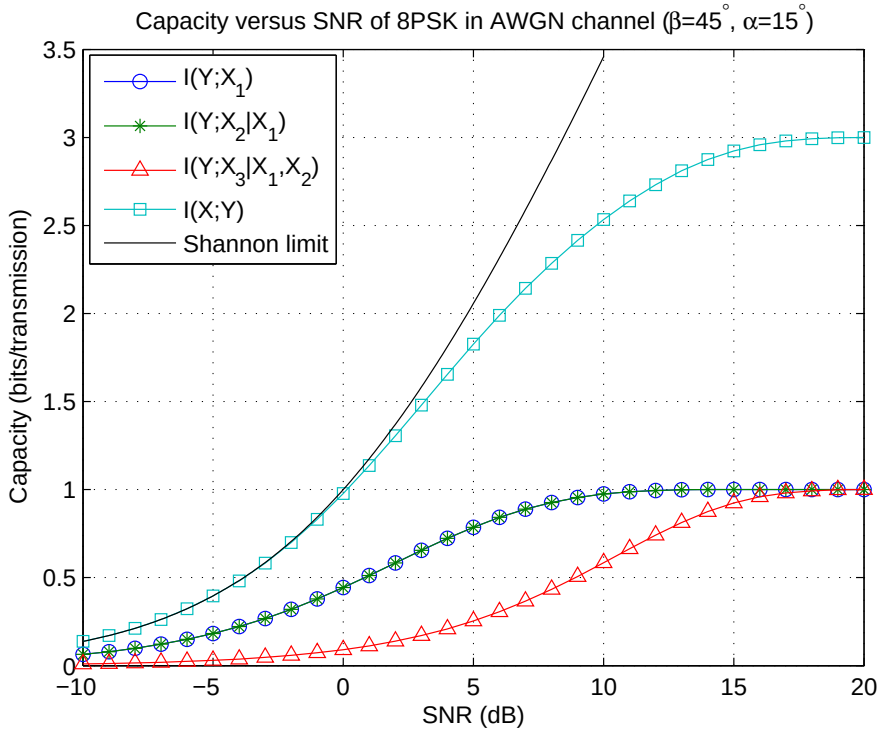

(d)

Figure 4.4: 8-PSK MLC capacity ($\beta = 45°$) (c)$\alpha = 10°$ (d)$\alpha = 15°$.

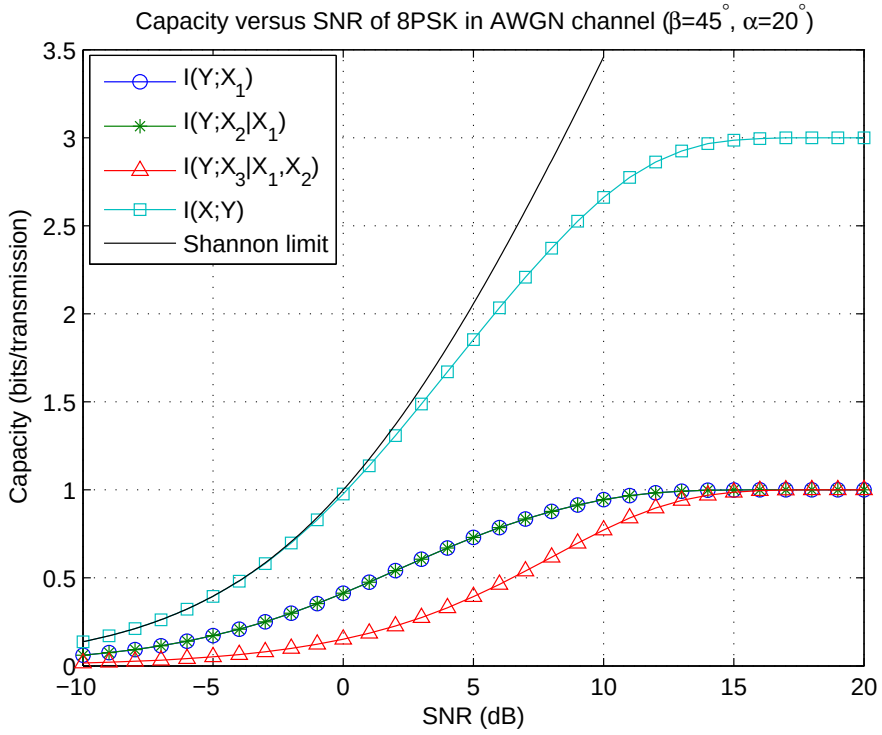

(e)

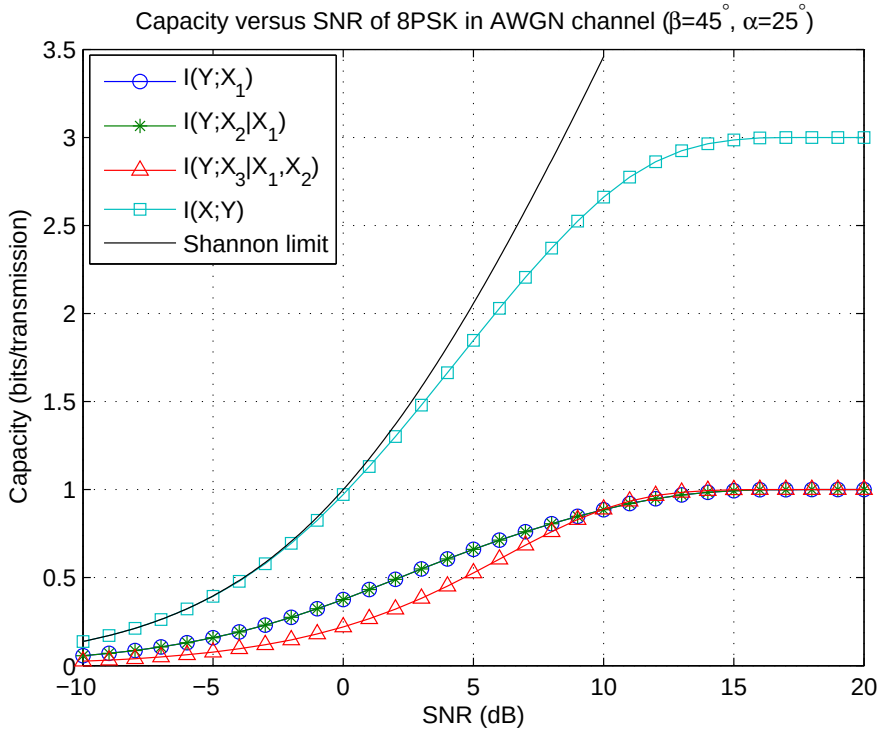

(f)

Figure 4.4: 8-PSK MLC capacity ($\beta = 45°$) (e)$\alpha = 20°$ (f)$\alpha = 25°$.

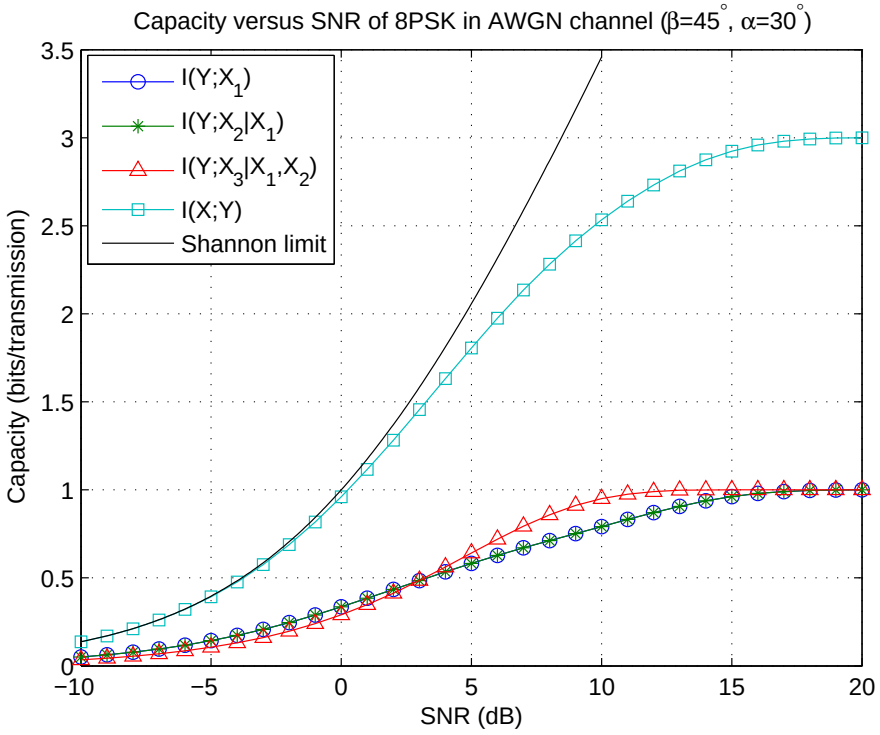

(g)

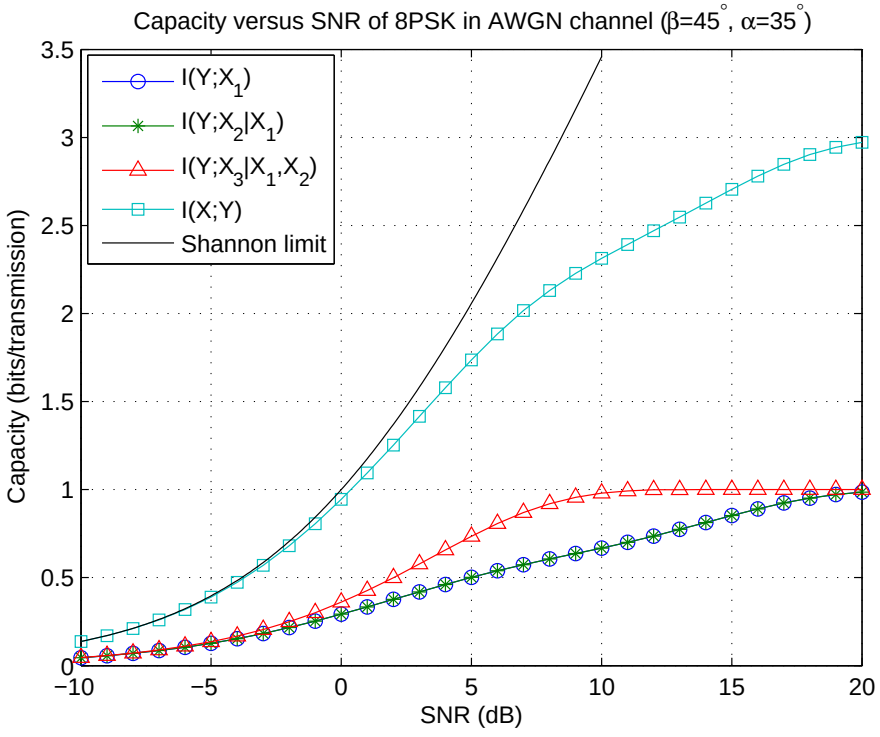

(h)

Figure 4.4: 8-PSK MLC capacity ($\beta = 45°$) (g)$\alpha = 30°$ (h)$\alpha = 35°$.

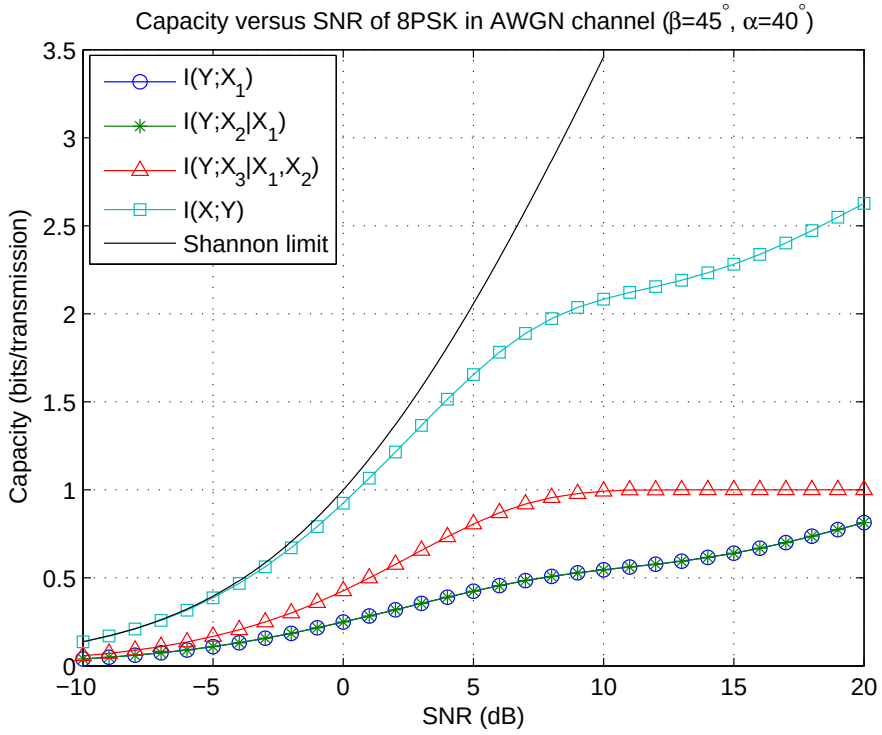

(i)

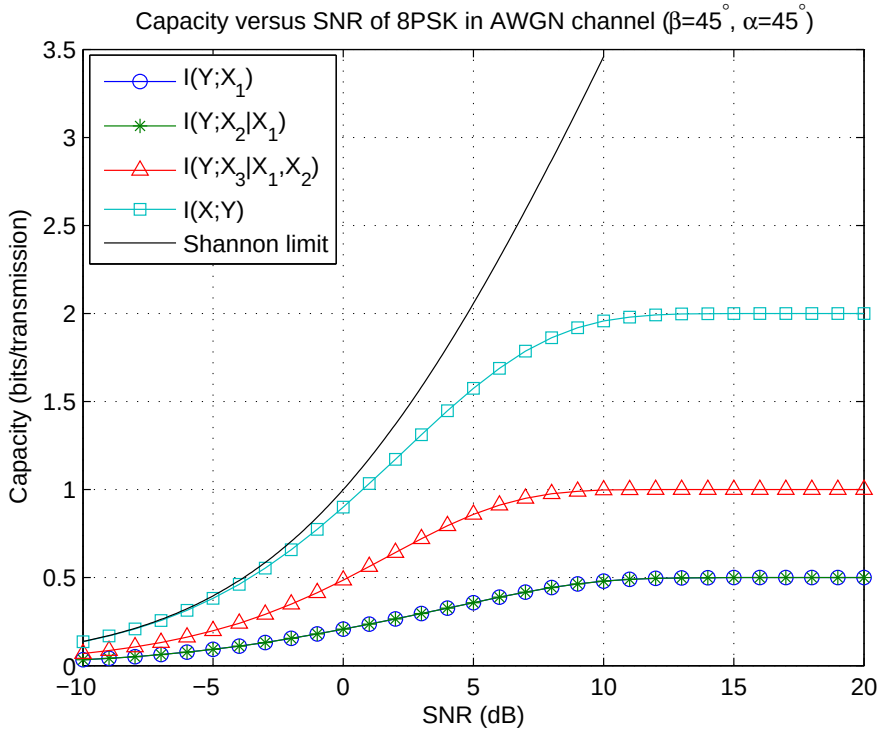

(j)

Figure 4.4: 8-PSK MLC capacity ($\beta = 45°$) (i)$\alpha = 40°$ (j)$\alpha = 45°$.

quantity includes both the cases of undetected errors and failure to decode. The probability of successful transmission of a packet is then given by $P_{S_i} = 1 - P_{E_i}$, and the throughput is given by

$$S_i = R_i P_{S_i} = R_i(1 - P_{E_i}) \tag{4.9}$$

where R_i is the rate of the channel code. The total throughput of the system is given by

$$S = S_1 + S_2 + S_3. \tag{4.10}$$

We want to compare the throughput of the 8-PSK MLC system with the throughput of system employing a regular coding scheme with 8-PSK modulation.

4.3.1 Throughput of 8-PSK with BCH Codes

The regular coding scheme for 8-PSK modulation with a (n, k, t) BCH code is to group every k information bits into the encoder and the output is a block of n bits. Then every three encoded bits are mapped to a 8-PSK symbol for transmission. The receiver demodulates the received symbol and makes a hard decision for detecting the three bits in the symbol. Then the demodulated bits are sent into the decoder for error detection and correction.

For uniform 8-PSK ($\beta = 45°$, $\alpha = 22.5°$) with Gray mapping, the exact bit error probability of the AWGN channel can be evaluated [27]. Then from equations (4.8) and (4.9), the throughput of each level can be computed. In the following, we plot the throughput of the regular coding scheme with BCH codes of block length $n = 15$, 31, and 63, and compare them with 8-PSK capacity and AWGN channel capacity.

Figure 4.5 shows the throughput with all possible BCH codes of length $n = 15$: [15,11,1], [15,7,2], [15,5,3], and [15,1,7]. The first three codes are used in the 8-PSK MLC system described in the previous sections. Notice that the cross-over of the throughput of different codes suggesting that different codes should be used in different

SNR region in order to achieve the maximum throughput.

A similar plot for BCH codes of length $n = 31$ is shown in Figure 4.6. With $n = 31$, there are more codes for various error-correcting capabilities. Again, the crossover of the throughput curves suggests the proper selection of codes depending on the SNR.

Figure 4.7 shows the throughput for BCH codes of length $n = 63$. It can be observed that most of the throughput cross-overs happen between SNR of 5 to 12 dB.

The comparison of the maximum throughput (envelope of the throughput of various codes) for $n = 15$, 31, and 63 BCH codes is shown in Figure 4.8. In the low SNR region, short block length codes have higher throughput than codes of longer length. In the high SNR region, the achievable rate actually depends on the code rate, in which case codes with long block length tend to have high throughput due to more selections of codes with higher rates.

Throughput of 8-PSK MLC with BCH Codes

The throughput of the MLC coded uniform 8-PSK scheme can be obtained in a similar way as the regular coding scheme with different detection error probability and the MSD decoding structure. Figure 4.9 shows the throughput of each level of the MLC scheme with $n = 15$ BCH codes, and the total throughput is shown in Figure 4.10. The comparison of the total throughput of the MLC scheme with the regular coding scheme in shown in Figure 4.11. As can be seen, the MLC scheme outperforms the regular coding scheme in the SNR region from about -6 dB to around 6 dB. At the rate of 0.5 bit/transmission, there is about 3.5 dB gain for the MLC scheme over the regular coding scheme when the block length is 15.

Similar plots are shown in Figure 4.12, Figure 4.13, and Figure 4.14 when three BCH codes of length $n = 31$ ([31,6,7], [31,16,3], and [31,26,1]) are chosen for the MLC scheme. The MLC scheme outperforms the regular coding scheme from SNR of -4 dB to abour 7.5 dB when comparing with $n = 31$ BCH codes, and from around -2 dB to

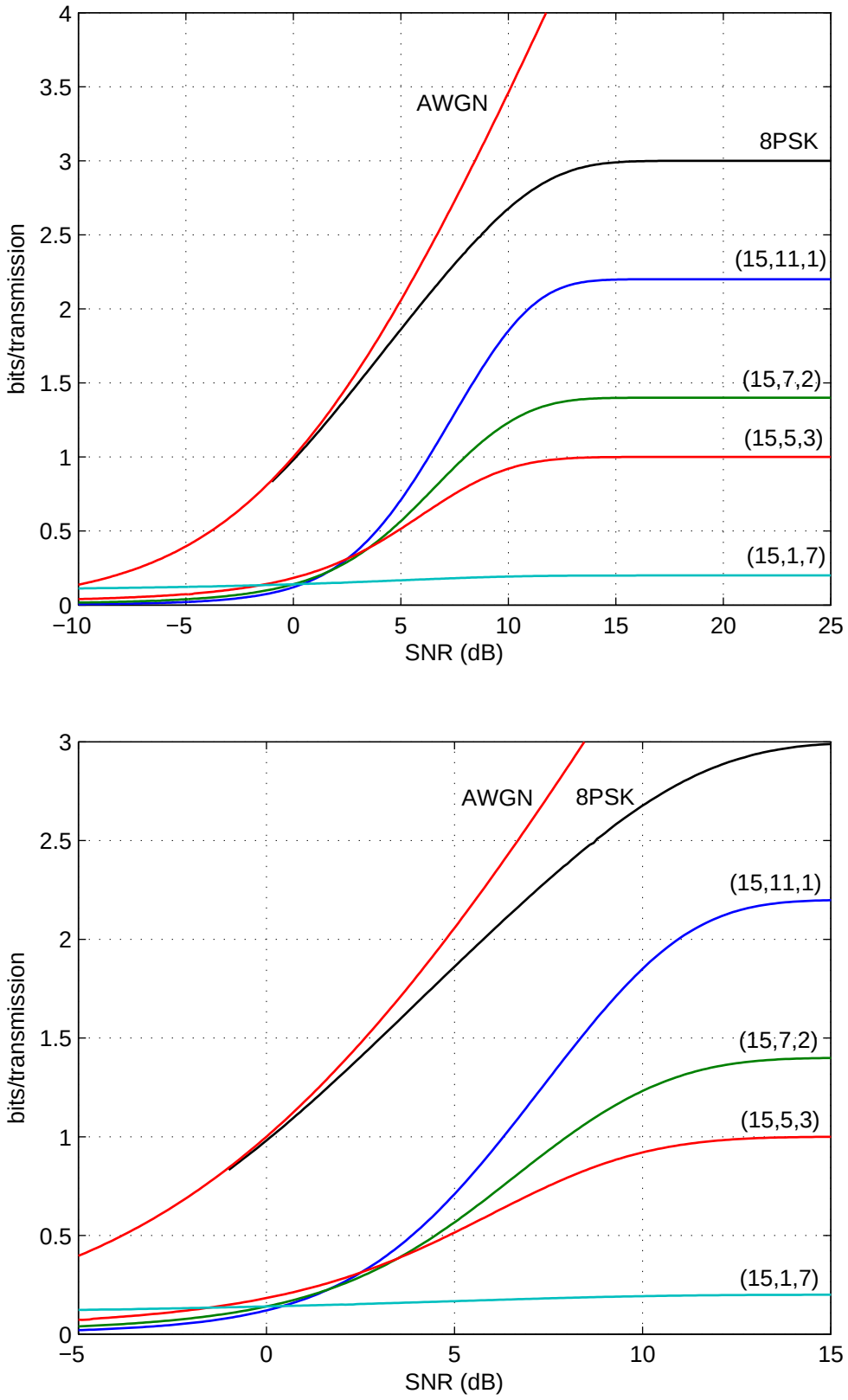

Figure 4.5: Throughput of 8-PSK with $n = 15$ BCH codes.

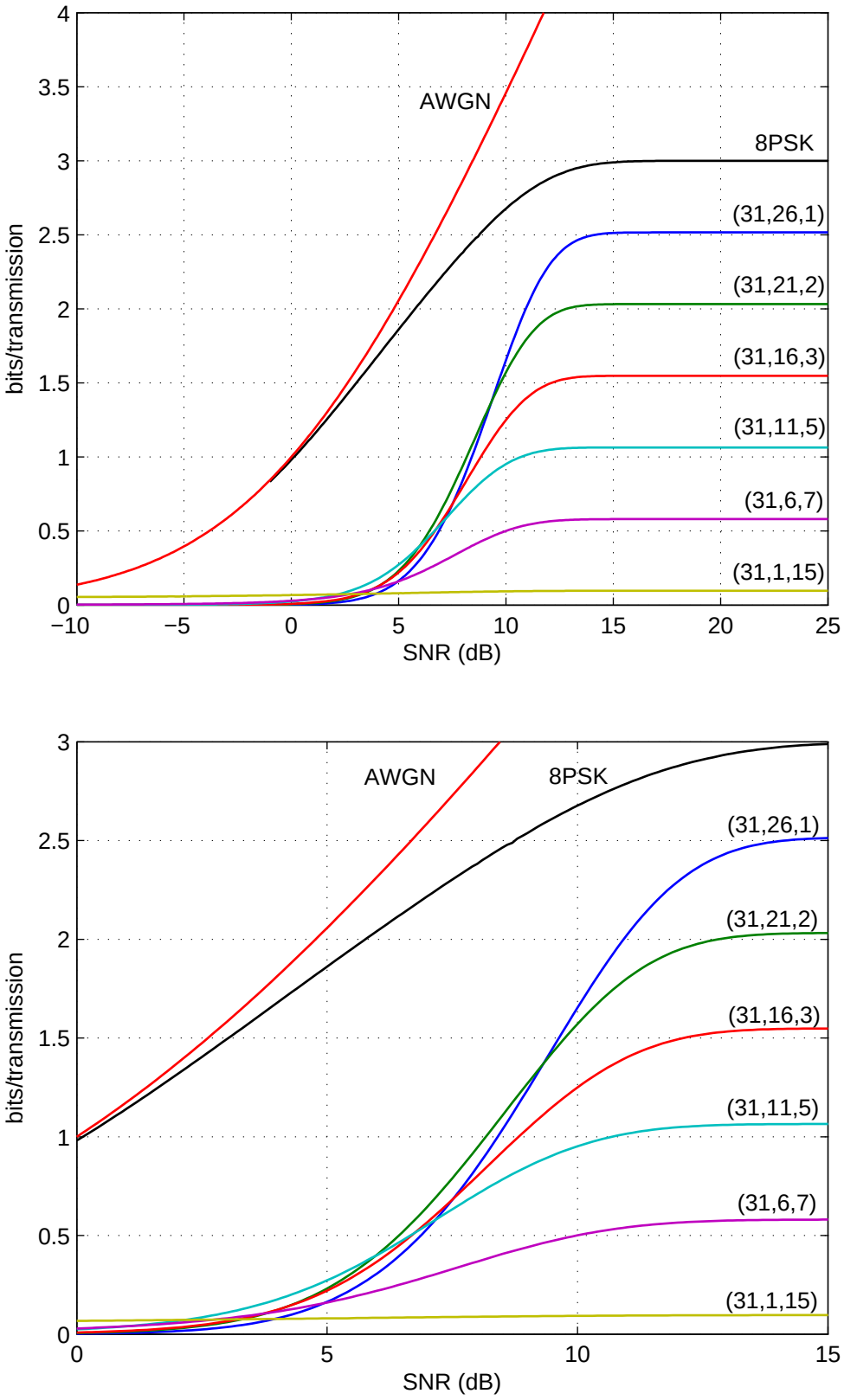

Figure 4.6: Throughput of 8-PSK with $n = 31$ BCH codes.

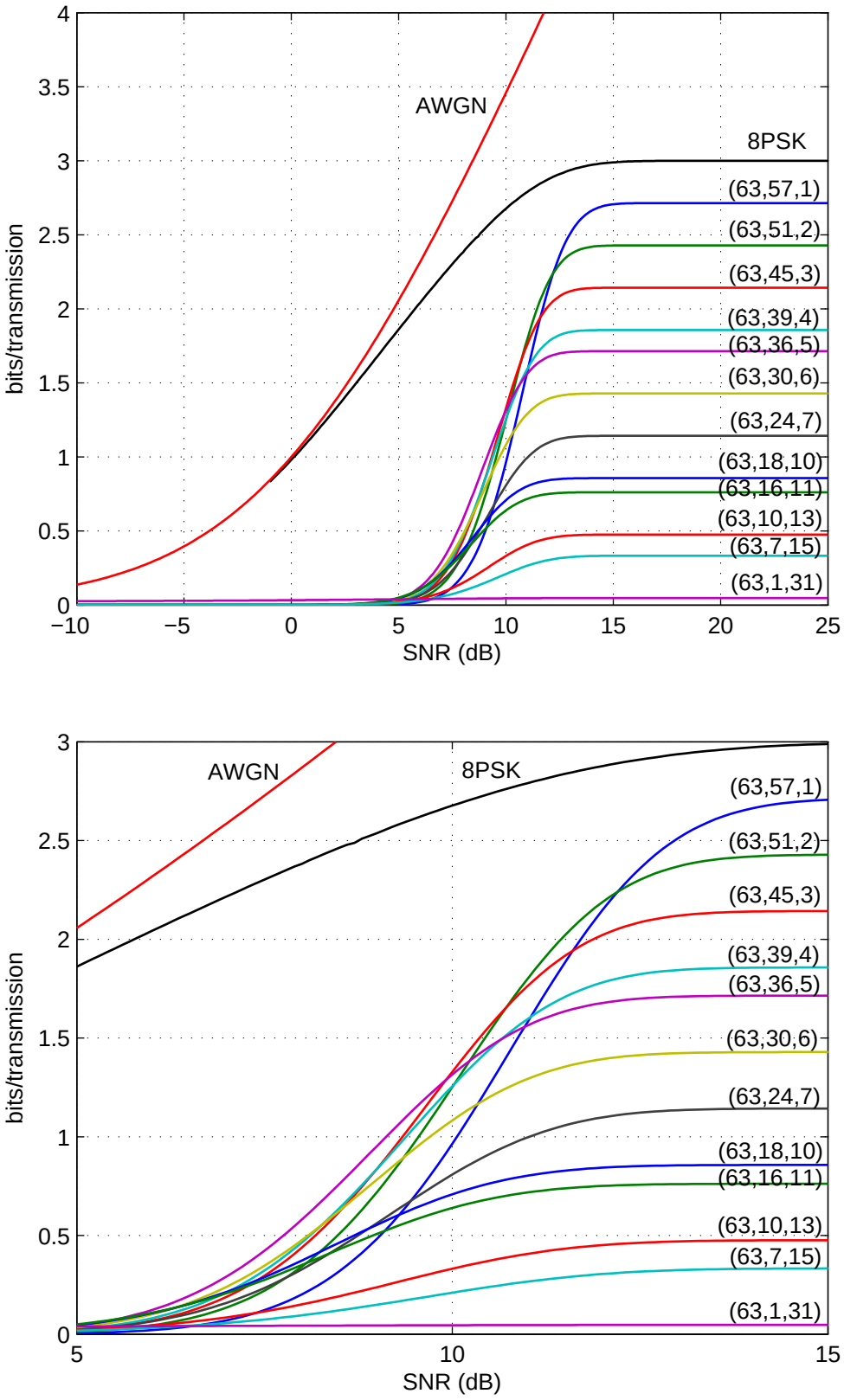

Figure 4.7: Throughput of 8-PSK with $n = 63$ BCH codes.

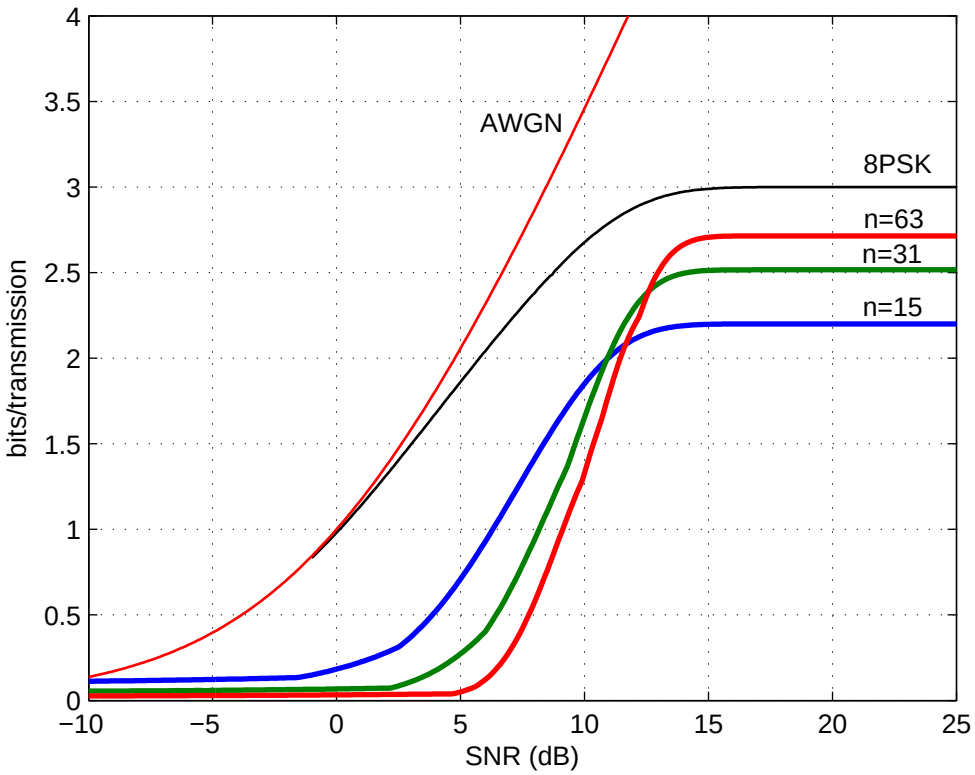

Figure 4.8: Comparison of maximum throughput of 8-PSK with $n = 15$, 31, and 63 BCH codes.

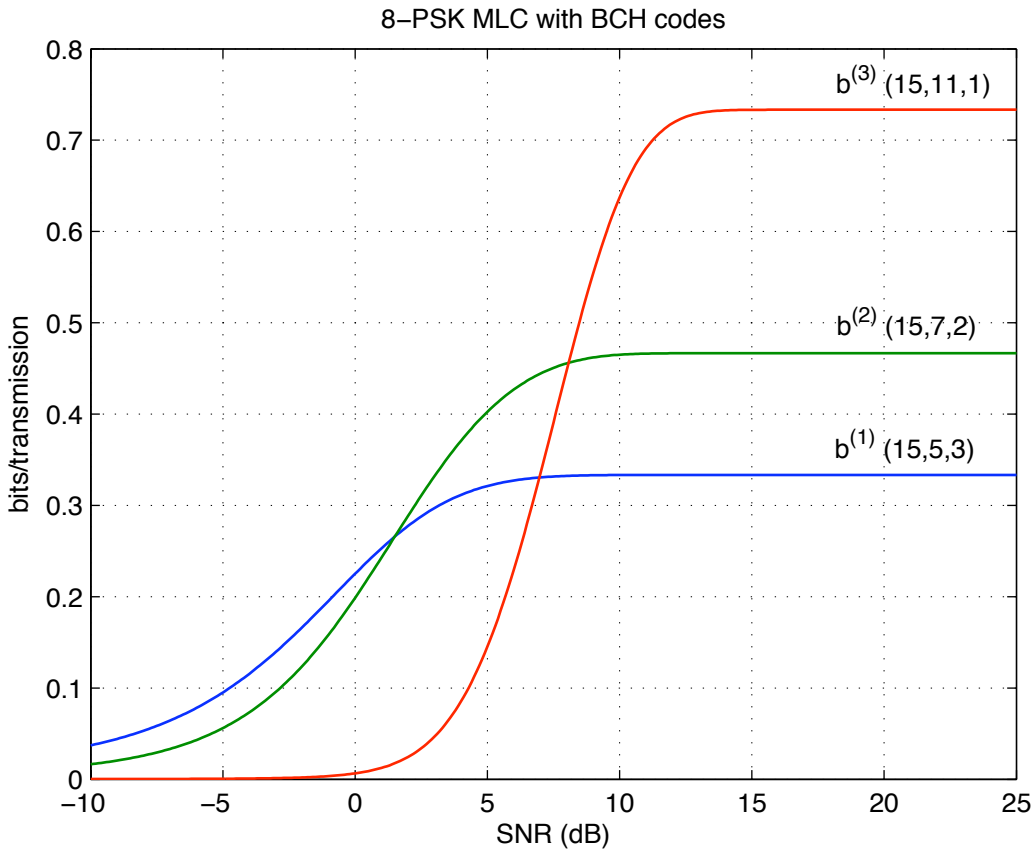

Figure 4.9: Throughput of each level of 8-PSK MLC with BCH codes ($n = 15$).

4 dB when comparing with $n = 15$ BCH codes.

Finally, the comparison of the MLC scheme using $n = 15$ and $n = 31$ codes is shown in Figure 4.15. Note that the total code rates of the two sets of codes are very close. For the $n = 15$ codes, the total rate is $\frac{(5+7+11)}{15} = 1.533$. For the $n = 31$ codes, the total rate is $\frac{(6+16+26)}{31} = 1.548$. As can be seen, the $n = 15$ codes have a higher total throughput throughout the low SNR region up to around 12 dB, the in the high SNR region there is very less difference. This is consistent with the results shown in Figure 4.8 in the regular coding scheme case.

Note that all the throughput plots shown are of the case of uniform 8-PSK constellation. Further improvement of the total throughput may be improved by using non-uniform constellation such that the first level ($b^{(1)}$) bit error rate can be decreased

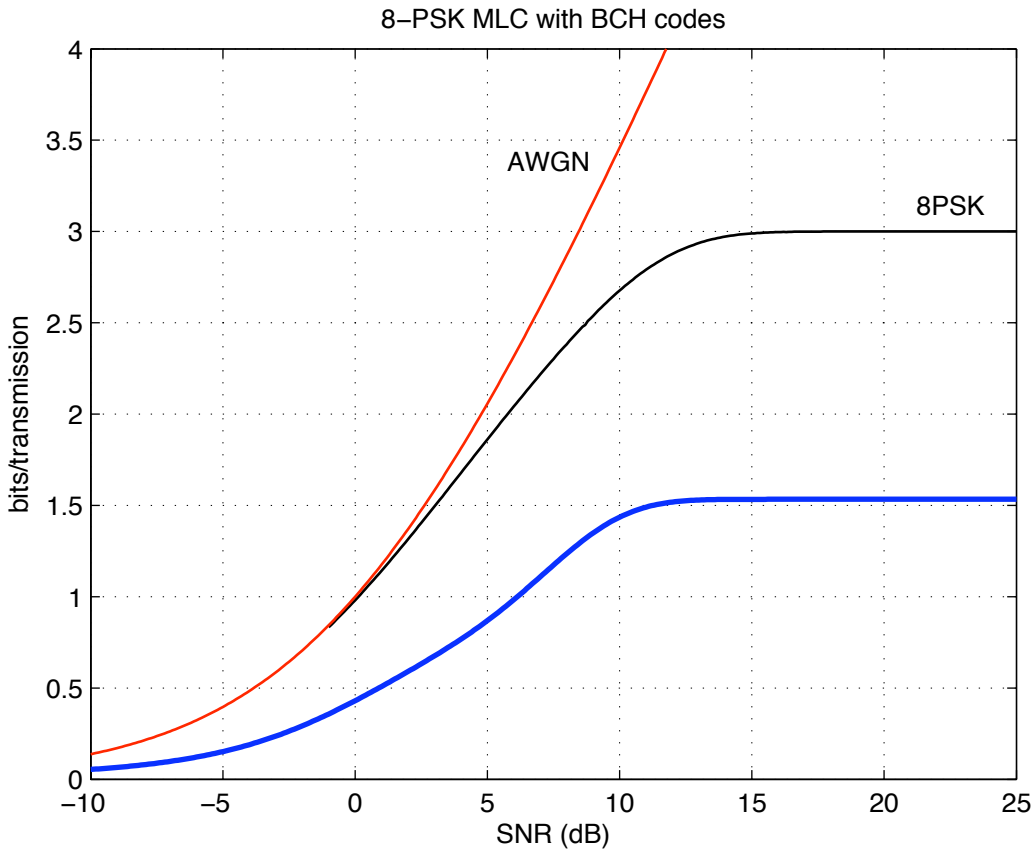

Figure 4.10: Total throughput of of 8-PSK MLC with BCH codes ($n = 15$).

to increase the throughput in the low SNR region.

4.4 Conclusions

In this chapter, we analyze the capacity and throughput of the proposed MLC system with 8-PSK modulation. Numerical results show that the MLC scheme outperforms the regular scheme in the low SNR region by sacrificing the throughput in the high SNR region due to the low reliability on the low level in the MLC scheme.

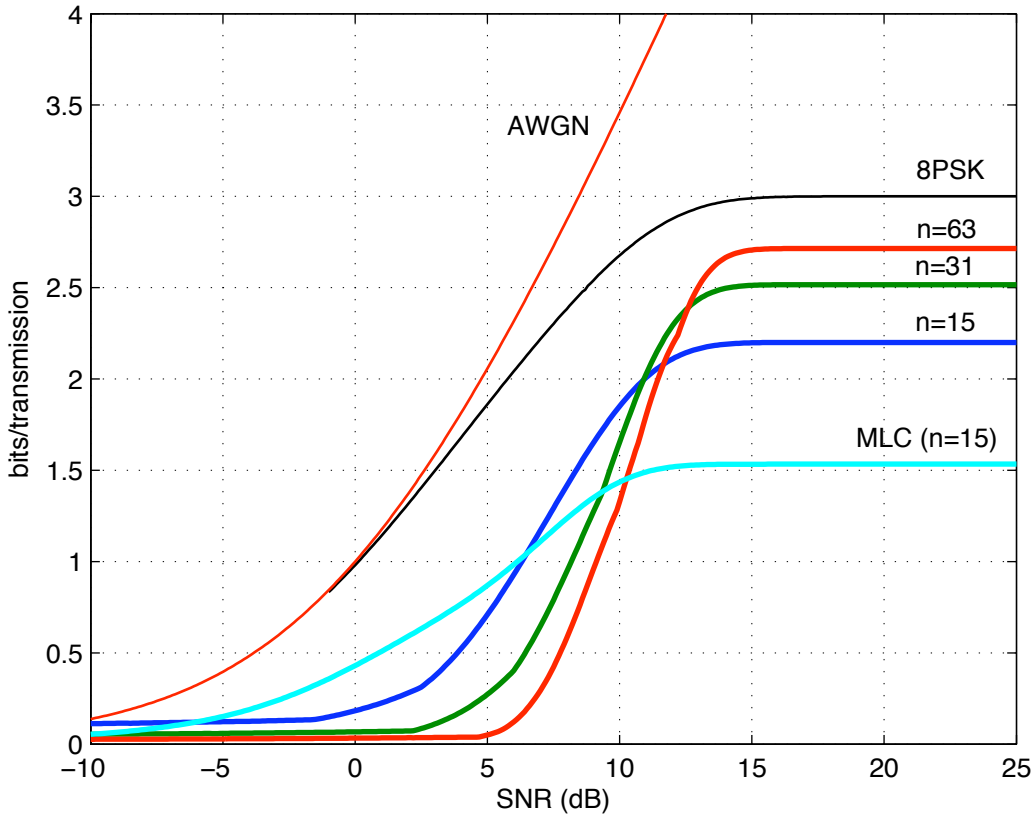

Figure 4.11: Comparison of total throughput for regular coded and MLC coded 8-PSK with BCH codes ($n = 15$).

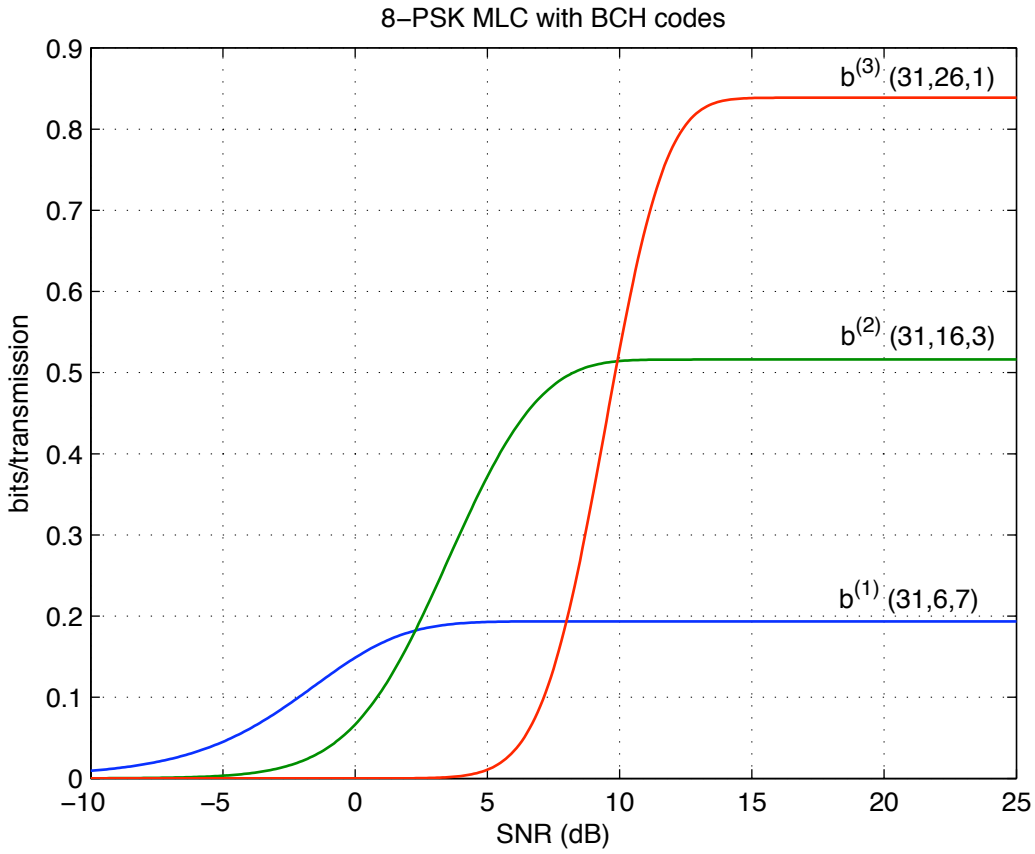

Figure 4.12: Throughput of each level of 8-PSK MLC with BCH codes ($n = 31$).

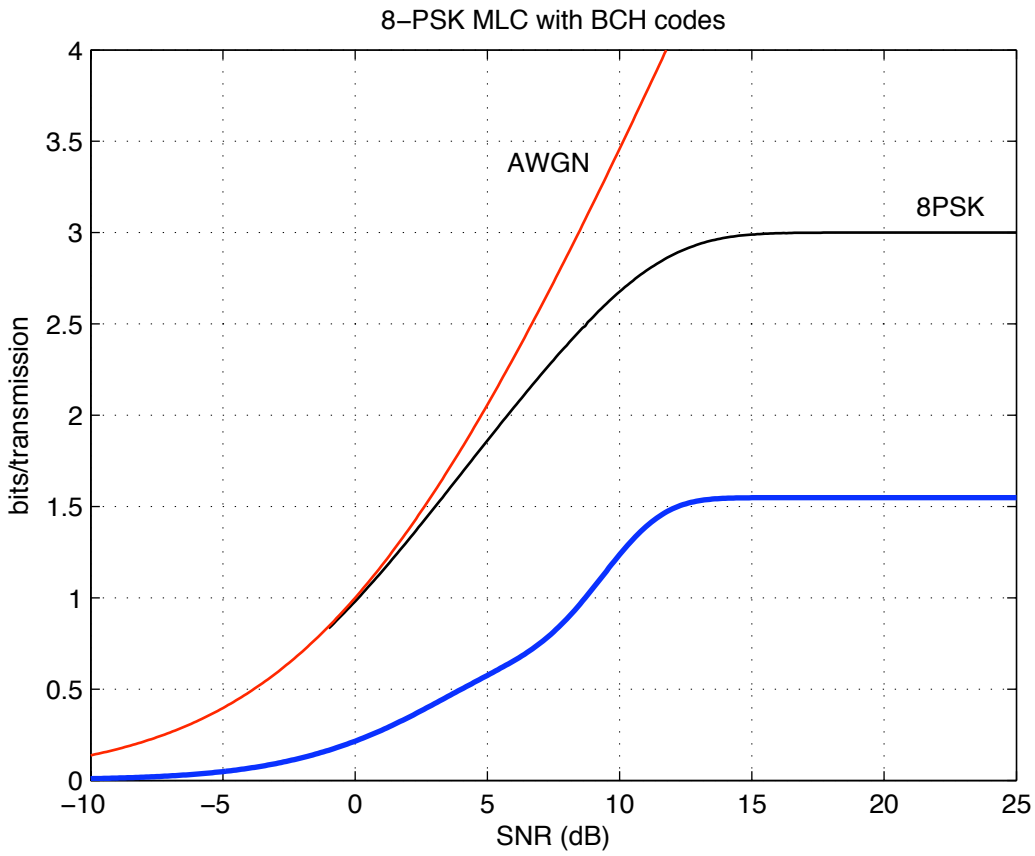

Figure 4.13: Total throughput of of 8-PSK MLC with BCH codes ($n = 31$).

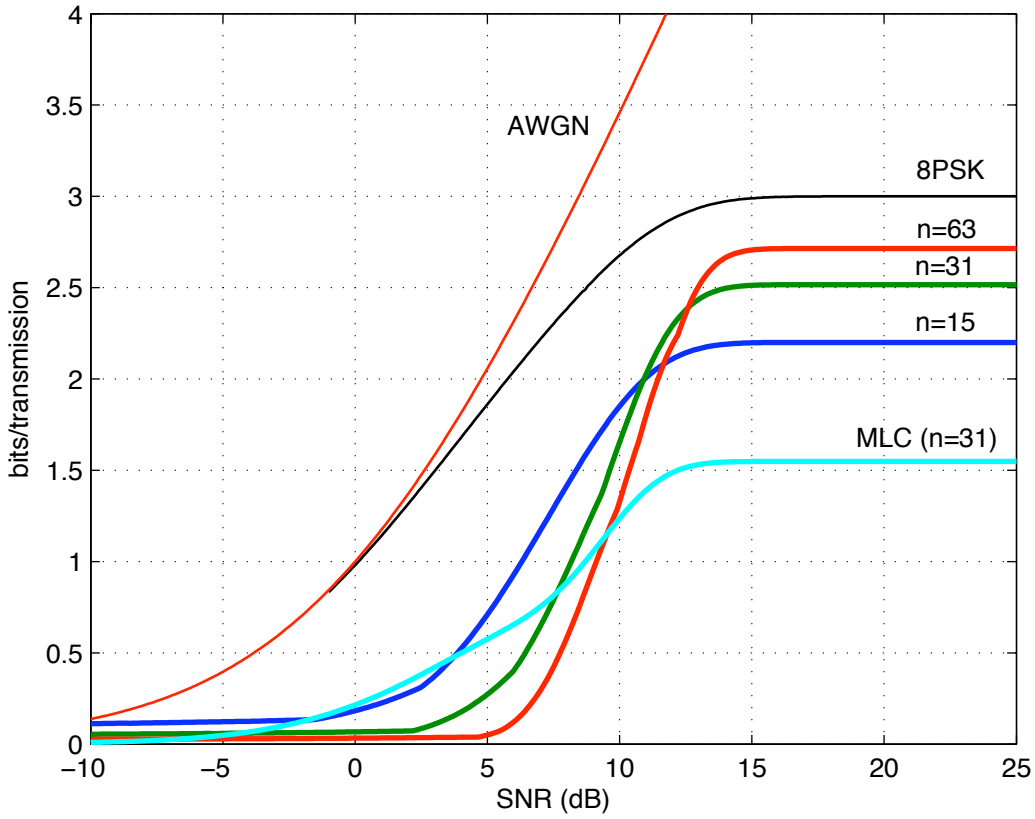

Figure 4.14: Comparison of total throughput for regular coded and MLC coded 8-PSK with BCH codes ($n = 31$).

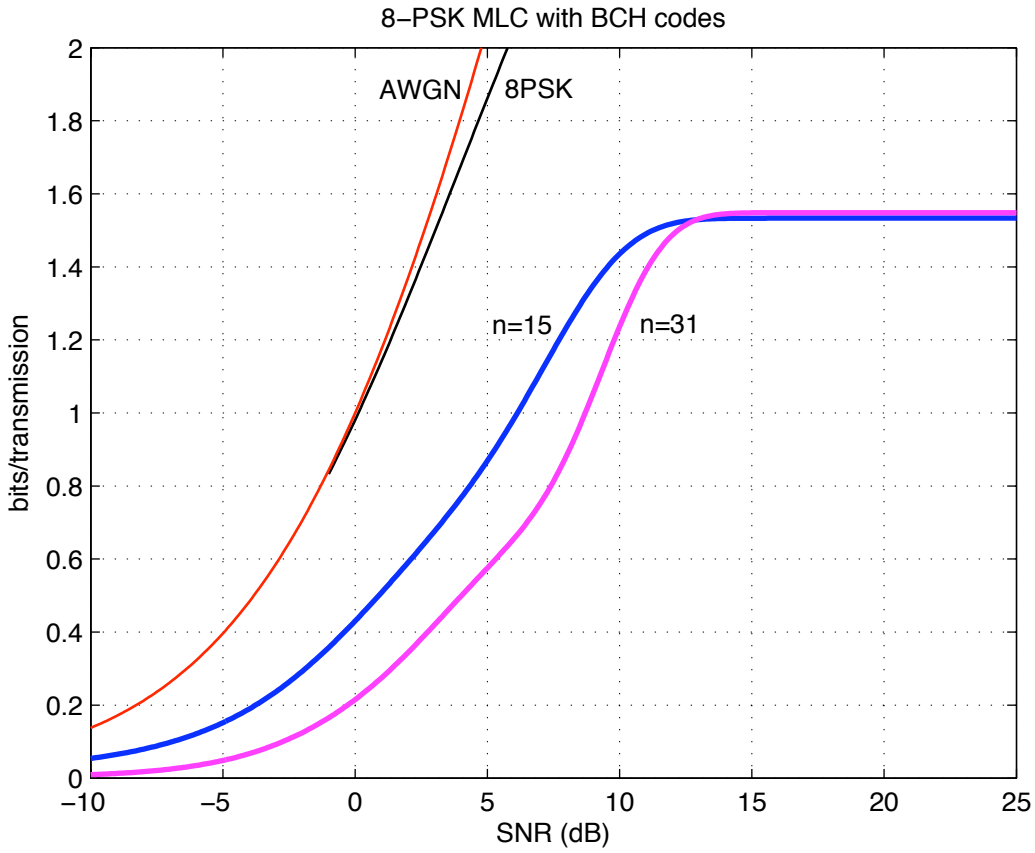

Figure 4.15: Comparison of total throughput for MLC coded 8-PSK with BCH codes of block length $n = 15$ and 31.

CHAPTER 5

Receiver Design for Multiple-Access Ultra-Wideband Communications

5.1 Introduction

One form of ultra-wideband (UWB) communications, originally referred to as impulse radio (IR), involves the transmission of signals that are short pulses with a relatively large fractional bandwidth. These UWB signals possess a bandwidth from over 500 MHz to several GHz that is larger than 25% of the center frequency. The Federal Communications Commission (FCC) and the International Telecommunication Union Radiocommunication Sector (ITU-R) define UWB in terms of a transmission from an antenna for which the emitted signal bandwidth exceeds 500 MHz or 20% of the center frequency. Like a spread spectrum (SS) system, UWB systems use pulse trains to spread energy over the ultra-wide bandwidth. The classical way to modulate data with such signals is to use pulse-position modulation (PPM) on the low duty-cycle pulse trains [28]. Figure 5.1 illustrates the bandwidth comparison of UWB PPM signals and narrowband signals.

For multiple-access communications, assigning different random time-hopping (TH) sequences to different users can be combined with PPM [29]. This TH-PPM scheme was originally proposed for UWB communications. A nice property of this modulation

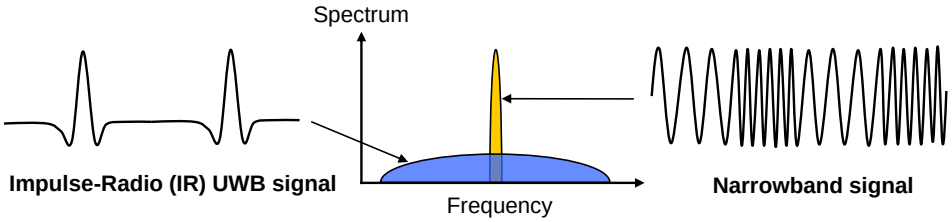

Figure 5.1: UWB vs narrowband signaling.

scheme is the excellent time resolution which comes from the fact that the pulse duration is on the order of a nanosecond. In a multipath environment, this provides the system with resolvable paths of differential delays on the order of the pulse duration. Therefore with appropriate signal processing, the effect of multipath can be mitigated to achieve high system performance.

Since UWB systems have a very large bandwidth, which overlays with other dedicated frequency bands for existing narrowband and wideband systems, the signals from UWB systems would interfere with narrowband and wideband radio systems, and vice versa. The impact of UWB system interference on narrowband systems is examined in [30]. To insure that UWB communications will not affect the already existing narrowband and wideband systems, the FCC has released strict regulations on the power spectral density, peak power, and bandwidth for UWB communication systems. More specifically, the FCC allocated 7.5 GHz of contiguous spectrum (3.1 - 10.6 GHz) for UWB communication systems with a minimum 500 MHz bandwidth regulation on UWB signals of -41.3 dBm/MHz permissible power over the entire 7.5 GHz band. This is shown in Figure 5.2

There are two problems arising from the FCC regulations. The first is that for the assigned spectrum, UWB systems have to be carrier-based systems in order to have the spectrum centered within the 3.1 to 10.6 GHz frequency band. The second problem is that under the low power level regulation, UWB systems are vulnerable to signals from co-existing narrowband and wideband systems, and subsequently encounter serious

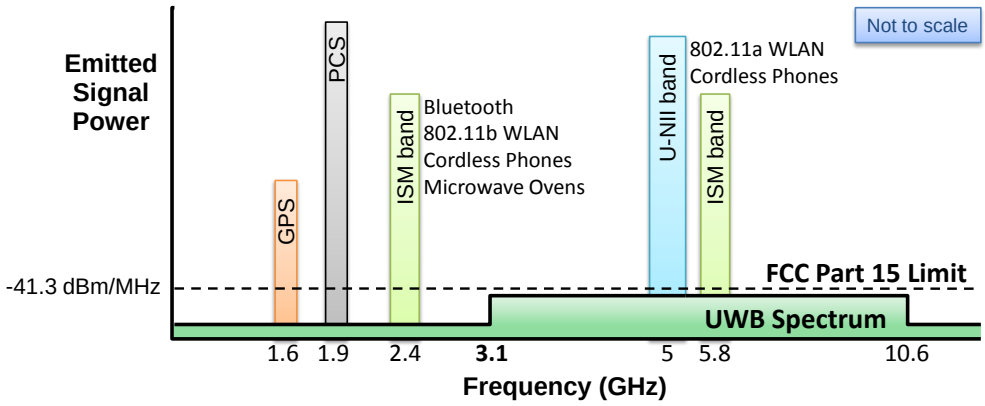

Figure 5.2: UWB spectrum allocation.

problems with the narrowband and wideband interference. This makes the interference mitigation an important issue in UWB communications. In this chapter, we focus on the mitigation of MAI in an AWGN channel.

For these different types of interference, there are different methods proposed in the previous research to deal with them. ISI exists due to the multipath propagation channels. Since UWB systems have a high time resolution, there are more resolvable paths in the receiver which can be utilized for different combining schemes to achieve a better system performance. This leads to the Rake receiver design for UWB systems. The performance of a Rake receiver for a PPM-based single-user UWB system is examined in [31]. For narrowband interference, an interference rejection method based on UWB pulse shape design was proposed in [32]. An interference suppression scheme based on the estimation of interference was proposed in [33]. There is also a linear interference suppression method based on the traditional Rake receiver investigated in [34]. The performance analysis of the multiple-access UWB system is examined in [29], [35], and [36]. In [36], the system performance is evaluated using the Gaussian quadrature rules (GQR) technique, which can overcome the problem of exactly evaluating the probability density function (PDF) of the MAI. For the MAI, an optimum multiuser detection (MUD) scheme is proposed in [37]. As to jamming signal interference, the system per-

formance is evaluated for a single-tone jammer in [38]. In [39], both cases of single-tone and multiple-tone jamming are considered in the system performance analysis.

The problem for the MAI mitigation in the current work lies in the choice of suitable probability model. Many previous research used the Gaussian approximation (GA) to describe the probability model of the MAI. However, as mentioned in [29] and [30], the GA for the distribution of the MAI is not always accurate. Thus the optimum receiver designed using this GA is actually not optimum. Analyzing a system with a GA will likely yield pessimistic results. The advantage of the GA is that the optimum decision rule is simple and the analysis is straightforward. But for an accurate system performance analysis and the actual optimum receiver design, we need to know the actual probability model of the MAI.

The optimum receiver design for UWB communication systems could be complicated due to the required accuracy of time synchronization and various sources of interference, and might not yield a practical receiver. Therefore, we propose a suboptimum receiver with nonlinear interference mitigation such that the complexity can be greatly reduced while the performance is still comparable to the optimum receiver.

The goal of the suboptimum receiver design is to reduce the complexity while preserving the performance very close to the optimum receiver. A suitable approach in the design of the suboptimum receiver for a UWB system is to use the locally optimum Bayes detection (LOBD) theory [40][41]. This is because the UWB signals generally have very low power, which satisfies the small signal per chip assumption in the LOBD algorithm. By using a locally optimum detection approach in a TH-PPM UWB system, the receiver is designed with the structure of having the conventional correlator at the first stage followed by a nonlinear processing element, which works to mitigate the interference. This function depends on the density function of the interference. However, it is not trivial to find the PDF of the total interference.

In this chapter, we look at the case of synchronous multiple-access time-hopping

PPM UWB communication and investigate the suboptimum nonlinear receiver performance by finding the exact PDF of the interference. The rest of the chapter is structured as follows. In Section 5.2, we consider the system model of the TH-PPM UWB system. In Section 5.3, we derive the PDF of the MAI. The receiver design is considered in Section 5.4. We first evaluate the linear receiver performance and check the validity of the Gaussian approximation to the MAI. Then we design the suboptimum receiver using the LOBD algorithm and evaluate the performance. In Section 5.5, we show numerical examples. We state the conclusions in Section 5.6.

5.2 System Model

Consider a multiple-access (MA) time-hopping (TH) pulse position modulation (PPM) ultra-wideband (UWB) communication system. The transmitted signal of the kth user is

$$s^{(k)}(t) = \sum_{j=-\infty}^{\infty} \sqrt{\frac{E_k}{N_s}}\, p(t - jT_f - c_j^{(k)} T_c - d_{\lfloor j/N_s \rfloor}^{(k)} \delta) \tag{5.1}$$

where T_f is the time duration of one *frame* (or say pulse repetition time), E_k is the energy per bit of the kth user, $p(t)$ is the transmitted pulse waveform of unit energy, $\int_0^{T_p} p^2(t)dt = 1$, where T_p is the duration of $p(t)$, $\{c_j^{(k)}\} \in \{0, 1, \cdots, N_c - 1\}$ is the time hopping sequence of the kth user, T_c is the chip duration for time hopping, $\{d_{\lfloor j/N_s \rfloor}^{(k)}\} \in \{0, 1\}$ is the binary data of the kth user, δ is the additional time shift due to PPM, and each data bit is transmitted in N_s consecutive slots. An example of the UWB frame structure is shown in Figure 5.3.

In our model, we assume $T_p = T_c = \delta$. In general, T_f has to be at least $(N_c + 1)T_c$. In the analysis, we assume $T_f = N_s$ by rewriting equation (5.1) as

$$s^{(k)}(t) = \sum_{j=-\infty}^{\infty} \sqrt{\frac{E_k}{N_s}}\, p(t - jT_f - w_j^{(k)} T_c) \tag{5.2}$$

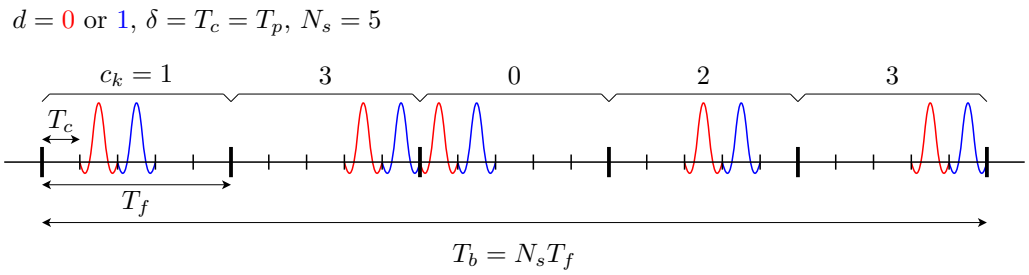

Figure 5.3: UWB frame structure.

where

$$w_j^{(k)} = c_j^{(k)} + d_{\lfloor j/N_s \rfloor}^{(k)} \mod N_c. \tag{5.3}$$

In a single frame, only one pulse, or say *chip*, is transmitted. Therefore, it takes $N_s T_f$ seconds to transmit a single data bit. The bit energy E_k is equally distributed to each chip, thus the power of a user is not increased when N_s increases. Assume there are total N_u users in the system. Then the received signal with just additional white Gaussian noise is

$$\begin{aligned} r(t) &= \sum_{k=1}^{N_u} s^{(k)}(t - \tau_k) + n(t) \\ &= \sum_{k=1}^{N_u} \sum_{j=-\infty}^{\infty} A_k \, p(t - jT_f - c_j^{(k)} T_c - d_{\lfloor j/N_s \rfloor}^{(k)} \delta - \tau_k) + n(t) \end{aligned} \tag{5.4}$$

where $A_k = \sqrt{E_k/N_s}$, τ_k is the time delay of the kth user's signal, and $n(t)$ is the AWGN with zero mean and one-sided power spectral density (PSD) N_0. Furthermore, we assume τ_k's are i.i.d. and uniformly distributed in $[\,0, T_f\,]$. The conventional receiver for the TH-PPM UWB system is the correlator receiver as shown in Figure 5.4. At the receiver of the kth user, the received signal $r(t)$ is correlated with the template signal $v^{(k)}(t) = p(t) - p(t - \delta)$ in each frame. We assume the desired user's receiver has perfect knowledge of the time-hopping sequence of the desired user, but not other users. For the detection of one bit (say $d_0^{(k)}$), the received signal is correlated with the template

signal of the desired user over the bit duration $N_s T_f$. That is,

$$r^{(k)} = \int_0^{N_s T_f} r(t) \left[\sum_{j=0}^{N_s-1} v^{(k)}(t - jT_f - c_j^{(k)} T_c) \right] dt = \sum_{j=0}^{N_s-1} r_j^{(k)} \tag{5.5}$$

where $r_j^{(k)}$ is the component in the jth frame

$$r_j^{(k)} = \int_{jT_f}^{(j+1)T_f} r(t) v(t - jT_f - c_j^{(k)} T_c) dt = s_j^{(k)} + I_j^{(k)} + n_j^{(k)} \tag{5.6}$$

where $s_j^{(k)}$, $I_j^{(k)}$, and $n_j^{(k)}$ are the correlation of $s^{(k)}(t - \tau_k)$, $\sum_{l=1, l\neq k}^{N_u} s^{(l)}(t - \tau_l)$, and $n(t)$ with the template signal in the jth frame, respectively, and can be derived from the following equations.

$$s_j^{(k)} = \int_{jT_f}^{(j+1)T_f} s^{(k)}(t - \tau_k) v(t - jT_f - c_j^{(k)} T_c) dt \tag{5.7}$$

$$I_j^{(k)} = \sum_{l=1, l\neq k}^{N_u} \int_{jT_f}^{(j+1)T_f} s^{(l)}(t - \tau_l) v(t - jT_f - c_j^{(k)} T_c) dt \tag{5.8}$$

$$n_j^{(k)} = \int_{jT_f}^{(j+1)T_f} n(t) v(t - jT_f - c_j^{(k)} T_c) dt. \tag{5.9}$$

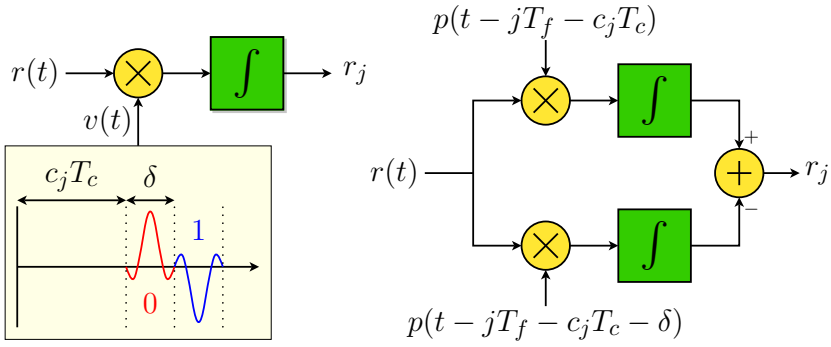

Figure 5.4: Conventional correlator receiver.

At the kth user's receiver, in order to decide if $d_q^{(k)}$ is "0" or "1", we need to observe

$r_j^{(k)}$ for $j = qN_s, qN_s + 1, \cdots, qN_s + N_s - 1$. That is, the decision is based on

$$\left\{ r_j^{(k)} \right\}_{j=qN_s}^{qN_s+N_s-1}.$$

In order to find the decision rule for $d_q^{(k)}$, we need to know the characteristics of $r_j^{(k)}$. First note that since $n(t)$ is AWGN with zero mean and one-sided PSD N_0, $n_j^{(k)}$ is a Gaussian random variable with zero mean and variance $\frac{N_0}{2}\left[2 - 2\int_0^{T_f} p(t)p(t-\delta)dt\right]$.

To derive $s_j^{(k)}$ and $I_j^{(k)}$, notice that they depend on $\{\tau_k\}_{k=1}^{N_u}$, as well as on the transmitted data of the users. Without loss of generality, we consider the receiver for the first user ($k = 1$). We want to make a decision on $d_0^{(1)}$ ($q = 0$) by observing $\{r_0^{(1)}, r_1^{(1)}, \cdots, r_{N_s-1}^{(1)}\}$. We assume $\tau_1 = 0$ and consider the relative delay between user 1 and other users. We also assume perfect knowledge of the channel at the receiver.

Now the problem becomes to characterize the following:

$$r_j^{(1)} = s_j^{(1)} + I_j^{(1)} + n_j^{(1)}$$

for $j = 0, 1, \cdots, N_s - 1$. By the above assumption,

$$s_j^{(1)} = A_1 \left[R_p\left(d_{\lfloor j/N_s \rfloor}^{(1)} \delta \right) - R_p\left((1 - d_{\lfloor j/N_s \rfloor}^{(1)})\, \delta \right) \right] \tag{5.10}$$

where we define $R_p(\tau) = \int_0^{T_f} p(t)p(t-\tau)dt$ as the autocorrelation of the pulse waveform $p(t)$. There are many ways to choose the value of δ. Here we simply choose $\delta = T_p$ so that the PPM pulses maintain orthogonality, i.e. $R_p(\delta) = \int_0^{T_f} p(t)p(t-\delta)dt = 0$. In this case, $R_p\left(d_{\lfloor j/N_s \rfloor}^{(1)} \delta \right) - R_p\left((1 - d_{\lfloor j/N_s \rfloor}^{(1)})\, \delta \right)$ is either 1 ($d_{\lfloor j/N_s \rfloor}^{(1)} = 0$) or -1 ($d_{\lfloor j/N_s \rfloor}^{(1)} = 1$). Thus, we have

$$s_j^{(1)} = \begin{cases} A_1, & d_{\lfloor j/N_s \rfloor}^{(1)} = 0 \\ -A_1, & d_{\lfloor j/N_s \rfloor}^{(1)} = 1. \end{cases} \tag{5.11}$$

Note that in this case, the variance of $n_j^{(k)}$ can be simplified as $\mathrm{Var}[n_j^{(k)}] = N_0$, and

therefore $n_j^{(k)}$ is Gaussian with zero mean and variance N_0. In the next section, we will characterize the interference term $I_j^{(1)}$.

5.3 Synchronous Multiple Access UWB Communications

In this section we consider the synchronous multiple-access (MA) TH-PPM UWB system, i.e., $\tau_1 = \tau_2 = \cdots = \tau_{N_u} = 0$, and derive the probability distribution of the interference. By assuming that all users are independent, the interference from all other users to user 1 over the N_s frames $\{I_k^{(1)}\}_{k=2}^{N_u}$ are independent and identically distributed (i.i.d.), and thus we only need to consider the interference from a specific user k.

In order to simplify the analysis for the distribution of the MAI, we need to make a further assumption, or equivalently, we look at a special case of this system. Assume that $T_f = N_c T_c$ and $T_p = T_c = \delta$. Also assume that the pulse waveform is rectangular. That is

$$p(t) = \begin{cases} \frac{1}{\sqrt{T_p}}, & 0 \le t \le T_p \\ 0, & \text{otherwise.} \end{cases} \tag{5.12}$$

Furthermore, in order to make the pulse waveform uniformly distributed within one frame duration, we define

$$w_j^{(k)} = c_j^{(k)} + d_{\lfloor j/N_s \rfloor}^{(k)} \mod N_c \tag{5.13}$$

In this case, the transmitted signal of the user becomes

$$s^{(k)}(t) = \sum_{j=-\infty}^{\infty} \sqrt{\frac{E_k}{N_s}}\, p(t - jT_f - w_j^{(k)} T_c) \tag{5.14}$$

Here we use the rectangular pulse shape so that we can have a closed form solution

of the interference PDF. The analysis shown here can be extended to other different kind of pulses, such as a Gaussian monocycle.

Consider the communication during the time from 0 to $N_s T_f$, which is the time to transmit a single bit. This time interval corresponds to the data bit $d_0^{(k)}$ of the kth user. Since we only consider a single bit transmission, we eliminate the subscript 0 and simply use $d^{(k)}$ to represent the data bit. For a given data bit $d^{(k)}$ of the kth user being transmitted, there are N_s frames. The interference from these N_s frames $I_{0,k}^{(1)}, I_{1,k}^{(1)}, \cdots, I_{N_s-1,k}^{(1)}$ are assumed to be identically distributed, but they are not independent since they all contain the information of the same data bit $d^{(k)}$ being transmitted by the kth user. However, they are conditionally independent when conditioned on $d^{(k)}$. In later analysis, we will show that the identical distribution assumption of the interference terms is not necessary.

We first consider the case when $d^{(k)} = 0$. In this case, the total shift of the pulse in the N_s frames of the kth user $\{w_j^{(k)}\}_{j=0}^{N_s-1}$ equals the time-hopping sequence of the kth user $\{c_j^{(k)}\}_{j=0}^{N_s-1}$. Therefore $\{w_j^{(k)}\}_{j=0}^{N_s-1}$ are uniformly distributed over $[0, N_c - 1]$. The time shift of the template signal of user 1 is simply the time-hopping sequence of user 1, $\{c_j^{(1)}\}_{j=0}^{N_s-1}$. Let X_j be the random variable of the time shift difference between user 1 and user k. That is, define

$$X_j = w_j^{(k)} - c_j^{(1)} = c_j^{(k)} - c_j^{(1)}. \tag{5.15}$$

Note that $c_j^{(k)}$'s are independent due to the randomness of the time hopping sequence. Thus, X_j is a discrete random variable ranging from $-(N_c - 1)$ to $N_c - 1$ with the probability distribution

$$P(X_j = x) = \begin{cases} \frac{N_c - |x|}{N_c^2}, & x = -(N_c - 1), \cdots, N_c - 1 \\ 0, & \text{otherwise.} \end{cases} \tag{5.16}$$

Given that $d^{(k)} = 0$, the pulses of the kth user will overlap with the template pulse of user 1 only when X_j is either 0 or 1. Therefore, the conditional density function is then given by

$$f_{I_{j,k}^{(1)}|d^{(k)}}(x|0) = \frac{1}{N_c}\delta(x - A_k) + \frac{N_c - 1}{N_c^2}\delta(x + A_k) + \left(\frac{N_c - 1}{N_c}\right)^2 \delta(x). \tag{5.17}$$

Now define the total interference of user k to user 1 during the N_s frames as $I_k^{(1)} = \sum_{j=0}^{N_s-1} I_{j,k}^{(1)}$. Given $d^{(k)} = 0$, $I_{j,k}^{(1)}$'s are independent. Thus the characteristic function (CF) of $I_k^{(1)}$ is the product of the CF's of $I_{j,k}^{(1)}$'s, i.e.

$$\Phi_{I_k^{(1)}|d^{(k)}}(v) = \prod_{j=0}^{N_s-1} \Phi_{I_{j,k}^{(1)}|d^{(k)}}(v) = \left[\Phi_{I_{0,k}^{(1)}|d^{(k)}}(v)\right]^{N_s} \tag{5.18}$$

where the last equality comes from the fact that $I_{j,k}^{(1)}$'s are identically distributed, therefore having the same CF. The CF of $I_{0,k}^{(1)}$ given $d^{(k)} = 0$ can be computed as

$$\Phi_{I_{0,k}^{(1)}|d^{(k)}=0}(v) = \frac{1}{N_c}e^{jvA_k} + \frac{N_c - 1}{N_c^2}e^{-jvA_k} + \left(\frac{N_c - 1}{N_c}\right)^2. \tag{5.19}$$

Thus, the CF of $I_k^{(1)}$ given $d^{(k)} = 0$ is

$$\Phi_{I_k^{(1)}|d^{(k)}=0}(v) = \frac{1}{N_c^{N_s}} \sum_{l=0}^{N_s} \sum_{m=0}^{N_s-l} \binom{N_s}{l, m} \frac{(N_c - 1)^q}{N_c^{N_s-l}} e^{jvA_k(l-m)} \tag{5.20}$$

where $q = 2N_s - 2l - m$, and the conditional PDF of $I_k^{(1)}$ is given by

$$f_{I_k^{(1)}|d^{(k)}}(x|0) = \frac{1}{2\pi}\int_{-\infty}^{\infty} e^{-jvx}\Phi_{I_k^{(1)}|d^{(k)}=0}(v)dv. \tag{5.21}$$

Similarly, when $d^{(k)} = 1$, the conditional density function of $I_{j,k}^{(1)}$ is given by

$$f_{I_{j,k}^{(1)}|d^{(k)}}(x|1) = \frac{N_c - 1}{N_c^2}\delta(x - A_k) + \frac{1}{N_c}\delta(x + A_k) + \left(\frac{N_c - 1}{N_c}\right)^2 \delta(x). \tag{5.22}$$

Then the CF of $I_{0,k}^{(1)}$ given $d^{(k)}=1$ can be written as

$$\Phi_{I_{0,k}^{(1)}|d^{(k)}=1}(v)=\frac{N_c-1}{N_c^2}e^{jvA_k}+\frac{1}{N_c}e^{-jvA_k}+\left(\frac{N_c-1}{N_c}\right)^2, \tag{5.23}$$

and the CF of the total interference over the N_s frames is given by

$$\Phi_{I_k^{(1)}|d^{(k)}=1}(v)=\frac{1}{N_c^{N_s}}\sum_{l=0}^{N_s}\sum_{m=0}^{N_s-l}\binom{N_s}{l,m}\frac{(N_c-1)^q}{N_c^{N_s-m}}e^{jvA_k(l-m)} \tag{5.24}$$

where $q=2N_s-l-2m$, and then the conditional PDF of $I_k^{(1)}$ can be computed.

Assume that $P(d^{(k)}=0)=P(d^{(k)}=1)=\frac{1}{2}$. Then the PDF of $I_k^{(1)}$ is given by

$$f_{I_k^{(1)}}(x)=\frac{1}{2}f_{I_k^{(1)}|d^{(k)}}(x|0)+\frac{1}{2}f_{I_k^{(1)}|d^{(k)}}(x|1) \tag{5.25}$$

and the CF of $I_k^{(1)}$ is given by

$$\Phi_{I_k^{(1)}}(v)=\frac{1}{2}\left(\Phi_{I_k^{(1)}|d^{(k)}=0}(v)+\Phi_{I_k^{(1)}|d^{(k)}=1}(v)\right). \tag{5.26}$$

For the total interference $I^{(1)}=\sum_{k=2}^{N_u}I_k^{(1)}$ from the N_u-1 users to user 1, we can compute its PDF by convolving the PDF of $I_k^{(1)}$'s

$$f_{I^{(1)}}(x)=f_{I_2^{(1)}}(x)*f_{I_3^{(1)}}(x)*\cdots*f_{I_{N_u}^{(1)}}(x). \tag{5.27}$$

The CF of $I^{(1)}$ is given by

$$\Phi_{I^{(1)}}(v)=\prod_{k=2}^{N_u}\Phi_{I_k^{(1)}}(v). \tag{5.28}$$

5.4 Receiver Design for UWB Communications

From the previous section, we have obtained the probability distribution of the MAI in the synchronous MA-TH-PPM UWB system. The next question is how to design

the receiver based on the MAI distribution to have the optimum system performance. In this section, we design the receiver for the synchronous system with the MAI in the AWGN channel. We first examine the optimum receiver. Then we design the suboptimum receiver with less complexity and asymptotically approach the performance of the optimum receiver.

5.4.1 Optimum Detection with MAI

Recall that to detect the desired user's data bit ($d_0^{(1)}$), the conventional linear receiver computes the correlation of $r(t)$ with the template signal within a single frame. From equation (5.6), we have

$$r_j^{(1)} = s_j^{(1)} + I_j^{(1)} + n_j^{(1)} = s_j^{(1)} + Z_j^{(1)} \tag{5.29}$$

and makes the decision by checking if $r^{(1)} = \sum_{j=0}^{N_s-1}$ is greater or less than the threshold 0. Generally the optimal receiver is not linear since the interference component $I_j^{(1)}$ is not Gaussian. Note that $I_j^{(1)} = \sum_{k=2}^{N_u} I_{j,k}^{(1)}$, and the PDF and CF of $I_{j,k}^{(1)}$ were derived in the previous section. Therefore, the CF of $I_j^{(1)}$ is given by

$$\Phi_{I_j^{(1)}}(v) = \prod_{k=2}^{N_u} \left[\left(\frac{2N_c - 1}{N_c^2} \right) \cos(vA_k) + \left(\frac{N_c - 1}{N_c} \right)^2 \right]. \tag{5.30}$$

The CF of $Z_j^{(1)}$ is

$$\begin{aligned} \Phi_{Z_j^{(1)}}(v) &= \Phi_{I_j^{(1)}}(v) \Phi_{n_j^{(1)}}(v) \\ &= \prod_{k=2}^{N_u} \left[\left(\frac{2N_c - 1}{N_c^2} \right) \cos(vA_k) + \left(\frac{N_c - 1}{N_c} \right)^2 \right] e^{-\frac{N_0}{2} v^2} \end{aligned} \tag{5.31}$$

and then the PDF of $Z_j^{(1)}$ can be computed from the characteristic function.

Now in order to derive the optimum receiver in this case, consider the binary hypothesis

$$\begin{cases} H_0: \ \underline{r}^{(1)} = \underline{s}_0^{(1)} + \underline{Z}^{(1)}, \\ H_1: \ \underline{r}^{(1)} = \underline{s}_1^{(1)} + \underline{Z}^{(1)}. \end{cases} \tag{5.32}$$

where $\underline{Z}^{(1)} = [Z_0^{(1)}, Z_1^{(1)}, \ldots, Z_{N_s-1}^{(1)}]$. Here the underline on the signal denotes the vector consists of correlator outputs of the signal indexed from 0 to $N_s - 1$. For example, $\underline{r}^{(1)} = [r_0^{(1)}, r_1^{(1)}, \cdots, r_{N_s-1}^{(1)}]$. Then the optimal decision rule based on observing $\underline{r}^{(1)}$ is given by

$$\Lambda(\underline{r}^{(1)}) = \frac{P(\underline{r}^{(1)}|H_0)}{P(\underline{r}^{(1)}|H_1)} = \frac{f_{\underline{Z}^{(1)}}(\underline{r}^{(1)} - \underline{s}_0^{(1)})}{f_{\underline{Z}^{(1)}}(\underline{r}^{(1)} - \underline{s}_1^{(1)})} \underset{\text{H}_1}{\overset{\text{H}_0}{\gtrless}} 1. \tag{5.33}$$

To further simplify the above equation to obtain the final decision statistic, we need to derive the PDF of $\underline{Z}^{(1)}$. Even though we already know the PDF of $Z_j^{(1)}$, it is not straightforward to obtain the PDF of $\underline{Z}^{(1)}$ from it. Even knowing the PDF of $\underline{Z}^{(1)}$, it would still be very complicated to implement the optimum decision rule. This leads us to the consideration of suboptimum receiver design for the system with MAI. The goal here is to design a suboptimum receiver with simple decision rule and performance that asymptotically approaches the performance of the optimum receiver (as the signal-to-noise ratio becomes small or as N_c becomes large).

5.4.2 Suboptimum Design with the Linear Receiver

As mentioned earlier, Gaussian approximation to the MAI is not accurate. In order to see that the Gaussian approximation is inappropriate, we first want to know the system performance in the case when the Gaussian approximation is used. Then, we compare the Gaussian approximation case with the case when the actual MAI distribution is taken into account in the system performance evaluation.

Performance of the Linear Receiver

Recall that the correlator receiver output of user 1

$$r_j^{(1)} = s_j^{(1)} + \sum_{k=2}^{N_u} I_{j,k}^{(1)} + n_j^{(1)}. \tag{5.34}$$

If we collect the correlator output over N_s frames ($j = 0, 1, \cdots, N_s - 1$), according to equation (5.5), we have

$$r^{(1)} = \sum_{j=0}^{N_s-1} r_j^{(1)} = s^{(1)} + \sum_{k=2}^{N_u} I_k^{(1)} + n^{(1)} \tag{5.35}$$

where $s^{(1)} = \sum_{j=0}^{N_s-1} s_j^{(1)} \in \{\pm N_s A_1\}$, $I_k^{(1)} = \sum_{j=0}^{N_s-1} I_{j,k}^{(1)}$, and $n^{(1)} = \sum_{j=0}^{N_s-1} n_j^{(1)} \sim N(0, N_s N_0)$. In the previous section, we derived the PDF and CF of $I_k^{(1)}$. By the assumption that all the users are independent, the CF of $I^{(1)} = \sum_{k=2}^{N_u} I_k^{(1)}$ is the product of the CF's of $I_k^{(1)}$'s. Let $Z^{(1)} = \sum_{j=0}^{N_s-1} Z_j^{(1)} = I^{(1)} + n^{(1)}$, then the CF of $Z^{(1)}$ is the product of the CF's of $I^{(1)}$ and $n^{(1)}$, and the PDF of $Z^{(1)}$ is given by

$$f_{Z^{(1)}}(x) = \frac{1}{2^{N_u}\pi} \int_{-\infty}^{\infty} e^{-jvx} \prod_{k=2}^{N_u} g_k(v) e^{-\frac{N_s N_0}{2} v^2} dv \tag{5.36}$$

where

$$\begin{aligned} g_k(v) &= \left[\frac{e^{jvA_k}}{N_c} + \frac{N_c - 1}{N_c^2} e^{-jvA_k} + \left(\frac{N_c - 1}{N_c} \right)^2 \right]^{N_s} \\ &\quad + \left[\frac{N_c - 1}{N_c^2} e^{jvA_k} + \frac{e^{-jvA_k}}{N_c} + \left(\frac{N_c - 1}{N_c} \right)^2 \right]^{N_s}. \end{aligned} \tag{5.37}$$

Now we have

$$r^{(1)} = s^{(1)} + Z^{(1)} \tag{5.38}$$

and the PDF of $Z^{(1)}$ is given above. This is a typical binary hypothesis problem. Note that $Z^{(1)}$ has zero mean and the PDF is symmetric about 0. Therefore under the assumption that $P(d_0^{(1)}=0)=P(d_0^{(1)}=1)=\frac{1}{2}$, the BER is given by

$$\begin{aligned}
P_e &= \frac{1}{2}\left[P(r^{(1)}<0|d_0^{(1)}=0)+P(r^{(1)}>0|d_0^{(1)}=1)\right] \\
&= P(r^{(1)}<0|d_0^{(1)}=0) \\
&= \int_{-\infty}^{0} f_{r^{(1)}}(x)dx \\
&= \int_{-\infty}^{-N_sA_1} f_{Z^{(1)}}(x)dx \\
&= \frac{1}{2^{N_u-1}}\frac{1}{2\pi}\int_{-\infty}^{-N_sA_1}\int_{-\infty}^{\infty} \\
&\quad e^{-jvx}\prod_{k=2}^{N_u}\left\{\left[\frac{1}{N_c}e^{jvA_2}+\left(\frac{1}{N_c}-\frac{1}{N_c^2}\right)e^{-jvA_2}+\left(\frac{N_c-1}{N_c}\right)^2\right]^{N_s}\right. \\
&\quad \left.+\left[\left(\frac{1}{N_c}-\frac{1}{N_c^2}\right)e^{jvA_k}+\frac{1}{N_c}e^{-jvA_k}+\left(\frac{N_c-1}{N_c}\right)^2\right]^{N_s}\right\}e^{-\frac{N_sN_0}{2}v^2}dvdx
\end{aligned} \tag{5.39}$$

With simplification, we have

$$P_e=\frac{1}{2^{N_u}\pi}\int_{-\infty}^{-N_sA_1}\int_{-\infty}^{\infty}e^{-jvx}\prod_{k=2}^{N_u}g_k(v)e^{-\frac{N_sN_0}{2}v^2}dvdx \tag{5.40}$$

which can be evaluated numerically.

Gaussian Approximation to the MAI

Now we look at the case if we evaluate the system performance by approximating the MAI as Gaussian. The variance of the interference $\mathrm{Var}[I]$ can be computed numerically from the interference PDF. The variance of the AWGN over N_s frames is $\mathrm{Var}[n]=$

$N_s \cdot N_0$. Then the variance of the total interference plus $\mathrm{Var}[I+n]$ is given by

$$\mathrm{Var}[I+n] = \mathrm{Var}[I] + N_s \cdot N_0. \tag{5.41}$$

The actual signal-to-inteference plus noise ratio (SINR) can then be computed and the approximated BER performance under the Gaussian approximation is given by

$$P_e \approx P_{e,GA} = Q\left(\sqrt{\mathrm{SINR}}\right). \tag{5.42}$$

When the number of users is large, the total interference is approximately Gaussian distributed by the central limit theorem (CLT), and the Gaussian linear receiver is approximately optimum. However, when the number of user is small, say 2 or 3, the CLT does not apply, and the Gaussian linear receiver is not optimum. Thus, we need to find other ways to design the suboptimum receiver which gives the approximate optimality.

5.4.3 Locally Optimum Bayes Detector

The basic idea of the LOBD algorithm is to approximate the interference PDF using the Taylor series expansion. As it is shown earlier, the optimum decision requires the computation of the total interference plus noise PDF $f_{Z_j^{(1)}}(x)$. However, since this PDF is a complicated function, the implementation complexity is high. Therefore, if we can find a good approximation to this PDF, we can reduced the receiver complexity. This can be done by first expanding the PDF into Taylor series, and then eliminating the higher order terms. For this to be a good approximation, the interference should be much stronger than the desired user's signal. This is called the *small signal assumption*.

For $i = 0, 1$, the Taylor series expansion of $f_{Z_j^{(1)}}(x)$ is given by

$$f_{\underline{Z}^{(1)}}(\underline{r}^{(1)} - \underline{s}_i^{(1)}) = f_{\underline{Z}^{(1)}}(\underline{r}^{(1)}) - \sum_{j=0}^{N_s-1} \frac{\partial f_{\underline{Z}^{(1)}}(\underline{r}^{(1)})}{\partial r_j^{(1)}} s_{i,j}^{(1)} + \frac{1}{2} \sum_{j=0}^{N_s-1} \sum_{l=0}^{N_s-1} \frac{\partial^2 f_{\underline{Z}^{(1)}}(\underline{r}^{(1)})}{\partial r_j^{(1)} \partial r_l^{(1)}} s_{i,j}^{(1)} s_{i,l}^{(1)} + \cdots . \tag{5.43}$$

Now under the small signal assumption, $s_{i,j}^{(1)}$'s are small, thus the higher order terms (order ≥ 2) should be small, and we have the approximation

$$f_{\underline{Z}^{(1)}}(\underline{r}^{(1)} - \underline{s}_i^{(1)}) \simeq f_{\underline{Z}^{(1)}}(\underline{r}^{(1)}) - \sum_{j=0}^{N_s-1} \frac{\partial f_{\underline{Z}^{(1)}}(\underline{r}^{(1)})}{\partial r_j^{(1)}} s_{i,j}^{(1)} \tag{5.44}$$

where $s_{0,j}^{(1)} = A_1$ and $s_{1,j}^{(1)} = -A_1$. The suboptimum decision rule is then given by

$$\Lambda(\underline{r}^{(1)}) \simeq r^* = \frac{f_{\underline{Z}^{(1)}}(\underline{r}^{(1)}) - A_1 \sum_{j=0}^{N_s-1} \frac{\partial f_{\underline{Z}^{(1)}}(\underline{r}^{(1)})}{\partial r_j^{(1)}}}{f_{\underline{Z}^{(1)}}(\underline{r}^{(1)}) + A_1 \sum_{j=0}^{N_s-1} \frac{\partial f_{\underline{Z}^{(1)}}(\underline{r}^{(1)})}{\partial r_j^{(1)}}} \underset{\mathrm{H}_1}{\overset{\mathrm{H}_0}{\gtrless}} 1. \tag{5.45}$$

Note that $Z_j^{(1)}$'s are identically distributed. If we define

$$h(x) = -\frac{d}{dx} \ln f_{Z_j^{(1)}}(x), \tag{5.46}$$

we can rewrite equation (5.45) and substitute $h(x)$ into it, and we have

$$\begin{aligned} r^* &= \frac{\frac{f_{\underline{Z}^{(1)}}(\underline{r}^{(1)})}{f_{\underline{Z}^{(1)}}(\underline{r}^{(1)})} - A_1 \sum_{j=0}^{N_s-1} \frac{\partial f_{\underline{Z}^{(1)}}(\underline{r}^{(1)})}{\partial r_j^{(1)}} / f_{\underline{Z}^{(1)}}(\underline{r}^{(1)})}{\frac{f_{\underline{Z}^{(1)}}(\underline{r}^{(1)})}{f_{\underline{Z}^{(1)}}(\underline{r}^{(1)})} + A_1 \sum_{j=0}^{N_s-1} \frac{\partial f_{\underline{Z}^{(1)}}(\underline{r}^{(1)})}{\partial r_j^{(1)}} / f_{\underline{Z}^{(1)}}(\underline{r}^{(1)})} \\ &= \frac{1 - A_1 \sum_{j=0}^{N_s-1} -\frac{d}{dx} \ln f_{Z_j^{(1)}}(x)}{1 + A_1 \sum_{j=0}^{N_s-1} -\frac{d}{dx} \ln f_{Z_j^{(1)}}(x)} \\ &= \frac{1 + A_1 \sum_{j=0}^{N_s-1} h(r_j^{(1)})}{1 - A_1 \sum_{j=0}^{N_s-1} h(r_j^{(1)})} \underset{\mathrm{H}_1}{\overset{\mathrm{H}_0}{\gtrless}} 1, \end{aligned} \tag{5.47}$$

and it can be further simplified to

$$\sum_{j=0}^{N_s-1} h(r_j^{(1)}) \underset{\mathrm{H}_1}{\overset{\mathrm{H}_0}{\gtrless}} 0. \tag{5.48}$$

Thus, by using the LOBD algorithm and under the small signal assumption, the decision rule can be greatly simplified to a threshold detection rule, similar to the Gaussian linear receiver. For different systems, the key point is to find the function $h(x) = -\frac{d}{dx} \ln f_{Z_j^{(1)}}(x)$. Obviously to derive the function $h(x)$ we need to know the distribution of the interference, which is the difficult part when implementing the suboptimum receiver.

5.4.4 LOBD Receiver for UWB Communications

As mentioned above, to design the suboptimum receiver using the LOBD algorithm for the UWB system, first we need to find the total interference plus noise PDF of a single chip. That is, for $r_j^{(1)} = s_j^{(1)} + Z_j^{(1)}$, where $Z_j^{(1)} = I_j^{(1)} + n_j^{(1)}$, we need to know the PDF of $Z_j^{(1)}$. From (5.30) and (5.31), it is given by

$$f_{Z_j^{(1)}}(x) = \frac{1}{2\pi} \int_{-\infty}^{\infty} e^{-jvx} \left\{ \prod_{k=2}^{N_u} f_k(v) e^{-\frac{N_0}{2} v^2} \right\} dv \tag{5.49}$$

where

$$f_k(v) = \left(\frac{2N_c - 1}{N_c^2}\right)\cos(vA_k) + \left(\frac{N_c - 1}{N_c}\right)^2. \tag{5.50}$$

The derivative of $f_{Z_j^{(1)}}(x)$ is

$$f'_{Z_j^{(1)}}(x) = \frac{1}{2\pi}\int_{-\infty}^{\infty} -jve^{-jvx}\left\{\prod_{k=2}^{N_u} f_k(v)e^{-\frac{N_0}{2}v^2}\right\}dv \tag{5.51}$$

and the function $h(x)$ is

$$h(x) = \frac{\int_{-\infty}^{\infty} jve^{-jvx}\left\{\prod_{k=2}^{N_u} f_k(v)e^{-\frac{N_0}{2}v^2}\right\}dv}{\int_{-\infty}^{\infty} e^{-jvx}\left\{\prod_{k=2}^{N_u} f_k(v)e^{-\frac{N_0}{2}v^2}\right\}dv}. \tag{5.52}$$

As can be seen, it is not easy to further simplify the above equation. However, we can always compute it numerically. In general, the function $h(x)$ is a nonlinear function. Thus, the suboptimum receiver obtained in this way is also called a *nonlinear* receiver in comparison to the Gaussian *linear* receiver. In the next subsection, we take a look at a special case when there are only two users in the system ($N_u = 2$). In this case, we can find a closed form expression for $h(x)$.

5.4.5 Special Case: 2-User Synchronous UWB Communications

Here we look at the special case when there are only two users ($N_u = 2$) in the system. In this case, $Z_j^{(1)} = \sum_{k=2}^{N_u} I_{j,k}^{(1)} + n_j^{(1)} = I_{j,2}^{(1)} + n_j^{(1)}$ has the PDF

$$f_{Z_j^{(1)}}(x) = \frac{1}{2\pi}\int_{-\infty}^{\infty} e^{-jvx} f_2(v)e^{-\frac{N_0}{2}v^2}dv. \tag{5.53}$$

However, it is not easy to further simplify the PDF from this form. Another way to compute the PDF is by convolving the PDF of $I_j^{(1)} = I_{j,2}^{(1)}$ and $n_j^{(1)}$. Then we have

$$f_{Z_j^{(1)}}(x) = \frac{1}{\sqrt{2\pi N_0}} \left[\left(\frac{2N_c - 1}{2N_c^2} \right) h_1(x) + \left(\frac{N_c - 1}{N_c} \right)^2 e^{-\frac{x^2}{2N_0}} \right] \tag{5.54}$$

where

$$h_1(x) = e^{-\frac{(x-A_2)^2}{2N_0}} + e^{-\frac{(x+A_2)^2}{2N_0}}. \tag{5.55}$$

By taking the derivative of $f_{Z_j^{(1)}}(x)$, we can obtain the following nonlinear function

$$h(x) = \frac{\left(\frac{2N_c-1}{2N_c^2} \right) h_2(x) + \left(\frac{N_c-1}{N_c} \right)^2 \left(\frac{x}{N_0} \right) e^{-\frac{x^2}{2N_0}}}{\left(\frac{2N_c-1}{2N_c^2} \right) h_1(x) + \left(\frac{N_c-1}{N_c} \right)^2 e^{-\frac{x^2}{2N_0}}} \tag{5.56}$$

where

$$h_2(x) = \frac{(x - A_2)}{N_0} e^{-\frac{(x-A_2)^2}{2N_0}} + \frac{(x + A_2)}{N_0} e^{-\frac{(x+A_2)^2}{2N_0}}. \tag{5.57}$$

Some plots of the density function and $h(x)$ for different parameters are shown in Figure 5.5 and 5.6. From these plots, we can see that the nonlinear function actually "suppress" the interference by the nonlinear mapping, especially at amplitudes where the "peak" happens in the interference PDF. Later it will becomes clear that this *interference mitigation* is the key to improve the system performance compared to the linear receiver performance.

5.4.6 Performance Analysis

In this section, we assume $P(H_0) = P(H_1) = \frac{1}{2}$. Let $y_j^{(1)} = h(r_j^{(1)})$ for $j = 0, 1, \cdots, N_s - 1$. The BER of this receiver is given by

$$P_e = P\left(\sum_{j=0}^{N_s-1} y_j^{(1)} < 0 \Big| H_0 \right). \tag{5.58}$$

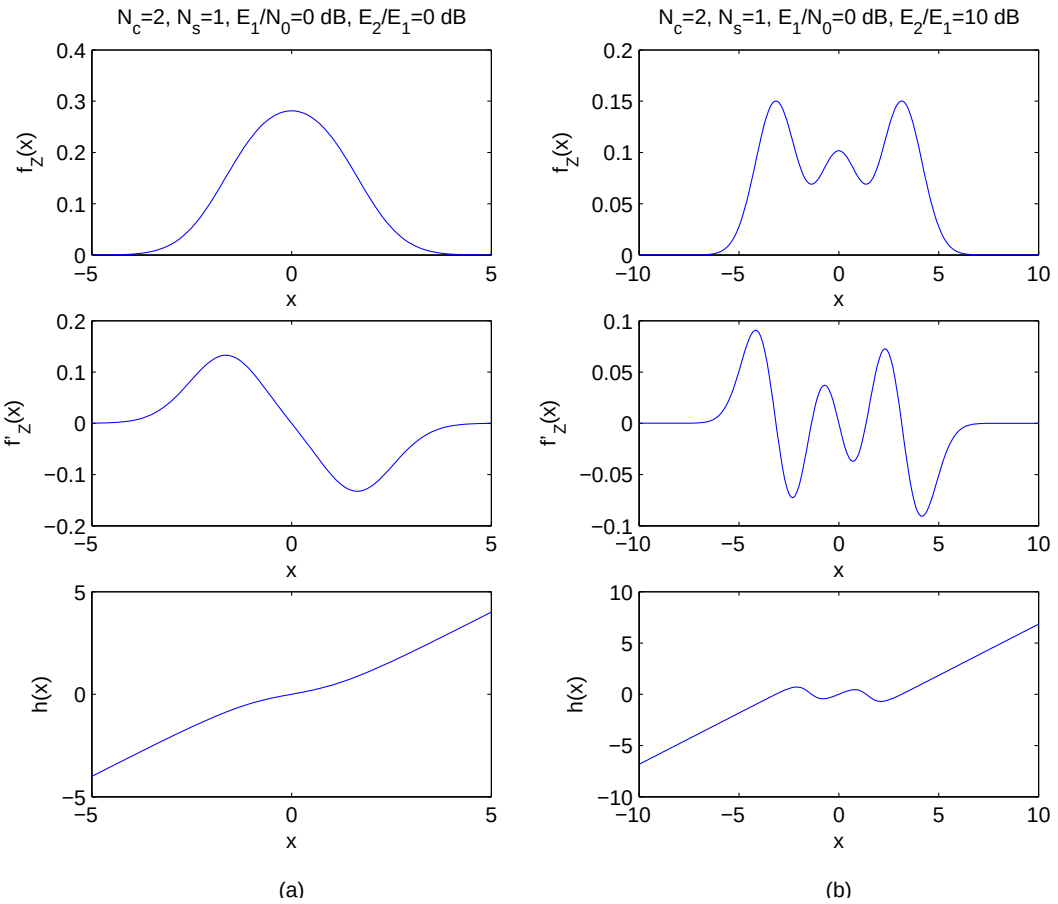

Figure 5.5: $h(x)$ for 2-user case.

To find the exact P_e, we need to find the probability distribution of $\sum_{j=0}^{N_s-1} y_j^{(1)}$ under H_0. However, this is not easy since $h(x)$ is quite complicated. A way to approximately evaluate P_e is to apply the CLT. Assume $r_j^{(1)}$'s are i.i.d under H_0. Then $y_j^{(1)}$'s are i.i.d under H_0 since they are functions of $r_j^{(1)}$'s. By the CLT for large N_s, we have

$$\sum_{j=0}^{N_s-1} \left\{ \frac{y_j^{(1)} - E\left[y_j^{(1)} \middle| H_0\right]}{\sqrt{N_s \mathrm{Var}\left(y_j^{(1)} \middle| H_0\right)}} \right\} \longrightarrow N(0,1). \tag{5.59}$$

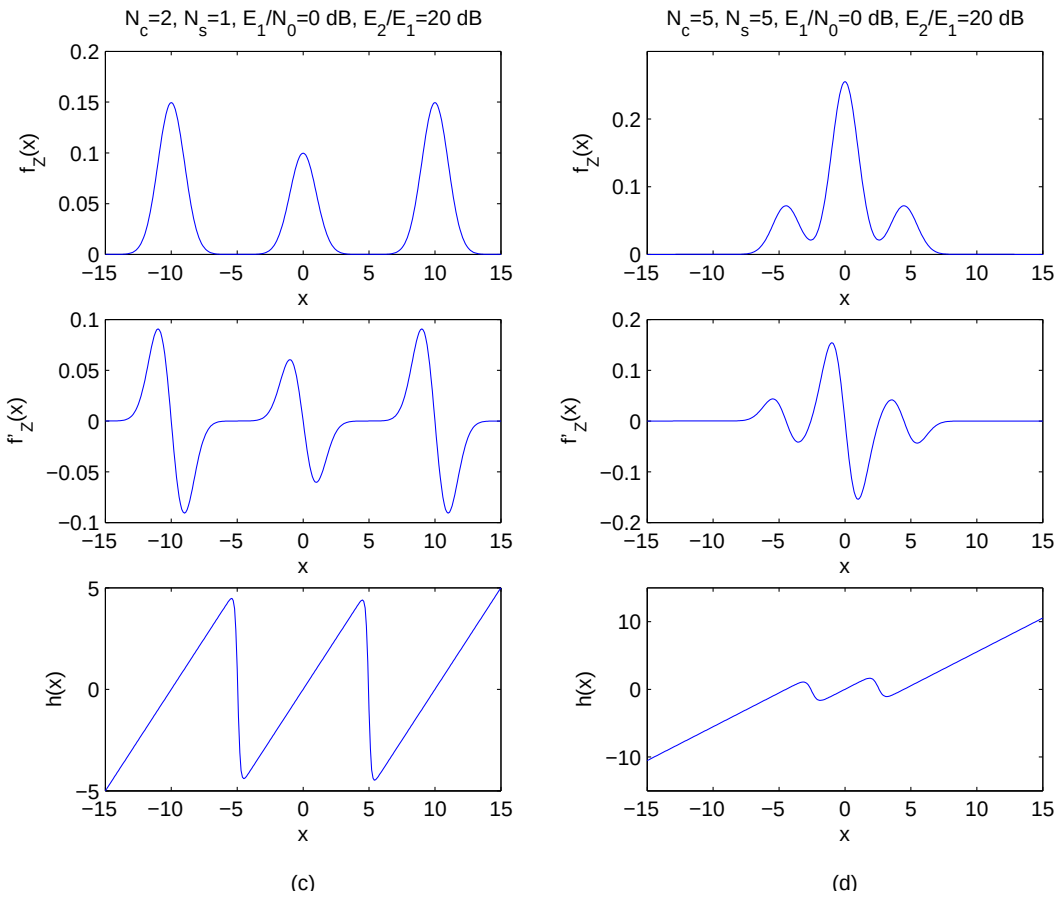

Figure 5.6: $h(x)$ for 2-user case.

Therefore, for large N_s,

$$P\left(\sum_{j=0}^{N_s-1} y_j^{(1)} < 0 \Big| H_0\right) \longrightarrow \Phi\left(-\frac{N_s E\left[y_j^{(1)} \big| H_0\right]}{\sqrt{N_s \mathrm{Var}\left(y_j^{(1)} \big| H_0\right)}}\right). \tag{5.60}$$

It can be shown that that mean of $y_j^{(1)}$ conditioned on H_0 is given by

$$\begin{aligned} E\left[y_j^{(1)}\middle|H_0\right] &= \int_{-\infty}^{\infty} y_j^{(1)} f(y_j^{(1)}) dy_j^{(1)} \\ &\simeq \int_{-\infty}^{\infty} h(r_j^{(1)}) \left[f_{Z_j^{(1)}}\left(r_j^{(1)}\right) - A_1 f'_{Z_j^{(1)}}\left(r_j^{(1)}\right)\right] dr_j^{(1)} \\ &= \int_{-\infty}^{\infty} \frac{f'_{Z_j^{(1)}}\left(r_j^{(1)}\right)}{f_{Z_j^{(1)}}\left(r_j^{(1)}\right)} A_1 f'_{Z_j^{(1)}}\left(r_j^{(1)}\right) dr_j^{(1)} \\ &= A_1 \int_{-\infty}^{\infty} \left[\frac{f'_{Z_j^{(1)}}\left(r_j^{(1)}\right)}{f_{Z_j^{(1)}}\left(r_j^{(1)}\right)}\right]^2 f_{Z_j^{(1)}}\left(r_j^{(1)}\right) dr_j^{(1)} \\ &= A_1 \int_{-\infty}^{\infty} h^2\left(r_j^{(1)}\right) f_{Z_j^{(1)}}\left(r_j^{(1)}\right) dr_j^{(1)} \\ &= A_1 L \end{aligned} \tag{5.61}$$

where

$$L = \int_{-\infty}^{\infty} h^2(x) f_{Z_j^{(1)}}(x) dx \tag{5.62}$$

Similarly, we have

$$\begin{aligned} E\left[\left(y_j^{(1)}\right)^2\middle|H_0\right] &= \int_{-\infty}^{\infty} h^2\left(r_j^{(1)}\right)\left[f_{Z_j^{(1)}}\left(r_j^{(1)}\right) - A_1 f'_{Z_j^{(1)}}\left(r_j^{(1)}\right)\right] dr_j^{(1)} \\ &= \int_{-\infty}^{\infty} h^2\left(r_j^{(1)}\right) f_{Z_j^{(1)}}\left(r_j^{(1)}\right) dr_j^{(1)} \\ &= L \end{aligned} \tag{5.63}$$

Therefore, the variance of $y_j^{(1)}$ conditioned on H_0 is given by

$$\mathrm{Var}\left(y_j^{(1)}\middle|H_0\right) = L - A_1^2 L^2. \tag{5.64}$$

Then we have the approximate error probability

$$P_e \simeq Q\left(\frac{N_s A_1 L}{\sqrt{N_s(L - A_1^2 L^2)}}\right) = Q\left(\sqrt{\frac{E_1}{L' - \frac{E_1}{N_s}}}\right) \tag{5.65}$$

where $L' = 1/L$ can be evaluated numerically. The quantity L represents the interference energy captured by the suboptimum receiver after passing the received signal through the nonlinear function. Intuitively, with strong interference, L is large, and thus L' is small. Therefore, the argument of the Q function becomes large, and thus P_e becomes small. For this approximate P_e to be valid, we need $L' > \frac{E_1}{N_s}$. Therefore, we need E_1 to be small, which is the same as the small signal assumption in the LOBD algorithm.

5.5 Numerical Example

In this section, we look at a special case when there are only two synchronized users in the system ($N_u = 2$). This is an extreme case that the interference is far from the Gaussian distribution. Let user 1 be the desired user and user 2 is the interfering user. The bit energy of the two users are E_1 and E_2, respectively. Note that $A_1 = \sqrt{E_1/N_s}$ and $A_2 = \sqrt{E_2/N_s}$ where N_s is the number of repetitions for transmitting one bit. We will examine the performance of both the linear and nonlinear receivers.

5.5.1 Linear Receiver

Figure 5.7 shows the exact BER performance for the synchronous case of the linear receiver for different N_s with $E_1 = E_2$. It is obtained by evaluating equation (5.40) numerically. We can see that by increasing N_s, there is very limited performance improvement when N_s is large, and there is a gap from the baseline AWGN performance. Figure 5.8 shows the BER of the linear receiver for different interference energy E_2 as N_s changes. The SNR in this case is $\frac{E_1}{N_0} = 10$ dB. As can be seen, when N_s increases from 1 to 50, the BER improvement is not in proportion to the the increment of N_s. Therefore, for the linear receiver, we can not improve the BER a great deal by increasing N_s.

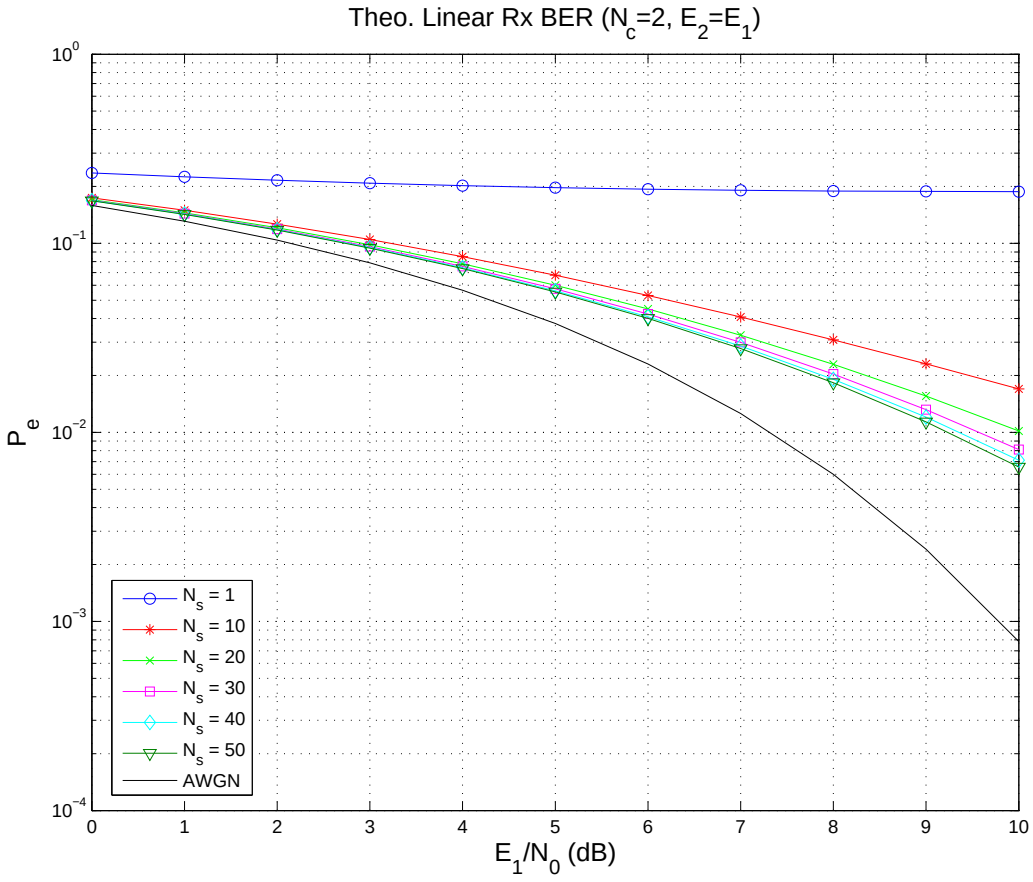

Figure 5.7: P_e vs. SNR for different N_s.

5.5.2 Gaussian Approximation

The comparison between the actual performance with a linear receiver and the one using Gaussian approximation is shown in Figure 5.8. It shows that by using Gaussian approximation, most of the time we would over estimate the system performance. With the interference plus noise variance, we can compare the PDF of the total interference using Gaussian approximation with the actual PDF. Some examples are shown in Figure 5.10.

The Gaussian linear receiver is simply a threshold receiver, which gives a very low complexity. However, from the numerical results, we can see that the linear receiver does not perform well with the MAI in the system.

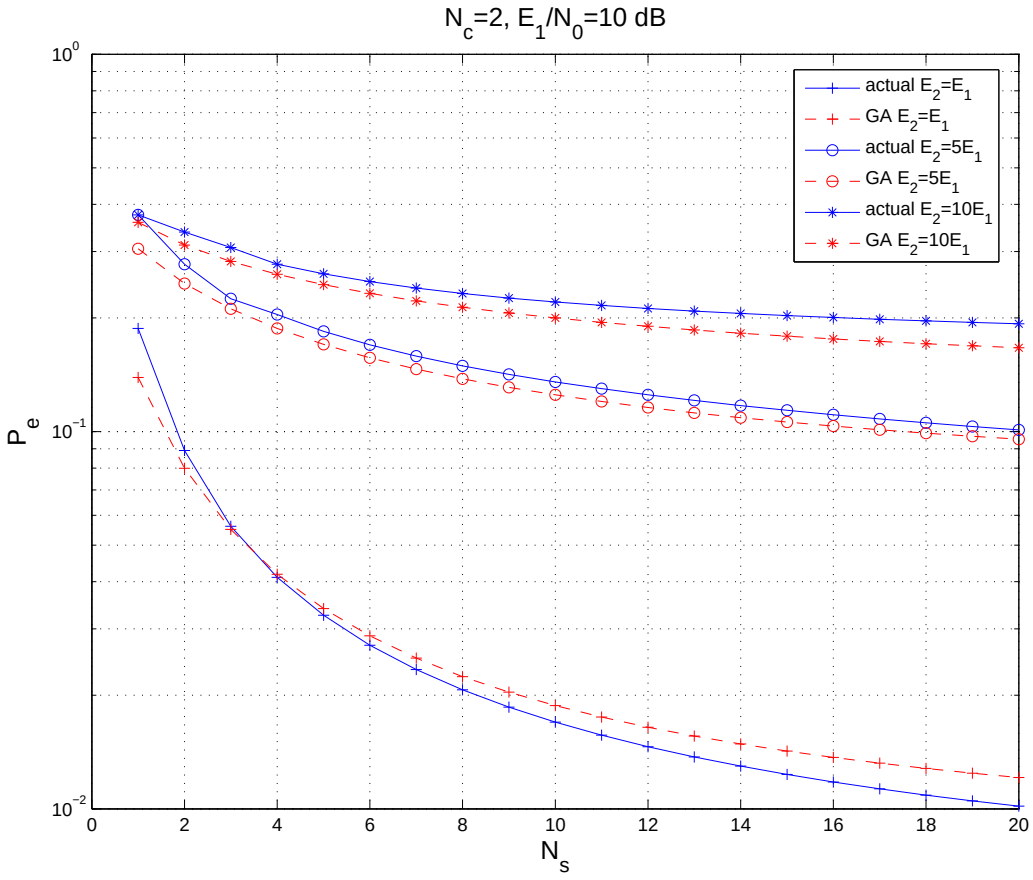

Figure 5.8: Performance comparison (actual vs. Gaussian approximation).

5.5.3 LOBD Nonlinear Receiver

The performance of the suboptimum nonlinear receiver for different N_s in the 2-user case is shown in Figure 5.11. We can see that the performance approaches the baseline AWGN performance when E_2 is large. This is consistent with the small signal assumption. Note that this is totally opposite to the linear receiver case: the performance gets worse as E_2 gets larger. The performance of the suboptimum nonlinear receiver compared to the linear receiver is shown in Figure 5.12 for the extreme case when $N_s = 1$. We can see that the nonlinear receiver outperforms the linear receiver, and is able to achieve the baseline AWGN performance when interference is strong. This is consistent with the small signal assumption required in the derivation of the nonlinear receiver.

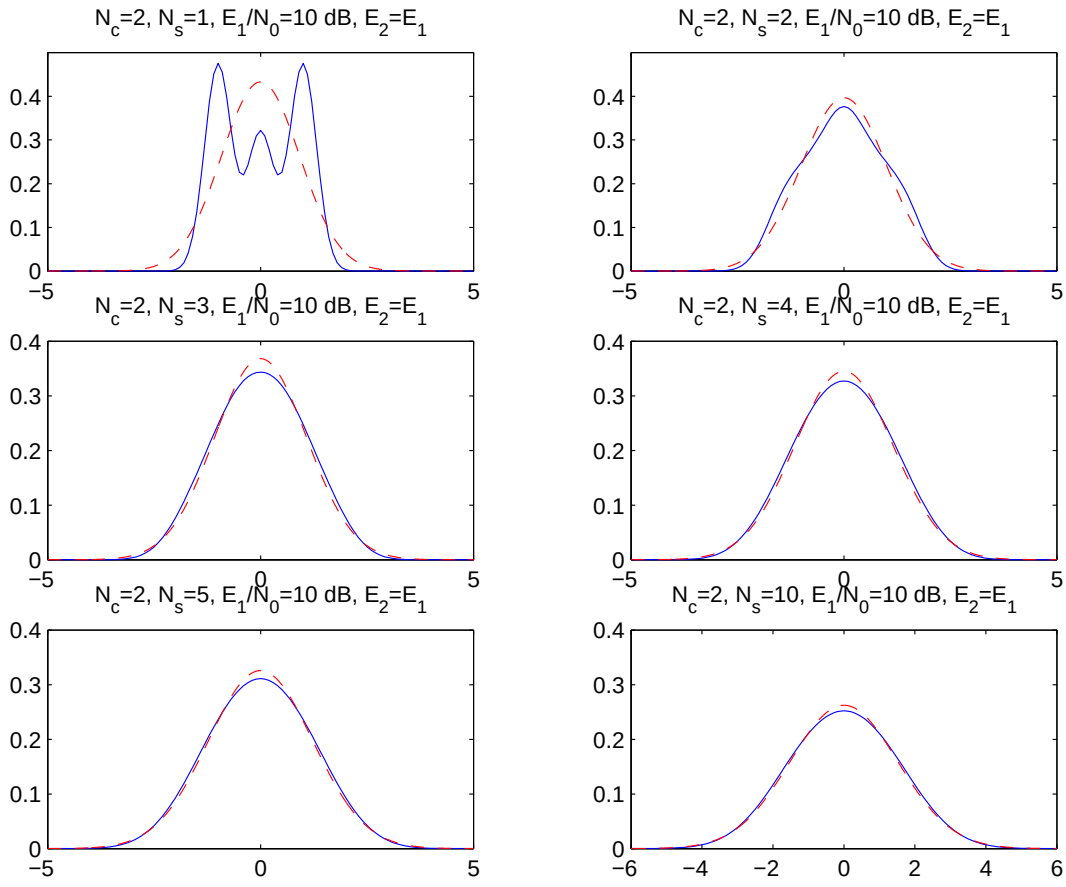

Figure 5.9: Interference PDF and Gaussian approximation.

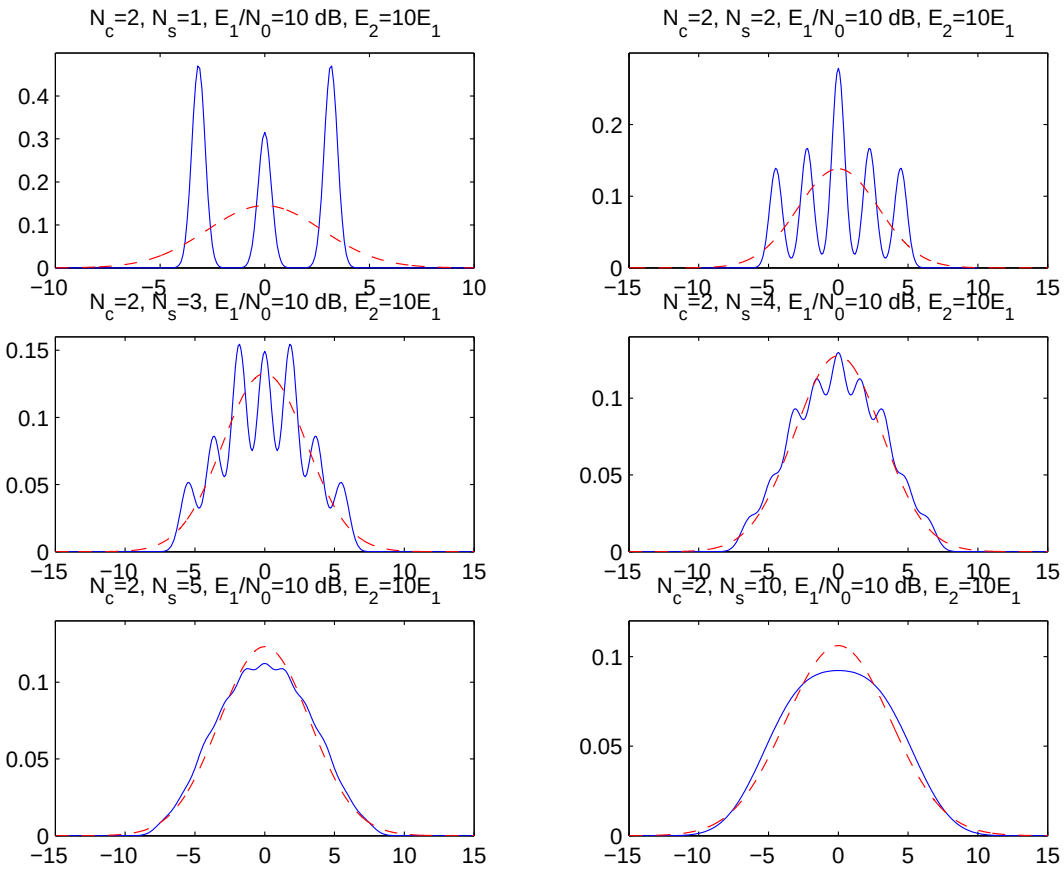

Figure 5.10: Interference PDF and Gaussian approximation.

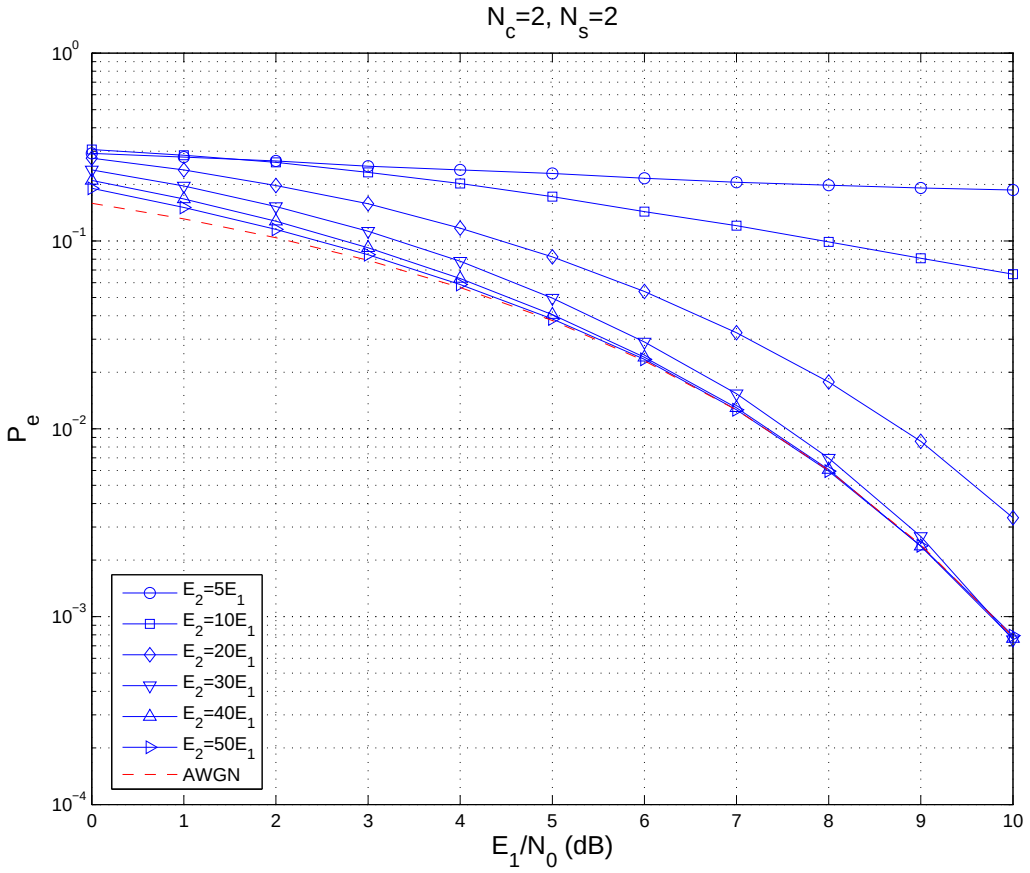

Figure 5.11: Suboptimum nonlinear receiver: 2-user case ($N_c = 2, N_s = 2$).

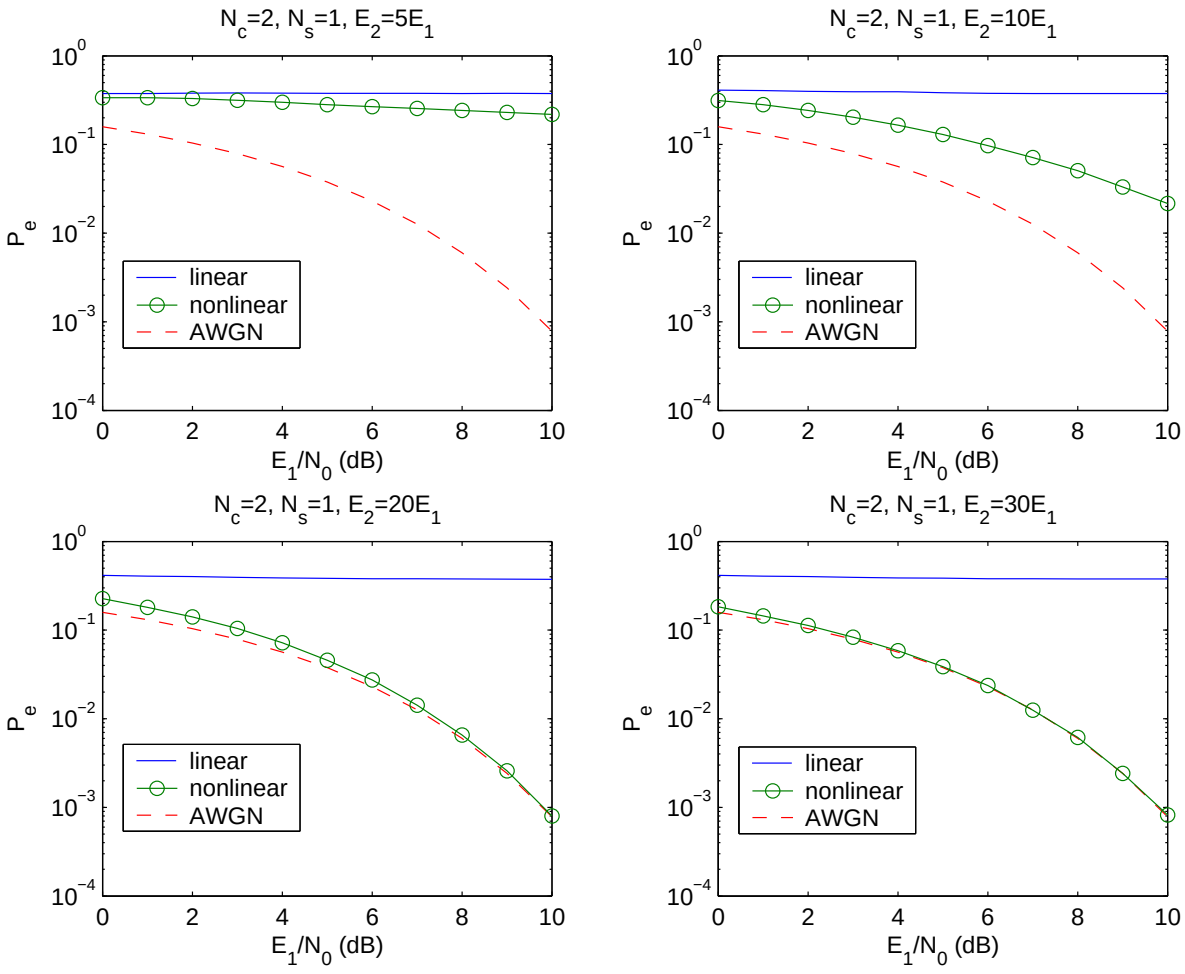

Figure 5.12: Linear v.s. nonlinear receiver: 2-user case ($N_c = 2, N_s = 1$).

5.6 Conclusions

In this chapter, we considered suboptimum receiver designs for UWB communications. The suboptimum *linear* receiver does not perform well with the MAI in the system even when the interference is not strong and N_s is large. The suboptimum *nonlinear* receiver designed according to the LOBD algorithm performs well and approaches the optimum performance when the interference is strong. The nonlinear receiver structure is simply a threshold receiver as the linear receiver, except with the extra complexity of mapping the received signal with a nonlinear function.

CHAPTER 6

Performance of UWB in Jamming

6.1 Introduction

In a military or commercial communication system, intentional or unintentional jamming interference can cause serious problems. Jammers emit noise-like interference to disrupt the communication link and degrade the performance. It is not easy to design a receiver that operates well in the presence of jammers, and it is necessary for a receiver to have the ability to suppress interference in such a hostile environment. Since ultra-wideband (UWB) communications co-exists with many narrowband systems, jamming interference is a crucial issue. Some of the analysis of the impact of jamming interference on UWB communications can found in [39][38][42][43][44].

The optimum receiver design for UWB communication systems in the presence of jamming is complicated. Suboptimum receivers with low complexity that can perform nearly as well as the optimum receiver are desirable. One of the methods to design suboptimum receivers is by using the locally optimum Bayes detection (LOBD) algorithm[41][40][45]. The idea is to pass the received signal samples through a nonlinear function designed according to the LOBD algorithm before the detection process. The nonlinear function can suppress the interference in the received signal and hence enhance the performance of the receiver. This technique is used in a direct sequence spread spectrum (DS-SS) system in [46] for the case of continuous wave and Gaussian

noise jamming in the system. An important assumption for the LOBD algorithm to work well is the *small signal assumption*, which says that the desired signal should be much smaller than the interfering signal. This is likely to be the case for UWB communications. In [47], the LOBD algorithm is applied to a multiple-access UWB system for multiple-access interference (MAI) suppression. In this chapter, we apply it to an UWB system with pulsed Gaussian noise jamming, and compare the performance of this suboptimum receiver with the performance of the optimum receiver and the suboptimum linear receiver designed according to the Gaussian approximation to the interference.

This chapter is organized as the follows. In Section 6.2, the system and signaling model are described. For the proposed system, different types of receiver designs are discussed in Section 6.3. In Section 6.4, we analyze the performance of different receivers introduced in the previous section. Numerical examples and simulation results are shown in Section 6.5. Finally, conclusions are presented in Section 6.6.

6.2 System Model

In this section, we consider an impulse radio (IR) based ultra-wideband (UWB) communication system using time-hopping (TH) pulse-position modulation (PPM). We consider the single-user case, an additive white Gaussian noise (AWGN) channel coexisting with jamming signals in the system. The user's signal $s(t)$ is given by

$$s(t) = \sum_{k=-\infty}^{\infty} \sqrt{\frac{E_b}{N_s}} p(t - kT_f - c_k T_c - d_{\lfloor k/N_s \rfloor}\delta) \tag{6.1}$$

where $p(t)$ is the UWB pulse with unit energy and time duration T_p, T_f is the frame duration or pulse repetition time, $\{c_k\}$ is the time hopping sequence known to both transmitter and receiver, T_c is the chip duration, $d \in \{0, 1\}$ is the binary data being transmitted, N_s is the repetition code length, and δ is the PPM modulation index. The

received signal is represented as

$$r(t) = s(t) + j(t) + n(t) \tag{6.2}$$

where $j(t)$ is the jamming signal, and $n(t)$ is the Gaussian process with zero mean and one-sided power spectral density (PSD) N_0.

6.2.1 Jamming Signal Model

We consider pulsed Gaussian noise jamming in our system model. Assume the jammer is synchronized with the communication system at the chip level. That is, for any chip duration, the jamming signal $j(t)$ is either on with probability ρ or off with probability $1 - \rho$. Let J be the average power of the jammer. Assume the wideband Gaussian noise jammer spreads its power evenly over the total frequency range of the spread bandwidth. That is, $W_J = W$ where W is the spread bandwidth of the signal. The equivalent single-sided PSD of the Gaussian noise jammer signal $j(t)$ is then $N_J = \frac{J}{W_J}$. According to the assumptions, when the jammer is on, $j(t)$ is a continuous-time Gaussian random process with bandwidth W_J and single-sided PSD N_J/ρ.

6.2.2 Correlator Receiver

The receiver correlates the received signal with the template signal

$$v(t) = \frac{1}{\sqrt{N_s}} \left[p(t - kT_f - c_k T_c) - p(t - kT_f - c_k T_c - \delta) \right] \tag{6.3}$$

and generates $r_k = r_{0k} - r_{1k}$, where r_{0k} and r_{1k} are the correlator outputs corresponding to the two PPM chip durations (0 and 1), respectively. Assume the receiver is synchronized to the transmitter. Consider one frame of the signal starting at time 0. Then we

have

$$r(t) = \sqrt{\frac{E_b}{N_s}} p(t - c_0 T_c - d_0 \delta) + j(t) + n(t) \tag{6.4}$$

for $0 \leq t \leq T_f$. The correlator output is

$$r_0 = \int_0^{T_f} r(t) v(t) dt = s_0 + j_0 + n_0 = s_0 + z_0 \tag{6.5}$$

where $z_0 = j_0 + n_0$ is the total interference plus noise. Since there are only two possible chip durations containing the desired signal in binary PPM, the integration from 0 to T_f is equivalent to integration from $c_0 T_c$ to $(c_0 + 2)T_c$ assuming $\delta = T_p = T_c$. The desired signal part s_0 in r_0 is given by

$$s_0 = \int_{c_0 T_c}^{(c_0+2)T_c} \sqrt{\frac{E_b}{N_s}} p(t - c_0 T_c - d_0 \delta) v(t) dt = (1 - 2d_0) \frac{\sqrt{E_b}}{N_s} \tag{6.6}$$

The noise part n_0 in r_0 is Gaussian with zero mean and variance N_0/N_s. In any chip duration, if the jammer is on, the correlator output due to the jammer is Gaussian distributed with zero mean and variance $\frac{N_J}{2\rho N_s}$. Within any frame duration T_f, the receiver correlates two consecutive chip durations depending on the time hopping offset. For the jammer, there are four different states during these two chip durations: (on,on), (on,off), (off,on), (off,off) with probabilities ρ^2, $\rho(1-\rho)$, $\rho(1-\rho)$, $(1-\rho)^2$, respectively. For the (off,off) state in which the jammer is off during these two chip durations, $j_0 = 0$. For the states (on,on), (on,off), and (off,on), the variance of j_0 is $\frac{N_J}{\rho N_s}$, $\frac{N_J}{2\rho N_s}$, and $\frac{N_J}{2\rho N_s}$, respectively. Therefore, the probability density function (PDF) of j_0 is given by

$$f_{j_0}(x) = \frac{\rho^2}{\sqrt{2\pi \frac{N_J}{\rho N_s}}} e^{-\frac{x^2}{2\frac{N_J}{\rho N_s}}} + \frac{2\rho(1-\rho)}{\sqrt{\pi \frac{N_J}{\rho N_s}}} e^{-\frac{x^2}{\frac{N_J}{\rho N_s}}} + (1-\rho)^2 \delta(x). \tag{6.7}$$

Based on the assumption of the jammer, the PDF of the total interference plus noise z_0 is then given by

$$f_{z_0}(x) = \frac{\rho^2}{\sqrt{2\pi\left(\frac{N_0}{N_s}+\frac{N_J}{\rho N_s}\right)}} e^{-\frac{x^2}{2\left(\frac{N_0}{N_s}+\frac{N_J}{\rho N_s}\right)}} + \frac{2\rho(1-\rho)}{\sqrt{2\pi\left(\frac{N_0}{N_s}+\frac{N_J}{2\rho N_s}\right)}} e^{-\frac{x^2}{2\left(\frac{N_0}{N_s}+\frac{N_J}{2\rho N_s}\right)}} + \frac{(1-\rho)^2}{\sqrt{2\pi\frac{N_0}{N_s}}} e^{-\frac{x^2}{2\frac{N_0}{N_s}}}. \tag{6.8}$$

6.3 Receiver Design

In this section, we examine different designs of the receiver for the communication system described in the previous section. We first design the optimum receiver to give us an idea of the best possible performance of such a system. Then we design suboptimum receivers with less complexity compared to the optimum receiver. The performance analysis of these receivers will be discussed in the next section.

6.3.1 Optimum Receiver

The design of the optimum receiver is based on the maximum-likelihood decision rule. The optimum receiver employs a maximum-likelihood diversity combining scheme to process the correlator outputs from different frame durations. The idea is that the correlator outputs that are corrupted by the interference are less reliable than those that are interference free. Therefore when they are combined to form a decision statistic, they should be weighted differently. The optimum receiver computes the weights for each frame output and compares the weighted sum with an optimum threshold to make the decision.

The receiver correlator outputs are $\{r_{ik}\}$ where $i = 0, 1$ and $k = 0, 1, \cdots, N_s - 1$. The subscript i indicates the output from the two binary PPM chip durations corresponding to 0 and 1 being transmitted, respectively. The subscript k indicates the frame in which the correlator outputs are generated. During the bit duration from time 0 to T_f, the

correlator receiver generates the following outputs:

$$\mathbf{r} = \begin{bmatrix} r_{00} & r_{01} & \cdots & r_{0N_s-1} \\ r_{10} & r_{11} & \cdots & r_{1N_s-1} \end{bmatrix}. \tag{6.9}$$

Depending on the chip being jammed or not, we can find the conditional PDF of r_{ik}. The conditional PDF of r_{ik} conditioned on the ith symbol being sent in the kth frame with the jammer off is given by

$$P_{ik}^{\text{off}}(x) = \frac{1}{\sqrt{\pi \frac{N_0}{N_s}}} \exp\left\{ -\frac{\left(x - \frac{\sqrt{E_b}}{N_s}\right)^2}{\frac{N_0}{N_s}} \right\}. \tag{6.10}$$

The conditional PDF of r_{ik} conditioned on the ith symbol being sent in the kth frame with the jammer on is given by

$$P_{ik}^{\text{on}}(x) = \frac{1}{\sqrt{\pi \left(\frac{N_0}{N_s} + \frac{N_J}{\rho N_s}\right)}} \exp\left\{ -\frac{\left(x - \frac{\sqrt{E_b}}{N_s}\right)^2}{\frac{N_0}{N_s} + \frac{N_J}{\rho N_s}} \right\}. \tag{6.11}$$

The conditional PDF of r_{ik} conditioned on the ith symbol not being sent in the kth frame with the jammer off is given by

$$Q_{ik}^{\text{off}}(x) = \frac{1}{\sqrt{\pi \frac{N_0}{N_s}}} \exp\left\{ -\frac{x^2}{\frac{N_0}{N_s}} \right\}. \tag{6.12}$$

The conditional PDF of r_{ik} conditioned on the ith symbol not being sent in the kth frame with the jammer on is given by

$$Q_{ik}^{\text{on}}(x) = \frac{1}{\sqrt{\pi \left(\frac{N_0}{N_s} + \frac{N_J}{\rho N_s}\right)}} \exp\left\{ -\frac{x^2}{\frac{N_0}{N_s} + \frac{N_J}{\rho N_s}} \right\}. \tag{6.13}$$

Let J_0 be the set of frames in $\{r_{0k}\}$ with interference on, and J_1 be the set of frames

in $\{r_{1k}\}$ with interference on. Let $|J_0|$ and $|J_1|$ denote the cardinality of J_0 and J_1, respectively. The joint PDF of $\mathbf{r}$ conditioned on 0 being sent is given by

$$\begin{aligned} f(\mathbf{r}|0, J_0, J_1) &= \left(\prod_{k\in J_0} P_{0k}^{\text{on}}(r_{0k})\right)\left(\prod_{k\notin J_0} P_{0k}^{\text{off}}(r_{0k})\right) \\ &\quad \left(\prod_{k\in J_1} Q_{1k}^{\text{on}}(r_{1k})\right)\left(\prod_{k\notin J_1} Q_{1k}^{\text{off}}(r_{1k})\right), \end{aligned} \tag{6.14}$$

and the joint PDF of $\mathbf{r}$ conditioned on 1 being sent is given by

$$\begin{aligned} f(\mathbf{r}|1, J_0, J_1) &= \left(\prod_{k\in J_1} P_{1k}^{\text{on}}(r_{1k})\right)\left(\prod_{k\notin J_1} P_{1k}^{\text{off}}(r_{1k})\right) \\ &\quad \left(\prod_{k\in J_0} Q_{0k}^{\text{on}}(r_{0k})\right)\left(\prod_{k\notin J_0} Q_{0k}^{\text{off}}(r_{0k})\right). \end{aligned} \tag{6.15}$$

Assume that 0 and 1 are equally likely being sent. Then the maximum-likelihood decision rule is given by

$$\frac{f(\mathbf{r}|0, J_0, J_1)}{f(\mathbf{r}|1, J_0, J_1)} \underset{\text{H}_1}{\overset{\text{H}_0}{\gtrless}} 1. \tag{6.16}$$

This rule can be further simplified to

$$\begin{aligned} r^* &= N_0\left[\sum_{k\in J_0} r_{0k} - \sum_{k\in J_1} r_{1k}\right] \\ &\quad + \left(N_0 + \frac{N_J}{\rho}\right)\left[\sum_{k\notin J_0} r_{0k} - \sum_{k\notin J_1} r_{1k}\right] \\ &\underset{\text{H}_1}{\overset{\text{H}_0}{\gtrless}} \frac{(|J_1| - |J_0|)\sqrt{E_b}N_J}{2\rho N_s}. \end{aligned} \tag{6.17}$$

Note that in the above equation, it requires the knowledge of J_0, J_1, N_0, N_J, and ρ to make the decision. It can be observed that the optimum receiver is a linear receiver

comparing the weighted sum of the correlator outputs with a threshold. The correlator outputs with and without interference are weighted differently. The frames without interference are weighted more than the frames with interference. This is reasonable since information from frames being jammed by the interference is less reliable than those that are not jammed.

6.3.2 Suboptimum Receiver

As can be seen, the optimum receiver is complicated in practice since it requires the knowledge of the channel and interference. Therefore, we seek suboptimum receivers that are feasible with limited knowledge about the channel and interference. A common way to design a suboptimum receiver is to model or approximate the interference as Gaussian distributed. However, depending on the type of interference, a Gaussian approximation may not always be accurate. In that case, substantial improvement can be made by considering a more accurate probability distribution of the interference. In the following we consider two suboptimum receiver designs. The suboptimum linear receiver is derived by employing a Gaussian approximation. Then we derive the suboptimum nonlinear receiver by using the actual probability distribution of the interference.

Linear Receiver

From (6.8), it can be seen that the probability distribution of the total interference plus noise is not Gaussian. By approximating the interference distribution as Gaussian, it is equivalent to the case of a single user in an AWGN channel without interference. In this case, the receiver is the simple threshold detector as shown in Figure 6.1. The suboptimum linear receiver collects and sums up the correlator outputs, and compare the sum with the threshold 0. This is given by

$$r^* = \sum_{k=0}^{N_s-1} r_k \underset{\mathrm{H}_1}{\overset{\mathrm{H}_0}{\gtrless}} 0. \tag{6.18}$$

This receiver structure is simple and easy to implement. However, due to the inaccuracy of Gaussian approximation, the performance can be poor, leaving the possibility for substantial improvement.

Figure 6.1: Suboptimum linear receiver.

Nonlinear Receiver

To further improve the suboptimum linear receiver, the accurate probability distribution of the interference has to be taken into consideration. However, by using the actual PDF in (6.8) and the maximum-likelihood detection, the decision rule is quite complicated. As mentioned in [47], under the small signal assumption, the LOBD algorithm can be applied, and the decision rule can be simplified to the structure as shown in Figure 6.2. The receiver structure is similar to the suboptimum linear receiver except that the correlator outputs are passed through a nonlinear function before the summation. According to the LOBD algorithm [41][40][45], the nonlinear function can be computed by

$$h(x) = -\frac{f'_{z_0}(x)}{f_{z_0}(x)} \tag{6.19}$$

where $f_{z_0}(x)$ is given by (6.8) and the derivative of $f_{z_0}(x)$ can be easily computed as

$$\begin{aligned} f'_{z_0}(x) \;=\; & \frac{\rho^2}{\sqrt{2\pi\left(\frac{N_0}{N_s}+\frac{N_J}{\rho}\right)}}\, e^{-\frac{x^2}{2\left(\frac{N_0}{N_s}+\frac{N_J}{\rho}\right)}} \left(-\frac{x}{\frac{N_0}{N_s}+\frac{N_J}{\rho}}\right) \\ & + \frac{2\rho(1-\rho)}{\sqrt{2\pi\left(\frac{N_0}{N_s}+\frac{N_J}{2\rho}\right)}}\, e^{-\frac{x^2}{2\left(\frac{N_0}{N_s}+\frac{N_J}{2\rho}\right)}} \left(-\frac{x}{\frac{N_0}{N_s}+\frac{N_J}{2\rho}}\right) \\ & + \frac{(1-\rho)^2}{\sqrt{2\pi\frac{N_0}{N_s}}}\, e^{-\frac{x^2}{2\frac{N_0}{N_s}}} \left(-\frac{x}{\frac{N_0}{N_s}}\right). \end{aligned} \tag{6.20}$$

Let $y_k = h(r_k)$ denote the nonlinear function output. Then the decision rule is given by

$$r^* = \sum_{k=0}^{N_s-1} y_k = \sum_{k=0}^{N_s-1} h(r_k) \underset{\mathrm{H_1}}{\overset{\mathrm{H_0}}{\gtrless}} 0. \tag{6.21}$$

An example of the nonlinear function is shown in Figure 6.3 for $E_b = 1$, $E_b/N_0 = 5$

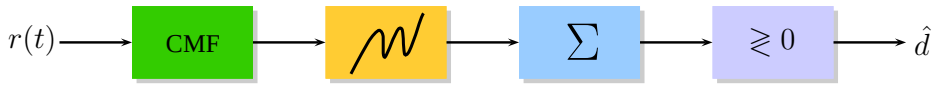

Figure 6.2: Suboptimum nonlinear receiver.

dB, $E_b/N_J = -10$ dB, $\rho = 0.3$, and $N_s = 10$. It can be observed that the plot can be

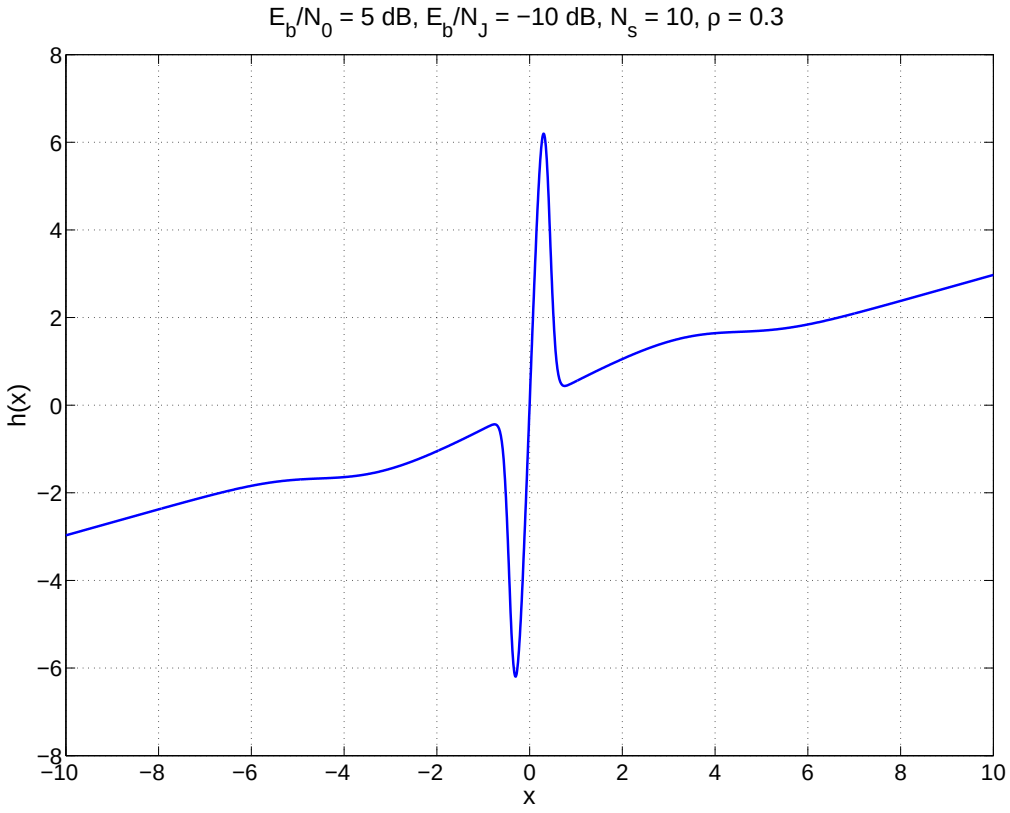

Figure 6.3: LOBD nonlinear function $h(x)$.

divided into two regions: the linear region close to the origin passing through (0,0), and the nonlinear (semi-linear) region. The linear region corresponds to the AWGN, and the

nonlinear region corresponds to the interference. Under the small signal assumption, if the interference is small, the AWGN dominates and the function operates in the linear region. With strong interference, the function operates in the nonlinear region and the interference is suppressed. As the interference gets weaker, the nonlinear region becomes less nonlinear. In the extreme case, the system is interference-free, and the nonlinear function becomes linear. Also note that the AWGN cannot be suppressed by the LOBD receiver.

6.4 Performance Analysis

In this section we analyze the performance of the optimum and suboptimum receivers described in the previous section.

6.4.1 Optimum Receiver

Now we investigate the performance of the optimum receiver in terms of the bit error probability. The decision rule of the optimum receiver derived earlier in (6.17) can be rearranged and written as

$$R_0 - R_1 \underset{\mathrm{H_1}}{\overset{\mathrm{H_0}}{\gtrless}} \frac{(|J_1| - |J_0|)\sqrt{E_b}N_J}{2\rho N_s} \tag{6.22}$$

where

$$R_0 = N_0 \sum_{k \in J_0} r_{0k} + \left(N_0 + \frac{N_J}{\rho}\right) \sum_{k \notin J_0} r_{0k} \tag{6.23}$$

and

$$R_1 = N_0 \sum_{k \in J_1} r_{1k} + \left(N_0 + \frac{N_J}{\rho}\right) \sum_{k \notin J_1} r_{1k}. \tag{6.24}$$

Without loss of generality, assume data bit 0 is sent. Conditioned on 0 being sent, each term in the above expression is Gaussian distributed and all terms are independent.

Then the mean (μ_{R_i}) and variance ($\sigma^2_{R_i}$) of R_0 and R_1 can be computed as

$$\mu_{R_0} = \frac{\sqrt{E_b}}{N_s}\left[|J_0|N_0 + (N_s - |J_0|)\left(N_0 + \frac{N_J}{\rho}\right)\right] \tag{6.25}$$

$$\sigma^2_{R_0} = a|J_0| + b(N_s - |J_0|) \tag{6.26}$$

$$\mu_{R_1} = 0 \tag{6.27}$$

$$\sigma^2_{R_1} = a|J_1| + b(N_s - |J_1|) \tag{6.28}$$

where $a = \frac{N_0^2}{2}\left(\frac{N_0}{N_s} + \frac{N_J}{\rho N_s}\right)$ and $b = \frac{N_0}{2N_s}\left(N_0 + \frac{N_J}{\rho}\right)^2$. Therefore, the decision statistic $R = R_0 - R_1$ is Gaussian with mean (μ_R) and variance (σ^2_R) given by

$$\mu_R = \frac{\sqrt{E_b}}{N_s}\left[|J_0|N_0 + (N_s - |J_0|)\left(N_0 + \frac{N_J}{\rho}\right)\right] \tag{6.29}$$

$$\sigma^2_R = a(|J_0| + |J_1|) + b(2N_s - |J_0| - |J_1|). \tag{6.30}$$

A bit error occurs when R is less than the threshold

$$t(J_0, J_1) = \frac{(|J_1| - |J_0|)\sqrt{E_b}N_J}{2\rho N_s}. \tag{6.31}$$

Thus, given (J_0, J_1), the bit error probability can be computed as

$$P_b(J_0, J_1) = \int_{-\infty}^{t} \frac{1}{\sqrt{2\pi\sigma^2_R}} \exp\left(-\frac{(x - \mu_R)^2}{2\sigma^2_R}\right) dx = Q\left(\frac{\mu_R - t}{\sigma_R}\right) \tag{6.32}$$

where $Q(\cdot)$ is defined as $Q(x) = \int_x^\infty \frac{1}{\sqrt{2\pi}} \exp\left(-\frac{x^2}{2}\right) dx$. The average bit error probability by averaging $P_b(J_0, J_1)$ over (J_0, J_1) and is given by

$$P_b = \sum_{|J_0|}\sum_{|J_1|}\left[\binom{N_s}{|J_0|}\binom{N_s}{|J_1|}\rho^{(|J_0|+|J_1|)} \cdot (1-\rho)^{(2N_s - |J_0| - |J_1|)} Q\left(\frac{\mu_R - t}{\sigma_R}\right)\right]. \tag{6.33}$$

Notice that this result can be easily computed.

6.4.2 Suboptimum Linear Receiver

For the linear receiver, during one bit duration, the receiver combines $2N_s$ chip correlator outputs to make the decision. Assume k out of these $2N_s$ chips are jammed. Then the variance of the total interference plus noise is given by $N_0 + \frac{kN_J}{2\rho N_s}$, and the conditional bit error probability is given by $Q\left(\sqrt{\frac{E_b}{N_0+\frac{kN_J}{2\rho N_s}}}\right)$. The average probability of bit error can then be derived by averaging the above expression over all possible values of k and is given by

$$P_b = \sum_{k=0}^{2N_s} \binom{2N_s}{k} \rho^k (1-\rho)^{2N_s-k} Q\left(\sqrt{\frac{E_b}{N_0 + \frac{kN_J}{2\rho N_s}}}\right). \tag{6.34}$$

6.4.3 Suboptimum Nonlinear Receiver

According to the decision rule obtained in (6.21), the bit error probability of the nonlinear receiver can be computed as

$$P_b = \frac{1}{2}\Pr(r^* < 0|\mathrm{H}_0) + \frac{1}{2}\Pr(r^* > 0|\mathrm{H}_1) = \Pr(r^* < 0|\mathrm{H}_0), \tag{6.35}$$

and the second equality is due to the assumption that 0 and 1 are equally likely to be transmitted. In order to compute the above probability, we need to know the probability distribution of r^*, and equivalently, the distribution of $y_k = h(r_k)$. The conditional mean of y_k can be computed in a similar way as in equation (5.61), and is given by [40]

$$\begin{aligned} \mathrm{E}\left[y_k|\mathrm{H}_0\right] &= \int_{-\infty}^{\infty} y_k f(y_k) dy_k \\ &\cong \int_{-\infty}^{\infty} h(r_k) \left[f_{Z_0}(r_k) - \frac{\sqrt{E_b}}{N_s} f'_{Z_0}(r_k)\right] dr_k \\ &= \frac{\sqrt{E_b}}{N_s} L \end{aligned} \tag{6.36}$$

where

$$L = \int_{-\infty}^{\infty} h^2(x) f_{Z_0}(x) dx. \tag{6.37}$$

Similarly to equation (5.63), we have

$$\mathrm{E}\left[y_k^2 | \mathrm{H}_0\right] = L, \tag{6.38}$$

and the conditional variance of y_k is given by

$$\mathrm{Var}\left[y_k | \mathrm{H}_0\right] = L - \frac{E_b}{N_s^2} L^2. \tag{6.39}$$

Therefore, the conditional mean and variance of r_k can be represented as

$$\mathrm{E}\left[r_k | \mathrm{H}_0\right] = \mathrm{E}\left[\sum_{k=0}^{N_s-1} y_k^2 | \mathrm{H}_0\right] = \sqrt{E_b} L \tag{6.40}$$

$$\mathrm{Var}\left[r_k | \mathrm{H}_0\right] = \sum_{k=0}^{N_s-1} \mathrm{Var}\left[y_k | \mathrm{H}_0\right] = N_s L - \frac{E_b}{N_s} L^2. \tag{6.41}$$

In the ideal case, the interference is suppressed after passing the correlator outputs through the nonlinear function. Thus, the nonlinear function output is interference free and the same as the single-user AWGN channel case. In practice, the interference suppression is not perfect and there is still residual interference in the nonlinear function output. If N_s is considerably large, the output can be approximated as a Gaussian random variable. The error probability can then be approximated by

$$P_b \simeq Q\left(\sqrt{\frac{E_b L^2}{N_s L - \frac{E_b}{N_s} L}}\right) = Q\left(\sqrt{\frac{E_b}{\frac{N_s}{L} - \frac{E_b}{N_s}}}\right). \tag{6.42}$$

Note that in this expression, L depends on the PDF of the interference and has to be evaluated numerically.

6.5 Numerical Examples

In this section we present numerical examples of the performance of the different receivers mentioned in the previous sections.

6.5.1 Optimum Receiver

Figure 6.4 shows the performance of the optimum receiver for $N_s = 1, 2, \cdots, 10$ with signal-to-interference ratio (SIR) $E_b/N_J = -10$ dB and jamming fractional probability $\rho = 0.3$. It can be observed that when N_s increases, the performance gets closer to the single-user AWGN channel case. However, there is a limitation of improvement by increasing N_s. For the bit error probability (BER) of 10^{-5} and $N_s = 10$, there is still a 2 dB performance gap to the single-user AWGN case. In Figure 6.5, the SNR is fixed at $E_b/N_0 = 15$ dB, and the BER is shown versus the SIR. The substantial BER improvement by increasing N_s can be seen clearly in the low SIR region. The BER versus jamming fraction is shown in Figure 6.6. It can be seen that ρ has a larger impact on large value of N_s than small value. However, in full-band jamming ($\rho = 1$), the performance is almost the same for any value of N_s.

6.5.2 Suboptimum Linear Receiver

For the suboptimum linear receiver, the BER performance versus SIR for $\rho = 0.1$ and 0.3 is shown in Figure 6.7. First note the crossover of the plots for $N_s = 1$ to 10 in both figures. The crossover divides the plots into two regions. In the high SIR region, the BER decreases as N_s increases. However, in the low SIR region, increasing N_s degrades the system performance. This is because when the signal to interference plus noise ratio is small, a coded system can perform worse than the uncoded system. Also note that the smaller jamming fraction has a higher impact on the performance difference among different values of N_s.

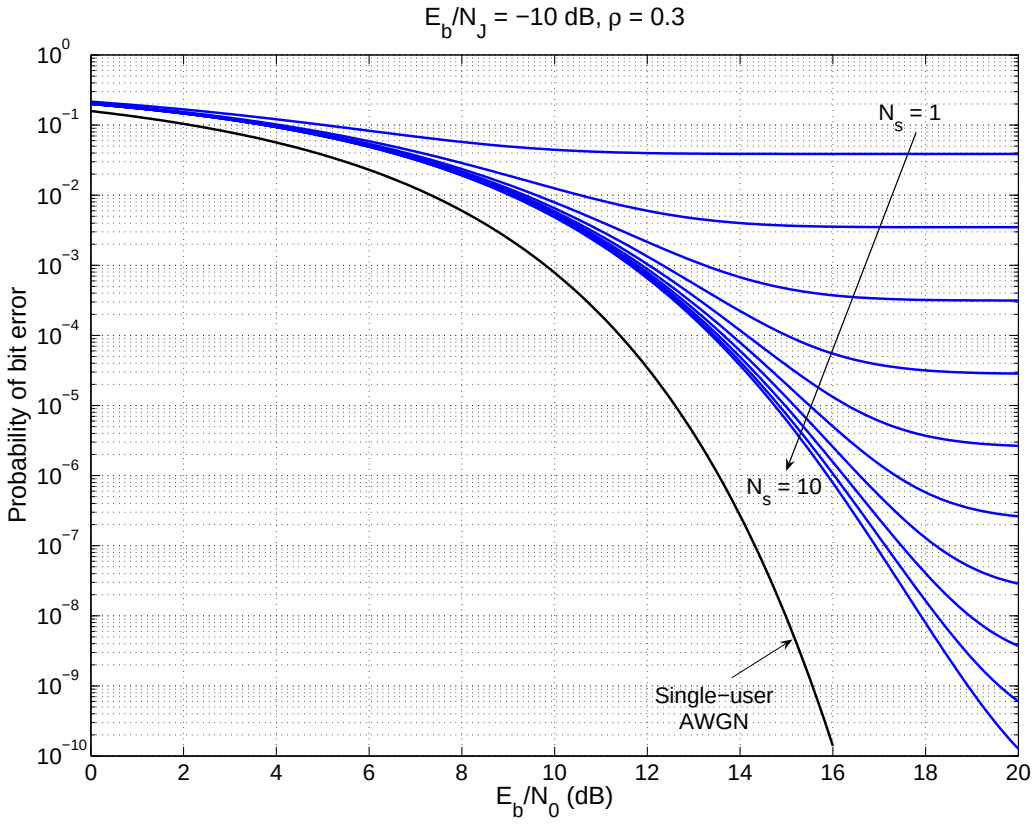

Figure 6.4: Performance of the optimum receiver.

6.5.3 Suboptimum Nonlinear Receiver

Figure 6.8 shows simulation results of the BER performance of the suboptimum nonlinear receiver versus the SNR for the SIR at -10 dB and $\rho = 0.3$. Notice that as the SNR increases, at some point, the BER bounces back and increases. Eventually when SNR is large enough (say 30 dB), increasing N_s degrades the performance. There are two main reasons for this phenomenon. First, within the N_s chips, not all of the are jammed. However, those non-jammed chips are still passed through the nonlinear function. For the non-jammed chips, the nonlinear function is not optimum since only AWGN is presented. The other reason is that when SNR is large, for the non-jammed chips, the small signal assumption does not hold, and the LOBD algorithm can not be applied to enhance performance. This can be seen in Figure 6.9. In this figure, for high

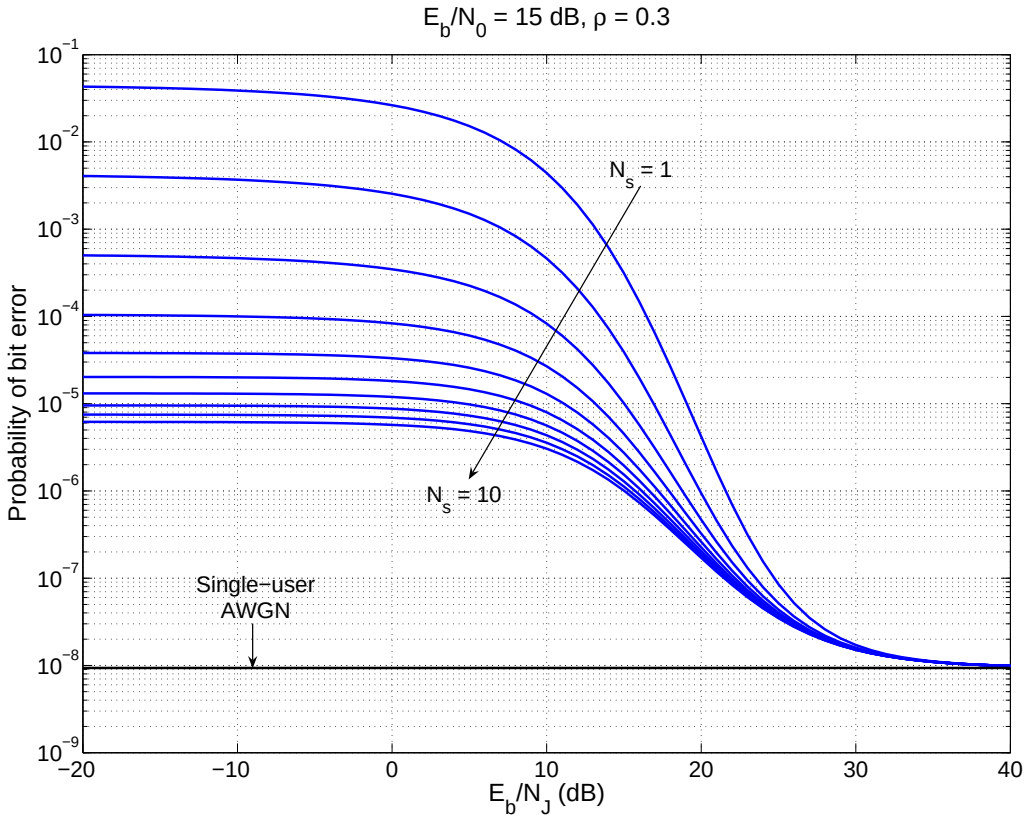

Figure 6.5: Performance of the optimum receiver.

SNR (say 25 dB), the linear region of the nonlinear function actually lies within the desired signal's amplitude. To demonstrate the ideas, if we pass the non-jammed chips through the function matched to the AWGN distribution (which is linear) instead of the original nonlinear function, the BER does not bounce back as SNR increases. This is shown in the dotted lines in Figure 6.10. Figure 6.11 shows the performance of the nonlinear receiver against the jamming fraction ρ. Note that for small ρ region, a large value of N_s can have a substantial performance improvement.

6.5.4 Comparison

Figure 6.12 shows the comparison of the performance of the optimum receiver and the suboptimum receivers for SIR $= -10$ dB, $N_s = 10$, and $\rho = 0.3$. It can be seen

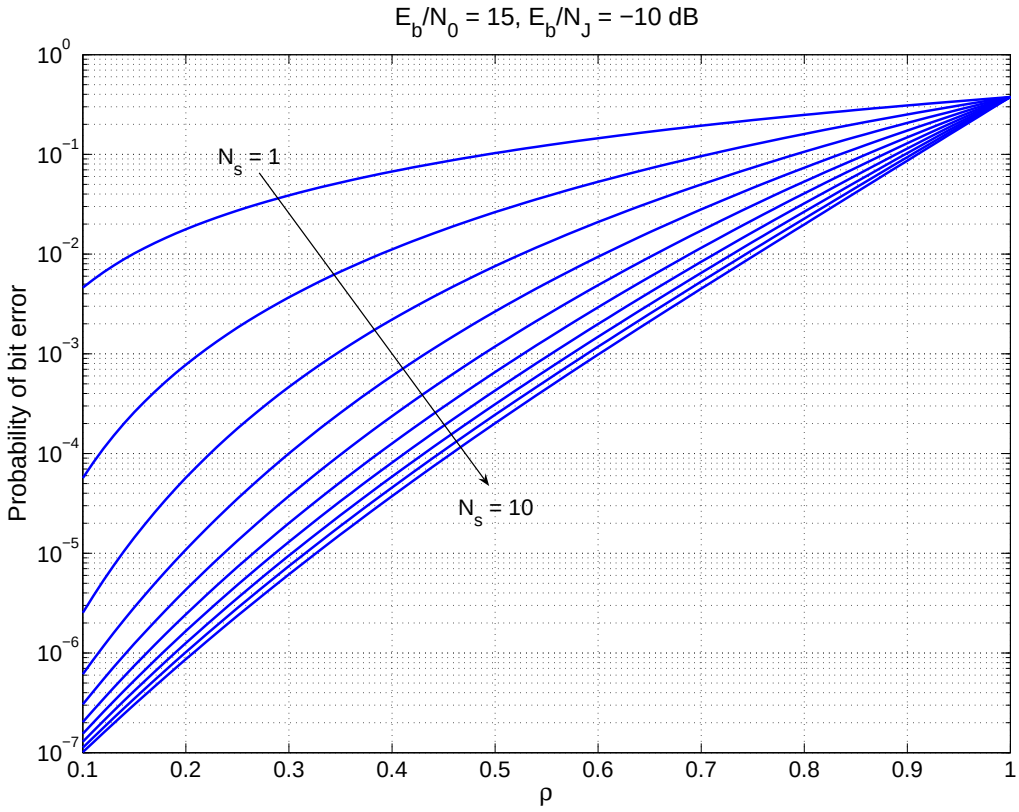

Figure 6.6: Performance of the optimum receiver.

that the nonlinear receiver outperforms the linear receiver in the low SNR region from 0 dB to about 17 dB. From 17 dB to 26 dB, the performance gap narrows down. This is because of the effect of the non-jammed chips. For the BER at 10^{-2}, there is still a performance gap a bit more than 5 dB between the nonlinear receiver and the optimum receiver. A more sophisticated coding scheme than the repetition code might be able to narrow the gap.

6.6 Conclusions

In this chapter, we designed and analyzed receivers for the ultra-wideband communication system in the presence of jamming interference. We compared the optimum

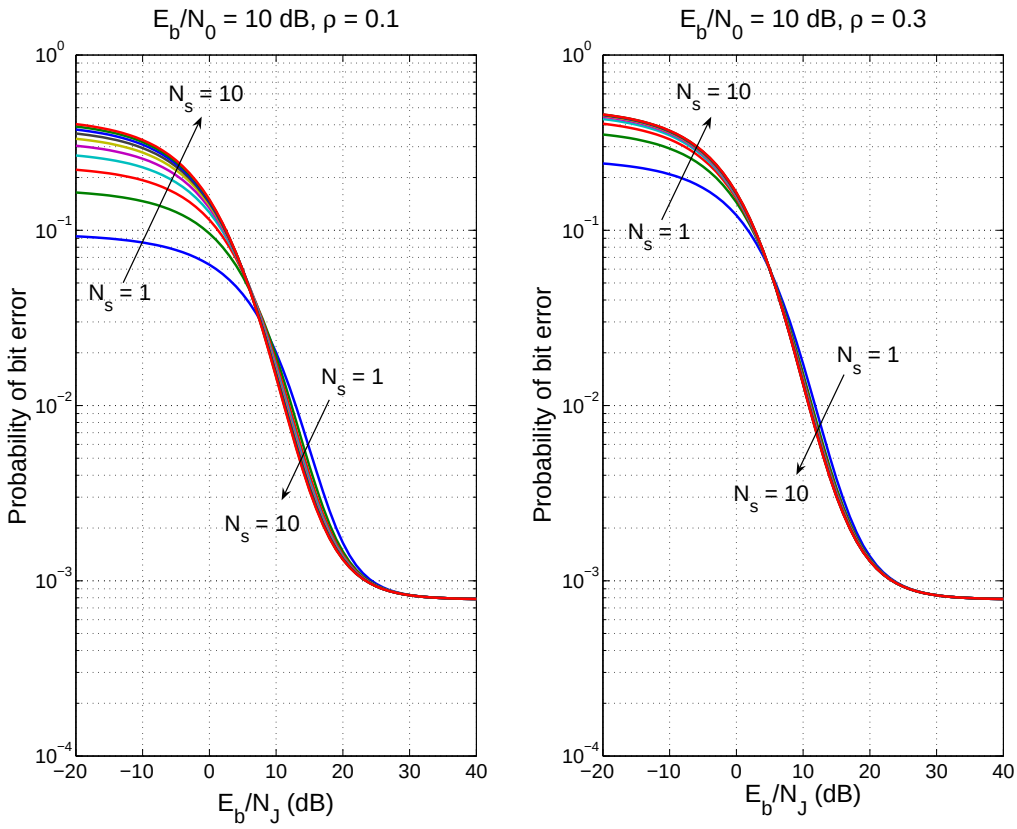

Figure 6.7: Performance of the suboptimum linear receiver.

receiver with two feasible suboptimum receivers. The suboptimum nonlinear receiver outperforms the linear one, especially when the interference is severe. Numerical results show the effectiveness of the repetition coding scheme in different conditions. The good thing about the suboptimum nonlinear receiver is that it has a simple threshold detector structure. The complexity comes in finding the probability distribution of the interference.

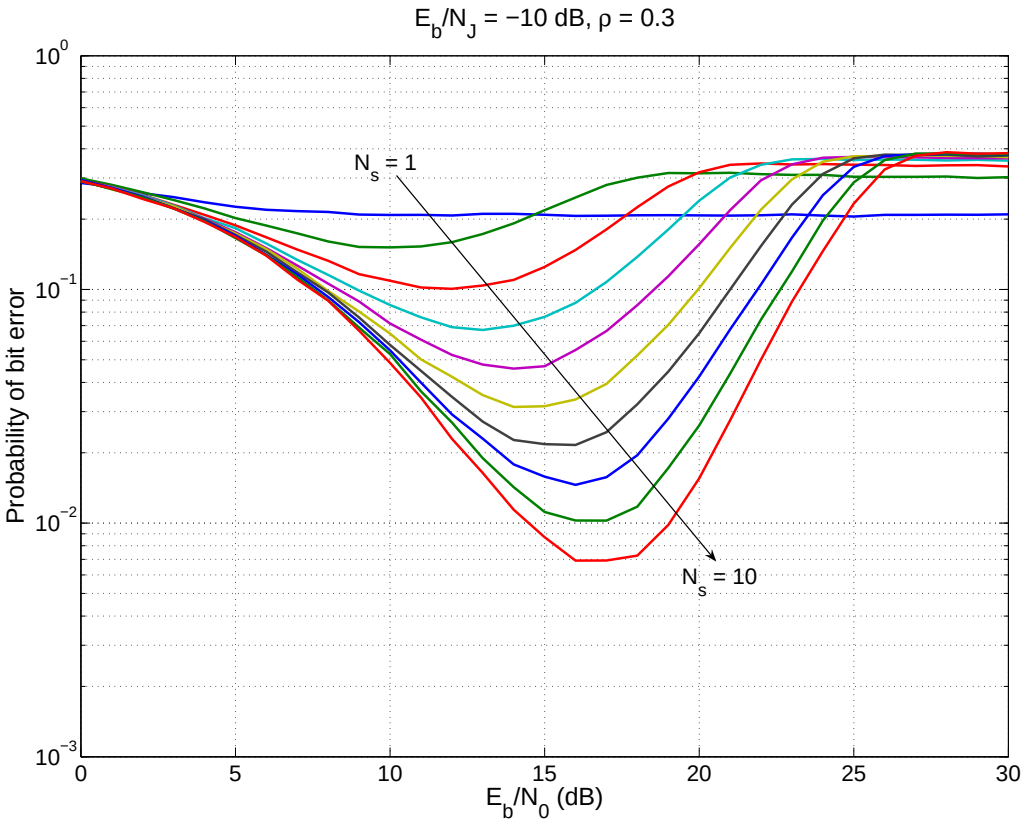

Figure 6.8: Performance of the suboptimum nonlinear receiver.

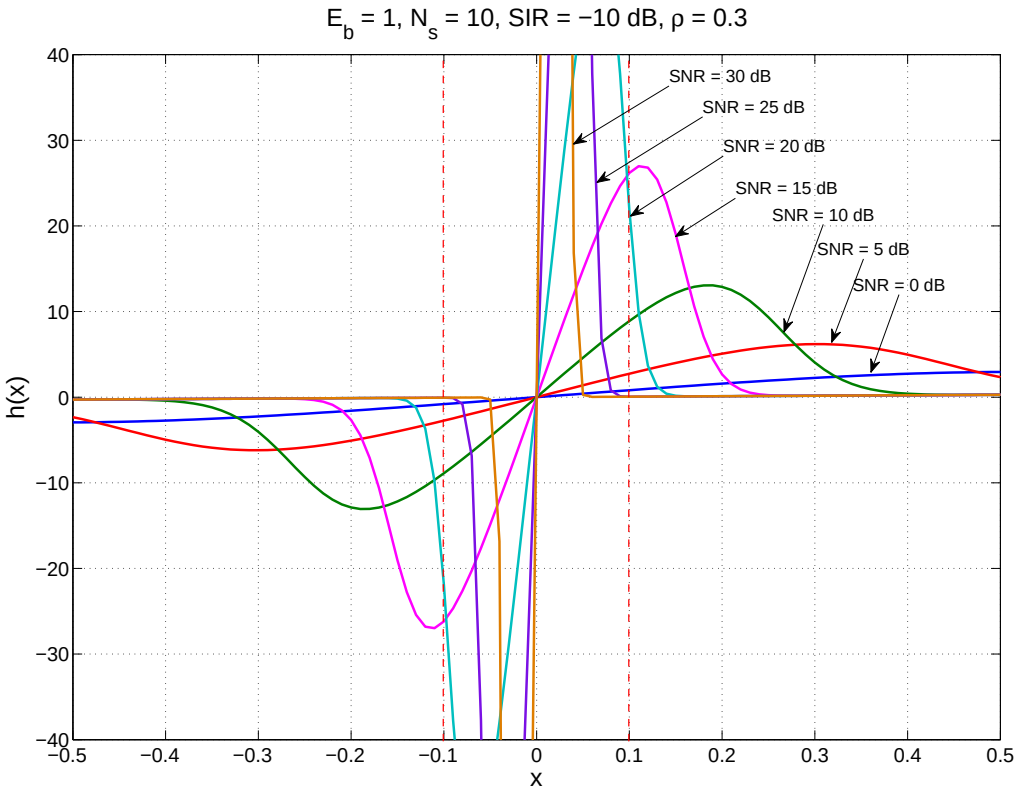

Figure 6.9: Nonlinear LOBD function of different SNR.

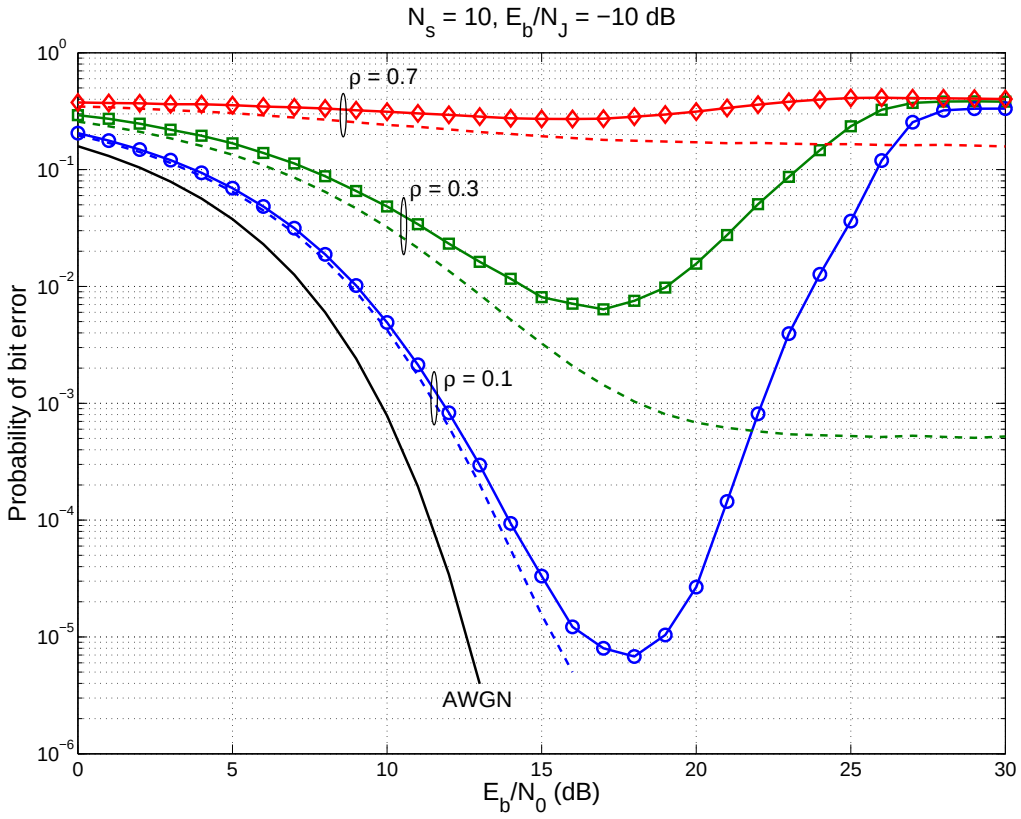

Figure 6.10: Performance of the suboptimum nonlinear receiver.

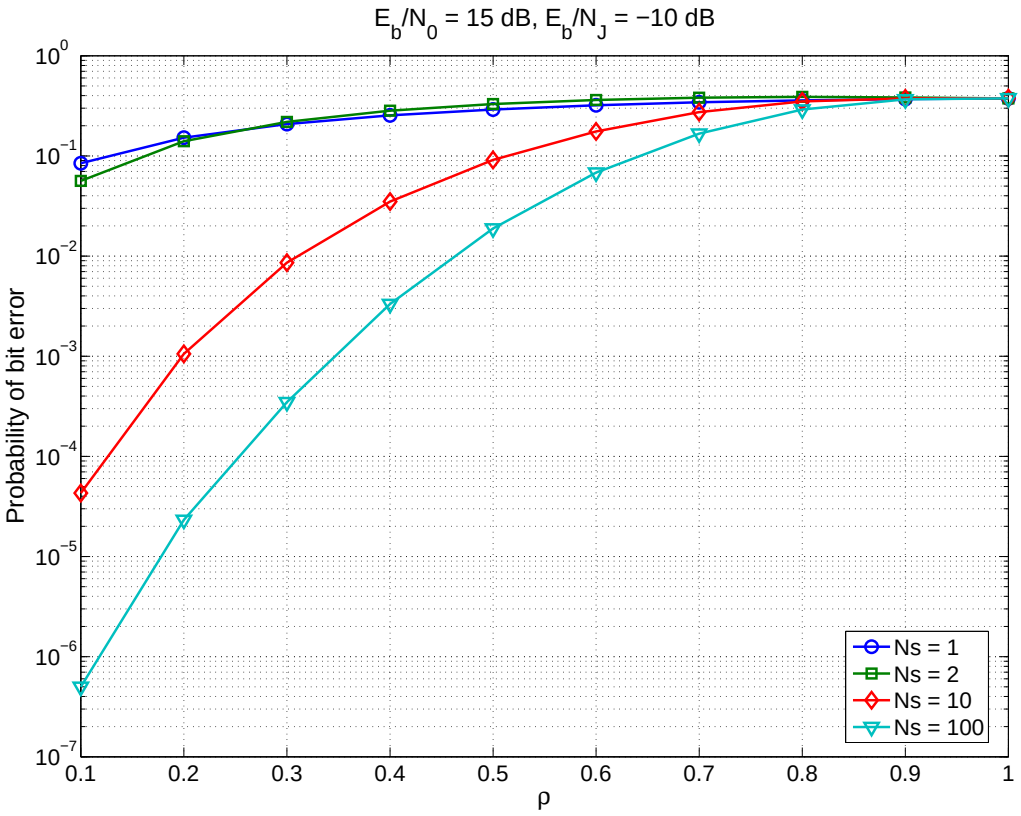

Figure 6.11: Performance of the suboptimum nonlinear receiver.

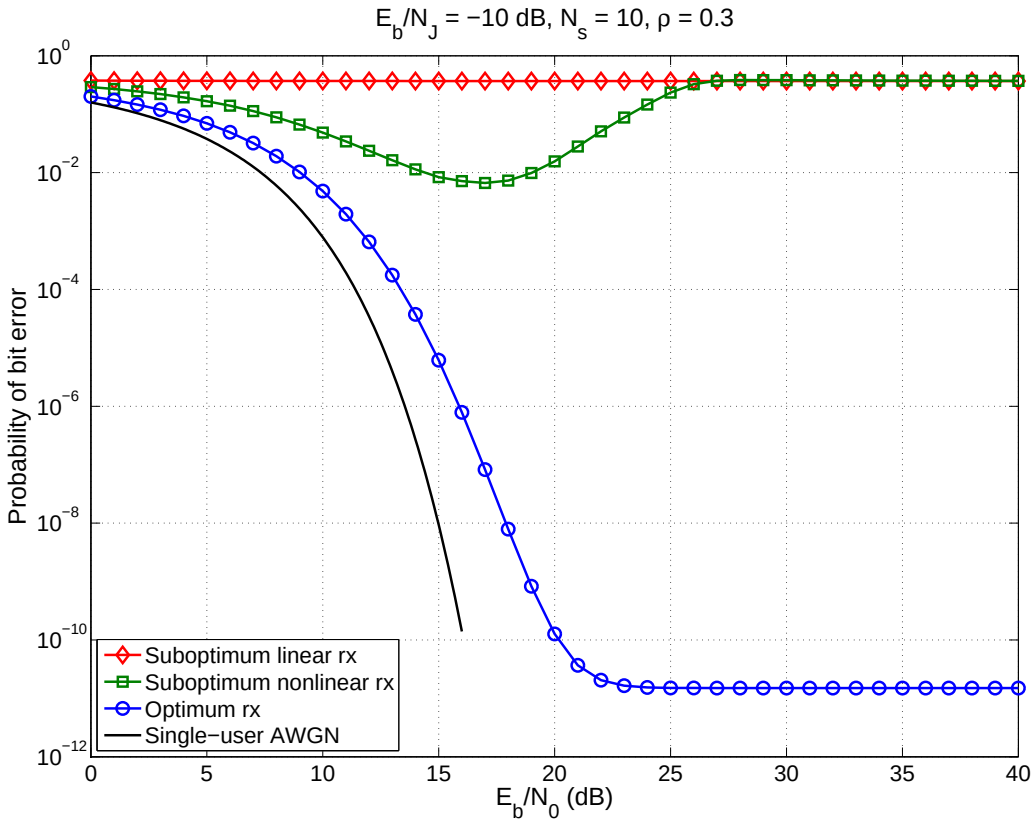

Figure 6.12: Performance comparison of different receivers.

CHAPTER 7

Adaptive Receiver for UWB Communications

7.1 Introduction

The nonlinear receiver design based on the LOBD algorithm in Chapters 5 and 6 requires the knowledge of the PDF of the interference. In the previous chapters, we demonstrated that in theory the receiver design can suppress interference with the knowledge of the interference PDF. In practice, the interference PDF is unknown to the receiver and needs to be estimated. For practical purpose, it is also necessary for the receiver to keep tracking the PDF of the interference due to the time-varying nature of the communication link. Therefore, for implementation, it requires the receiver to estimate the PDF or the nonlinear signal processing function in real-time in order to successfully suppress interference. The adaptive receiver structure for an impulse radio based UWB system is shown in Figure 7.1. The receiver keeps taking interference samples and updating the nonlinear function in order to ensure the suppression of the interference.

There are many ways to estimate the PDF of a random signal. In general, the PDF of a random signal can be estimated using *parametric* or *nonparametric* estimators. Parametric estimation assumes the density to be some known parametric distribution. By identifying the characteristics of the signal, an estimate of the parameters of that distribution is made. This type of estimator can generate poor estimates if the dis-

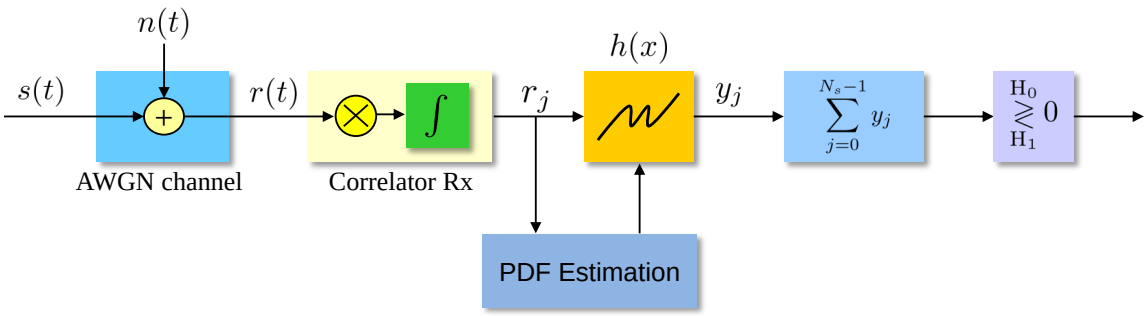

Figure 7.1: Adaptive LOBD receiver.

tribution of the signal is unknown a priori, or if the signal distribution is not of the form of the assumed distribution. Nonparametric estimation, on the other hand, does not make any assumption about the distribution of the signal. An intuitive nonparametric way to estimate the density function is to use the histogram of the signal. The histogram of a set of samples of a random signal is a plot showing the proportion of samples falling into adjacent, non-overlapping intervals called *bins*. The intervals are generally of the same size (bin width). The histogram representation of the PDF runs into difficulties when the signal is changing dynamically, and can not guarantee an efficient description of the distribution [48]. Another problem of the histogram estimation is that it is sensitive to the choice of bin width. Without careful selection of the bin width, important information may be lost in the histogram representation. A general form of nonparametric density estimation is *kernel density estimation* (KDE). The idea is to extrapolate the set of samples of the signal to the entire range of the distribution. To be specific, let $x_1, x_2, \ldots, x_n$ be a set of i.i.d. samples of a random signal, then the kernel density approximation of its probability density function is given by [49]

$$\hat{f}(x) = \frac{1}{nh} \sum_{i=1}^{n} K\left(\frac{x - x_i}{h}\right) \tag{7.1}$$

where $K(\cdot)$ is some *kernel function* and h is a smoothing parameter called the *bandwidth*. Quite often $K(\cdot)$ is taken to be a standard Gaussian function with zero mean and

unit variance. Thus the variance is controlled indirectly through the parameter h. A histogram can be regarded as a collection of point samples from a kernel density estimate for which the kernel is a uniform box the width of the histogram bin. As can be seen from equation (7.1), the computation of the PDF requires the summation of the kernel function evaluated over the set of samples. With a large size of samples, this computation can take quite some time and this does not suit the needs of a real-time estimator for the LOBD receiver.

In [48], cumulative distribution function (CDF) and quantiles are used for interference PDF estimation, and combined with the LOBD algorithm for interference suppression. It is then applied in [46] in a direct-sequence spread-spectrum (DS-SS) system with turbo coding for the continuous wave and Gaussian jamming interference cases. The nice thing about using quantiles for PDF estimation is that it does not change radically with the dynamic change of the signal. Quantile representation is also less likely to cause the loss of important information with equal-bin-width histogram counts. When combining quantile representation with LOBD algorithm, the computation of the nonlinear function output can be very simple, and makes it suitable for the real-time estimation purpose.

For IR-based UWB systems, interference PDF estimation might be done by collecting interference samples during the non-PPM chip duration as shown in Figure 7.2 and then form and update the CDF. Typically, the frame time or pulse repetition time may be a hundred to a thousand times of the monocycle width, therefore a sufficient number of interference samples can be obtained between two UWB pulses. The accuracy of the PDF estimation depends on the number of interference samples in the CDF. Note that the "interference sounding" process requires extra energy at the receiver. The more samples are collected, the more energy is required.

In this chapter, we will investigate the quantile PDF estimation method, and apply it to the adaptive receiver design for UWB communications to combat interference.

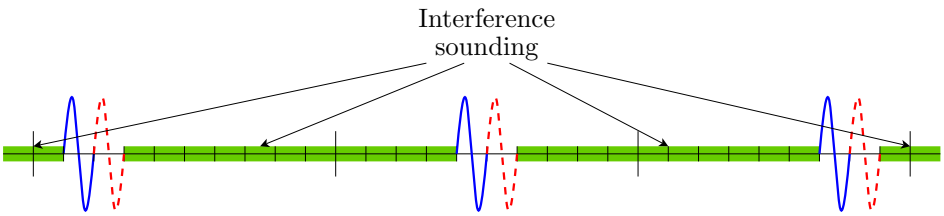

Figure 7.2: Interference sounding for PDF estimation.

7.2 Quantile for PDF Estimation

The histogram of a signal can be regarded as representation of the PDF of the random signal. The quantile representation can be thought of as the cumulative histogram, which can be used to represent or estimate the CDF of a random signal. Once the CDF is estimated from the quantile, the PDF can be estimated from the CDF by derivation.

Let $x = \{x_1, x_2, \ldots, x_{N_s}\}$ be the set of N_s samples of a random signal. We can sort the samples so that they are in ascending order ($x_1 \leq x_2 \leq \ldots \leq x_{N_s}$). Let $A_0, A_1, \ldots, A_N$ represent the quantile of the samples where A_k is the sample $x_k \in x$ in the k/N percentile position of the sample set x. For example, when $k = N/2$ (assume that N is even), $A_{N/2}$ is the median of x. When $k = N$, $A_N = x_{N_s}$ is the maximum of the set x. For $k = 0$, we can set $A_0 = x_1$ to be the minimum of the set x with the assumption that $N_s \gg N$ in most cases. Thus, the empirical CDF is formed by mapping A_k to k/N. Figure 7.3 shows the histogram and quantile representation of a Gaussian distribution with zero mean and unit variance with $N_s = 8192$ samples and $N = 16$ bins. As can be seen, the quantile is closely matched to the actual CDF of a Gaussian distribution. The estimate of the PDF from the quantile representation can be done by taking the ratio of the difference of the quantile bins ($1/N$) and the difference of A_k's. Figure 7.4 shows the estimated PDF from the quantile plot shown in Figure 7.3b. As can be seen, the PDF estimate is not smooth and does not closely match the actual PDF. However, it does have the general trend of the actual PDF. For the case of increasing the number of bins to $N = 64$, the estimated PDF is shown in

Figure 7.5. It can be observed that the estimation is closer to the actual PDF in general shape, but in detail it is spiky. Similar to the KDE method in which the selection of the bandwidth can vary the smoothness of the estimate, when using quantile to estimate the PDF, the number of bins can also affect the smoothness of the result. However, the quantile method requires much less computation compared to the KDE method.

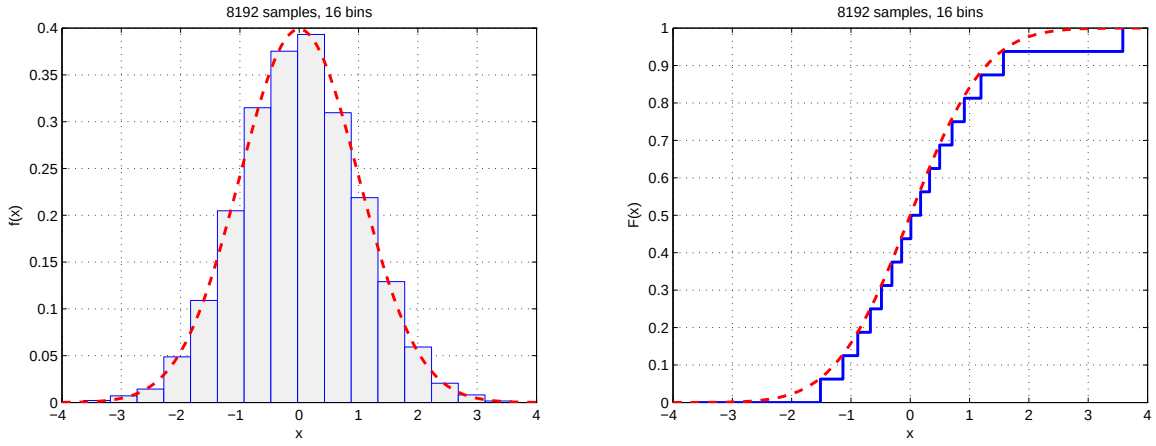

(a) (b)

Figure 7.3: Gaussian distribution $N(0,1)$ (a) histogram representation (b) quantile representation.

7.3 Adaptive LOBD Receiver

In this section, we demonstrate how to apply quantile PDF estimator to the implementation of the LOBD receiver to estimate and update the nonlinear function. It is shown in Chapters 5 and 6 that the signal processing function of the LOBD receiver is nonlinear in general and is of the form

$$h(x) = -\frac{f^{'}(x)}{f(x)} \tag{7.2}$$

where $f(x)$ is the PDF of the interference. With the quantile representation of the CDF at A_k, we have the estimate of the CDF $F_k = k/N$. To obtain f from the derivative of

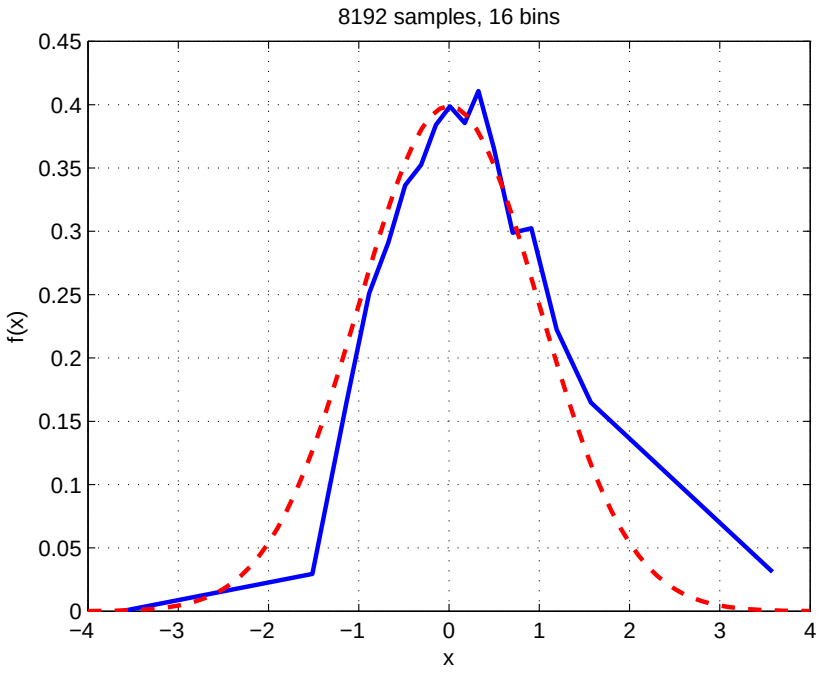

Figure 7.4: Estimated PDF from quantile representation.

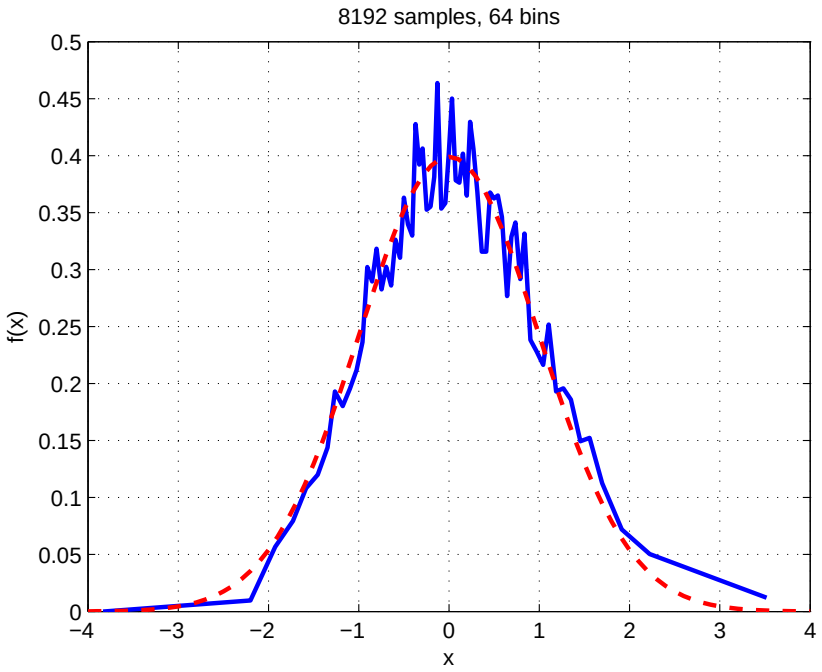

Figure 7.5: Estimated PDF from quantile representation.

F, the technique used in [48] is to evaluate F_k at "half a quantile" from A_k.

$$f_k = \left(\frac{dF}{dA}\right)_k = \frac{F_{k+\frac{1}{2}} - F_{k-\frac{1}{2}}}{A_{k+\frac{1}{2}} - A_{k-\frac{1}{2}}} = \frac{1}{N\left(A_{k+\frac{1}{2}} - A_{k-\frac{1}{2}}\right)}. \tag{7.3}$$

To obtain $f^{'}$ from the derivative of f, we can compute in a similar way

$$f_k^{'} = \left(\frac{df}{dA}\right)_k = \frac{f_{k+\frac{1}{2}} - f_{k-\frac{1}{2}}}{A_{k+\frac{1}{2}} - A_{k-\frac{1}{2}}} = \frac{\frac{1}{N(A_{k+1}-A_k)} - \frac{1}{N(A_k-A_{k-1})}}{A_{k+\frac{1}{2}} - A_{k-\frac{1}{2}}}. \tag{7.4}$$

The LOBD nonlinear function is then given by

$$h_k = -\frac{f_k'}{f_k} = -\frac{\frac{1}{A_{k+1}-A_k} - \frac{1}{A_k-A_{k-1}}/N\left(A_{k+\frac{1}{2}} - A_{k-\frac{1}{2}}\right)}{1/N\left(A_{k+\frac{1}{2}} - A_{k-\frac{1}{2}}\right)} = \frac{1}{A_k - A_{k-1}} - \frac{1}{A_{k+1} - A_k} \tag{7.5}$$

Equation (7.5) provides the desired receiver output with simple computation. with an input x to the LOBD function, it is first sorted to the nearest quantile A_k, and the corresponding h_k is the function output. In actual implementation, the receiver has to maintain the quantile $A_0, A_1, \ldots, A_N$ using the most recent samples of the interference. For the input to the LOBD function, a sorting process is required to find the nearest quantile value for generating the output. Due to the simple arithmetic of the output computation, the most time consuming part in the processing is to perform sorting to form the quantile and match it to the function input.

Receiver Implementation

The implementation of the adaptive LOBD algorithm at the receiver requires a buffer of size N_s to store interference samples, and another buffer of size N to store the quantile $A_1, A_2, \ldots, A_N$. For an IR-based UWB system with PPM modulation, interference samples can be collected during the non-PPM chip durations. Initially, the receiver collects N_s interference samples and store them in the interference buffer.

The interference samples need to be sorted in order to generating the quantile. Let $x = \{x_1, x_2, \ldots, x_{N_s}\}$ be the sorted samples (in ascending order) of interference stored in the buffer. The quantile is formed by assigning the sample at the k/N percentile position, $x_{\lfloor \frac{kN_s}{N} \rfloor}$, to A_k. The quantile $A_1, A_2, \ldots, A_N$ is stored in the quantile buffer. The adaptive LOBD algorithm can be summarized in the following steps:

1. During the PPM chip duration, the correlator receiver output r is first sorted to the nearest quantile A_k. Then the LOBD function output is computed according to equation (7.5).

2. During the non-PPM chip duration, whenever the correlator receiver outputs a interference sample, the interference buffer is updated by replacing the oldest interference sample with the current one. Then the new set of interference samples $x = \{x_1, x_2, \ldots, x_{N_s}\}$ is sorted and stored in the buffer.

3. The quantile $A_1, A_2, \ldots, A_N$ is updated with the current interference buffer.

4. Go back to step 1.

7.3.1 Adaptive Receiver for MAI

For the multiple-access UWB system described in Chapter 5, consider the MAI in the case shown in Figure 5.6 with the system parameters $N_c = 2$, $N_s = 1$, $E_1/N_0 = 0$ dB, $E_2/E_1 = 20$ dB. By taking 8192 samples from the MAI, the 16-bin histogram and quantile representations of the PDF and CDF is shown in Figure 7.6. The estimated LOBD function is shown in Figure 7.7 (solid line) compared with the theoretical LOBD function (dash line). Both the histogram and quantile plots give us pretty good ideas about the distribution. The estimated LOBD function does have three regions close to the three linear regions in the theoretical function. Even though the "linear" region in the estimated function is smaller than that in the original function, it can still suppress interference since the function output is limited to roughly -1.5 to 1.5 as shown in the

figure. Figure 7.8 shows the probability of bit error of the adaptive LOBD receiver for the two-user case as shown in Figure 5.12. It can be observed that the performance of the adaptive LOBD receiver is very close to the theoretical performance with the perfect knowledge of the interference PDF. When the interference is strong, the adaptive LOBD receiver is able to suppress interference and performance is comparable to the interference-free single-user AWGN case. This is consistent with the results shown in Chapter 5.

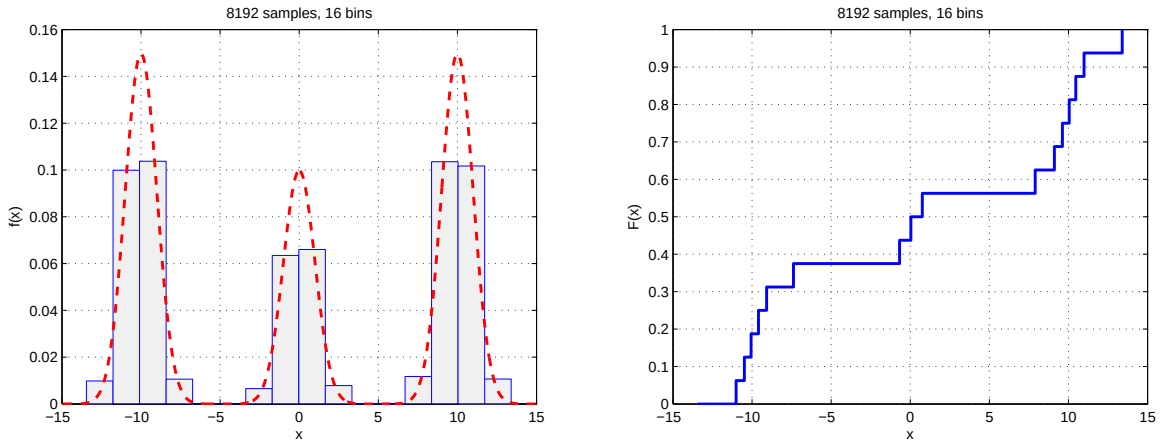

(a) (b)

Figure 7.6: MAI ($N_c = 2$, $N_s = 1$, $E_1/N_0 = 0$ dB, $E_2/E_1 = 20$ dB) (a) histogram representation (b) quantile representation.

7.3.2 Adaptive Receiver for Gaussian On-Off Jamming

For the on-off Gaussian jammer in UWB communications described in Chapter 6, one of the examples of the LOBD function is shown in Figure 6.3 with parameters $E_b/N_0 = 5$ dB, $E_b/N_J = -10$ dB, $N_s = 10$, and $\rho = 0.3$. The histogram and quantile plots representing PDF and CDF using 8192 samples in 8 bins are shown in Figure 7.9. The estimated LOBD function is shown in Figure 7.10 (solid line) compared with the theoretical LOBD function (dash line). Similar to the MAI case, the linear region of the theoretical LOBD function is clearly shown in the estimated function. Again,

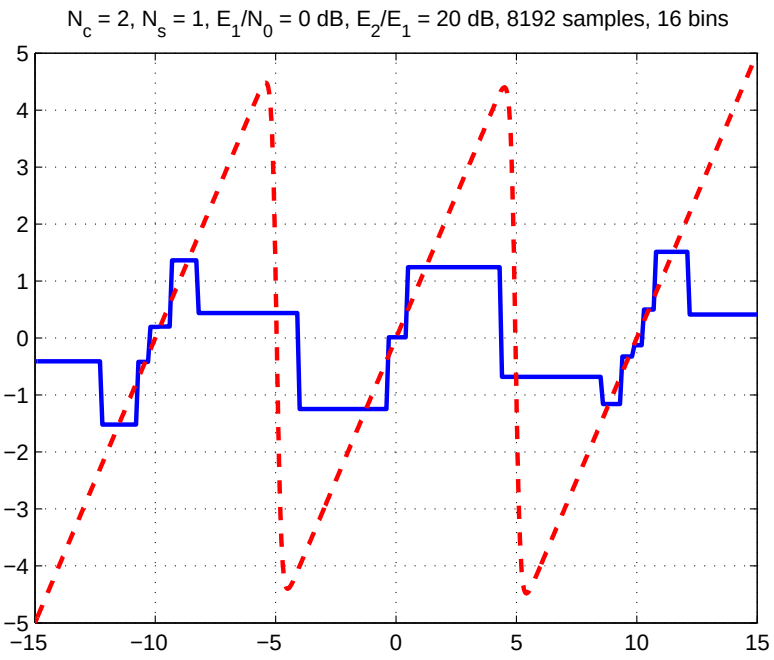

Figure 7.7: Estimated LOBD function for MAI.

even though the estimated function does not follow the theoretical function exactly, the interference suppression capability can still be observed. The probability of bit error of the adaptive LOBD receiver is shown in Figure 7.11. The adaptive receiver performance is very close to the theoretical LOBD receiver performance in the low SNR region before the BER curve bounces back. In the high SNR region when the theoretical BER bounces back, the adaptive receiver BER has a similar trend, but it outperforms the theoretical LOBD receiver. This is because the adaptive algorithm cannot perfectly estimate the theoretical LOBD function, which performs poorly in the high SNR region where the small signal assumption does not hold as discussed in Chapter 6. The adaptive algorithm is not able to create the estimate of the LOBD function with sharp transition from the linear region to the nonlinear region as shown in Figure 6.9, which unintentionally improved the BER performance. This is shown in Figure 7.12 when SNR is 20 dB. Compare it Figure 7.10, it can be seen clearly that the estimate of LOBD function when SNR = 20 dB does not match the theoretical one as

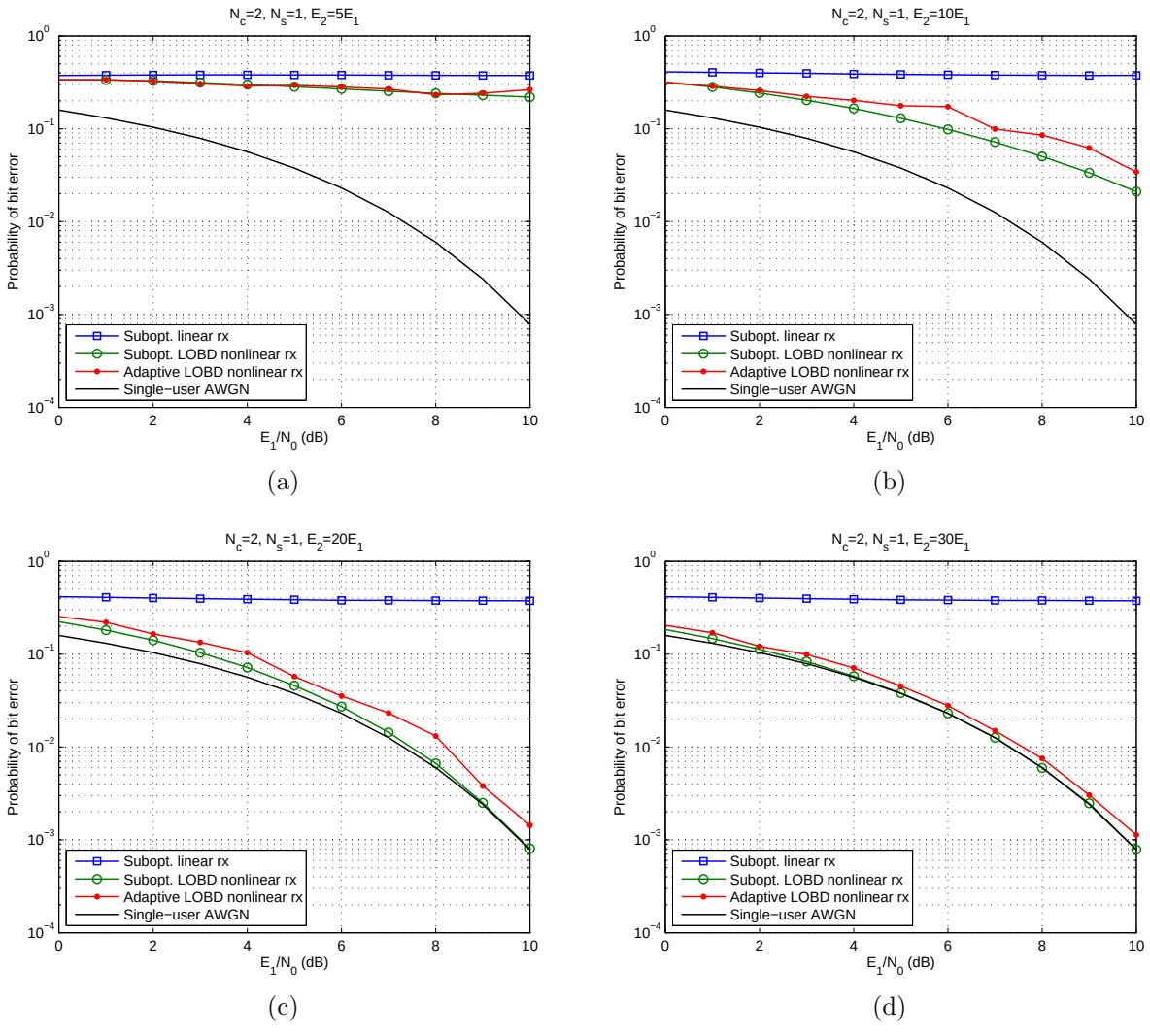

Figure 7.8: Adaptive LOBD receiver for MAI suppression ($N_c = 2, N_s = 1$) (a)$E_2 = 5E_1$ (b)$E_2 = 10E_1$ (c)$E_2 = 20E_1$ (d)$E_2 = 30E_1$.

well as the case when SNR = 5 dB.

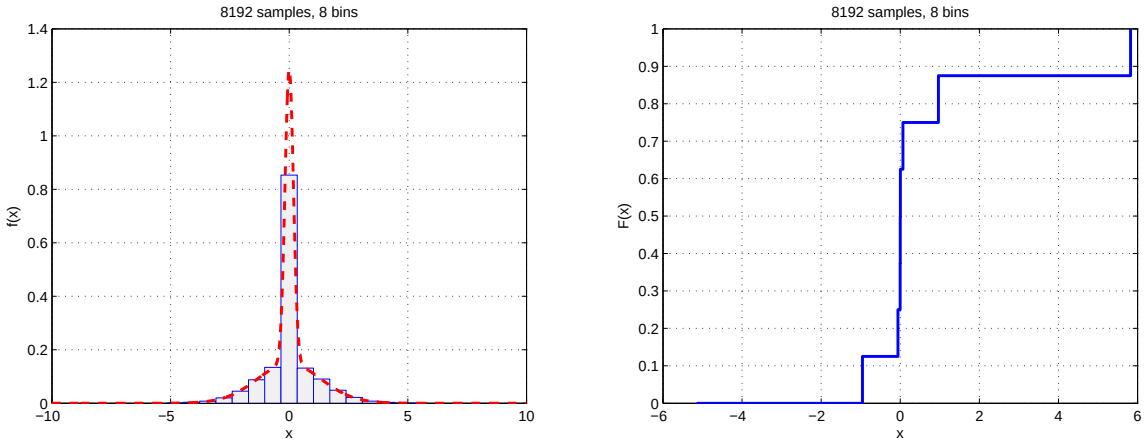

(a) (b)

Figure 7.9: Gaussian on-off jammer ($E_b/N_0 = 5$ dB, $E_b/N_J = -10$ dB, $N_s = 10$, $\rho = 0.3$) (a) histogram representation (b) quantile representation.

7.4 Conclusions

In this chapter, we investigate a real-time PDF estimation technique that can be applied to the LOBD receiver for UWB communications to adaptively estimate and update the LOBD function for signal processing to suppress interference. Numerical results show that the LOBD function can be estimated in an efficient way with small number of quantile bins, and can be close to the theoretical LOBD function derived from the actual interference PDF for the MAI and Gaussian on-off jammer. This adaptive receiver scheme makes the suboptimum receiver design for UWB systems practical with low complexity for easy implementation.

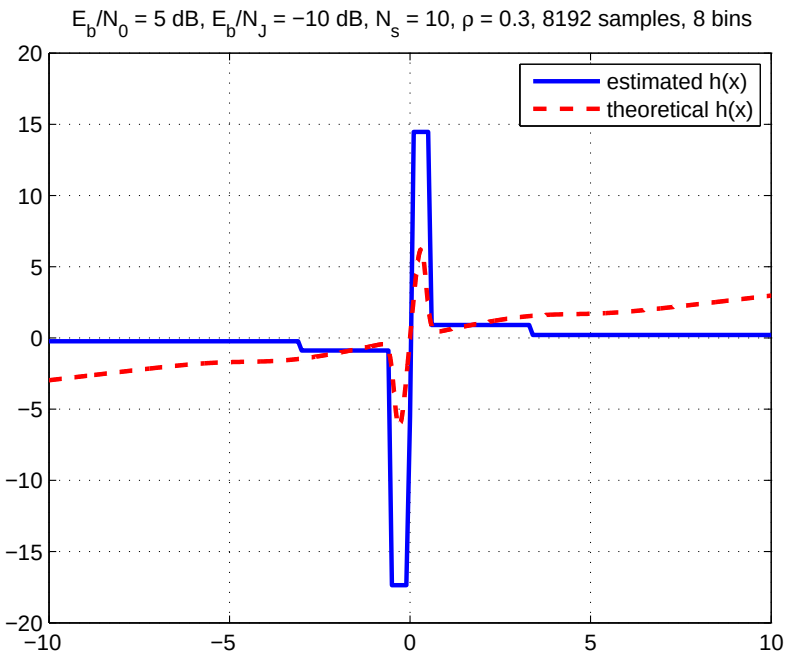

Figure 7.10: Estimated LOBD function for Gaussian on-off jammer.

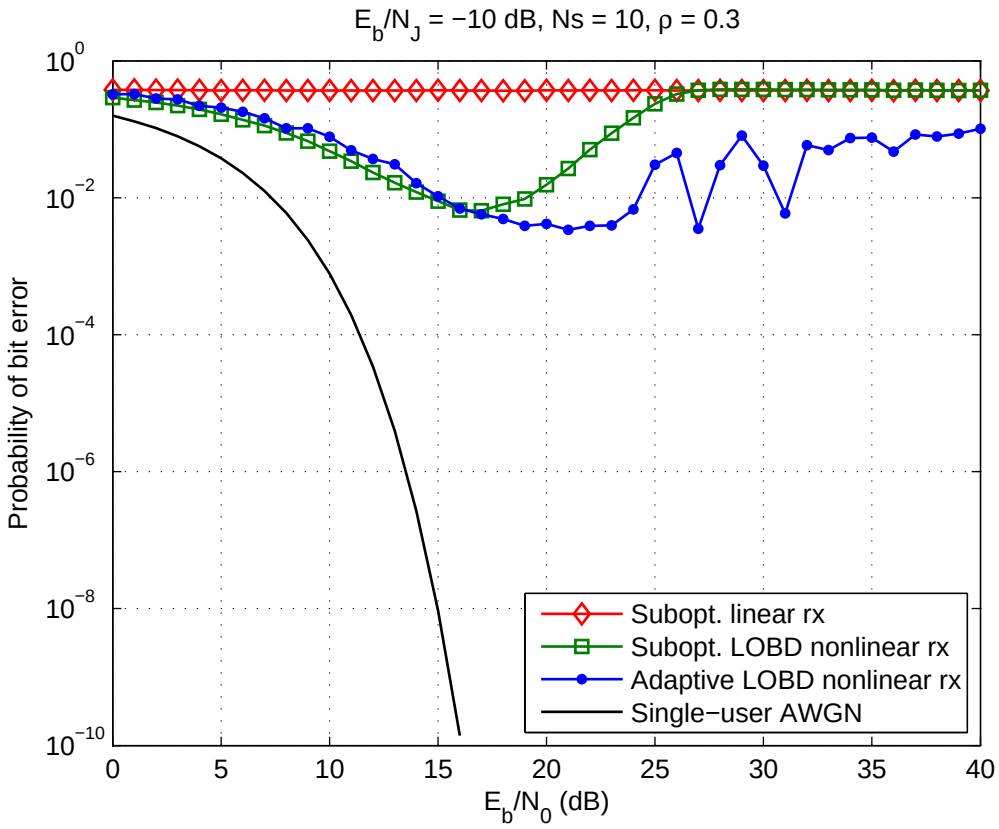

Figure 7.11: Adaptive LOBD receiver for Gaussian on-off jamming suppression ($E_b/N_J = -10$ dB, $N_s = 10$, $\rho = 0.3$).

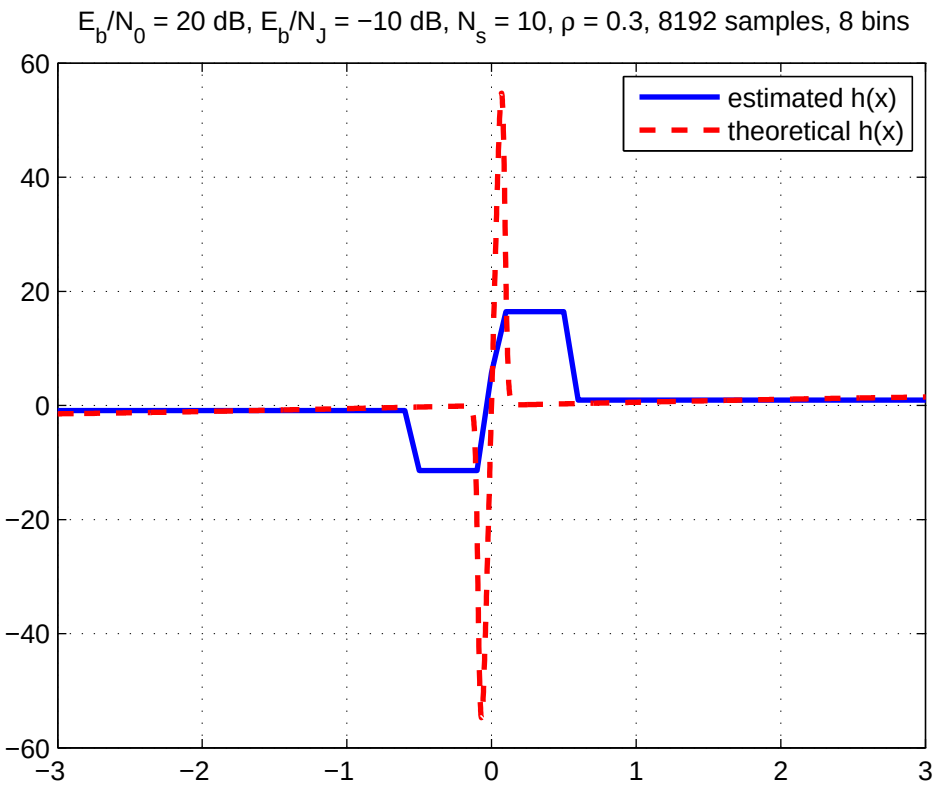

Figure 7.12: Estimated LOBD function for Gaussian on-off jammer.

CHAPTER 8

Conclusions and Future Research

In this chapter, we conclude this thesis by summarizing the content of this thesis and discussing possible future research directions.

8.1 Summary of Contributions

The major goal and contributions of this thesis is present and analyze the design of communication systems to combat interference. In Chapters 2 through 4, we investigate the use of multilevel coding (MLC) and asymmetric modulation in a multiple-access system to transmit data with various levels of importance and quality of service (QoS) constraints. Although the capability of unequal error protection (UEP) of a system cannot be easily quantified, we demonstrated that different QoS requirements (BER) of different data streams can be achieved through the choice of asymmetric modulation and MLC components codes combined into one simple coded modulation scheme. We considered MLC with asymmetric 8-PSK modulation using block partitioning, and apply multistage decoding (MSD) for data recovery. The performance of the proposed scheme using BCH codes is evaluated using the upper bound of decoding error probability of BCH codes. In order to analyze the BER performance, we use characteristic functions to derive the probability density function (PDF) of multiple-access interference (MAI) of a quaternary DS-CDMA system. The capacity and throughput analysis shows that

the MLC scheme (coded modulation) outperforms the regular coding scheme (independent coding and modulation) in the low SNR region. This means that the MLC scheme is an effective design for noisy environments. The combination of MLC and asymmetric modulation also enables the flexibility in designing systems for the (UEP) purpose.

Another way to combat interference presented in this thesis is through the design of the receiver to suppress interference. Specifically, in Chapters 5 through 7, we designed receivers to mitigate interference for ultra-wideband (UWB) communications. We consider impulse radio (IR) based UWB system with pulse-position modulation (PPM) and time-hopping (TH) for multiple-access. The simple repetition coding is applied for reliability enhancement. The goal is to design a simple, low-complexity receiver that can perform asymptotically as well as the optimum receiver. The receiver design based on locally optimum Bayes detection (LOBD) algorithm can effectively suppress interference while maintain a low complexity. It is demonstrated with the examples of MAI and jamming interference. The LOBD algorithm requires the knowledge of the PDF of the interference. For the MAI case, the PDF is derived using characteristic function method. For the jamming interference, a Gaussian on-off jammer is considered and PDF is obtained in a closed form. Numerical results show that the LOBD receiver performance well under strong interference. An adaptive algorithm for estimating and updating the interference PDF and the signal processing function of the LOBD algorithm is presented to address the practical issues of the receiver implementation. The use of quantile to represent the cumulative density function (CDF) results in simple arithmetic of the signal processing function, which suits well with the purpose of a simple, low-complexity receiver structure. Numerical results show that the adaptive receiver performance is very close to the theoretical performance of the case when the receiver has perfect knowledge of the interference PDF.

8.2 Future Research

8.2.1 Autonomous Radio with MLC and UEP

As mentioned in Chapters 2 and 3, we investigated techniques to equip a communication system with unequal error protection capability. One of the intentions is to design an autonomous radio with simple transmitter using a fixed coding and modulation scheme without feedback from the receiver. The receiver can demodulate and decode the received signal successfully in different stages depending on the channel condition.

The analysis in Chapters 2 and 3 assumes the channel is a simple AWGN channel. Therefore, there is no need for channel estimation. For realistic modeling of a wireless channel, we have take into account the effect of multipath fading and shadowing. In this case, even without feedback from receiver to the transmitter, channel estimation can still be done at the receiver for the decoder to improve the performance. One direction of future research is to consider fading channel in the autonomous radio system employing multilevel coding. At the receiver, channel estimation and decoding can be jointly considered when designing the system in order to attain the optimum performance. The channel estimator and the decoder can iteratively exchange information, and it is crucial to find what information should be exchanged between the two entities to enhance performance.

8.2.2 Impact of Interference Mitigation on Wireless Networks

Traditional wireless network design is based on the layering structure, and the physical and MAC layers are considered separately. Radio resource access is considered as a MAC layer problem. It is shown in [50] that this might not be an efficient way to design routing, scheduling, and power control for wireless ad hoc networks.

Most resource allocation algorithms considering cross-layer design use the receiver

SINR as an indication of the link quality. Based on the SINR measurement, optimization can be done to achieve the goals such as maximizing the throughput or minimizing the power consumption. One key component in the design is to control interference so that a desired link quality can be maintained to achieve a desired rate. Interference control can be done through scheduling, power control, exclusion regions, etc. These are MAC layer protocols and do not take into account interference mitigation that can be done in the physical layer.

It is not straightforward to quantify the effectiveness of interference mitigation algorithms. SINR seems to be a reasonable measurement. However, different interference mitigation algorithms work differently in different aspects affecting the network. Therefore, it is crucial to create a framework that abstracts the concept of interference mitigation in order to understand its fundamental impact on a wireless network.

One of the possible directions to continue the research carried out in this thesis is to examine the impact of interference mitigation to different network resource allocation issues in UWB networks. For example, by considering interference mitigation through physical layer signal processing, it is possible to achieve the same desired receiver SINR with a lower transmission power. This can change the power control algorithms, enable more different combinations of target link quality requirements, and increase the network throughput. This can be beneficial for low-power, energy-constrained networks. For networks without energy constraints, the gain in throughput might still worth the extra signal processing in the physical layer. We can investigate the balance for energy consumption and data rate for low-power systems such as UWB [51] through cross-layer design. This concept can also be applied to general wireless network models.

APPENDICES

APPENDIX A

Characteristic Function of I_I

To further simplify Equation (2.76), we have

$$\Phi_{I_I}(v) = \prod_{k=2}^{K} \left\{ \frac{1}{32\pi T} \sum_{l=0}^{N-1} \int_0^{2\pi} \int_0^T \sum_{\underline{b}_k^I} \sum_{\underline{b}_k^Q} \exp\left[jv \frac{1}{T} (\Delta) \right] d\tau d\phi \right\} \tag{A.1}$$

where

$$\begin{aligned} \Delta \;=\; & \Big[\cos\phi (b_{k,-1}^I C_{k,1}^{II}(l-N) + b_{k,0}^I C_{k,1}^{II}(l)) \\ & + \tan\beta \cdot \sin\phi (b_{k,-1}^Q C_{k,1}^{QI}(l-N) + b_{k,0}^Q C_{k,1}^{QI}(l)) \Big] \cdot \widehat{R}_\psi(\tau) \\ & + \Big[\cos\phi (b_{k,-1}^I C_{k,1}^{II}(l+1-N) + b_{k,0}^I C_{k,1}^{II}(l+1)) \\ & + \tan\beta \cdot \sin\phi (b_{k,-1}^Q C_{k,1}^{QI}(l+1-N) + b_{k,0}^Q C_{k,1}^{QI}(l+1)) \Big] \cdot R_\psi(\tau). \end{aligned} \tag{A.2}$$

To evaluate the summations over $\underline{b}_k^I$ and $\underline{b}_k^Q$, we note that there are 16 cases for $(\underline{b}_k^I, \underline{b}_k^Q) = (b_{k,-1}^I, b_{k,0}^I, b_{k,-1}^Q, b_{k,0}^Q)$ as in Table A.1.

Table A.1: Sixteen cases for ($\underline{b}_k^I$,$\underline{b}_k^Q$).

Case	$b_{k,-1}^I$	$b_{k,0}^I$	$b_{k,-1}^Q$	$b_{k,0}^Q$
1	1	1	1	1
2	1	1	1	-1
3	1	1	-1	1
4	1	1	-1	-1
5	1	-1	1	1
6	1	-1	1	-1
7	1	-1	-1	1
8	1	-1	-1	-1
9	-1	1	1	1
10	-1	1	1	-1
11	-1	1	-1	1
12	-1	1	-1	-1
13	-1	-1	1	1
14	-1	-1	1	-1
15	-1	-1	-1	1
16	-1	-1	-1	-1

Introducing the periodic cross-correlation functions

$$\theta_{k,i}^{II}(l) = C_{k,i}^{II}(l) + C_{k,i}^{II}(l-N), \tag{A.3}$$

$$\widehat{\theta}_{k,i}^{II}(l) = C_{k,i}^{II}(l) - C_{k,i}^{II}(l-N), \tag{A.4}$$

$$\theta_{k,i}^{QI}(l) = C_{k,i}^{QI}(l) + C_{k,i}^{QI}(l-N), \tag{A.5}$$

$$\widehat{\theta}_{k,i}^{QI}(l) = C_{k,i}^{QI}(l) - C_{k,i}^{QI}(l-N). \tag{A.6}$$

we evaluate Δ for the above 16 cases with the following results.

Case 1:

$$\begin{aligned}\Delta_1 = & \left[\cos(\phi)\theta_{k,1}^{II}(l) + \tan(\beta)\sin(\phi)\theta_{k,1}^{QI}(l)\right]\widehat{R}_\psi(\tau) \\ & + \left[\cos(\phi)\theta_{k,1}^{II}(l+1) + \tan(\beta)\sin(\phi)\theta_{k,1}^{QI}(l+1)\right]R_\psi(\tau).\end{aligned} \tag{A.7}$$

Case 2:

$$\begin{aligned}\Delta_2 &= \left[\cos(\phi)\theta_{k,1}^{II}(l) - \tan(\beta)\sin(\phi)\widehat{\theta}_{k,1}^{QI}(l)\right]\widehat{R}_{\psi}(\tau) \\ &\quad + \left[\cos(\phi)\theta_{k,1}^{II}(l+1) - \tan(\beta)\sin(\phi)\widehat{\theta}_{k,1}^{QI}(l+1)\right]R_{\psi}(\tau). \qquad \text{(A.8)}\end{aligned}$$

Case 3:

$$\begin{aligned}\Delta_3 &= \left[\cos(\phi)\theta_{k,1}^{II}(l) + \tan(\beta)\sin(\phi)\widehat{\theta}_{k,1}^{QI}(l)\right]\widehat{R}_{\psi}(\tau) \\ &\quad + \left[\cos(\phi)\theta_{k,1}^{II}(l+1) + \tan(\beta)\sin(\phi)\widehat{\theta}_{k,1}^{QI}(l+1)\right]R_{\psi}(\tau). \qquad \text{(A.9)}\end{aligned}$$

Case 4:

$$\begin{aligned}\Delta_4 &= \left[\cos(\phi)\theta_{k,1}^{II}(l) - \tan(\beta)\sin(\phi)\theta_{k,1}^{QI}(l)\right]\widehat{R}_{\psi}(\tau) \\ &\quad + \left[\cos(\phi)\theta_{k,1}^{II}(l+1) - \tan(\beta)\sin(\phi)\theta_{k,1}^{QI}(l+1)\right]R_{\psi}(\tau). \qquad \text{(A.10)}\end{aligned}$$

Case 5:

$$\begin{aligned}\Delta_5 &= -\Big(\left[\cos(\phi)\widehat{\theta}_{k,1}^{II}(l) - \tan(\beta)\sin(\phi)\theta_{k,1}^{QI}(l)\right]\widehat{R}_{\psi}(\tau) \\ &\quad + \left[\cos(\phi)\widehat{\theta}_{k,1}^{II}(l+1) - \tan(\beta)\sin(\phi)\theta_{k,1}^{QI}(l+1)\right]R_{\psi}(\tau)\Big). \qquad \text{(A.11)}\end{aligned}$$

Case 6:

$$\begin{aligned}\Delta_6 &= -\Big(\left[\cos(\phi)\widehat{\theta}_{k,1}^{II}(l) + \tan(\beta)\sin(\phi)\widehat{\theta}_{k,1}^{QI}(l)\right]\widehat{R}_{\psi}(\tau) \\ &\quad + \left[\cos(\phi)\widehat{\theta}_{k,1}^{II}(l+1) + \tan(\beta)\sin(\phi)\widehat{\theta}_{k,1}^{QI}(l+1)\right]R_{\psi}(\tau)\Big). \qquad \text{(A.12)}\end{aligned}$$

Case 7:

$$\begin{aligned}\Delta_7 &= -\Big(\Big[\cos(\phi)\widehat{\theta}^{II}_{k,1}(l) - \tan(\beta)\sin(\phi)\widehat{\theta}^{QI}_{k,1}(l)\Big]\,\widehat{R}_\psi(\tau) \\ &\quad + \Big[\cos(\phi)\widehat{\theta}^{II}_{k,1}(l+1) - \tan(\beta)\sin(\phi)\widehat{\theta}^{QI}_{k,1}(l+1)\Big]\,R_\psi(\tau)\Big). \quad \text{(A.13)}\end{aligned}$$

Case 8:

$$\begin{aligned}\Delta_8 &= -\Big(\Big[\cos(\phi)\widehat{\theta}^{II}_{k,1}(l) + \tan(\beta)\sin(\phi)\theta^{QI}_{k,1}(l)\Big]\,\widehat{R}_\psi(\tau) \\ &\quad + \Big[\cos(\phi)\widehat{\theta}^{II}_{k,1}(l+1) + \tan(\beta)\sin(\phi)\theta^{QI}_{k,1}(l+1)\Big]\,R_\psi(\tau)\Big). \quad \text{(A.14)}\end{aligned}$$

The latter 8 cases are simply the negative of the first 8 and thus we have 8 pairs of cases. For case 1 and case 16, we have

$$\exp\left(jv\frac{1}{T}\Delta_1\right) + \exp\left(jv\frac{1}{T}\Delta_{16}\right) = e^{jv\frac{\Delta_1}{T}} + e^{-jv\frac{\Delta_1}{T}} = 2\cos\left(\frac{v}{T}\Delta_1\right) \qquad \text{(A.15)}$$

with similar results for the other pairs of cases. Therefore, we have

$$\Phi_{I_I}(v) = \prod_{k=2}^{K}\left\{\frac{1}{8N}\sum_{l=0}^{N-1}\left(\sum_{i=1}^{8}\frac{1}{2\pi T_c}\int_0^{2\pi}\int_0^{T_c}\cos\left(\frac{v}{T}\Delta_i\right)\right)\right\}. \qquad \text{(A.16)}$$

If we further define

$$\begin{aligned}f(v;l,g(l),h(l),\alpha) &\triangleq \frac{1}{2\pi T_c}\int_0^{2\pi}\int_0^{T_c}\cos\Big\{\frac{v}{T}\Big[(\cos\phi\cdot g(l) + \alpha\sin\phi\cdot h(l))\,\widehat{R}_\psi(\tau) \\ &\quad + (\cos\phi\cdot g(l+1) + \alpha\sin\phi\cdot h(l+1))\,R_\psi(\tau)\Big]\Big\}d\tau d\phi \quad \text{(A.17)}\end{aligned}$$

then the characteristic function can be written as

$$\Phi_{I_I}(v) = \prod_{k=2}^{K}\left\{\frac{1}{8N}\sum_{l=0}^{N-1}\left(\sum_{i=1}^{8}f(v;l,g_i(l),h_i(l),\alpha_i)\right)\right\} \qquad \text{(A.18)}$$

where

$$g_1(l) = \theta_{k,1}^{II},\ h_1(l) = \theta_{k,1}^{QI},\ \alpha_1 = +\tan\beta, \tag{A.19}$$

$$g_2(l) = \theta_{k,1}^{II},\ h_2(l) = \widehat{\theta}_{k,1}^{QI},\ \alpha_2 = -\tan\beta, \tag{A.20}$$

$$g_3(l) = \theta_{k,1}^{II},\ h_3(l) = \widehat{\theta}_{k,1}^{QI},\ \alpha_3 = +\tan\beta, \tag{A.21}$$

$$g_4(l) = \theta_{k,1}^{II},\ h_4(l) = \theta_{k,1}^{QI},\ \alpha_4 = -\tan\beta, \tag{A.22}$$

$$g_5(l) = \widehat{\theta}_{k,1}^{II},\ h_5(l) = \theta_{k,1}^{QI},\ \alpha_5 = -\tan\beta, \tag{A.23}$$

$$g_6(l) = \widehat{\theta}_{k,1}^{II},\ h_6(l) = \widehat{\theta}_{k,1}^{QI},\ \alpha_6 = +\tan\beta, \tag{A.24}$$

$$g_7(l) = \widehat{\theta}_{k,1}^{II},\ h_7(l) = \widehat{\theta}_{k,1}^{QI},\ \alpha_7 = -\tan\beta, \tag{A.25}$$

$$g_8(l) = \widehat{\theta}_{k,1}^{II},\ h_8(l) = \theta_{k,1}^{QI},\ \alpha_8 = +\tan\beta. \tag{A.26}$$

As can be seen, in order to evaluate the characteristic function, we need to evaluate $f(v; l, g(l), h(l), \alpha)$, which involves the computation of double integrals that can be complicated. We can further simplify this by integrating over τ when considering the chip waveform $\Psi(t)$ to be the rectangular pulse. In this case, $\widehat{R}_\psi(\tau) = T_c - \tau$ and $R_\psi(\tau) = \tau$. Now the integrand can be written as

$$\begin{aligned}
E &= \cos\Big\{\frac{v}{T}\Big[\left(\cos\phi\cdot g(l) + \alpha\sin\phi\cdot h(l)\right)\widehat{R}_\psi(\tau) \\
&\quad + \left(\cos\phi\cdot g(l+1) + \alpha\sin\phi\cdot h(l+1)\right)R_\psi(\tau)\Big]\Big\} \\
&= \cos\Big\{\frac{v}{T}\Big[\left(\cos\phi\cdot g(l) + \alpha\sin\phi\cdot h(l)\right)(T_c - \tau) \\
&\quad + \left(\cos\phi\cdot g(l+1) + \alpha\sin\phi\cdot h(l+1)\right)\tau\Big]\Big\} \\
&= \cos\Big\{\frac{v}{T}\Big[\cos\phi\Big((g(l+1) - g(l))\tau + g(l)T_c\Big) \\
&\quad + \alpha\sin\phi\Big((h(l+1) - h(l))\tau + h(l)T_c\Big)\Big]\Big\} \\
&= \cos\Big\{\frac{v}{T}\Big[\Big(\cos\phi((g(l+1) - g(l)) + \alpha\sin\phi((h(l+1) - h(l))\Big)\tau \\
&\quad + \Big(\cos\phi g(l) + \alpha\sin\phi h(l)\Big)T_c\Big]\Big\} \\
&= \cos\Big(F\tau + G\Big)
\end{aligned} \tag{A.27}$$

where

$$F = \frac{v}{T}\Big(\cos\phi((g(l+1) - g(l)) + \alpha \sin\phi((h(l+1) - h(l))\Big), \tag{A.28}$$

and

$$G = \frac{v}{T}\Big(\cos\phi g(l) + \alpha \sin\phi h(l)\Big) T_c. \tag{A.29}$$

Next, we integrate E over τ to obtain

$$\begin{aligned}
\frac{1}{T_c}\int_0^{Tc} \cos\Big(F\tau + G\Big) d\tau &= \frac{1}{FT_c} \sin\Big(F\tau + G\Big)\Big|_0^{T_c} \\
&= \frac{1}{FT_c}\Big\{ \sin\Big(FT_c + G\Big) - \sin\Big(G\Big)\Big\} \\
&= \frac{1}{FT_c}\Big\{ 2\sin\Big(\frac{1}{2}FT_c\Big)\cos\Big(\frac{1}{2}FT_c + G\Big)\Big\} \\
&= \mathrm{sinc}(\frac{1}{2\pi}FT_c)\cos\Big(\frac{1}{2}FT_c + G\Big)
\end{aligned} \tag{A.30}$$

where

$$\mathrm{sinc}(x) = \frac{\sin(\pi x)}{\pi x}, \tag{A.31}$$

$$\begin{aligned}
\frac{1}{2\pi}FT_c &= \frac{1}{2\pi}\frac{v}{T}\Big(\cos\phi((g(l+1) - g(l)) + \alpha \sin\phi((h(l+1) - h(l))\Big) T_c \\
&= \frac{v}{2\pi N}\Big(\cos\phi((g(l+1) - g(l)) + \alpha \sin\phi((h(l+1) - h(l))\Big),
\end{aligned} \tag{A.32}$$

and

$$\begin{aligned}
\frac{1}{2}FT_c + G &= \frac{v}{2N}\Big(\cos\phi((g(l+1) - g(l)) + \alpha \sin\phi((h(l+1) - h(l))\Big) \\
&\quad + \frac{v}{T}\Big(\cos\phi h_1(l) + \alpha \sin\phi h_2(l)\Big) T_c \\
&= \frac{v}{2N}\Big(\cos\phi((g(l+1) + g(l)) + \alpha \sin\phi((h(l+1) + h(l))\Big).
\end{aligned} \tag{A.33}$$

Therefore we have

$$
\begin{aligned}
f(v;l,g(l),h(l),\alpha) \;=\; & \frac{1}{2\pi}\int_0^{2\pi} \operatorname{sinc}\Big\{\frac{v}{2\pi N}\Big(\cos\phi((g(l+1)-g(l)) \\
& + \alpha\sin\phi((h(l+1)-h(l))\Big)\Big\} \\
& \cdot\cos\Big\{\frac{v}{2N}\Big(\cos\phi((g(l+1)+g(l)) \\
& + \alpha\sin\phi((h(l+1)+h(l))\Big)\Big\}d\phi.
\end{aligned}
\tag{A.34}
$$

APPENDIX B

Variance of the Interference

The derivation here follows the work in [18]. According to Equations (2.68) and (2.69), we can expand Equation (2.92) as

$$\begin{aligned} W_k^{II} &= \left[b_{k,-1}^I \cdot C_{k,1}^{II}(\gamma_k - N) + b_{k,0}^I \cdot C_{k,1}^{II}(\gamma_k)\right] \widehat{R}_\psi(S_k) \\ &\quad + \left[b_{k,-1}^I \cdot C_{k,1}^{II}(\gamma_k + 1 - N) + b_{k,0}^I \cdot C_{k,1}^{II}(\gamma_k + 1)\right] R_\psi(S_k) \end{aligned} \tag{B.1}$$

where $S_k = \tau_k - \gamma_k T_c$ and $\gamma_k = \lfloor \tau_k / T_c \rfloor$. If we use Equation (2.74) to expand Equation (B.1), we obtain

$$\begin{aligned} W_k^{II} &= \left[\sum_{j=0}^{\gamma_k - 1} b_{k,-1}^I a_{k,j-\gamma_k+N}^I a_{1,j}^I + \sum_{j=\gamma_k}^{N-1} b_{k,0}^I a_{k,j-\gamma_k}^I a_{1,j}^I\right] \widehat{R}_\psi(S_k) \\ &\quad + \left[\sum_{j=0}^{\gamma_k} b_{k,-1}^I a_{k,j-\gamma_k-1+N}^I a_{1,j}^I + \sum_{j=\gamma_k+1}^{N-1} b_{k,0}^I a_{k,j-\gamma_k-1}^I a_{1,j}^I\right] R_\psi(S_k) \end{aligned} \tag{B.2}$$

which can be further expanded to obtain

$$\begin{aligned} W_k^{II} &= \left[\sum_{j=0}^{\gamma_k - 1} b_{k,-1}^I a_{k,j-\gamma_k+N}^I a_{1,j}^I + \sum_{j=\gamma_k}^{N-2} b_{k,0}^I a_{k,j-\gamma_k}^I a_{1,j}^I + b_{k,0}^I a_{k,N-\gamma_k-1}^I a_{1,N-1}^I\right] \widehat{R}_\psi(S_k) \\ &\quad + \left[b_{k,-1}^I a_{k,N-\gamma_k-1}^I a_{1,0}^I + \sum_{j=0}^{\gamma_k - 1} b_{k,-1}^I a_{k,j-\gamma_k+N}^I a_{1,j+1}^I + \sum_{j=\gamma_k}^{N-2} b_{k,0}^I a_{k,j-\gamma_k}^I a_{1,j+1}^I\right] R_\psi(S_k). \end{aligned} \tag{B.3}$$

Finally, the terms in Equation (B.3) can be rearranged to obtain

$$\begin{aligned} W_k^{II} &= b_{k,-1}^I \sum_{j=0}^{\gamma_k-1} a_{k,j-\gamma_k+N}^I \left(a_{1,j}^I \widehat{R}_\psi(S_k) + a_{1,j+1}^I R_\psi(S_k) \right) \\ &\quad + b_{k,0}^I \sum_{j=\gamma_k}^{N-2} a_{k,j-\gamma_k}^I \left(a_{1,j}^I \widehat{R}_\psi(S_k) + a_{1,j+1}^I R_\psi(S_k) \right) \\ &\quad + b_{k,0}^I a_{k,N-\gamma_k-1}^I a_{1,N-1}^I \widehat{R}_\psi(S_k) + b_{k,-1}^I a_{k,N-\gamma_k-1}^I a_{1,0}^I R_\psi(S_k). \end{aligned} \tag{B.4}$$

In order to reduce the complexity of evaluating Equation (B.4), we consider it conditioned on the signature sequence of the first user $\{a_{1,j}^I\}$ and the random variable γ^k, which is uniformly distributed on the set $\{0, \cdots, N-1\}$. We condition on $\gamma^k = \hat{\gamma}^k$ and $\{a_{1,j}^I\} = \{\hat{a}_{1,j}^I\}$, and define a set of $N+1$ random variables $\Omega_j,\ 0 \le j \le N$, by

$$\Omega_j = \begin{cases} b_{k,-1}^I a_{k,j-\hat{\gamma}_k+N}^I \hat{a}_{1,j}^I, & j = 0, \cdots, \hat{\gamma}_k - 1 \\ b_{k,0}^I a_{k,j-\hat{\gamma}_k}^I \hat{a}_{1,j}^I, & j = \hat{\gamma}_k, \cdots, N-2 \\ b_{k,0}^I a_{k,N-\hat{\gamma}_k-1}^I \hat{a}_{1,N-1}^I, & j = N-1 \\ b_{k,-1}^I a_{k,N-\hat{\gamma}_k-1}^I \hat{a}_{1,0}^I, & j = N \end{cases} \tag{B.5}$$

Then Equation (B.4) can be simplified to

$$W_k^{II} = \sum_{j=0}^{N-2} \Omega_j \left[\widehat{R}_\psi(S_k) + \hat{a}_{1,j}^I \hat{a}_{1,j+1}^I R_\psi(S_k) \right] + \Omega_{N-1} \widehat{R}_\psi(S_k) + \Omega_N R_\psi(S_k) \tag{B.6}$$

where the random variables $\Omega_j,\ 0 \le j \le N$, are mutually independent and satisfy $\Pr(\Omega_j = +1) = \Pr(\Omega_j = -1) = 1/2$. If we further define $f(s) = \widehat{R}_\psi(s) + R_\psi(s)$, $g(s) = \widehat{R}_\psi(s) - R_\psi(s)$, the set Γ_1 to be the set of all nonnegative integers i less than $N-1$ such that $\hat{a}_{1,i}^I \hat{a}_{1,i+1}^I = 1$ and the set Γ_2 to be the set of all nonnegative integers i less than $N-1$ such that $\hat{a}_{1,i}^I \hat{a}_{1,i+1}^I = -1$, then Equation (B.6) can be written as

$$W_k^{II} = \sum_{j \in \Gamma_1} \Omega_j f(S_k) + \sum_{j \in \Gamma_2} \Omega_j g(S_k) + \Omega_{N-1} \widehat{R}_\psi(S_k) + \Omega_N R_\psi(S_k). \tag{B.7}$$

If we let $X_k^{II} = \sum_{j\in\Gamma_1} \Omega_j$, $Y_k^{II} = \sum_{j\in\Gamma_2} \Omega_j$, $\Pi_k^{II} = \Omega_{N-1}$, and $\Lambda_k^{II} = \Omega_N$, then we have

$$W_k^{II} = \Pi_k^{II}\widehat{R}_\psi(S_k) + \Lambda_k^{II}R_\psi(S_k) + X_k^{II}f(S_k) + Y_k^{II}g(S_k). \tag{B.8}$$

Similarly, W_k^{QI} can be written as

$$W_k^{QI} = \Pi_k^{QI}\widehat{R}_\psi(S_k) + \Lambda_k^{QI}R_\psi(S_k) + X_k^{QI}f(S_k) + Y_k^{QI}g(S_k) \tag{B.9}$$

with Π_k^{QI}, Λ_k^{QI}, X_k^{QI}, and Y_k^{QI} defined in a similar way.

At this point, in order to simplify the notation, we ignore the superscript of W_k, Π_k, Λ_k, X_k, and Y_k. The random variables Π_k and Λ_k are uniform on $\{-1, 1\}$, and X_k and Y_k have PDFs

$$p_{X_k}(i) = \binom{L}{\frac{i+L}{2}} 2^{-L},\ i \in \{-L, -L+2, \cdots, L-2, L\} \tag{B.10}$$

$$p_{Y_k}(i) = \binom{M}{\frac{i+M}{2}} 2^{-M},\ i \in \{-M, -M+2, \cdots, M-2, M\} \tag{B.11}$$

where $L = (N-1+U)/2$, $M = (N-1-U)/2$. The random variable U is defined as

$$U = \sum_{j=0}^{N-2} a_{1,j} \cdot a_{1,j+1} \tag{B.12}$$

where $\{a_{1,j}\}$ is the signature sequence of user 1. By assuming random signature sequences, the PDF of U is given by

$$p_U(i) = \binom{N-1}{\frac{i+N-1}{2}} 2^{-N+1},\ i \in \{-N+2, -N+3, \cdots, N-3, N-1\}. \tag{B.13}$$

If $\psi(t)$ is a rectangular pulse, we have

$$W_k = P_k S_k + Q_k(T_c - S_k) + X_k T_c + Y_k(T_c - 2S_k). \tag{B.14}$$

Let $\mathbf{S} = (S_1, \cdots, S_K)$ and $\mathbf{\Phi} = (\phi_1, \cdots, \phi_K)$. Then the conditional variance of W^I is given by

$$\begin{aligned}
\mathrm{Var}\left[W \mid \mathbf{S}, \mathbf{\Phi}, M\right] &= E\left[\left(\sqrt{P/2} \cdot \cos\beta \sum_{k=2}^{K} W_k \cdot \cos\phi_k\right)^2 \mid \mathbf{S}, \mathbf{\Phi}, M\right] \\
&= \frac{P}{2}\cos^2\beta \sum_{k=2}^{K} E\left[W_k^2 \mid S_k, M\right] \cdot E\left[\cos^2\phi_k \mid \phi_k\right] \\
&= \frac{P}{2}\cos^2\beta \sum_{k=2}^{K} \frac{1}{2}\left[1 + \cos(2\phi_k)\right] \cdot \mathrm{Var}\left[W_k \mid S_k, M\right]. \quad \text{(B.15)}
\end{aligned}$$

The conditional variance of W_k can be computed as

$$\begin{aligned}
\mathrm{Var}\left[W_k \mid S_k, M\right] &= E\left[\Pi_k^2 S_k^2 \mid S_k\right] + E\left[\Lambda_k^2 (T_c - S_k)^2 \mid S_k\right] + E\left[X_k^2 T_c^2 \mid M\right] \\
&\quad + E\left[Y_k^2 (T_c - 2S_k)^2 \mid S_k, M\right]. \quad \text{(B.16)}
\end{aligned}$$

The random variables Π_k and Λ_k have variances equal to 1. Then we have

$$E\left[\Pi_k^2 S_k^2 \mid S_k\right] = S_k^2, \quad \text{(B.17)}$$

$$E\left[\Lambda_k^2 (T_c - S_k)^2 \mid S_k\right] = (T_c - S_k)^2, \quad \text{(B.18)}$$

$$E\left[X_k^2 T_c^2 \mid M\right] = T_c^2 (N - M - 1), \quad \text{(B.19)}$$

$$E\left[Y_k^2 (T_c - 2S_k)^2 \mid S_k, M\right] = M(T_c - 2S_k)^2. \quad \text{(B.20)}$$

Substituting Equations (B.17) through (B.20) in Equation (B.16) gives

$$\mathrm{Var}\left[W_k \mid S_k, M\right] = 2(2M + 1)(S_k^2 - T_c S_k) + N T_c^2, \quad \text{(B.21)}$$

and thus from Equation (B.15),

$$\begin{aligned}\mathrm{Var}\left[W \mid \mathbf{S}, \mathbf{\Phi}, M\right] &= \frac{P}{2}\cos^2\beta \sum_{k=2}^{K} \frac{1}{2}\left[1+\cos(2\phi_k)\right]\left[2(2M+1)(S_k^2 - T_c S_k) + NT_c^2\right] \\ &= \frac{P}{2}\cos^2\beta \sum_{k=2}^{K} \left[1+\cos(2\phi_k)\right]\left[(2M+1)(S_k^2 - T_c S_k) + \frac{NT_c^2}{2}\right].\end{aligned} \tag{B.22}$$

By averaging over ϕ_k,

$$\begin{aligned}\mathrm{Var}\left[W \mid \mathbf{S}, M\right] &= \frac{P}{2}\cos^2\beta \sum_{k=2}^{K} \left[(2M+1)(S_k^2 - T_c S_k) + \frac{NT_c^2}{2}\right] \\ &= \frac{P}{2}\cos^2\beta \left[\sum_{k=2}^{K}(2M+1)(S_k^2 - T_c S_k)\right] + \frac{(K-1)NPT_c^2}{4}\cos^2\beta.\end{aligned} \tag{B.23}$$

By averaging over S_k, since $E[S_k^2 - T_c S_k] = -T_c^2/6$, we have

$$\mathrm{Var}[W \mid M] = \frac{(K-1)NPT_c^2}{4}\cos^2\beta - \frac{PT_c^2}{12}\cos^2\beta \sum_{k=2}^{K}(2M+1). \tag{B.24}$$

For random signature sequences, $E[M] = \frac{N-1}{2}$, thus we have

$$\begin{aligned}\mathrm{Var}[W] &= \frac{(K-1)NPT_c^2}{4}\cos^2\beta - \frac{PT_c^2}{12}\cos^2\beta \sum_{k=2}^{K}(2\frac{N-1}{2}+1) \\ &= \frac{(K-1)NPT_c^2\cos^2\beta}{6}.\end{aligned} \tag{B.25}$$

Therefore, the variance of W^I is given by

$$\mathrm{Var}[W^I] = \frac{(K-1)NPT_c^2\cos^2\beta}{6}. \tag{B.26}$$

Similarly, it can be shown that

$$\mathrm{Var}[W^Q] = \frac{(K-1)NPT_c^2 \sin^2 \beta}{6}. \tag{B.27}$$

APPENDIX C

Probability of Detection Error of P_{det_3}

The detection error probability of $c_k^{(3)}$ is defined as

$$\begin{aligned} P_{det_3} &= P(c_k^{(3)} \neq \widetilde{c}_k^{(3)}) && \text{(C.1)} \\ &= P(c_k^{(3)} \neq \widetilde{c}_k^{(3)}, c_k^{(1)} = \widehat{c}_k^{(1)}, c_k^{(2)} = \widehat{c}_k^{(2)}) && \text{(C.2)} \\ &\quad + P(c_k^{(3)} \neq \widetilde{c}_k^{(3)}, c_k^{(1)} = \widehat{c}_k^{(1)}, c_k^{(2)} \neq \widehat{c}_k^{(2)}) && \text{(C.3)} \\ &\quad + P(c_k^{(3)} \neq \widetilde{c}_k^{(3)}, c_k^{(1)} \neq \widehat{c}_k^{(1)}, c_k^{(2)} = \widehat{c}_k^{(2)}) && \text{(C.4)} \\ &\quad + P(c_k^{(3)} \neq \widetilde{c}_k^{(3)}, c_k^{(1)} \neq \widehat{c}_k^{(1)}, c_k^{(2)} \neq \widehat{c}_k^{(2)}) && \text{(C.5)} \end{aligned}$$

The first term in the summation of (C.1) can be written as

$$\begin{aligned} \text{(C.2)} &= P(c_k^{(3)} \neq \widetilde{c}_k^{(3)} | c_k^{(1)} = \widehat{c}_k^{(1)}, c_k^{(2)} = \widehat{c}_k^{(2)}) P(c_k^{(1)} = \widehat{c}_k^{(1)}, c_k^{(2)} = \widehat{c}_k^{(2)}) \\ &= P(c_k^{(3)} \neq \widetilde{c}_k^{(3)} | c_k^{(1)} = \widehat{c}_k^{(1)}, c_k^{(2)} = \widehat{c}_k^{(2)})(1 - P_{dec_1})(1 - P_{dec_2}) && \text{(C.6)} \end{aligned}$$

The conditional probability in the above equation is given by

$$P(c_k^{(3)} \neq \widetilde{c}_k^{(3)} | c_k^{(1)} = \widehat{c}_k^{(1)}, c_k^{(2)} = \widehat{c}_k^{(2)}) = Q\left(\sqrt{\frac{4E_s \sin^2 \alpha}{N_0}}\right) \qquad \text{(C.7)}$$

Similarly, the second term in the summation of (C.1) can be written as

$$\begin{aligned} (\text{C.3}) \quad &= P(c_k^{(3)} \neq \widetilde{c}_k^{(3)} | c_k^{(1)} = \widehat{c}_k^{(1)}, c_k^{(2)} \neq \widehat{c}_k^{(2)}) P(c_k^{(1)} = \widehat{c}_k^{(1)}, c_k^{(2)} \neq \widehat{c}_k^{(2)}) \\ &= P(c_k^{(3)} \neq \widetilde{c}_k^{(3)} | c_k^{(1)} = \widehat{c}_k^{(1)}, c_k^{(2)} \neq \widehat{c}_k^{(2)}) (1 - P_{dec_1}) P_{dec_2} \qquad (\text{C.8}) \end{aligned}$$

The conditional probability in the above equation is given by

$$\begin{aligned} P(c_k^{(3)} \neq \widetilde{c}_k^{(3)} | c_k^{(1)} = \widehat{c}_k^{(1)}, c_k^{(2)} \neq \widehat{c}_k^{(2)}) &= \frac{1}{2} \left[1 + Q\left(\sqrt{\frac{4E_s \sin^2(2\beta - \alpha)}{N_0}} \right) \right. \\ &\quad \left. - Q\left(\sqrt{\frac{4E_s \sin^2(2\beta + \alpha)}{N_0}} \right) \right] \qquad (\text{C.9}) \end{aligned}$$

The third term in the summation of (C.1) can be written as

$$\begin{aligned} (\text{C.4}) \quad &= P(c_k^{(3)} \neq \widetilde{c}_k^{(3)} | c_k^{(1)} \neq \widehat{c}_k^{(1)}, c_k^{(2)} = \widehat{c}_k^{(2)}) P(c_k^{(1)} \neq \widehat{c}_k^{(1)}, c_k^{(2)} = \widehat{c}_k^{(2)}) \\ &= P(c_k^{(3)} \neq \widetilde{c}_k^{(3)} | c_k^{(1)} \neq \widehat{c}_k^{(1)}, c_k^{(2)} = \widehat{c}_k^{(2)}) P_{dec_1} (1 - P_{dec_2}) \qquad (\text{C.10}) \end{aligned}$$

The conditional probability in the above equation is given by

$$\begin{aligned} P(c_k^{(3)} \neq \widetilde{c}_k^{(3)} | c_k^{(1)} \neq \widehat{c}_k^{(1)}, c_k^{(2)} = \widehat{c}_k^{(2)}) &= \frac{1}{2} \left[1 - Q\left(\sqrt{\frac{4E_s \sin^2(2\beta - \alpha)}{N_0}} \right) \right. \\ &\quad \left. + Q\left(\sqrt{\frac{4E_s \sin^2(2\beta + \alpha)}{N_0}} \right) \right] \qquad (\text{C.11}) \end{aligned}$$

Finally, the last term in the summation of (C.1) can be written as

$$\begin{aligned} (\text{C.5}) \quad &= P(c_k^{(3)} \neq \widetilde{c}_k^{(3)} | c_k^{(1)} \neq \widehat{c}_k^{(1)}, c_k^{(2)} \neq \widehat{c}_k^{(2)}) P(c_k^{(1)} \neq \widehat{c}_k^{(1)}, c_k^{(2)} \neq \widehat{c}_k^{(2)}) \\ &= P(c_k^{(3)} \neq \widetilde{c}_k^{(3)} | c_k^{(1)} \neq \widehat{c}_k^{(1)}, c_k^{(2)} \neq \widehat{c}_k^{(2)}) P_{dec_1} P_{dec_2} \qquad (\text{C.12}) \end{aligned}$$

The conditional probability in the above equation is given by

$$P(c_k^{(3)} \neq \widetilde{c}_k^{(3)} | c_k^{(1)} \neq \widehat{c}_k^{(1)}, c_k^{(2)} \neq \widehat{c}_k^{(2)}) = 1 - Q\left(\sqrt{\frac{4E_s \sin^2 \alpha}{N_0}}\right) \tag{C.13}$$

By combining the above equations, we can obtain P_{det_3} as

$$\begin{aligned} P_{det_3} &= Q\left(\sqrt{\frac{4E_s \sin^2 \alpha}{N_0}}\right)(1 - P_{dec_1})(1 - P_{dec_2}) \\ &\quad + \frac{1}{2}\left[1 + Q\left(\sqrt{\frac{4E_s \sin^2(2\beta - \alpha)}{N_0}}\right)\right. \\ &\qquad \left. - Q\left(\sqrt{\frac{4E_s \sin^2(2\beta + \alpha)}{N_0}}\right)\right](1 - P_{dec_1})P_{dec_2} \\ &\quad + \frac{1}{2}\left[1 - Q\left(\sqrt{\frac{4E_s \sin^2(2\beta - \alpha)}{N_0}}\right)\right. \\ &\qquad \left. + Q\left(\sqrt{\frac{4E_s \sin^2(2\beta + \alpha)}{N_0}}\right)\right]P_{dec_1}(1 - P_{dec_2}) \\ &\quad + \left[1 - Q\left(\sqrt{\frac{4E_s \sin^2 \alpha}{N_0}}\right)\right]P_{dec_1}P_{dec_2} \end{aligned} \tag{C.14}$$

With further simplification, we have

$$\begin{aligned} P_{det_3} &= Q\left(\sqrt{\frac{4E_s \sin^2 \alpha}{N_0}}\right)(1 - P_{dec_1} - P_{dec_2}) \\ &\quad + \frac{1}{2}\left[1 - Q\left(\sqrt{\frac{4E_s \sin^2(2\beta - \alpha)}{N_0}}\right) + Q\left(\sqrt{\frac{4E_s \sin^2(2\beta + \alpha)}{N_0}}\right)\right]P_{dec_1} \\ &\quad + \frac{1}{2}\left[1 + Q\left(\sqrt{\frac{4E_s \sin^2(2\beta - \alpha)}{N_0}}\right) - Q\left(\sqrt{\frac{4E_s \sin^2(2\beta + \alpha)}{N_0}}\right)\right]P_{dec_2} \end{aligned} \tag{C.15}$$

APPENDIX D

Variance of the MAI

From (3.67), we know that $W_{k,1}^I$ is a function of μ_k, θ_k, $R_{k,1}^{II}$, and $R_{k,1}^{QI}$. The cross-correlations are functions of the signature sequences $\{a_{1,j}^I\}$, $\{a_{k,j}^I\}$, and $\{a_{k,j}^Q\}$. Therefore, we can obtain the distribution of $R_{k,1}^{II}$ and $R_{k,1}^{QI}$ by conditioning on $\{a_{1,j}^I\}$. By doing so, the conditional distribution is given by

$$p_R(rT_c) = \binom{N}{\frac{r+N}{2}} 2^{-N} \tag{D.1}$$

where $r = -N, -N+2, \cdots, N-2, N$. The conditional variance of $W_{k,1}^I$ conditioned on $\{a_{1,j}^I\}$ and θ_k is given by

$$\begin{aligned}
\mathrm{Var}[W_{k,1}^I|\{a_{1,j}^I\},\theta_k] &= \mathrm{Var}[\sqrt{2P}\cos\phi_k\cos\theta_k R_{k,1}^{II}|\{a_{1,j}^I\},\theta_k] \\
&\quad +\mathrm{Var}[\sqrt{2P}\sin\phi_k\sin\theta_k R_{k,1}^{QI}|\{a_{1,j}^I\},\theta_k] \\
&= \frac{P}{2}\cos^2\theta_k\mathrm{Var}[\cos\phi_k R_{k,1}^{II}|\{a_{1,j}^I\}] \\
&\quad +\frac{P}{2}\sin^2\theta_k\mathrm{Var}[\sin\phi_k R_{k,1}^{QI}|\{a_{1,j}^I\}]
\end{aligned} \tag{D.2}$$

In the above equation, the variance of $\cos\phi_k R_{k,1}^{II}$ conditioned on $\{a_{1,j}^I\}$ is given by

$$\mathrm{Var}[\cos\phi_k R_{k,1}^{II}|\{a_{1,j}^I\}] = \mathrm{E}[\cos^2\phi_k (R_{k,1}^{II})^2|\{a_{1,j}^I\}] = \mathrm{E}[\cos^2\phi_k]\mathrm{E}[(R_{k,1}^{II})^2|\{a_{1,j}^I\}] \tag{D.3}$$

where the two terms in the product are

$$\mathrm{E}[\cos^2\phi_k] = \frac{1}{2}(\cos^2(\beta-\alpha)+\cos^2(\beta+\alpha)) \tag{D.4}$$

$$\mathrm{E}[(R^{II}_{k,1})^2|\{a^I_{1,j}\}] = NT_c^2 \tag{D.5}$$

and

$$\mathrm{Var}[\cos\phi_k R^{II}_{k,1}|\{a^I_{1,j}\}] = \frac{1}{2}NT_c^2(\cos^2(\beta-\alpha)+\cos^2(\beta+\alpha)) \tag{D.6}$$

Similarly,

$$\mathrm{Var}[\sin\phi_k R^{QI}_{k,1}|\{a^I_{1,j}\}] = \frac{1}{2}NT_c^2(\sin^2(\beta-\alpha)+\sin^2(\beta+\alpha)) \tag{D.7}$$

Thus we have

$$\begin{aligned}\mathrm{Var}[W^I_{k,1}|\{a^I_{1,j}\},\theta_k] &= \frac{NPT_c^2}{4}\big\{\cos^2\theta_k[\cos^2(\beta-\alpha)+\cos^2(\beta+\alpha)] \\ &\qquad +\sin^2\theta_k[\sin^2(\beta-\alpha)+\sin^2(\beta+\alpha)]\big\}\end{aligned} \tag{D.8}$$

Average over θ_k, we have

$$\begin{aligned}\mathrm{Var}[W^I_{k,1}] &= \mathrm{E}_{\theta_k}[\mathrm{Var}[W^I_{k,1}|\theta_k]] \\ &= \frac{NPT_c^2}{4}\big\{\mathrm{E}[\cos^2\theta_k][\cos^2(\beta-\alpha)+\cos^2(\beta+\alpha)] \\ &\qquad +\mathrm{E}[\sin^2\theta_k][\sin^2(\beta-\alpha)+\sin^2(\beta+\alpha)]\big\} \\ &= \frac{NPT_c^2}{4}\left\{\frac{1}{2}[\cos^2(\beta-\alpha)+\cos^2(\beta+\alpha)+\sin^2(\beta-\alpha)+\sin^2(\beta+\alpha)]\right\} \\ &= \frac{NPT_c^2}{4}\end{aligned} \tag{D.9}$$

Therefore,

$$\mathrm{Var}[W^I_1] = \sum_{k=2}^{K}\mathrm{Var}[W^I_{k,1}] = \frac{(K-1)NPT_c^2}{4}. \tag{D.10}$$

Similarly, we have

$$\mathrm{Var}[W_1^Q] = \frac{(K-1)NPT_c^2}{4}. \tag{D.11}$$

APPENDIX E

8-PSK MLC Capacity

The AWGN channel output Y is complex and can be decomposed into I and Q components Y_I and Y_Q, respectively. The mutual information of Y and X_1 can be written as

$$I(Y;X_1) = I(X_1;Y) = I(X_1;Y_Q,Y_I) = I(X_1;Y_Q) + \underbrace{I(X_1;Y_I|Y_Q)}_{0} \tag{E.1}$$

The last term $I(X_1;Y_I|Y_Q) = 0$ is due to the fact of independence of X_1 and X_2 (I and Q components) introduced by block partitioning. Similarly,

$$\begin{aligned} I(Y;X_2|X_1) = I(X_2;Y|X_1) = I(X_2;Y_Q,Y_I|X_1) &= \underbrace{I(X_2;Y_Q|X_1)}_{0} + I(X_2;Y_I|Y_Q,X_1) \\ &= I(X_2;Y_I) \end{aligned} \tag{E.2}$$

We start the analysis of $I(Y;X_1) = I(X_1;Y_Q)$ with the assumption that $P(X_1 =$

$0) = P(X_1 = 1) = \frac{1}{2}$. Let $\Delta_1 = \sqrt{E_s}\cos(\beta + \alpha)$, $\Delta_2 = \sqrt{E_s}\cos(\beta - \alpha)$. Then we have

$$\begin{aligned} f(y_Q) &= \frac{1}{2} f(y_Q|x_1 = 0) + \frac{1}{2} f(y_Q|x_1 = 1) \\ &= \frac{1}{2}\left\{\frac{1}{2}\frac{1}{\sqrt{2\pi\sigma^2}}\exp\left(-\frac{(y_Q - \Delta_1)^2}{2\sigma^2}\right) + \frac{1}{2}\frac{1}{\sqrt{2\pi\sigma^2}}\exp\left(-\frac{(y_Q - \Delta_2)^2}{2\sigma^2}\right)\right\} \\ &+ \frac{1}{2}\left\{\frac{1}{2}\frac{1}{\sqrt{2\pi\sigma^2}}\exp\left(-\frac{(y_Q + \Delta_1)^2}{2\sigma^2}\right) + \frac{1}{2}\frac{1}{\sqrt{2\pi\sigma^2}}\exp\left(-\frac{(y_Q + \Delta_2)^2}{2\sigma^2}\right)\right\} \end{aligned} \tag{E.3}$$

The mutual information $I(X_1; Y_Q)$ can be computed as the sum of conditional mutual information

$$\begin{aligned} I(X_1; Y_Q) &= \frac{1}{2}\int_{-\infty}^{\infty} f(y_Q|x_1 = 0)\log_2\left(\frac{f(y_Q|x_1 = 0)}{f(y_Q)}\right) dy_Q \\ &+ \frac{1}{2}\int_{-\infty}^{\infty} f(y_Q|x_1 = 1)\log_2\left(\frac{f(y_Q|x_1 = 1)}{f(y_Q)}\right) dy_Q \end{aligned} \tag{E.4}$$

Let

$$I(X_1 = i; Y_Q) = \int_{-\infty}^{\infty} f(y_Q|x_1 = i)\log_2\left(\frac{f(y_Q|x_1 = i)}{f(y_Q)}\right) dy_Q,\ i = 0, 1 \tag{E.5}$$

we have

$$I(X_1; Y_Q) = \frac{1}{2} I(X_1 = 0; Y_Q) + \frac{1}{2} I(X_1 = 1; Y_Q) \tag{E.6}$$

When $X_1 = 0$, $I(X_1 = 0; Y_Q)$ can be computed as

$$\begin{aligned} I(X_1 = 0; Y_Q) &= \int_{-\infty}^{\infty} f(y_Q|x_1 = 0)\log_2\left(\frac{f(y_Q|x_1 = 0)}{f(y_Q)}\right) dy_Q \\ &= \frac{1}{2\sqrt{2\pi\sigma^2}}\int_{-\infty}^{\infty}\left(e^{-\frac{(y_Q - \Delta_1)^2}{2\sigma^2}} + e^{-\frac{(y_Q - \Delta_2)^2}{2\sigma^2}}\right)\log_2 W\, dy_Q \end{aligned} \tag{E.7}$$

where

$$\begin{aligned} W &= \frac{\frac{1}{2\sqrt{2\pi\sigma^2}}\left(e^{-\frac{(y_Q-\Delta_1)^2}{2\sigma^2}}+e^{-\frac{(y_Q-\Delta_2)^2}{2\sigma^2}}\right)}{\frac{1}{4\sqrt{2\pi\sigma^2}}\left(e^{-\frac{(y_Q-\Delta_1)^2}{2\sigma^2}}+e^{-\frac{(y_Q+\Delta_1)^2}{2\sigma^2}}+e^{-\frac{(y_Q-\Delta_2)^2}{2\sigma^2}}+e^{-\frac{(y_Q+\Delta_2)^2}{2\sigma^2}}\right)} \\ &= \frac{2\left(e^{-\frac{(y_Q-\Delta_1)^2}{2\sigma^2}}+e^{-\frac{(y_Q-\Delta_2)^2}{2\sigma^2}}\right)}{e^{-\frac{(y_Q-\Delta_1)^2}{2\sigma^2}}+e^{-\frac{(y_Q+\Delta_1)^2}{2\sigma^2}}+e^{-\frac{(y_Q-\Delta_2)^2}{2\sigma^2}}+e^{-\frac{(y_Q+\Delta_2)^2}{2\sigma^2}}} \end{aligned} \tag{E.8}$$

Let $u=\frac{y_Q}{\sigma}$, $\frac{du}{dy_Q}=\frac{1}{\sigma}$, $dy_Q=udu$, then

$$W=\frac{2\left(e^{-\frac{(u-\frac{\Delta_1}{\sigma})^2}{2}}+e^{-\frac{(u-\frac{\Delta_2}{\sigma})^2}{2}}\right)}{e^{-\frac{(u-\frac{\Delta_1}{\sigma})^2}{2}}+e^{-\frac{(u+\frac{\Delta_1}{\sigma})^2}{2}}+e^{-\frac{(u-\frac{\Delta_2}{\sigma})^2}{2}}+e^{-\frac{(u+\frac{\Delta_2}{\sigma})^2}{2}}} \tag{E.9}$$

With the factorization

$$e^{-\frac{(u+\frac{\Delta_1}{\sigma})^2}{2}}=e^{-\frac{(u-\frac{\Delta_1}{\sigma})^2}{2}}\cdot e^{-2\frac{\Delta_1}{\sigma}u} \tag{E.10}$$

and

$$e^{-\frac{(u+\frac{\Delta_2}{\sigma})^2}{2}}=e^{-\frac{(u-\frac{\Delta_2}{\sigma})^2}{2}}\cdot e^{-2\frac{\Delta_2}{\sigma}u} \tag{E.11}$$

it can be simplified to

$$W=\frac{2\left(e^{-\frac{(u-\frac{\Delta_1}{\sigma})^2}{2}}+e^{-\frac{(u-\frac{\Delta_2}{\sigma})^2}{2}}\right)}{e^{-\frac{(u-\frac{\Delta_1}{\sigma})^2}{2}}\left(1+e^{-2\frac{\Delta_1}{\sigma}u}\right)+e^{-\frac{(u-\frac{\Delta_2}{\sigma})^2}{2}}\left(1+e^{-2\frac{\Delta_2}{\sigma}u}\right)} \tag{E.12}$$

Let

$$\begin{aligned} g_1(x,y) &= \frac{1}{2\sqrt{2\pi}}\int_{-\infty}^{\infty}\left(e^{-\frac{(u-x)^2}{2}}+e^{-\frac{(u-y)^2}{2}}\right)\cdot \\ &\quad \log_2\left(\frac{2\left(e^{-\frac{(u-x)^2}{2}}+e^{-\frac{(u-y)^2}{2}}\right)}{e^{-\frac{(u-x)^2}{2}}\left(1+e^{-2xu}\right)+e^{-\frac{(u-y)^2}{2}}\left(1+e^{-2yu}\right)}\right)du \end{aligned} \tag{E.13}$$

Then we have

$$\begin{aligned} I(X_1 = 0; Y_Q) &= g_1\left(\frac{\Delta_1}{\sigma}, \frac{\Delta_2}{\sigma}\right) \\ &= g_1\left(\frac{\sqrt{E_s}\cdot\cos(\beta+\alpha)}{\sigma}, \frac{\sqrt{E_s}\cdot\cos(\beta-\alpha)}{\sigma}\right) \end{aligned} \tag{E.14}$$

Similarly, we have

$$\begin{aligned} I(X_1 = 1; Y_Q) &= g_1\left(-\frac{\Delta_1}{\sigma}, -\frac{\Delta_2}{\sigma}\right) \\ &= g_1\left(-\frac{\sqrt{E_s}\cdot\cos(\beta+\alpha)}{\sigma}, -\frac{\sqrt{E_s}\cdot\cos(\beta-\alpha)}{\sigma}\right) \end{aligned} \tag{E.15}$$

Therefore,

$$\begin{aligned} I(X_1; Y_Q) &= \frac{1}{2}g_1\left(\frac{\sqrt{E_s}\cdot\cos(\beta+\alpha)}{\sigma}, \frac{\sqrt{E_s}\cdot\cos(\beta-\alpha)}{\sigma}\right) \\ &\quad +\frac{1}{2}g_1\left(-\frac{\sqrt{E_s}\cdot\cos(\beta+\alpha)}{\sigma}, -\frac{\sqrt{E_s}\cdot\cos(\beta-\alpha)}{\sigma}\right) \end{aligned} \tag{E.16}$$

Similarly, it can be shown that

$$\begin{aligned} I(X_2; Y_I) &= \frac{1}{2}g_1\left(\frac{\sqrt{E_s}\cdot\sin(\beta+\alpha)}{\sigma}, \frac{\sqrt{E_s}\cdot\sin(\beta-\alpha)}{\sigma}\right) \\ &\quad +\frac{1}{2}g_1\left(-\frac{\sqrt{E_s}\cdot\sin(\beta+\alpha)}{\sigma}, -\frac{\sqrt{E_s}\cdot\sin(\beta-\alpha)}{\sigma}\right) \end{aligned} \tag{E.17}$$

To compute the mutual information of Y and X_3, we have to consider the four cases of the pair (X_1, X_2). Thus,

$$\begin{aligned} I(Y; X_3|X_1X_2) &= \frac{1}{4}\left[I(Y; X_3|X_1X_2 = 00) + I(Y; X_3|X_1X_2 = 01)\right. \\ &\quad \left.+I(Y; X_3|X_1X_2 = 10) + I(Y; X_3|X_1X_2 = 11)\right] \end{aligned} \tag{E.18}$$

With similar derivation, we have

$$I(Y;X_3|X_1X_2=00)=\frac{1}{2}g_2\left(\frac{\sqrt{E_s}\cdot\sin\alpha}{\sigma}\right)+\frac{1}{2}g_2\left(-\frac{\sqrt{E_s}\cdot\sin\alpha}{\sigma}\right) \tag{E.19}$$

where

$$g_2(x)=\frac{1}{\sqrt{2\pi}}\int_{-\infty}^{\infty}e^{-\frac{(u-x)^2}{2}}\cdot\log_2\left(\frac{2}{1+e^{-2xu}}\right)du \tag{E.20}$$

Due to the symmetry of the constellation, $I(Y;X_3|X_1X_2=00)=I(Y;X_3|X_1X_2=01)=I(Y;X_3|X_1X_2=10)=I(Y;X_3|X_1X_2=11)$, we have

$$I(Y;X_3|X_1X_2)=\frac{1}{2}g_2\left(\frac{\sqrt{E_s}\cdot\sin\alpha}{\sigma}\right)+\frac{1}{2}g_2\left(-\frac{\sqrt{E_s}\cdot\sin\alpha}{\sigma}\right) \tag{E.21}$$

BIBLIOGRAPHY

BIBLIOGRAPHY

[1] M. M. Khairy and E. Geraniotis, "Asymmetric modulation and multistage coding for multicasting with multi-level reception over fading channels," in *Proc. IEEE Military Communications MILCOM 1999*, vol. 1, 31 Oct.–3 Nov. 1999, pp. 92–96.

[2] M. B. Pursley and J. M. Shea, "Phase-shift-key modulation for multimedia multicast transmission in mobile wireless networks," in *Proc. IEEE Military Communications Conference MILCOM '96*, vol. 1, 21–24 Oct. 1996, pp. 210–214.

[3] ——, "Convolutionally encoded phase-shift-key modulation for multimedia multicast transmission in mobile wireless networks," in *Proc. MILCOM 97*, vol. 2, 2–5 Nov. 1997, pp. 978–982.

[4] ——, "Nonuniform phase-shift-key modulation for multimedia multicast transmission in mobile wireless networks," *IEEE J. Sel. Areas Commun.*, vol. 17, no. 5, pp. 774–783, May 1999.

[5] ——, "Multicast transmission with nonuniform phase-shift-key modulation and convolutional coding over Rayleigh fading channels," in *Proc. IEEE Military Communications MILCOM 1999*, vol. 1, 31 Oct.–3 Nov. 1999, pp. 306–310.

[6] ——, "Multimedia multicast wireless communications with phase-shift-key modulation and convolutional coding," *IEEE J. Sel. Areas Commun.*, vol. 17, no. 11, pp. 1999–2010, Nov. 1999.

[7] ——, "Adaptive nonuniform phase-shift-key modulation for multimedia traffic in wireless networks," *IEEE J. Sel. Areas Commun.*, vol. 18, no. 8, pp. 1394–1407, Aug. 2000.

[8] J. H. Park and C. W. Lee, "Asymmetric 8-PSK modulation with embedded bpsk," *Electronics Letters*, vol. 30, no. 17, pp. 1376–1378, 18 Aug. 1994.

[9] M. Sajadieh, F. R. Kschischang, and A. Leon-Garcia, "Modulation-assisted unequal error protection over the fading channel," *IEEE Trans. Veh. Technol.*, vol. 47, no. 3, pp. 900–908, Aug. 1998.

[10] L. F. Wei, "Coded modulation with unequal error protection," *IEEE Trans. Commun.*, vol. 41, no. 10, pp. 1439–1449, Oct. 1993.

[11] H. Imai and S. Hirakawa, "A new multilevel coding method using error-correcting codes," *IEEE Trans. Inf. Theory*, vol. 23, no. 3, pp. 371–377, May 1977.

[12] S. Vishwanath and A. Goldsmith, "Adaptive turbo-coded modulation for flat-fading channels," *IEEE Trans. Commun.*, vol. 51, no. 6, pp. 964–972, June 2003.

[13] A. Goldsmith, "Adaptive modulation and coding for fading channels," in *Proc. IEEE Information Theory and Communications Workshop*, 20–25 June 1999, pp. 24–26.

[14] A. J. Goldsmith and S. G. Chua, "Adaptive coded modulation for fading channels," *IEEE Trans. Commun.*, vol. 46, no. 5, pp. 595–602, May 1998.

[15] S. M. Alamouti and S. Kallel, "Adaptive trellis-coded multiple-phase-shift keying for rayleigh fading channels," *IEEE Trans. Commun.*, vol. 42, no. 6, pp. 2305–2314, June 1994.

[16] J. Hayes, "Adaptive feedback communications," *IEEE Trans. Commun. Technol.*, vol. 16, no. 1, pp. 29–34, February 1968.

[17] M. B. Pursley, "Spread-spectrum multiple-access communications," in *Multi-user Communication Systems*, G. Longo, Ed. New York: Springer-Verlag, 1981, pp. 139–199.

[18] J. Lehnert and M. Pursley, "Error probabilities for binary direct-sequence spread-spectrum communications with random signature sequences," *IEEE Trans. Commun.*, vol. 35, no. 1, pp. 87–98, Jan 1987.

[19] R. K. J. Morrow and J. S. Lehnert, "Bit-to-bit error dependence in slotted DS/SSMA packet systems with random signature sequences," *IEEE Trans. Commun.*, vol. 37, no. 10, pp. 1052–1061, Oct. 1989.

[20] E. Geraniotis and M. Pursley, "Error probability for direct-sequence spread-spectrum multiple-access communications–part ii: Approximations," *IEEE Trans. Commun.*, vol. 30, no. 5, pp. 985–995, May 1982.

[21] M. Pursley and H. Roefs, "Numerical evaluation of correlation parameters for optimal phases of binary shift-register sequences," *IEEE Trans. Commun.*, vol. 27, no. 10, pp. 1597–1604, Oct 1979.

[22] G. Ungerboeck, "Channel coding with multilevel/phase signals," *IEEE Trans. Inf. Theory*, vol. 28, no. 1, pp. 55–67, Jan 1982.

[23] R. H. Morelos-Zaragoza, M. P. C. Fossorier, S. Lin, and H. Imai, "Multilevel coded modulation for unequal error protection and multistage decoding .i. symmetric constellations," *IEEE Trans. Commun.*, vol. 48, no. 2, pp. 204–213, Feb. 2000.

[24] M. Isaka, M. P. C. Fossorier, R. H. Morelos-Zaragoza, S. Lin, and H. Imai, "Multilevel coded modulation for unequal error protection and multistage decoding. ii. asymmetric constellations," *IEEE Trans. Commun.*, vol. 48, no. 5, pp. 774–786, May 2000.

[25] G. C. Clark and J. B. Cain, *Error-Correction Coding for Digital Communications*. Plenum Press, 1981.

[26] C.-W. Wang and W. E. Stark, "Performance analysis of direct-sequence code-division multiple-access communications with asymmetric quadrature phase-shift-keying modulation," *The Interplanetary Network Progress Report by Jet Propulsion Laboratory*, vol. 42-163, 2005.

[27] M. I. Irshid and I. S. Salous, "Bit error probability for coherent M-ary PSK systems," *IEEE Trans. Commun.*, vol. 39, no. 3, pp. 349–352, Mar. 1991.

[28] M. Z. Win and R. A. Scholtz, "Impulse radio: how it works," *IEEE Commun. Lett.*, vol. 2, no. 2, pp. 36–38, Feb. 1998.

[29] ——, "Ultra-wide bandwidth time-hopping spread-spectrum impulse radio for wireless multiple-access communications," *IEEE Trans. Commun.*, vol. 48, no. 4, pp. 679–689, April 2000.

[30] R. J. Fontana, "An insight into UWB interference from a shot noise perspective," in *Proc. Digest of Papers Ultra Wideband Systems and Technologies 2002 IEEE Conference on*, 21–23 May 2002, pp. 309–313.

[31] J. D. Choi and W. E. Stark, "Performance of ultra-wideband communications with suboptimal receivers in multipath channels," *IEEE J. Sel. Areas Commun.*, vol. 20, no. 9, pp. 1754–1766, Dec. 2002.

[32] A. Taha and K. M. Chugg, "A theoretical study on the effects of interference on uwb multiple access impulse radio," in *Asilomar Conference on Signals, Systems and Computers*, 2002.

[33] E. Baccarelli, M. Biagi, and L. Taglione, "A novel approach to in-band interference mitigation in ultra wide band radio systems," in *Proc. of 2002 UWBST*, 2002, pp. 297–302.

[34] I. Bergel, E. Fishler, and H. Messer, "Narrow-band interference suppression in time-hopping impulse-radio systems," in *Proc. of 2002 UWBST*, 2002, pp. 303–307.

[35] B. Hu and N. C. Beaulieu, "Exact bit error rate analysis of th-ppm uwb systems in the presence of multiple-access interference," *IEEE Commun. Lett.*, vol. 7, no. 12, pp. 572–574, Dec. 2003.

[36] G. Durisi and S. Benedetto, "Performance evaluation of th-ppm uwb systems in the presence of multiuser interference," *IEEE Commun. Lett.*, vol. 7, no. 5, pp. 224–226, May 2003.

[37] Y. C. Yoon and R. Kohno, "Optimum multi-user detection in ultra-wideband (uwb) multiple-access communication systems," in *Proc. 2002 ICC*, vol. 2, 2002, pp. 812–816.

[38] L. Zhao and A. Haimovich, "Performance of ultra-wideband communications in the presence of interference," *IEEE J. Sel. Areas Commun.*, vol. 20, no. 9, pp. 1684–1691, 2002.

[39] J. Choi and W. Stark, "Performance analysis of ultra-wideband spread-spectrum communications in narrowband interference," in *Proc. MILCOM 2002*, vol. 2, 2002, pp. 1075–1080 vol.2.

[40] A. Spaulding and D. Middleton, "Optimum reception in an impulsive interference environment–Part I: Coherent detection," *IEEE Trans. Commun.*, vol. 25, no. 9, pp. 910–923, Sep 1977.

[41] A. Spaulding, "Locally optimum and suboptimum detector performance in a non-gaussian interference environment," *IEEE Trans. Commun.*, vol. 33, no. 6, pp. 509–517, 1985.

[42] X. Chu and R. Murch, "The effect of NBI on UWB time-hopping systems," *IEEE Trans. Wireless Commun.*, vol. 3, no. 5, pp. 1431–1436, 2004.

[43] T. Quek, M. Win, and D. Dardari, "Unified analysis of UWB transmitted-reference schemes in the presence of narrowband interference," *IEEE Trans. Wireless Commun.*, vol. 6, no. 6, pp. 2126–2139, 2007.

[44] Y. D. Alemseged and K. Witrisal, "Modeling and mitigation of narrowband interference for transmitted-reference UWB systems," *IEEE J. Sel. Topics Signal Process.*, vol. 1, no. 3, pp. 456–469, Oct. 2007.

[45] A. Spaulding and D. Middleton, "Optimum reception in an impulsive interference environment–Part II: Incoherent reception," *IEEE Trans. Commun.*, vol. 25, no. 9, pp. 924–934, Sep 1977.

[46] C.-P. Liang and W. Stark, "Turbo codes in DS-SS with adaptive nonlinear suppression of impulsive interference," in *Proc. IEEE Military Communications MILCOM 1999*, vol. 1, 1999, pp. 408–412 vol.1.

[47] C.-W. Wang and W. E. Stark, "Nonlinear interference mitigation in multiple-access ultra-wideband communications," in *Proc. IEEE Military Communications Conference MILCOM 2007*, 2007.

[48] J. H. Higbie, "Adaptive nonlinear suppression of interference," in *Proc. Conference record Military Communications Conference MILCOM 88 '21st Century Military Communications - What's Possible?'. 1988 IEEE*, 23–26 Oct. 1988, pp. 381–389.

[49] J. E. Gentle, *Elements of Computational Statistics*. Springer-Verlag, 2002.

[50] A. J. Goldsmith and S. B. Wicker, "Design challenges for energy-constrained ad hoc wireless networks," *IEEE Wireless Commun. Mag.*, vol. 9, no. 4, pp. 8–27, Aug. 2002.

[51] A. El Fawal, J. Y. Le Boudec, R. Merz, B. Radunovic, J. Widmer, and G. M. Maggio, "Trade-off analysis of PHY-aware MAC in low-rate low-power UWB networks," *IEEE Commun. Mag.*, vol. 43, no. 12, pp. 147–155, Dec. 2005.